PHD DISSERTATION

Propagation and effects of vibrations in densely populated urban environments

by Paulius Bucinskas

AARHUS
UNIVERSITY

SOLIDUM PETIT IN PROFUNDIS · UNIVERSITAS ARHUSIENSIS ·

Propagation and effects of vibrations in densely populated urban environments

PhD Dissertation

Paulius Bucinskas

October 31, 2019

AARHUS
UNIVERSITY
DEPARTMENT OF ENGINEERING

Thesis submitted: October 31, 2019

PhD Supervisor: Prof. Lars Vabbersgaard Andersen
Department of Engineering, Aarhus University

ISBN: 978-87-7507-489-1
DOI: 10.7146/aul.389

Assessment Committee: Prof. Amir M. Kaynia, NGI / NTNU, Norway
Prof. Pedro Alves Costa, University of Porto, Portugal
Prof. Steffen Petersen, Aarhus University, Denmark

PhD Series: Faculty of Science and Technology, Aarhus University

Abstract

Environmental vibration generated by sources such as rail lines, road traffic and construction work is a serious concern, especially in the urban environment. It leads to annoyance of the exposed population, creating uncomfortable living and working spaces. Thus, prediction and mitigation of these effects is an important research area, investigated by an increasing number of engineers and researchers. In this regard, computational models are especially useful. They enable the prediction of environmental vibration levels in the planning stages of a new project, reducing or, ideally, completely removing the need for in-situ investigations. Currently available numerical approaches are highly capable and can be used to model the complex cases encountered in the urban environment. However, the largest drawback of these approaches is the long computational times needed to obtain the solution, thus limiting their usage for real applications. The thesis aims to create environmental vibration prediction tools, with particular interest in their computational efficiency. This way, the created methodologies could be easier applicable to a wider audience.

Modelling of the vibration propagation through soil, in most cases, is the most time consuming task. Thus, the thesis mostly focuses on this part of the system. A semi-analytical soil modelling approach was chosen to model the soil, using a Thomson-Haskell transfer matrix method. The method is advantageous, due to the analytical formulation of the soil, which does not require the discretization of the full soil domain and incorporates the infinite nature of the soil. The semi-analytical method is coupled to the finite element method, where the soil is accounted for using the semi-analytical approach, while the external structures can be modelled with finite elements. This way, the computational efficiency of the semi-analytical approach is combined with the modelling freedom of the finite elements method, allowing the application of the created model for a wide range of application cases.

The thesis investigates a number of modelling cases that are commonly encountered when analysing dynamic soil–structure interaction and vibration propagation through soil. A railway bridge structure is analysed using lumped-parameter models to obtain a solution in the time domain. The work presents a novel lumped-parameter model fitting technique that is needed to obtain a numerically stable solution. Further, the semi-analytical soil model is used to analyse cases commonly encountered in the urban environment. For that purpose, various configurations of soil interacting with structure are tested, such as: rigid blocks, pile foundations, railway tracks, embedded structures, and cavities inside the soil. The proposed modelling methods are validated by comparison with other numerical methods. Very good agreement is found, demonstrating the high accuracy and the reduced computational effort of the proposed modelling approaches. A novel numerical method for predicting railway-induced vibrations is also proposed. The method utilizes the semi-analytical soil model formulated in both moving and fixed frames of reference. This way, it is possible to model the railway track and the vehicle in a moving frame of reference, while the nearby structures are formulated in a fixed frame of reference. The approach offers a flexible and numerically stable approach of modelling the full vibration propagation path, using a single-step solution procedure.

Resumé

Miljøvibrationer genereret af kilder såsom jernbanelinjer, vejtrafik og byggeri er et alvorligt problem, især i bymiljøet. Vibrationer generer befolkningen og skaber ubehagelige boliger og arbejdspladser. Forudsigelse og afbødning af disse effekter er således et vigtigt forskningsområde, der undersøges af et stigende antal ingeniører og forskere. I denne forbindelse er beregningsmodeller især nyttige. De muliggør forudsigelse af miljøvibrationsniveauer i planlægningsfasen i et nyt projekt, hvilket reducerer eller, ideelt set, fjerner behovet for in-situ-undersøgelser fuldstændigt. De i øjeblikket tilgængelige numeriske tilgange er generelt anvendelige og kan bruges til at modellere de komplekse problemer, man støder på i bymiljøet. Den største ulempe ved disse metoder er de lange beregningstider, der er nødvendige for at bestemme løsningen, hvilket begrænser metodernes anvendelighed i forhold til virkelige applikationer. Afhandlingen sigter mod at skabe miljømæssige vibrationsforudsigelsesværktøjer med særlig interesse i deres beregningseffektivitet. På denne måde kan de oprettede metoder være lettere at anvende for et bredere publikum.

Modellering af vibrationsudbredelse gennem jord er i de fleste tilfælde den mest tidskrævende opgave. Afhandlingen fokuserer således mest på denne del af systemet. En semi-analytisk jordmodelleringsmetode blev valgt til at modellere jorden ved hjælp af en Thomson-Haskell transfermatrixmetode. Fremgangsmåden er fordelagtig på grund af den analytiske formulering af jorden, som ikke kræver diskretisering af det fulde jorddomæne og indkorporerer den uendelige natur af jorden. Den semianalytiske metode er koblet til finite-elementmetoden, idet jorden modelleres ved hjælp af den semi-analytiske tilgang, mens strukturer kan modelleres med finite elementer. På denne måde kombineres beregningseffektiviteten af den semi-analytiske tilgang med modelleringsfriheden ved elementmetoden, hvilket gør det muligt at anvende den oprettede model til en lang række applikationer.

Afhandlingen undersøger en række modelleringstilfælde, der ofte opstår, når man analyserer dynamisk jord–strukturinteraktion og vibrationsudbredelse gennem jord. En jernbanebro analyseres ved hjælp af en såkaldt lumped-parameter model for at få en løsning i tidsdomænet. Afhandlingen præsenterer en ny metode til kalibrering af lumped-parameter modeller, som er nødvendig for at opnå en numerisk stabil løsning. Den halvanalytiske jordmodel bruges desuden til at analysere problemer, der ofte optræder i bymiljøet. Til dette formål testes forskellige konfigurationer af jord, der interagerer med strukturer, såsom: stive blokke, pælefundamenter, jernbanespor, indlejrede strukturer og hulrum inde i jorden. De foreslåede modelleringsmetoder valideres ved sammenligning med andre numeriske metoder. God overensstemmelse findes mellem resultaterne, hvilket demonstrerer en høj nøjagtighed til trods for den reducerede beregningsindsats i de foreslåede modelleringsmetoder. En ny numerisk metode til forudsigelse af jernbaneinducerede vibrationer foreslås også. Metoden anvender den semi-analytiske jordmodel, der er formuleret i både bevægelige og faste koordinater. På denne måde er det muligt at modellere jernbanesporet og køretøjet i en bevægelig referenceramme, mens de nærliggende strukturer er formuleret i en fast referenceramme. Der opnås herved en fleksibel og numerisk stabil fremgangsmåde til modellering af hele vibrationsudbredelsen, løst ved anvendelse af en enkelttrinsmetode.

Table of contents

Thesis Details

Thesis Title: Propagation and effects of vibrations in densely populated urban environments

PhD Student: Paulius Bucinskas

Supervisor: Prof. Lars Vabbersgaard Andersen, Aarhus University

The main body of this thesis consist of the following papers, separated into three groups.

Bridge modelling group:

B1. P. Bucinskas, L.V. Andersen, K. Persson, Numerical modelling of ground vibration caused by elevated high-speed railway lines considering structure–soil–structure interaction, INTER-NOISE and NOISE-CON Congress and Conference Proceedings. 253 (2016) 2119–2130.

B2. P. Bucinskas, L.V. Andersen, Lumped-parameter models for structure–soil interaction of multi-span railway bridges, Proceedings of the 30th Nordic Seminar on Computational Mechanics (NSCM-30). (2017) 50–53.

B3. P. Bucinskas, L.V. Andersen, Dynamic response of vehicle–bridge–soil system using lumped-parameter models for structure–soil interaction. Under review in Computers and Structures, initial submission 2019 April 30, revised submission 2019 September 18.

Structure–soil interaction group:

S1. P. Bucinskas, L.V. Andersen, Semi-analytical approach to modelling the dynamic behaviour of soil excited by embedded foundations, Procedia Engineering, X International Conference on Structural Dynamics, EURODYN 2017. 199 (2017) 2621–2626.

S2. P. Bucinskas, L.V. Andersen, Excitation of structures near railway tracks — analysis of the wave propagation path, Proceedings of the 6th International Conference on Computational Methods in Structural Dynamics and Earthquake Engineering, COMPDYN 2017. (2017).

S3. P. Bucinskas, L.V. Andersen, Dynamic soil excitation from railway tunnels, Numerical Methods in Geotechnical Engineering IX, Proceedings of the 9th European Conference on Numerical Methods in Geotechnical Engineering, NUMGE 2018. Volume 2 (2018) 1551–1556.

S4. P. Bucinskas, L.V. Andersen, Dynamic structure response using surrogate models, Advances in Engineering Materials, Structures and Systems: Innovations, Mechanics and Applications, Proceedings of the 7th International Conference on Structural Engineering, Mechanics and Computation, SEMC 2019. (2019) 109–114.

S5. P. Bucinskas, L.V. Andersen, Semi-analytical model of soil interacting dynamically with rigid blocks, cavities and piles. Under review in Computers and Geotechnics, initial submission 2019 October 11.

Railway vibration group:

R1. P. Bucinskas, L.V. Andersen, Effects of railway track modelling to surrounding soil and structure excitation, 25th International Congress on Sound and Vibration, ICSV 25. (2018), 4148–4155.

R2. P. Bucinskas, E. Ntotsios, D.J. Thompson and L.V. Andersen, Modelling train-induced vibration of structures using a mixed-frame-of-reference approach. Under review in Journal of Sound and Vibration, initial submission 2019 September 17.

In addition to the main papers, the following publications have also been co-authored.

A1. L.V. Andersen, P. Bucinskas, P. Persson, M. Muresan, L.I. Muresan, I.O. Paven, Mitigating ground vibration by periodic inclusions and surface structures, INTER-NOISE and NOISE-CON Congress and Conference Proceedings. 253 (2016) 6984–6995.

A2. L.V. Andersen, A. Peplow, P. Bucinskas, Efficiency of nearly periodic structures for mitigation of ground vibration, Proceedings of the 6th International Conference on Computational Methods in Structural Dynamics and Earthquake Engineering, COMPDYN 2017. (2017).

A3. L.V. Andersen, A. Peplow, P. Bucinskas, P. Persson, K. Persson, Variation in models for simple dynamic structure-soil-structure interaction problems, Procedia Engineering, X International Conference on Structural Dynamics, EURODYN 2017. 199 (2017) 2306–2311.

A4. P. Persson, L.V. Andersen, K. Persson, P. Bucinskas, Effect of structural design on traffic-induced building vibrations, Procedia Engineering, X International Conference on Structural Dynamics, EURODYN 2017. 199 (2017) 2711–2716.

A5. A. Peplow, L.V. Andersen, P. Bucinskas, Environmental vibration reduction utilizing an array of mass scatterers, Procedia Engineering, X International Conference on Structural Dynamics, EURODYN 2017. 199 (2017) 1368–1373.

A6. L.V. Andersen, P. Bucinskas, P. Persson, Probabilistic assessment of ground-vibration transfer in layered soil, Numerical Methods in Geotechnical Engineering IX, Proceedings of the 9th European Conference on Numerical Methods in Geotechnical Engineering, NUMGE 2018. Volume 2 (2018) 1577–1586.

A7. L.V. Andersen, P. Bucinskas, P. Nguyen, L. Manuel, P. Persson, A surrogate model for vibration transmission in layered soil, Advances in Engineering Materials, Structures and Systems: Innovations, Mechanics and Applications, Proceedings of the 7th International Conference on Structural Engineering, Mechanics and Computation, SEMC 2019. (2019) 31–36.

A8. P. Bucinskas, J. Sneideris, L. Agapii, L.V. Andersen. Validation of a Numerical Model for Dynamic Three-Dimensional Railway Bridge Analysis by Comparison with a Small-Scale Laboratory Model, International Journal of Railway Technology. (2019).

This thesis has been submitted for assessment in partial fulfilment of the PhD degree. The thesis is based on the submitted or published scientific papers which are listed above. Parts of the papers are used directly or indirectly in the extended summary of the thesis. As part of the assessment, co-author statements have been made available to the assessment committee and are also available at the Faculty. The thesis is not in its present form acceptable for open publication but only in limited and closed circulation as copyright may not be ensured.

Preface

The present thesis ‘‘Propagation and effects of vibrations in densely populated urban environments’’ is submitted in partial fulfilment of the requirement of the degree of PhD from Aarhus University. The work was conducted during the period April 2016 – January 2018 in Department of Civil Engineering, Aalborg University and during the period February 2018 – October 2019 in Department of Engineering, Aarhus University. The work was partially funded by the European Regional Development Fund, under the Interreg V programme and project ‘‘Urban Tranquillity’’. Additional support was provided by the Graduate School of Science and Technology in Aarhus University. Their support is greatly appreciated.

I would like to express my deepest gratitude to my supervisor Professor Lars Vabbersgaard Andersen. His continued support, endless knowledge and sincere interest made working together a rewarding and fulfilling experience. Additionally, his coordination and support during the change of universities made the process as easy as possible. I would also like to thank Professor David Thompson and Evangelos Ntotsios for their guidance during my four-month visit to Institute of Sound and Vibration Research, University of Southampton.

Furthermore, I would like to thank my colleagues from both Aalborg and Aarhus Universities. Our discussions over coffee provided the needed breaks in between the hours spent debugging codes and writing publications.

Finally, I would like to thank my family for the unwavering moral support throughout my time spent studying abroad. The thesis would have not been possible without them.

Paulius Bucinskas

Aarhus University, October 31, 2019

Part I
Introduction

1 Introduction

Motivation for the research, with a brief introduction into environmental vibrations. The international and national standards, considered frequency ranges and commonly used assumptions are covered. The overview of the thesis structure is also provided.

Around 75% of the population living in the EU live in urban environments and this number is expected to further increase in the future [1], with the same trends observed all over the world. Living in such an environment has many advantages, such as short commute time to work or school, greater opportunities, convenience of having a wide range of facilities available, etc. At the same time, densely populated areas are better for the environment, as less land area is used, shorter commutes mean less energy is used on transportation, and a convenient public transport system reduces the use of personal vehicles.

Rail transportation is especially attractive for these conditions, allowing to move a large amount of passengers from one urban centre to another urban centre, or inside an urban area. This way, the emission levels per passenger are much lower compared to personal transportation. Due to these reasons, railway transportation is being upgraded and expanded through the world. A white paper by the European Union [2], discussing the future of sustainable transportation, places high-speed railways as the main mode of transportation for medium-distance travel. Therefore, large-scale expansion and creation of a unified European high-speed network can be expected in the future.

However, densification of urban environments and development of rail transportation poses some challenges. High concentration of traffic and industry causes not only air pollution, but also high levels of noise and vibration. The predominant factor leading to environmental vibration is the rail transportation, where a large portion of new projects already need to consider vibration mitigation measures [3]. Both sound and vibration are unpleasant and disturbing to the populace, and can even cause negative health effects [4,5]. Unfortunately current rules and regulations governing the sound and vibration pollution are not well defined and can lead to under or over prediction, which in turn causes “noisy” buildings or unnecessary expenses. Therefore, costly and time-consuming on-site measurements have to be carried out for every new construction project. New numerical prediction tools together with better understanding of noise and vibrations propagation could reduce noise and vibration in the cities as well as the associated costs.

The thesis aims to investigate the ground vibration in the built environment and focuses on creating numerical models for prediction of its effects. The exact mechanism of vibration propagation through soil is rather complicated and especially hard to predict in a densely populated environment, and thus there is a need for complex computational models. At the same time, computational efficiency is also an important factor. Precise but slow to compute models are often not utilized for practical applications, due to the difficulty of using them, and

they are instead substituted by imprecise and quick models. Therefore, computationally efficiency of numerical models is highlighted throughout the work.

1.1 Environmental vibration

Main contributors to the vibrations observed in the urban environment are rail and road transportation, construction work and various types of vibrating machinery. Especially prevalent and thus the most investigated vibration sources are the rail transportation and pile driving during construction. The generated vibrations propagate through the soil and enter nearby structures as shown in Figure 1.1, directly effecting the inhabitants or generating structure-borne noise.

Generally the vibration frequency range affecting humans, where whole body vibration is observed, is considered to be 1–80 Hz [6], sometimes expanded up to 100 Hz [7]. The audible sounds generated by structure-borne vibration are considered in the 20–250 Hz range [7]. It is evident that the two frequency ranges have a significant overlap, and it is often difficult to differentiate between the effects of the vibration itself and the resulting sound. This work is mostly concerned with whole body vibration range of 1–80 Hz [8]. The vibrations propagating through soil are generally modelled using linear elastic models, due to the low amplitude displacements observed. This is a fair assumption for most cases, except very close to the excitation source, like the ballast of the railway track or the nearfield of a driven pile, where plastic deformations might occur. Therefore, the thesis is limited to linear elastic behaviour of the soil. Further, only structures relatively close to vibration sources are considered, as the waves propagating through soil quickly dissipate due to geometrical and material damping.

Environmental vibration is recognized as a serious concern to the exposed population that needs to be addressed. However, a clear definition of environmental vibration and its effects is difficult, due to several reasons. Firstly, the problem is hard to predict and mostly in-situ measurements need to be used, which also have a large degree of uncertainty. Secondly, the human response to vibrations is rather hard to define, as it greatly depends on the personal perception of each individual human. The most commonly used measurement for human

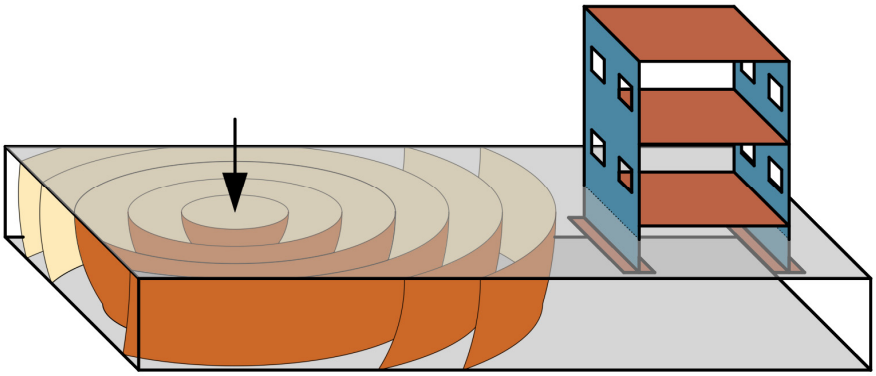

Figure 1.1. Environmental vibrations propagating through soil and entering structures.

exposure to vibration is *annoyance*. A study conducted by Waddington et al. [5] for the EU project CargoVibes provides equations for estimating the portions of the exposed population that are slightly annoyed, annoyed or highly annoyed. Further, experimental studies were conducted to determine the vibration effects on sleep by Smith et al. [9]. The work concluded that higher vibration levels do lead to worse sleep, even when the noise levels remain constant through the tested scenarios. Interestingly, a study conducted by Sharp et al. [4], concluded that people are more annoyed by vibrations of freight trains, when compared to passenger trains, even though the vibration exposure levels are the same from the two sources. This shows that exposure to vibration is not a simple problem and the type of the source also has to be considered, not only the vibration levels. Further, it is often difficult to distinguish the effects of vibrations and the corresponding noise. However, noise exposure does show similar annoyance effects to exposed population and can even lead to potential cardiovascular issues, as shown by Fyhri and Aasvang [10].

The internationally used standard for human exposure are provided by ISO [8,11–13]. Additional guidelines for maximum vibration levels can be found in various countries national standards. Commonly used national standards are: German [14,15], that is also used in other European countries, United States noise and vibration assessment for transit [16] and for high-speed railways [17], United Kingdom [18,19], Switzerland [20]. Further, the European project RIVAS proposed expose–response curves for vibration levels from railways transportation and corresponding human response in [21]. An overview of the most commonly used standards was created by Kouroussis et al. [22], finding that the problem assessment is difficult and different standards might even provide contradictory results. Some of the standards also provide structure-damage-assessment methodologies [15,20]. It has been observed that the property owners near railway tracks might be concerned regarding possible damage to structures due to vibrations [23]. However, the structural damage risk is assumed to be low from the most frequently observed environmental vibration sources [6].

1.2 Overview of the thesis

Part I of the thesis introduces and gives a broad overview of the work done during the project. Firstly, a literature review describing the current state of the art is given. The most popular numerical modelling approaches, structure interaction with the soil, and vibration sources are discussed. Further, the hypothesis and aims of the thesis are formulated, indicating their contribution to the field. Short descriptions of papers, composing the main part of the work, are then provided, listing the main findings and the evolution of the created models. Finally, the conclusions and ideas for future work are discussed.

Part II provides the papers written during the course of the project. The collection of papers is the main part of the work. For ease of reading, the papers are split into three groups:

- Bridge modelling—deals with dynamic modelling of a bridge structure excited by a traversing vehicle. The most important phenomena affecting such structures are included into the developed computational model. The papers investigate the structure coupling via the soil, lumped-parameter models for such coupling, railway excitation, and modelling of nonlinear interactions. The papers in this group are denoted B1–B3.

- Structure–soil interaction using a semi-analytical approach—the usage of a well-known semi-analytical modelling approach is investigated. The semi-analytical model is coupled to finite-element structures, creating a versatile and efficient dynamic soil–structure modelling tool. Modelling of various types of foundations, soil cavities and railway tracks is described. The model is also used for training a surrogate model for assessment of vibration in a building. The papers in this group are denoted S1–S5.
- Railway vibration modelling—deals with vibrations from surface railway lines. The modelling of a railway track and the excitation from a passing vehicle is investigated. A novel approach of modelling such systems is proposed, using a mixed frame of reference formulation. The papers in this group are denoted R1–R2.

Each of the groups deals with specific topics, related to vibration propagation and dynamic structure–soil interaction. At the same time, the covered topics have significant overlap and similar concepts are applied throughout all of the works. The papers in each group are organized chronologically. However, all three groups were developed simultaneously during the course of the project, with new developments being incorporated in all groups at the same time.

2 State of the art

Overview of the current state of the art. The section covers the basics of ground wave propagation, analytical and semi-analytical models, and numerical methods. Further, dynamic soil–structure interaction modelling and railway induced vibration are covered.

An overview of the works dealing with structure–soil interaction (SSI) and environmental vibration problems is given. Starting with Section 2.1.1, simple concepts inherent to dynamic modelling of elastic media are given, such as the waves propagating through the soil. Further, in Sections 2.1.2 and 2.1.3, more advanced semi-analytical and discretized soil modelling methods are introduced. Section 2.2 describes the approaches used for modelling SSI, including rigid structures, piled foundations and vibration mitigation measures. Section 2.3 deals with railway induced vibrations, providing a more detailed look into one of the most prominent vibration sources. Section 2.4 discusses empirical models and experimental measurements, with particular interest of their influence on numerical modelling.

The overview focuses on semi-analytical and numerical modelling, and only a brief look into experimental measurements is provided. The list of publications mentioned in the section is in no way exhaustive and is only intended to illustrate the discussed methodologies and approaches. Where possible, references to works providing a more detailed literature review are given.

2.1 Dynamic soil modelling

2.1.1 Basics of soil modelling

For purposes of modelling environmental vibration, the soil is considered as a linear elastic material with homogeneous layers. It is often considered as being a full-space, infinite in all directions, or as a half-space, where the only boundary is the soil surface. Solution of the governing equation for an isotropic linear elastic solid, used as an idealization of the soil, shows that there are two types of waves propagating through the soil strata. The waves are: the primary wave (P-wave) propagating as compression deformation, and the secondary wave (S-wave) propagating as shear deformation. The P-wave is the fastest propagating wave. Using the Lame constants, the P-wave speed can be found as

$$c_{\mathrm{P}} = \sqrt{\frac{\lambda + 2\mu}{\rho}}, \tag{1}$$

where λ is the first Lame constant, μ is the second Lame constant (Shear modulus) and ρ is the density of the soil. The S-wave speed depends on the shear modulus and the density, and it can be found as

$$c_S = \sqrt{\frac{\mu}{\rho}}. \tag{2}$$

From Equations 1 and 2, it is evident that the P-wave will always be faster than the S-wave. However, the secondary wave generally carries more energy and is therefore more important when analysing environmental vibrations.

When a free surface is introduced into the system (for example, analysing a half-space of soil) the Rayleigh wave (R-wave) appears [24], travelling in the surface of the soil. The Rayleigh wave is slower than the S-wave, typically with a speed of around $0.9c_S$. However, it is carrying even more energy than the S-wave. Therefore, the R-wave is often the most important factor for modelling environmental vibrations, especially when surface vibration sources are considered. To determine the exact R-wave speed the following equation is solved:

$$\left(2 - \frac{c_R^2}{c_S^2}\right) = 4\left(1 - \frac{c_R^2}{c_P^2}\right)^{0.5}\left(1 - \frac{c_R^2}{c_S^2}\right)^{0.5}. \tag{3}$$

It can be seen that the R-wave speed depends on both the S and P waves speeds, as it is a mixture if the two waves. All three types of waves are non-dispersive, as their speed is independent of wavenumber or frequency. Additionally, other waves can appear in the soil, such as the Love wave, which can appears when a soft soil layer is placed on or in-between stiffer soil layers. A more detailed description of wave propagation through soil, including analytical derivations for S, P and R-waves is available in [25–27].

Further, a wave is reflected when it impinges on a free surface or another boundary. The phenomenon is similar to any other waves, such as light, sound and water. However, P and S-waves reflected at a surface interact with each other. Thus, an incoming P-wave will create reflected P-waves as well as reflected S-waves. Only horizontally polarized S-waves reflect fully as S-waves, as they only contain movement parallel to the soil surface. Similar phenomena are observed when a wave reaches an interface between two layers with different material properties. In that case, reflection and refraction of the waves is observed, as some of the energy is reflected back and some is transmitted into the next layer.

The energy contained in the propagating waves is affected by geometric and material damping. The geometric damping is due to the increasing size of the wave front with increasing distance from the source. P and S-waves propagate through the whole soil medium, while the R-wave is constrained to the soil surface, leading to less increase in the size of the wave front with increasing distance from the source. Thus, the P and S-waves decay faster, compared to the R-wave. Material damping is due to movement energy being transformed into heat. Generally, frequency independent hysteric damping is used. However, viscous damping or combination of the two are also encountered. Using frequency-domain solution procedures, material damping in the soil can easily be introduced via a complex-valued Young's modulus.

Overall, the dynamic soil behaviour is a complex problem, where multiple interacting phenomena need to be considered. Implied infinite boundaries make it difficult to model using

many standard approaches. The problem becomes even more complex when external structures interacting with the soil are introduced. The waves interacting with the structures, soil surface and layer interfaces create a system where analytical analysis quickly becomes impossible. Thus, numerical models are used, as described in the following sections.

2.1.2 Semi-analytical methods

The basic theory for waves propagating through a homogeneous elastic half-space were developed already in 1904 by Lamb [28], describing wave propagation for two and three-dimensional cases. Modelling a layered half-space is a more difficult task, for which a semi-analytical method is commonly used. The method is based on an analytical solution to the Green's function, which is obtained using a methodology originally derived by Thomson [29]. Soon hereafter, the work was reformulated into matrix notation by Haskell [30], and now it is commonly known as the Thomson-Haskell transfer matrix method. The Green's function is obtained analytically in the frequency–wavenumber domain, assuming linear behaviour and perfectly horizontal soil stratification. Only the horizontal coordinates are considered as wavenumbers, which are inverse Fourier transformed back into spatial coordinates after the Green's function has been obtained. The transformation is discrete, making the method semi-analytical. The originally proposed formulation is based on the flexibility of the system, where displacements and traction at an interface can be transmitted through a layer by multiplication with the layer transfer matrix. The method is computationally efficient, as assembly of multiple layers only requires multiplication of relatively small matrices, without the need of global system assembly. Infinite boundaries are also already part of the analytical formulation, making the approach very useful for SSI problems. The formulation can be expanded to model poroelastic system behaviour using the Biot [31–34] theory. Examples of semi-analytical models with poroelasticity can be found in [35,36].

However, numerical issues quickly arise using the flexibility-based approach, when high frequencies and deep layers are considered. This is due to the limited precision in the representation of numbers used in computers, which are not able to handle the mathematical operations needed. As the layer assembly involves large exponentially growing terms, the accumulated error from the performed mathematical operations leads to computational instabilities. The Thomson-Haskell transfer matrix method is widely used for geophysics and seismology, where several approaches have been developed for solving the instability issue [37–40]. One of the approaches, proposed by Wang [41], identifies that the problem arises due to the coupling of two waves (the P-wave and the so-called SV-wave) propagating through the layers and mixing in the interfaces. The problem can, however, be solved by a local coordinate transformation within each layer to remove the coupling terms. This way, the whole system is rotated every time a new interface is encountered in the solution procedure. Computational times are effected by incorporation of additional stabilization techniques, but the increase is relatively low. It is noted that the method proposed by Wang [41] has been incorporated in the numerical models developed during this thesis. An example of soil modelled using the Thomson-Haskell transfer matrix method is shown in Figure 2.1.

Alternatively, the original transfer matrix can be reorganized into a stiffness expression, as proposed by Kausel and Roesset [42]. The method assembles the stiffness of soil layers into a

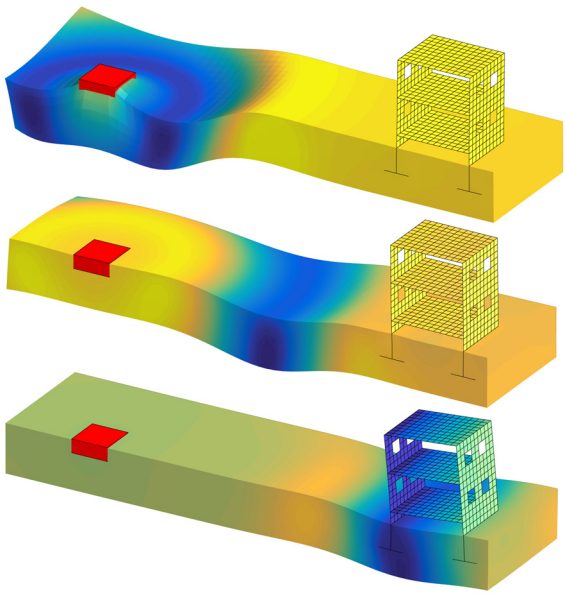

Figure 2.1. Environmental vibration propagation modelled using the semi-analytical soil model with finite element building model.

stiffness matrix defined within the wavenumber–frequency domain, similarly to the finite element method. In that case, the assembled stiffness matrix size depends on the total number of layers considered in the system. Nevertheless, the approach is still computationally efficient and is widely used. Through the years, the direct stiffness matrix method has been further developed and expanded, with detailed descriptions available in the works by Kausel [43,44]. The method can also be applied for anisotropic layers and wave propagation through fluids as described by Park and Kaynia [45].

Another approach of finding the Green's function is the thin layer method (TLM). Here, the Thomson-Haskell transfer matrix, reformulated into the stiffness formulation, is still used, with the simplification that the displacements vary linearly through a layer. For the assumption to be correct, the modelled layers have to be sufficiently small when compared to the S-wave length. In theory, the method cannot be used to model a half-space to infinite depth. This is overcome by utilizing the direct stiffness matrix method to model the half-space underneath the layers, or applying non-reflecting boundary conditions, which will be discusses in the next subsection. Early works describing the TLM were conducted by Waas [46] and by Lysmer and Wass [47]. The method was further expanded by Kausel and Roesset [42]. Both the stiffness matrix and thin layer methods have been used for the development of the ElastoDynamics Toolbox at K.U. Leuven [48].

After the Green's function in the frequency–wavenumber domain has been established using any of the methods, it is converted into frequency–space domain, using discrete double inverse Fourier transformation. If the system is considered in a fixed frame of reference, the polar symmetry of the Green's function can be utilized, essentially simplifying the inverse transformation problem from a two-dimensional field to a one-dimensional line. The method greatly reduces the computational effort and allows a more precise evaluation of the Green's

function, as described in detail by Andersen and Clausen [49,50]. Methods for finding the Green's function directly in the time domain are also available. For example, Kausel [51] uses the TLM for a direct time domain solution, where the governing equations formulated in the frequency domain are transformed analytically into the time domain. More recent works [52,53] propose a direct time–wavenumber domain formulation for layered half-space. After the Green's function has been obtained, it can be used directly or as part of other approaches. The methodologies described in this section are also used as parts of other methods, for example, the boundary element (BE) method, or for modelling non-reflecting boundary conditions.

The main advantage of the semi-analytical models is their computational efficiency. The analytical formulation with implied infinite boundaries is quick to compute. Further, the frequency–wavenumber domain formulations can be easily parallelized, allowing multiple frequencies/wavenumbers to be solved simultaneously. This is especially well suited for modern multi-core computer CPUs. The main drawback is the simplifications needed to obtain an analytical Green's function expression. Thus, it is not possible to directly model cavities inside the soil, trenches, non-horizontal soil stratification and other conditions, commonly found in urban environments. Further, for practical application, the analytical formulations are rather complex and not well known in industry.

2.1.3 Numerical methods

Various numerical methods can be used when semi-analytical approaches are not sufficient. They offer much greater flexibility for modelling complex geometry, material properties or nonlinear interactions. All of the methods discretize the analysed system to numerically approximate the differential equations, describing the system behaviour.

The finite difference method (FDM) is one of the approaches used for modelling the soil strata. The continuous system is discretized into a number of nodes at which the strong form of the governing partial differential equation is solved, approximating the spatial and temporal derivatives by finite differences. Differently from the semi-analytical approaches, the nodes are only directly interacting with other nearby nodes, leading to sparse system matrices. Virieux [54,55] describes finite-difference (FD) modelling of wave propagation through two-dimensional elastic media, using a staggered grid for velocities and stresses. Similarly a three-dimensional staggered grid is used by Graves [56], who also described an optimized computation technique for large modelled domains. The methodology has been applied for predicting railway induced ground vibration in [57]. However, compared to other numerical approaches, it is rarely used. The advantages of the method are that it can be more computationally efficient, and application of non-reflecting boundary conditions is easier, when compared to finite element method (FEM). However, modelling more complex geometries, such as buildings or detailed railway tracks, is difficult [57,58].

The FEM method [59] is another commonly used approach for modelling the soil. Here the weak form of the differential equations is used. It is an attractive solution procedure, as it is well suited for modelling complex geometries. Structures and soil can be modelled using the same method, and a direct time-domain formulation is available. The FEM is widely utilized

for ground vibration propagation problems, and examples of works using the methods can be found in [60–63]. A large advantage of the FEM is the widespread, commercially available software, such as COMSOL Multiphysics [64] and ABAQUS [65]. The main consideration when using finite elements (FE) is to ensure proper discretization of the waves travelling through the soil, with the general rule being six to ten elements per wavelength. It can become a limiting factor for high-frequency excitation, where the waves have very short wavelengths. Further, when modelling the soil as an infinite domain, the FEM has significant issues. Namely, the waves propagating through the soil are reflected from the boundaries of the domain, leading to unphysical system behaviour. This can be solved by modelling the soil domain to be large enough for the waves to dissipate before the waves reflected at the artificial boundaries re-enter the domain of interest. However, such models are generally very large, in turn requiring long computation times.

A more efficient way of dealing with reflections from the boundaries is to introduce non-reflective boundary conditions. There is a number of different approaches to account for the non-reflecting boundary conditions. One of the most simple approaches was proposed by Lysmer and Kuhlemeyer [66]. It is based on impedance boundary conditions that are applied to the artificial boundary of the system. Physically, this is equivalent to lining the boundaries of the domain with dashpots, with their damping dependent on the soil properties. The impedance is determined according to P and S-wave speeds, thus the R-waves are not well accounted for. A method proposed by Bamberger et al. [67] introduces R-wave 'ears' in the model, essentially enlarging the modelled domain close to the soil surface allowing R-waves to dissipate. Further, the waves are best absorbed when they reach the boundary orthogonally, leading to overall low-reflecting boundary condition. This can be improved using formulations accounting for the direction of the wave propagation, as shown by Higdon [68] and Krenk and Kirkegaard [69]. However, then it is required that the direction of wave propagation is known, which is difficult when the soil is interacting with structures and creating additional reradiated waves. Infinite elements can also be used to introduce low-reflecting boundaries, as described by Bettess [70]. Examples of works using this approach can be found in [60,61,63]. A more recent, and a very promising development, is the perfectly matched layer (PML) method. The PML method utilizes complex valued coordinate stretching, leading to much more efficient non-reflecting boundary conditions. Originally, PMLs were developed for electromagnetic wave propagation by Berenger [71]. Application for electrodynamics was then introduced by Chew and Liu [72]. Further, an FE–PML coupling methodology was developed in, e.g., [73,74]. The application range for PML is wide, the boundary can be formulated in time-domain [75] and in a moving frame of reference [76]. An example of an FE–PML model applied for environmental vibration prediction can be found in [77].

The boundary element method (BEM) [78] is another commonly used numerical approach. Here only the surface of the modelled domain needs to be discretized, essentially reducing the discretization of three-dimensional problems into two-dimensions. The method uses the Green's functions as weight functions for the BE formulation, which can be obtained analytically or from the previously described semi-analytical approaches. Differently than for FDM and FEM methods, the non-reflecting boundary conditions are already part of the formulation, since the Green's function ensure radiation of waves into an infinite domain,

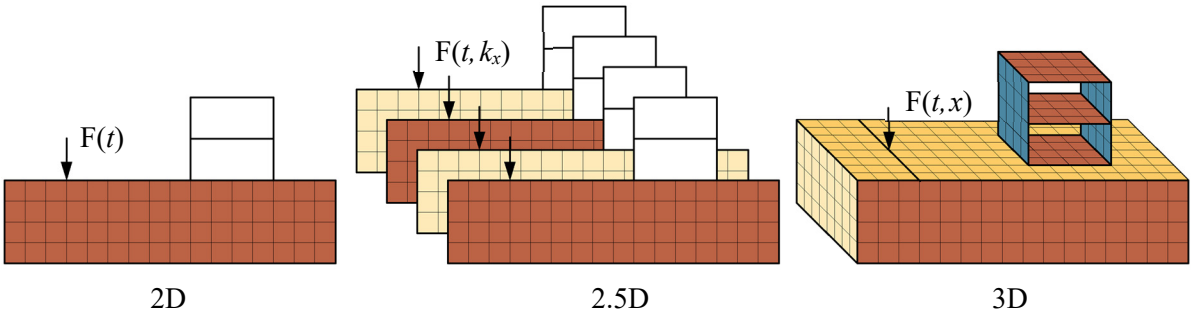

Figure 2.2. Two-dimensional, two and half-dimensional and three-dimensional modelling approaches.

making the BE method well suited for modelling the soil. Pure BE formulations have been applied for SSI problems in, e.g., [79,80]. However, it is not well suited for modelling complicated geometries, such as a building structure. Thus, in most cases the approach is combined with FE method, creating coupled FE–BE models. Then the structures are modelled using the FE method, and the soil domain is modelled using BEs. A good overview of FE and BE approaches is provided by Clouteau [81]. Combined FE–BE models can be found in a large number of works, for example, [82–87].

The numerical methods in this section can be formulated in either two or three-dimensions. Generally, two-dimensional methods are quicker to compute, but the three-dimensional solution is needed to model the system fully, especially considering moving loads and complex geometries. An alternative 2.5D (two-and-a-half-dimensional) approach was proposed by Yang and Hung [88] for modelling systems with invariant geometry along the movement line. The method simplifies the three-dimensional system into a series of two-dimensional problems, which are solved for discrete wavenumbers. Thus the method lies in-between the two and three-dimensional approaches, see Figure 2.2. The method is computationally efficient, as the system is only discretized in two dimensions. Further, it is easy to parallelise the solution procedure for efficient computations and the requirements for computer random access memory (RAM) are reduced. The largest drawback of the method is that it is limited to structures invariant in one direction. Thus, it is well suited for modelling railway tracks and tunnels but cannot be used to represent discrete supports of the track, bridge pylons or other finite building structures. A comparison between 2D and 2.5D tunnel models was performed by Yang et al. [89]. It was determined that, while a 2D model is less computationally demanding, it overestimates the obtained vibration levels for all tested cases and is generally less accurate. A periodic formulation using Floquet transform was introduced by Degrande et al. [90], that can be used for periodically varying infinite geometry in the third direction.

Thus, numerical methods are a commonly used for a wide array of applications, with their popularity increasing historically together with the improving computer hardware technology. At the same time, the limiting factor for more complex problems remains the computational effort needed. This often makes numerical models unsuitable for the early stages of a project, where large numbers of possible design cases need to be tested. Further, continued improvement of computer hardware is not guaranteed, with current technologies approaching the physical limits of silicon chips, and there is a market for computational methods that can

be used on standard laptop and desktop computers, as opposed to large super computers that are not commonly available for early design of civil structures. Therefore, in the author's opinion, numerical methods cannot fully replace analytical and semi-analytical methods.

2.2 Structures interacting with soil

SSI is an integral part of environmental vibration prediction. The underlying soil can often completely change the response of a structure; thus, it is also important for analysis of dynamic structure behaviour. A significant amount of research has been carried out into the development of various approaches to account for SSI. An overview of early, mainly analytical, methods was written by Kausel [91]. An overview of more recent developments of the FE and the BE methods can be found in [81,92].

Rigid blocks are often used to represent the building foundations. The assumption is that the footings are significantly stiffer compared to the surrounding soil and the local deformations of the footing can be neglected. It is a fair assumption when modelling smaller sized foundations, such as surface or strip type footings, unless the soil is very stiff. In any case, the assumption is not suitable for modelling piles or slab type foundations, which can deform significantly during loading. An additional advantage of modelling the foundations as rigid is the reduced number of degrees of freedom needed, as a single node with six degrees of freedom can fully represent the displacements of a three-dimensional rigid object. Likely the most simple approach for obtaining the response of a rigid footing is by using the dynamic stiffness tables described by Wong and Luco [93]. Another approach is to use lumped parameter models (LPMs). LPMs represent the underlying soil behaviour through relatively simple systems consisting of springs, dashpots and masses. In some cases, some types of LPMs introduce additional degrees of freedom into the system, but the number is low. Standard and fundamental LPMs can be obtained directly from the material properties of the soil and the dimensions of the rigid footing, as described in [27,94]. The simple models are generally limited to circular and square footings placed on the surface of a half-space.

Simplified models used to model rigid footings are very limited in their application cases. Thus, more flexible BE [79,95,96] and FE–BE [83] approaches are commonly used to account for soil stratification, unusual foundation shapes or separate footings coupling through the soil. Semi-analytical soil modelling methods are also a viable approach, especially considering the reduced computational effort needed. A semi-analytical model for rigid surface footings was used by Andersen and Clausen [49]. The work discretized the soil–footing interface into a number of discretization nodes. Using the semi-analytical soil model, a global flexibility matrix was established, describing the receptance between all the discretization nodes. The matrix was then inverted and condensed to account for the rigid footing movements, resulting in a dynamic stiffness matrix. The obtained frequency-domain stiffness matrix describes SSI interaction of separate rigid footings and the coupling between the footings through the soil. It can be directly added to FE matrices, used to model external structures connected to the rigid footings. Rigid surface footings were also investigated by Lin et al. [97] using a different semi-analytical soil model. The work was recently further expanded including three-dimensional rigid foundations and a time-domain solution by Han et al. [98].

Another type of LPMs, named consistent LPMs, has been developed by Wolf [99,100]. This type of LPMs can recreate complex soil behaviour, including the effects of layered soil or unconventional foundation shapes. The approach is based on fitting a polynomial fraction function to the desired system response in the frequency domain. Increasing the order of the fitted polynomials enables more complex system behaviour to be recreated. The function can then be reorganised into partial fraction form and physically represented as series of simple LPM systems. Consistent LPMs can be used for the direct and the coupling terms of a stiffness matrix, allowing an accurate representation of the SSI, including coupling of separate footings through the soil. The largest drawback of the approach is that the frequency domain dynamic stiffness matrix of the soil is required. It can be obtained by any of the previously described approaches, or it can be measured directly through physical experiments in the field or in the laboratory. The main application case for consistent LPMs is when a system formulated in the frequency domain needs to be transformed into a time-domain solution. The usage of consistent LPMs is further investigated in papers B2 and B3 of the thesis.

Piles are another popular type of foundations for buildings. Dynamic pile foundation modelling is similar to modelling any other type of foundation, but the piles are not modelled as rigid, which requires additional consideration. Semi-analytical [101–103] and numerical [104,105] methods are commonly used. In regard to environmental vibration, the pile foundations are also interesting during the installation phase. Piles installed using impact driving or vibration driving produce environmental vibration in the surrounding areas. Modelling the installation process is difficult using the linear elastic approaches described in this work, as the near-field soil behaviour is nonlinear. However, for the far-field response, linear models are still used, for example, in [106,107]. The effects of pile driving are beyond the scope of this work, but more detailed descriptions are available in [108,109].

Evaluation of vibration reduction measures is often the main objective for using computational ground vibration models. This way, the optimum solution can be found even before the construction process begins. A large amount of works investigates various vibration mitigation measures; thus, only examples of the measures are given here. A more detailed overview can be found in a literature review by Connolly et al. [58]. The vibration mitigation approaches are generally split into three groups relating to: the source, the transmission path, and the receiver of vibrations. The measures that can be taken at the source of vibration include floating-slab track design [110], ballast mats [111], dynamic vibration absorbers [112] or changing the vehicle suspension properties [113]. Transmission path measures include trenches and other barriers embedded inside the soil [87,114] and heavy blocks placed on the soil surface [115–118]. An overview of transmission path measures can be found in [119]. The receiver of the vibrations is usually a building structure, where measures such as base isolation [120] or adjusting the structural design [121] can be taken. Some of the vibration mitigation methods are investigated in the supplementary papers of the thesis (A1–A8), but they are not the focus of the thesis. Overall, the range of possible measures is large, with various computational approaches used for their evaluation, the choice of methodology being dependent on the model complexity and the available computational resources.

As can be seen, dynamic SSI modelling takes various forms depending on the considered system. However, if modelling of a full vibration propagation path is desired, the computational model should be able to account for most of the discussed cases. This is possible to achieve using three-dimensional FE models, but—as discussed previously—the computational effort needed for such models is very large. Another possible candidate for modelling the full system is a coupled semi-analytical–FE approach. SSI modelling using the semi-analytical soil model coupled to FE models of structures is explored in papers S1–S5 of the thesis.

2.3 Railway excitation

Railways are one of the main sources of environmental vibration, due to the large moving mass of the train and wheel–rail interaction between two steel surfaces. This leads to both low frequency vibrations due to the moving mass and high frequency vibration from the wheel–rail interaction. Well-developed railway infrastructure is an environmentally friendly alternative to personal vehicles. Therefore, the industry is seeing an increased surge in development of new railway lines, especially in European and Asian countries. Due to these reasons, the vast majority of research regarding environmental vibrations is carried out for railway excitation. Computational modelling of railway vibrations poses some unique challenges. The vibration source is moving through the system, requiring large modelling domains or moving-frame-of-reference formulations. Further, the dynamic excitation is due to multiple phenomena.

Here only a small part of the overall research is provided. Much wider overviews of the research regarding railways can be found in, for example, [6,58,122,123], with a broader overview of vehicle and track modelling, including their interaction, provided by Popp et al. [124]. This section is focused on railways, but vibration modelling from road traffic is largely the same, just with different properties of the track and vehicle suspension systems.

2.3.1 Dynamic excitation mechanisms

The effects of a passing train are generally separated into the quasi-static loads and the dynamic loads [125]. The quasi-static loads are caused by the moving vehicle mass and are therefore independent on the characteristics of the vehicle suspension. The resulting system response is mostly affected in the low-frequency range, though with increasing frequencies with increasing speeds of the vehicle. The quasi-static loads lead to a well-predictable system response. The positions of the peaks and valleys, observed in a frequency spectrum, depend on the spacing between the wheel sets and bogies as well as the number of carriages in the train. The predicted frequency response from quasi-static forces is described in [6,123,126].

The dynamic loads induced by trains are due to the wheel–rail interactions and generally lead to higher-frequency vibrations in the range relevant to reradiated structure-borne noise. Naturally, the produced vibration is highly dependent on the quality of the track. For numerical simulations, the uneven track profiles are obtained from power spectral density (PSD) spectra. These spectra are defined in a number of standards; the most commonly used are the Federal Railroad Association (FRA, United States), Chinese and German spectra. Overall, comparison between different PSD spectra is difficult, as they are defined for different wavelength ranges and use different input parameters. An overview of the PSD spectra and their application can be found in [123,127,128]. In most cases, only the vertical irregularities of the track are

considered, and the system is simplified into a single rail, assuming the irregularities between two rails are identical. However, as shown by Ntotsios et al. [129], this is not always sufficient, and two rails with uncorrelated unevenness profiles are needed for certain unevenness wavelengths. Like railways, road roughness can also be described using PSD spectra [82].

The wheel–rail interaction can be accounted for in several different ways. The circular shape of the wheel combined with the small interaction area with the rail lead to nonlinear wheel–rail interaction. This can be modelled using the nonlinear Hertzian springs, accounting for the varying stiffness of the wheel dependent on the relative deformations. Further, with high vehicle speed and large unevenness amplitude, the wheels can lose contact with the rails leading to no interaction force. Wheel–rail interaction mechanisms including Hertzian springs and loss of contact was used by, e.g., Lei and Noda [130]. However, to account for nonlinear wheel–rail interaction, an iterative time-domain solution of the system is needed. This is a significant complication for solving the system, as the underlying soil is commonly modelled in the frequency domain. Alternatively, the Hertzian spring stiffness can be linearized around the force levels corresponding to wheel deformation when loaded only by the vehicle weight. This is a commonly used approach which can be found in, for example, [131,132]. Generally, it is accepted that the linearized wheel–rail interaction is adequate. However, when analysing singular defects of a rail, such as a rail joint, nonlinear interaction might be necessary, as found by Kouroussis et al. [133].

Another excitation mechanism from a passing vehicle is due to the local rail defects. This poses a significant problem for computational modelling, as some of the commonly used approaches—such as two-and-a-half-dimensional models (2.5D models) and frequency domain solutions—are not suitable for this case. Therefore, time-domain solutions are used, often included into multi-step solution procedures. For example, in [133,134] two-step solution procedures are used, where wheel–rail interaction is accounted for in time domain, while the resulting soil displacements are found in the frequency domain. Connolly et al. [135] uses a three-step solution, where the additional third step calculates the resulting building response in time domain.

Other types of excitation also exist. Parametric excitation arises due to discrete supports of the rail by the sleepers, which lead to varying stiffness of the track. Similarly, assessment of local rail defects requires a time-domain-solution procedure as shown by Nielsen et al. [136,137]. Time-domain solutions are also used when modelling the effects of wheel flats [138,139]. Seemingly, the effects of a wheel flat should be harmonic and solvable in the frequency domain. However, due to the possibility of losing contact and potentially having large deformations of the wheels, nonlinear wheel–rail interaction is needed. As found by Pieringer et al. [139], even using the nonlinear Hertzian springs might not be sufficient when modelling large wheel flats. Here, more advanced models of the wheel may be required. Alternatively, the smaller irregularities of the wheels have an insignificant effect on the ground vibration, compared to the track irregularities [140], and are often not considered.

2.3.2 Modelling approaches

One of the early analytical models for modelling railway-generated ground vibration has been developed by Krylov [141–144]. Here the train is represented as moving constant loads with the underlying soil modelled as a homogeneous half-space, utilizing a formulation for the Green's function developed by Lamb [28]. Only the Rayleigh wave is considered for the Green's function. The work can be expanded by introducing more complex formulations of the Green's function as described by Degrande and Lombaert [145]. A similar modelling approach was proposed by Sheng et al. for stationary harmonic loads [146] and moving harmonic loads [147]. Here, the underlying soil is modelled using the transfer-matrix method developed by Thomson and Haskell [29,30], allowing the modelling of layered soil. Further, the track is modelled analytically in the frequency–wavenumber domain as a layered structure with springs, masses and dashpots representing the track elements. This way, an infinite track can be represented. The effects of the track were investigated using the semi-analytical model in [148]. Further, the model was expanded to include a two-dimensional multi-degree-of-freedom vehicle model and an uneven vertical track profile in [131]. This way, the developed model can account for both the quasi-static load and the dynamic wheel–rail interaction. The modelling approach was further expanded by modelling both rails and their interaction with separate vehicle wheels by Ntotsios et al. [129]. The usage of the semi-analytical soil modelling approach for rail vibration prediction are investigated in papers R1 and R2 of the thesis.

A semi-analytical approach has also been used for modelling railway tunnels embedded inside the soil, and for determining the resulting environmental vibrations. A popular approach is the Pipe-in-Pipe (PiP) method, developed in [110,149], as part of MOTIV project [150]. The method uses a full-space formulation for the soil, not accounting for the effects of the soil surface. Generally, it is assumed as a fair assumption, especially considering tunnels embedded deep inside the soil. For shallow tunnels, a methodology to model the surface response of a half-space was introduced by Hussein et al. [151]. The methodology assumes that the tunnel response is not affected by the surface of the soil, and after the tunnel response is obtained the Green's functions are used to determine the response of soil half-space. As discussed by Andersen and Jones [152], this approach may, however, not be useful for tunnels placed near the surface, i.e. cut-and-cover tunnels. In any case, the PiP method has recently been used for modelling double-deck tunnel structures [153] and for investigation of vibration reduction methods using dynamic dampers [112].

Three-dimensional FE and BE methods are commonly used for modelling geometrically more complex problems or when time domain analysis is needed. An FE–BE tunnel model has been described by Andersen and Jones [152]. The same work compared the agreement between two and three-dimensional models, concluding that, while two-dimensional model might suffice in some cases and for some frequencies, three-dimensional models are needed for accurate results. O'Brien and Rizos [154] used a coupled FE–BE model in time domain. A staggered time-integration scheme was used, ensuring the compatibility of forces and displacements between the FE and BE solutions [83]. The created model only accounts for the quasi-static loads of the train. A similar three-dimensional FE–BE model was used by Galvín et al. [85]. However, the described method also includes a multi-degree-of-freedom vehicle

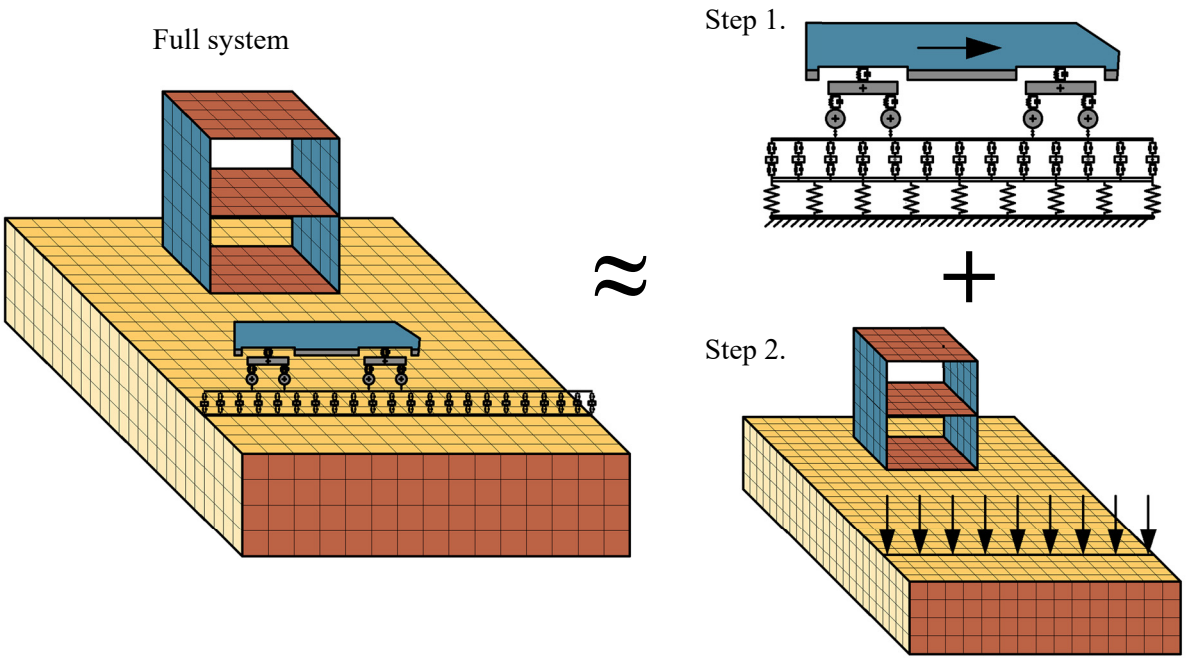

Figure 2.3. Typical two-step solution approach separating the vehicle–track and the soil–structure systems.

model and direct coupling between the FE and BE parts of the system. Both works model the track structure using the FEM and the underlying soil using the BEM. Works utilizing the FEM to model both the track and the soil are also popular. In that case, commercially available FE software packages are generally used [60,63,155,156]. As already mentioned, the large advantage of FE models is the widely available commercial software tools. For example, both the works by Connolly et al. [60] and Kouroussis and Verlinden [156] used ABAQUS [65] to model the underlying soil. However, in both cases it was not possible to introduce a vehicle model directly into the ABAQUS model; hence, additional steps were taken. In [156], the solution procedure is split into two parts: firstly, the vehicle–track system with a simplified soil layer is modelled; secondly, the detailed soil model is loaded by the forces obtained from the first step. On the other hand [60] employed a staggered solution procedure for every time step, where the nonlinear wheel–rail interaction forces are applied to the ABAQUS soil model through user-defined FORTRAN subroutines. Similar approaches are often needed when utilizing three-dimensional FE models. Further, the 2.5D modelling approach is particularly well suited for modelling railway vibration and is widely used. The 2.5 formulation been applied to most of the previously described soil modelling methods: finite/infinite element formulations are used in [157–159], BE model in [160], FE–BE models in [161–164], FE–PML models in [77,165,166].

Lopes et al. [77] modelled a full vibration propagation path from a multi-degree-of-freedom vehicle model to a building structure. Due to the limitations of the 2.5D approach, the solution procedure was split into three parts: the vehicle–track model, the 2.5D FE–PML tunnel model, and a three-dimensional FE building structure. This way, some of the direct coupling terms are excluded from the system, such as the vehicle model does not directly couple to the building. However, these effects are considered very small, and they are further reduced by increasing

distance between the source and the receiver. Similar solution procedures are common, especially, when considering the full vibration propagation path. Hussein et al. [167] used a so-called sub-modelling technique for predicting building response from railway tunnels. Once again, a multi-step solution procedure was used, assuming that the presence of a building has no effect on the tunnel response. The PiP tunnel model was used and the building response was found from the free-field displacements of the soil surface. Similar multi-step approaches can be found in [132,168]. A typical two-step approach is illustrated in Figure 2.3. An alternative to multi-step solution procedures would be a fully coupled time-domain solution. For example, Ju [140] used a time-domain solution procedure and a three-dimensional FE model, modelling the full propagation path from the vehicle up to the building structure. Unfortunately, such models are limited due to time-domain modelling limitations, mainly the long computation times and overall difficult implementation.

2.4 Empirical models and experimental measurements

Experimental measurements are an integral part of environmental vibration prediction tools. A large part of currently used models is fully or partially data driven, providing quick estimates without the need for detailed information about the site conditions. The more complex computational models also need to be calibrated according to measurement data in order to provide accurate results. This section provides an overview of how the computational modelling methods are affected by field measurements.

The most simple environmental vibration prediction methods are based on in-situ measurements, as proposed in [17,169]. These empirical methods are still widely utilized for practical applications, as they are simple and straightforward to use. However, the usage cases are rather limited and not suitable for more complex building structures or soil conditions. A number of so-called semi-empirical models for predicting vibrations caused by railways have been developed. They generally model an extremely simplified railway track and soil system with the results calibrated according to measurement data [170–173]. An alternative approach of creating data-driven models was presented by Connolly et al. [174]. Here an efficient estimate of environmental vibrations is obtained using machine learning with neural networks, where the data points needed are obtained from a detailed three-dimensional FE model. Further, Kouroussis et al. [175] proposed an approach for estimating the effects of localized rail defects, such as rail joints.

More advanced computational models have been also successfully used for railway induced vibration prediction. A study investigating high-speed trains was performed by Galvín and Domínguez [84]. A theoretical FE–BE model was created modelling the track including the surrounding structures such as pylons supporting the electricity lines above the track. The model was validated by comparison with field measurements. The obtained results showed good agreement between the measured and simulated results. Costa et al. [164] also obtained similar results comparing a coupled FE–BE model with field measurements. However, the accuracy of the models greatly depends on the quality of input parameters, such as the Young's modulus and Poisson's ratio of the soil.

Generally, conventional site investigations do not provide sufficient data for analysing environmental vibrations [58]. Thus, more specific site investigations need to be performed, often by measuring the wave propagation speeds in the soil. A measurement technique based on an impact method for soil transmission was proposed by Bovey [176]. Other methods of determining dynamic soil properties from field measurements can be found in [177–179], and a full waveform inversion was used by Kallivokas et al. [180] to characterize a site. Milne et al. [126] showed a way of finding the vehicle speed and track system support modulus using data obtained from measured train passages. Similarly, [181] also presents an approach of calculating train speed from vibration measurements.

The critical train speed is often analysed, as the train speed can exceed the wave propagation speeds in the soil, creating an equivalent to a Mach cone in the soil. An extreme case where the train speed was approaching the critical Rayleigh wave speed has been observed at Ledsgard in Sweden and described by Madshus and Kaynia [182]. However, when critical speeds are not approached, the vibration levels are often not highly dependent on the train speed. Degrande and Schillemans [183] performed a free-field soil vibration measurements from passing high-speed trains, measuring speeds from 160 km/h to 330 km/h. There, only a weak dependence of the observed vibration levels on the train speeds was found. Similarly, based on a numerical study, Connolly et al. [135] concluded that there is no correlation between the train speed and observed vibrations in a building structure. Auersch and Said [184] investigated the attenuation of vibrations with increasing distance, for various sources of vibration. They found that the attenuation of vibration greatly depends on the type of the source, with source types such as trains producing slower attenuating vibrations than, for example, explosion-type sources.

Generally, the precision of computational models is limited due to reasons such as oversimplification of the system and imprecise input parameters. However, achieving extremely high precision might be impossible due to the stochastic nature of the problem. A study performed by Connolly et al. [185], encompassing a large number of measurement data collected from various studies, observed that differences of ±2 VdB (vibration metric defined by FRA [17]) are observed even between separate train passages. Indicating that there is a rather large degree of uncertainty in the system, at the same time defining the upper precision limit that numerical methods can most likely achieve.

3 Scope of the thesis

Conclusions and findings obtained from the state of the art. The scope of the thesis is defined, with the formulation of hypothesis and accompanying overall aims.

3.1 Findings of state of the art

Environmental vibration prediction is a difficult task that becomes even more demanding when a densely built up urban area is considered. In that case, simple analytical approaches will not suffice for predicting the vibration levels with an adequate accuracy. Further, advanced fully three-dimensional FE and BE models can model complex systems. However, they are limited by the large computational effort required and by the limited information about the site conditions that is typically available. Additionally, experimental measurement campaigns indicate that perfect predictions of environmental vibrations might not be possible, due to the stochastic nature of the system. Thus, a middle ground between the complexity of the computational model and the effort needed to obtain the solution needs to be found.

The literature overview provides insight into the approaches that various authors use to obtain an accurate but at the same time usable computational model. Simplifications such as linear elastic soil behaviour, hysteric damping and no slippage between the foundations of a structure and the soil are almost universally accepted. Further, it is common to disregard secondary coupling effects, for example, by assuming that the vehicle response is not affected by a nearby building structure. The most computationally efficient formulations of the soil are usually obtained in the frequency domain, leading to multi-step solution procedures, when accounting for nonlinear excitation mechanisms. Similarly, hybrid-modelling approaches are often used, combining two or more modelling methods. Works modelling the full vibration propagation path including the source of vibration and the receiving structure are quite rare, especially for railway excitation cases.

A single best overall approach for predicting environmental vibrations does not exist. Three-dimensional FE models could most likely be used to model all the described cases, including the soil and the structures interacting with it. However, FE models are limited by quickly increasing computational times with increasing domain size. Thus, more specialized, but more efficient, models are used, depending on the analysed case. The disadvantage of that is the difficulty of combining these approaches into a single large model.

The work done during the thesis focuses on the semi-analytical modelling approach, used by Sheng et al. [146,147] for railway vibration prediction and by Andersen and Clausen [49] for modelling rigid footings. The modelling approach capabilities and applications for modelling various cases, described in the literature review, are investigated. The model is applied for modelling rigid and piled foundations, coupled to FE structures, transformed into the time domain using LPMs and finally utilized for modelling the full vibration propagation path from a passing train to a building structure. The approach could be a promising solution

procedure, allowing modelling various structures interacting with the soil using one unified approach.

3.2 Objectives of the thesis

With onset in the literature review, the hypothesis of the thesis is as follows:

> *"Applying a semi-analytic ground model coupled with a structural finite-element model, the ground-borne vibration in a building placed within an urban environment can be estimated with an adequate accuracy but also with a reasonable computational effort".*

The main objective is therefore to create numerical models for environmental vibration prediction, with emphasis on computational efficiency. The created computational models should be able to account for the full vibration propagation path starting at the source of the vibrations, propagating through the soil, and entering the building structure through its foundations. It should, if necessary, account for the back coupling, for example, from the building to the soil. Additionally, the work should be applicable to a wide range of application cases and not be limited to narrow, specific applications. In particular, the vibration propagating through soil is of interest, with most of the effort focused on modelling the soil medium and the dynamic structure–soil interaction. Analysis is limited to measurable excitation of structures, without considering the human response to vibrations.

The work done during the thesis is split into three groups, analysing railway bridges, dynamic soil–structure interaction and railway vibrations. The semi-analytical ground model is used throughout the whole work. However, each group deals with unique issues that arise due to the specifics of the considered problem. The publications written for each group are given is Section 5. Additionally, the developed computational model is included as part of the thesis, and a brief description of it given in Section 4.

4 Computational model

Short description of developed computational model covering its capabilities, requirements and file structure. An example case is provided, demonstrating the structure of the input files and the resulting system.

4.1 Description of the computational model

As part of the PhD thesis, an in-house computational model for environmental vibration prediction was developed. The model can be used to model dynamic soil behaviour and structures interacting with the soil, including coupling through the soil. The results are obtained in the frequency–space domain, in a fixed frame of reference. The computational model is intended as an open-access software, freely available for download and use. It was developed during the course of the project and encompasses cases investigated in Papers S1–S5.

The model utilizes the Thomson-Haskell [29,30] transfer matrix with the stabilization technique proposed by Wang [41]. For thick layers and high frequencies, the model also automatically detects exponential terms exceeding the limits of double precision floating-point numbers and divides the effected layers. The flexibility approach is used, assembling the system by multiplying matrices of the dimension six by six. A fixed frame of reference is considered, where the polar symmetry of the Green's function in frequency–wavenumber domain is utilized, requiring discretization only along a single wavenumber dimension. Optionally, the polar symmetry of the solution in the frequency–space domain can be utilized. In that case, the results are pre-calculated at a number of spatial positions, from which the results at exact positions are determined by interpolation. This way, the computational cost is reduced significantly, without significant loss of precision.

The calculations relating to the semi-analytical model are performed in an executable file, which is programmed using FORTRAN and compiled with the Intel® Fortran Compiler. The code is specifically optimized for parallel calculations using multi-core CPUs. The user can choose to either run separate frequencies or separate wavenumbers, inside a single frequency, as parallel calculations. This way, the computational load can be adjusted according to the analysed case. The input for the executable file can be written directly into an ascii text file with the extension '.txt.', which is read by the executable. The user can choose to either directly export the dynamic flexibility matrix of the soil, or to take its inverse and output the stiffness matrix. The output files are saved as binary files with the extension '.dat', allowing them to be imported efficiently into other software. The FORTRAN part of the code does not perform the calculations to determine the system displacements. It is only used to discretize the system and obtain the matrices governing the system behaviour, which are then used to solve the system directly or couple it to external structures.

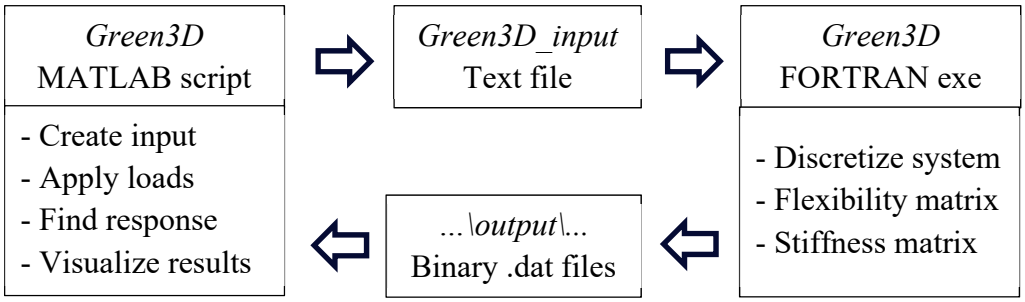

Figure 4.1. Workflow chart of the computational model.

An accompanying MATLAB script is also included. It loads the output files from the executable, applies the user prescribed loads and obtains the system displacements. Additionally, the script offers an alternative way to input parameters into the FORTRAN part of the code, run the code, and display the obtained results, all included into a single script file. The MATLAB script generally follows the same input structure as the text file read by the FORTRAN executable. The flowchart showing the interaction between the two parts of the code and the task they perform can be seen in Figure 4.1. The MATLAB part of the code is not necessary, as the user can directly write the input file and load the obtained results into other software. An example of the structure for the input text file is discussed in Section 4.2.

The desired geometry of the investigated problem is defined using *instances*. Each instance has an associated node, defining the position, and a profile, defining the shape and discretization. Profiles for square and circular shapes are predefined in the code and can easily be modified by the user. Properties of the profiles, such as their dimensions, discretization, placement of the master node, etc., can easily be defined. A profile is assigned one of the types:

- *flexible*—the discretization nodes of the created instance are independent and can be coupled separately to structures for analysis of soil–structure interaction;
- *rigid*—all nodes of the instance move according to the six degrees of freedom of the master node which is the only node coupled to a structure; or
- *observation*—creates an instance with nodes that can only be used to visualise the soil behaviour, i.e. no SSI can be introduced via such instances.

The observation type only reacts to the movement of instances of the other two types, and it cannot used independently. However, it provides a significant reduction in calculation time compared to flexible instances that account for SSI. If the predefined shapes are insufficient, it is possible to define a shape manually, by directly defining the coordinates of nodes used for discretization of the body. The flexible, rigid and observation types of the shape can still be used. A more detailed explanation of the input structure can be found in the user manual included in the downloadable files.

The computational model was named ‘Green3D’. The download includes a short user manual, explaining the input parameters in the MATLAB part of the code. It can be downloaded using the following link or using the QR code (requires a computer with Microsoft Windows 10 operating system):

https://drive.google.com/open?id=1a_akCbuZU1H1hX_KghWxy1drwMIb9Yuk

Additionally, the source files for coupling FE structures to the semi-analytical model are provided. The code acts as an additional layer on top of the provided Green3D code, automatically coupling external FE structures to the soil. The input structure to define the geometry and properties of the system is similar to the previous code. However, no user manual is available. Solid, shell and beam finite elements are included, which can be used independently or as parts of predefined structures. The predefined FE structures afre parametric, allowing the user to define the properties manually, and they include a simple building model, piled foundations, and a railway track. The MATLAB suite of files can be downloaded from the following link or using the QR code:

https://drive.google.com/open?id=1UndTmhjeAuRBgKCKqMQkuiKx-MRawB04

4.2 Example case

A system of two rigid blocks is investigated. Each block is a three-dimensional square with dimensions 3 m × 3 m × 1 m and is positioned, so that the top of the block is equal to the soil surface. The centre-to-centre distance between the two blocks is 8 m. The blocks are embedded inside a layered half-space of soil. The top layer is 5 m thick, with a Young’s modulus of 80 MPa and a Poisson’s ratio of 0.48. The underlying half-space has a Young’s modulus of 600 MPa and a Poisson’s ratio of 0.30. Both layers have a density of 2000 kg/m^3 and a loss factor of 0.05, used to define hysteretic damping. Additionally, the response of the surrounding soil is investigated, visualising the behaviour of a 14 m × 14 m × 2 m block, centred around the rigid blocks. The steady state response of the system at 30 Hz is investigated.

The text file given bellow has been produced with the MATLAB suite of files, and it provides the input for the computational model, analysed using the FORTRAN executable program. Comments written in italic and placed after exclamation marks provide explanations of the input structure. Alternatively, the provided code could be written directly as the input file in the same way that, for example, input files for commercial finite element programs can typically be developed via a user interface or directly as a text file.

Green3D_input.txt

```
* Identifier
     vibSurf                        ! The name of the project, used to name the output files;

* Frequencies
     30                             ! Analysed frequency;

* Settings                          ! General code settings (set to default values, if excluded);
     + LoadShape bell               ! Bell shaped load in wavenumber domain;
     + Damping hysteric             ! Hysteric damping;
     + Wavenumbers   8000           ! Total number of discrete wavenumbers;
     + aMax   10                    ! Maximum investigated wavenumber;
     + Interpolated                 ! Interpolated solution in spatial domain;
     + Radial 500                   ! Number of discrete points used for spatial interpolation;
     + ParType  local               ! Parallelization over wavenumbers inside single frequency;
     + RigidDiscretization 0.6      ! Discretization spacing parameter, see Paper S5;
     + OutStiffness  yes            ! Produces the stiffness matrix of the system;

* Nodes                             ! Defines the coordinates of the nodes used in the system;
     0.0      0.0    0.0    1       ! Numbers 1-3 (x,y,z)-coordinates; 4-assigned node number;
     4.0      0.0    0.0    2
     8.0      0.0    0.0    3

* Profile Box  rig block            ! Creates a box profile, with user given name 'rig block';
     + Rigid                        ! Defines the type of profile, in this case rigid;
     + Radius 1.5                   ! Half-length of one side for the horizontal cross-section;
     + Depth  1.0                   ! Vertical height;
     + Points  4                    ! Discretization, number of points for one radius;
     + Solid                        ! The shape is fully discretised, including the internal nodes;

* Profile Box  obs plane            ! Creates another box profile, with given name 'obs plane';
     + Observation                  ! Defines the type of profile, in this case observation;
     + Radius 7.0
     + Depth  2.0
     + Points 20
     + Hollow                       ! Outer shell of the shape discretized, excluding internal nodes;

* Soil soft clay                    ! Creates soil material profile, with user given name 'soft clay';
     + Youngs 80E+06                ! Young's modulus;
     + Poissons      0.48           ! Poisson's ratio;
     + Density       2000           ! Mass density;
     + LossFactor 0.05              ! Loss factor;

* Soil sand                         ! Creates another soil material profile, with name 'sand';
     + Youngs 600E+06
     + Poissons      0.3
     + Density       2000
     + LossFactor 0.05

* Instances                         ! Assembly of geometry, assigns nodes to created profiles
     +       1      rig block       ! Profile 'rig block' is placed at node number 1;
     +       3      rig block       ! Profile 'rig block' is also placed at node number 3;
     +       2      obs plane       ! Profile 'obs plane' is placed at node number 2;

* Stratification                    ! Assembly of soil layers, starting at the surface;
     +       soft clay     5.0     ! Soil material profile 'soft clay', with 5 m thickness;
     +       sand          0       ! Soil material profile 'sand', 0 indicates half-space.
```

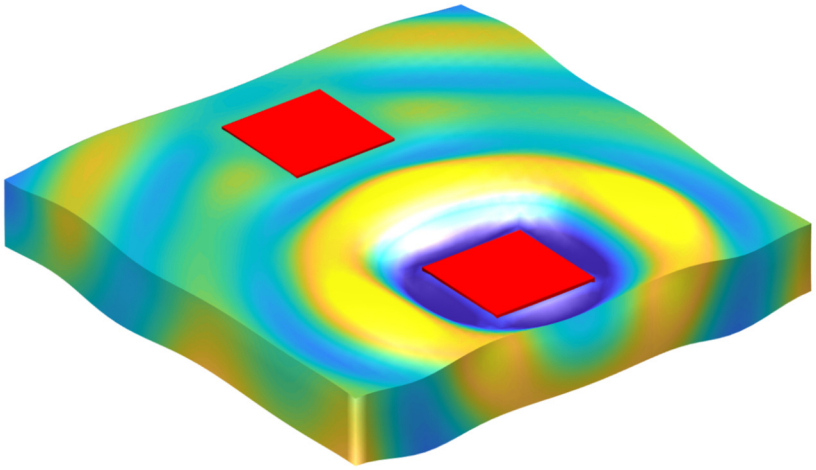

Figure 4.2. Example system created using Green3D software.

The obtained system is shown in Figure 4.2. The rigid blocks, named '*rig block*' in the input file, are coloured in red, while the shaded surfaces is the instance '*obs plane*', used for visualising the soil response. The shown system is loaded with a vertical unit load applied on the first rigid block. In this case, the system response is plotted using the included MATLAB script.

5 Summary of publications

This section provides summaries of the publications written during the course of the thesis, covering the main points from the used methodologies, the proposed novelties and the obtained conclusions. An overview of the works and their relation to each other is discussed.

The main part of the work done during the project was disseminated in ten scientific papers, including seven papers in the peer reviewed proceedings of international conferences and three papers under review for publication in high-ranking international journals. Short descriptions providing the main ideas and findings of the papers are provided in this section, with the full papers given in Part II of the thesis. As already mentioned, the papers are split into three groups, each group dealing with similar topics. The papers inside the groups are given in chronological order, with later publications incorporating the findings and new developments from the previous ones. All groups include, first, a number of conference publications and then a final journal publication. The journal publications encompass the developments of the previous works and introduce new findings; however, the conference papers include several case studies and some findings that cannot be found in the journal papers. Each paper therefore has some contributions to the thesis in its own right. At the same time, the papers in all groups have some overlap in terms of methodology and problems considered, overall dealing with similar topics.

5.1 Dynamic railway bridge excitation (Papers B1–3)

The dynamic behaviour of railway bridges due to passing trains is a complex problem, requiring consideration of multiple phenomena and the interaction between different parts of a large, intricate system. All the papers in Group B deal with a similar structural system: a multi-span elevated railway line, with rigid surface footings, placed on a layered or homogeneous half-space of soil. A sketch of the system is shown in Figure 5.1. The model includes the bridge deck and the pylons modelled using beam finite elements, a layered deck structure modelled using springs, dashpots and masses, and a multi-degree-of-freedom vehicle model. The system is excited by the traversing vehicle, including both the quasi-static and dynamic excitation forces. The dynamic excitation is due to the rail unevenness, which is accounted for by the nonlinear wheel–rail interaction forces.

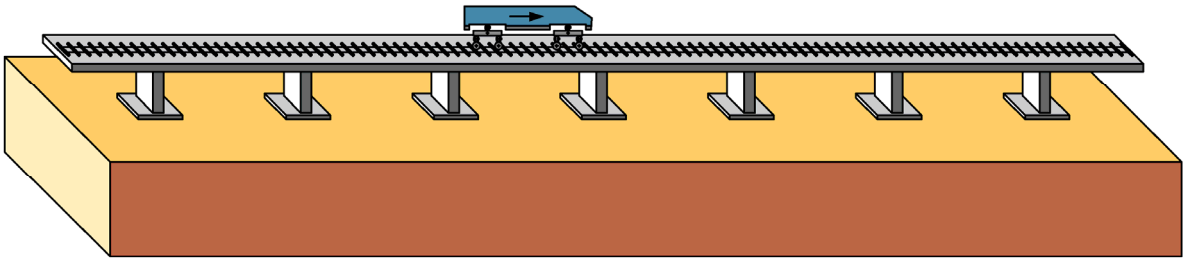

Figure 5.1. Analysed bridge structure.

The numerical model is based on a previous work by Bucinskas et al. [186], developed as part of the master thesis. The work proposed a hybrid modelling technique, where an iterative solution technique is used to combine the time and the frequency domain solutions. The same technique is also used in paper B1 and partly in paper B3.

Due to the discrete representation of the bridge structure, i.e. pylons are present with some spacing, it is not possible to utilize direction invariant computation methods based on, for example a 2.5D FE or BE approach as mentioned in Section 2.1.3. Alternatively, a periodic structure could have been analysed by using the Floquet theory. However, the methodology proposed in paper Group B is suggested to be more general as it allows the analysis of structures of any shape interacting with the soil. It is indeed not limited to the analysis of linear, periodically repeated structures, even though the papers only consider such structures in the computational examples. Additionally, including a moving multi-degree-of-freedom vehicle model into the system requires time-domain solution procedure. At the same time, the semi-analytical soil model is used, which is formulated in the frequency domain. Thus, different hybrid solution procedures are utilized, combining different modelling techniques.

5.1.1 Paper B1: Numerical modelling of ground vibration caused by elevated high-speed railway lines considering structure–soil–structure interaction

P. Bucinskas, L. V. Andersen, K. Persson.
INTER-NOISE and NOISE-CON Congress and Conference Proceedings (2016).

The paper concerns the dynamic response of a low-rise multi-span bridge structure, with particular interest in the behaviour of the foundations and the surrounding soil during the passage of a train. Several ways of accounting for the soil are introduced and compared, while analysing the effects of the vehicle speed and the soil stratification.

Key points and novelties of the paper:

- The rigid footings are modelled in two ways. The first approach accounts for structure–soil–structure interaction (SSSI), including the cross coupling of footings through the soil, while the second accounts only for the structure–soil interaction (SSI), i.e. only including the coupling of each individual footing to the soil. The more complex first model requires analysis of the full soil system interacting with the full array of rigid footings, while the simpler SSI model only requires the solution for a single footing, which is then applied to all bridge footings. Using a simpler model is beneficial due to the reduced computational cost, while the more complex model is more accurate. To the knowledge of the author, the direct comparison of the two approaches (dynamic SSSI vs. SSI) for a multi-span railway bridge is novel.
- A parametric analysis investigating the effects of the vehicle speed is performed, with some results given in Figure 5.2. It is determined that, if the vehicle approaches the R-wave speed in the soil, the vibration levels are amplified. The amplification is more prevalent if the soil is modelled as a homogeneous half-space. The effects are reduced when a layered soil cases are analysed. Similar findings are available in the literature for tracks placed directly on the ground, but the analysis of a low-rise multi-span bridge was new at the time of the study.

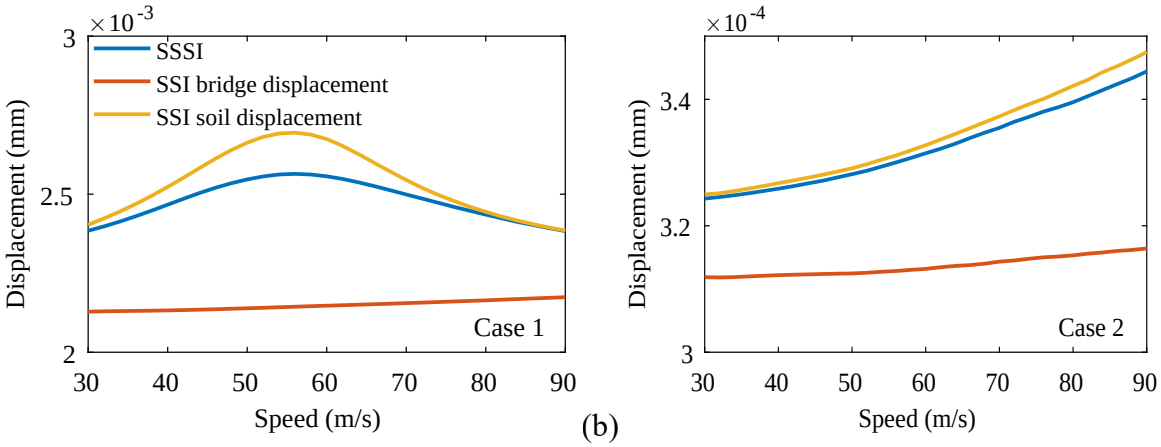

Figure 5.2. Maximum absolute bridge footing displacement dependency on vehicle speed: (a) a half-space of soft soil; (b) a layer of soft soil over a half-space of stiff soil. The figure is part of Figure 5 from Paper B1.

- A modelling approach only accounting for a single footing at a time is not able to predict the response amplification due to the critical speed, thus providing inaccurate results. However, for layered soil, the differences between the two approaches are not large. This observation may be of interest for practical design, since real soil is always stratified.
- The stress experienced by the bridge pylon was analysed for the worst loading case (half-space of soft soil with critical vehicle speed), including the vehicle model and uneven track. It was determined, that the differences between the modelling approaches are very small, i.e. for the analysis of the structure the SSI approach may suffice.
- Analysing the soil surface response further away from the bridge structure, the model including the cross coupling through the soil (the SSSI model) predicts lower vibration amplitudes for the whole analysed frequency range.

Main conclusion of the paper:

Comparing the two proposed modelling approaches, it is evident that the full model is preferable, especially when the response of the bridge footings or the surrounding soil is of interest. However, for the bridge deck response, the simpler SSI model could be successfully used without a significant loss of precision. This could be useful if simple rigid-footing-modelling approaches, which can model only a single rigid footing at a time, are utilized.

5.1.2 Paper B2: Lumped-parameter models for structure–soil interaction of multi-span railway bridges

P. Bucinskas, L. V. Andersen
Proceedings of the 30th Nordic Seminar on Computational Mechanics, NSCM-30 (2017).

The paper concerns the dynamic response of a short railway bridge structure, supported by three pylons. A time-domain solution procedure is utilized to analyse the effects of track unevenness on the structural response.

Key points and novelties of the paper:

- Consistent lumped-parameter models (LPMs) are used to approximate the soil response obtained from the semi-analytical soil model, formulated in frequency domain. Standard stiffness, mass and damping matrices are obtained, that can be used for a pure time domain solution, with non-linear wheel rail interaction. The use of LPMs for SSI and SSSI of multi-span bridges is, to the authors knowledge, novel.
- The created model is used to analyse the effects of track unevenness on the response of the structure. Randomly generated track unevenness profiles are tested with three vehicle speeds. In total, 100 unevenness profiles are tested, generating envelopes for maximum and minimum response of the system.
- The stochastic nature of rail unevenness leads to significant differences between separate realizations. The largest differences between the maximum and minimum response are observed in the frequency range up to 100 Hz. At the same time, the effects due to vehicle wheels passing over sleepers and the quasi-static loads produce distinct peaks with little scatter of data.

Main conclusion of the paper:

For the analysed case, consistent LPMs work well to recreate the system response in time domain, including the foundation coupling through soil. The obtained system is computationally efficient and can be used to run crude Monte-Carlo simulations. Further, the pure time-domain solution is more efficient and with better convergence compared to the hybrid approach used in Paper B1.

5.1.3 Paper B3: Dynamic response of vehicle–bridge–soil system using lumped-parameter models for structure–soil interaction

P. Bucinskas, L. V. Andersen
Under review in Computers and Structures, initial submission 2019 April 30, revised and resubmitted after first review 2019 September 18.

The paper concerns the modelling of a multi-span railway bridge structure in time domain using consistent LPMs. The paper provides a detailed description of the modelling approaches, solution procedures, polynomial fraction function fitting for LPMs, and problems that can be encountered when modelling such systems.

Key points and novelties of the paper:

- The hybrid solution procedure, from Paper B1, is compared to a pure time-domain solution using consistent LPMs. For the analysed case, the hybrid solution procedure requires additional filtering to obtain a converging solution. For the considered structure, track and vehicle, filtering for frequencies above 70 Hz is needed, making the results beyond that limit inaccurate. Thus, a pure time-domain solution using LPMs is preferable, when high-frequency vibration is of interest.
- Cross-coupling terms up to three footings away have a significant effect on the system response and should thus be represented by LPMs. This is especially important for higher-frequency response. Meanwhile, the low-frequency response, up to 15 Hz, can be recreated

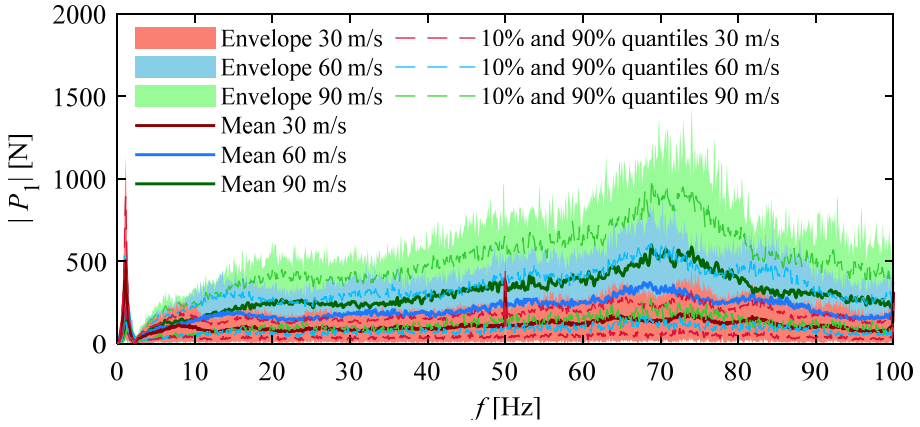

Figure 5.3. Fourier coefficients of wheel-rail interaction force. The figure is an unmodified version of Figure 13 from Paper B3.

by modelling only the direct terms (diagonal terms of the dynamic stiffness matrix). The systematic study of the importance of cross coupling between pylons via the soil is, the knowledge of the author, novel.

- The analysed frequency range up to 100 Hz requires a high-order polynomial-fraction function to properly match the variation observed in the frequency-dependent dynamic stiffness of the footing–soil system. The cross-coupling terms between two footings, separated by multiple footings in-between, are especially difficult to recreate using LPMs. In some cases, polynomial orders exceeding 50 are required. Nonetheless, such high-order LPMs were successfully calibrated, which may be novelty of the paper. Usually, in the literature, LPMs of much lower orders are used, and the experience of the author is that the same type of instability issues will not occur in such cases.
- The high-order, multi-degree-of-freedom LPMs can have numerical stability issues, even if the standard constraints of negative real parts for the poles are enforced. An LPM fitting procedure is intruded to obtain stable models. The procedure uses three test conditions to eliminate the numerically unstable LPMs. This procedure can be considered novel.
- The effects of the stochastic track unevenness are investigated by analysing 100 track profiles. Compared to Paper B2, the track properties and the power-spectral density (PSD) functions for the unevenness are changed, leading to different system response. The analysis is carried out for the wheel–rail interaction forces and for the accelerations of the deck and one footing. The obtained wheel–rail interaction forces are shown in Figure 5.2. The figure shows overall increasing interaction forces with increasing vehicle speed, also the distinct peaks caused by the vehicle weight at very low frequencies, and a peak at 50 Hz due to the wheel passing over sleepers.

Main conclusion of the paper:

Using consistent LPMs to recreate complex system behaviour with multiple cross couplings through a wide frequency range is possible. However, some numerical stability issues are encountered, requiring additional consideration. In those cases, the proposed fitting procedure should be followed.

5.2 Dynamic soil–structure interaction using the semi-analytical approach for modelling a layered ground (Papers S1–5)

Papers in this group deal with dynamic SSI modelling and vibration propagation through soil. The semi-analytical soil model based on the Thomson-Haskell transfer matrix [29,30] is employed, with Papers S3–S5 utilizing an additional stabilization technique [41] to avoid precision errors in the computer implementation. The computational model described in Section 4 was developed together with the papers in this group.

The capabilities of the model are explored for modelling various structures, such as rigid blocks, piles and tunnels. All papers deal with the system in the frequency domain, excited by fixed harmonic forces. Beam, shell and solid finite elements are used to model external structures coupled to the soil, with the coupling between the two approaches achieved through so-called SSI nodes. This modelling approach is beneficial, as the soil can be modelled efficiently using the semi-analytical approach, while complex structural geometries can be modelled using the finite-element method (FEM).

Computational efficiency is key; thus, the efforts are concentrated on finding the optimum numerical approaches. One of the papers investigates the use of surrogate models as an alternative approach. However, the surrogate model is still calibrated according to data obtained from the semi-analytical model.

5.2.1 Paper S1: Semi-analytical approach to modelling the dynamic behaviour of soil excited by embedded foundations

P. Bucinskas, L. V. Andersen
X International Conference on Structural Dynamics, EURODYN 2017.

The paper analyses the behaviour of two types of foundations: rigid footings and piles. The semi-analytical soil model is used with a derived formulation for embedded source and receiver positions. A procedure for the coupling of finite elements to the semi-analytical soil model is introduced.

Key points and novelties of the paper:

- The proposed approach to modelling rigid footings is validated by comparison with an FE model. The same surface footing is modelled as a completely rigid plate and as an FE shell model that is then coupled to the soil. It is determined that the differences between the two approaches are small for all analysed soil stratifications and loading cases, indicating that the assumption of rigid footings, usually made for engineering design, is acceptable.
- Pile modelling using the semi-analytical approach is investigated. The piles are modelled as beams by the FEM and coupled to the soil in three different ways. Firstly, the embedded FE nodes are directly coupled to the corresponding SSI nodes. In this case, only the translational degrees of freedom are coupled to the soil. Two other approaches use rigid discs or rigid rings (the two approaches are illustrated in Figure 5.4), with the diameter of the pile, which are then coupled to the nodes of the FE pile. This way, the rotational degrees of freedom of the pile are also coupled to the soil.

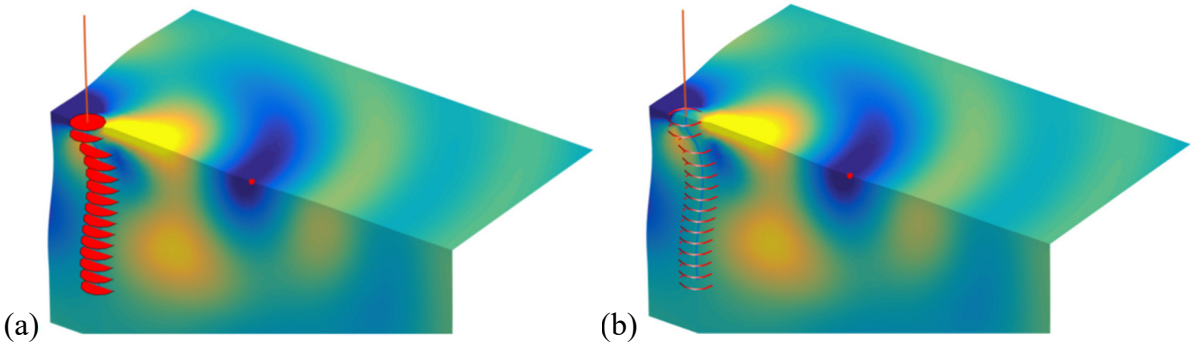

Figure 5.4. Pile modelled with: (a) rigid disks and (b) rings. The system is excited at 45 Hz. The figure is an unmodified version of Figure 4 from Paper S1.

- Comparison between the three pile modelling approaches is performed by modelling a single pile, loaded by unit moment. As expected, the modelling approach without rigid objects underestimates the stiffness of the system, due to the lack of rotational stiffness in the pile. The other two approaches show very similar results, with the best approach dependent on the considered pile type~~.~~ For example, large diameter monopiles are better represented with rigid rings, while small diameter drilled piles are better represented with rigid disks.

Main conclusion of the paper:

The paper introduces an early version of the coupled semi-analytical and FE model, which is further developed in the subsequent publications of paper Group S. Overall, the used computational model is efficient and can be used for a wide range of application cases. The proposed novel pile modelling method is promising, as it is easy to implement into existing semi-analytical models and it is not limited by the number or configuration of piles. The modelling approach for rigid footings and the proposed pile modelling with rigid discs is further investigated and developed in Paper S5.

5.2.2 Paper S2: Excitation of structures near railway tracks—analysis of the wave propagation path

P. Bucinskas, L. V. Andersen,
Proceedings of the 6th International Conference on Computational Methods in Structural Dynamics and Earthquake Engineering, COMPDYN 2017.

The work concerns the ground vibration propagation path and the effects of additional structures placed within the propagation path. Embedded structures and structures placed on the ground surface, commonly encountered within an urban environment, are investigated. The source of vibration is a railway track, and the receiver is a rigid surface footing placed at some distance from the source, with additional structures placed in between the two.

Key points and novelties of the paper:

- A three-dimensional railway track model is constructed. FE beams are used to model the rails, while FE shells model the embankment. The embankment is a structure with considerable thickness. The effects of the thickness are accounted for by introducing an

offset between the reference plane for the embankment structure and the ground surface. Rigid links between the two parts of the model are established using Lagrange multipliers.

- Several different cases are analysed: a rigid block embedded within the soil, a single-lane road on the surface parallel to the track, and a concrete pipe embedded inside the soil, with various orientations relative to the railway track. The cases are compared to a free-field case, i.e. a case with no structures present within the wave propagation path.
- In most cases, the additional structures mitigate the vibrations, with the largest effects observed in the 7–30 Hz frequency range. However, in some cases the vibration levels are increased in the 30–40 Hz range for the considered soil and source conditions.
- The orientation relative to the wave propagation front is extremely important for elongated structures (the surface road and the buried pipe). Structures placed parallel to the railway track have little effect, whereas structures orthogonal to the track provide strong mitigation of the ground vibration compared to the reference case.

Main conclusion of the paper:

Structures placed within the ground vibration propagation path can have significant effect on the system behaviour. They mostly act as vibration dissipaters, in some extreme cases leading to 70 % vibration reduction. However, some amplification effects have been also observed, shifting the system response to higher, otherwise unpredicted, frequencies. Thus, when analysing environmental vibration in urban environments, it might be necessary to account for these effects, requiring computational models accounting for the full vibration propagation path and any major obstacles placed within it, whether these obstacles are placed on the ground or buried within the soil. In practise, this is rarely performed, in part due to the limitations of the used environmental vibration prediction tools.

5.2.3 Paper S3: Dynamic soil excitation from railway tunnels

P. Bucinskas, L. V. Andersen
Proceedings of the 9th European Conference on Numerical Methods in Geotechnical Engineering, NUMGE 2018.

The paper investigates the possibility of using the semi-analytical modelling approach combined with the FEM to model tunnels embedded within the soil. Tunnel structures are difficult to model, as it involves a cavity inside the soil, which cannot be represented using the semi-analytical model directly. Thus, a sub-structuring solution procedure is introduced.

Key points and novelties of the paper:

- A sub-structuring approach is proposed, in which the cavity is modelled using solid finite elements with negative material properties. This way, a continuous soil is modelled using the semi-analytical approach and only the cavity is discretized with the FEM. In the modelled case, additional stiffness is added to model the tunnel lining.
- A cut-and-cover tunnel is modelled using the proposed methodology. The results are compared with simplified versions of the model: only the tunnel lining is modelled using shell elements; the tunnel lining is modelled as a single FE beam; or no tunnel model is included the system at all.

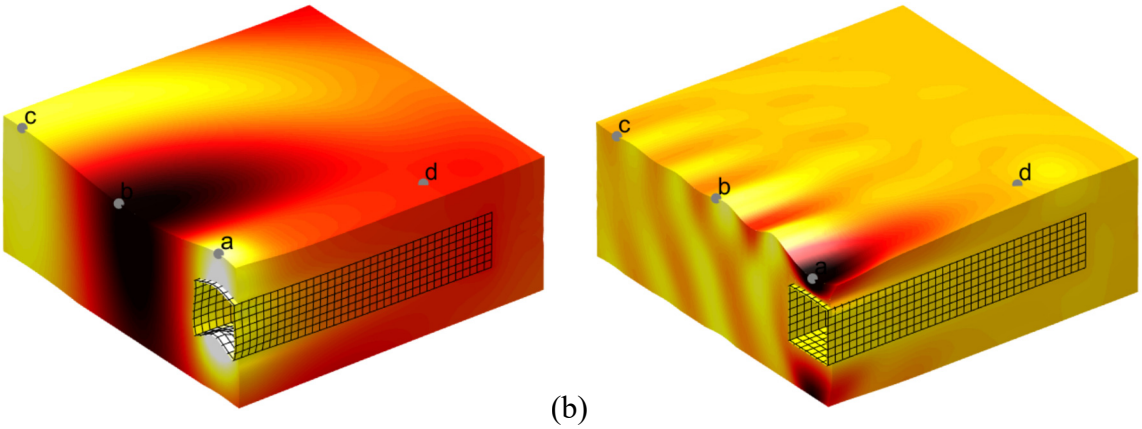

(a) (b)

Figure 5.5. Created tunnel model including a cavity. Response at (a) 10 Hz; (b) 50 Hz. Parts of the figure are taken from Figures 5 and 6 in Paper S3.

- The vibrations produced by a unit-magnitude time-harmonic load applied on the tunnel floor are observed on the soil surface. The created system and its response are shown in Figure 5.5. When the tunnel lining is present, the comparison between the different models indicates that the cavity does not significantly influence the soil surface response, especially further away from the tunnel. However, the cavity is important if the dynamic response of the tunnel structure itself is in focus.
- A simple beam model is not suitable for modelling the tunnel structure. The obtained response is completely different compared to the full model. Modelling only the soil with no tunnel present at all produces better matching results. It should be noted, that the used beam model only couples the translational degrees of freedom to the soil, and could potentially be improved by modelling the SSI differently, for example using rigid surfaces as in paper S1.

Main conclusion of the paper:

The proposed sub-structuring approach, subtracting the stiffness of the removed material, can successfully be used to model cavities inside the soil. However, care should be taken to properly discretize the system. Thus, differences between the dynamic stiffness obtained from the semi-analytical and that obtained with the FE models can lead to unphysical waves propagating in the system. The method is further developed and validated in Paper S5.

5.2.4 Paper S4: Dynamic structure response using surrogate models

P. Bucinskas, L. V. Andersen
Proceedings of the 7th International Conference on Structural Engineering, Mechanics and Computation, SEMC 2019.

The usage of surrogate models for environmental vibration prediction inside buildings is investigated. Calibration and application of surrogate models for this purpose could be a useful solution method, due to the ability of the methodology to provide almost instantaneous results. However, high-quality data, based on a "truth model", are needed to train the surrogate model, which can be obtained both experimentally and numerically. In this paper, the surrogate model is trained using data from a coupled semi-analytical and FE model.

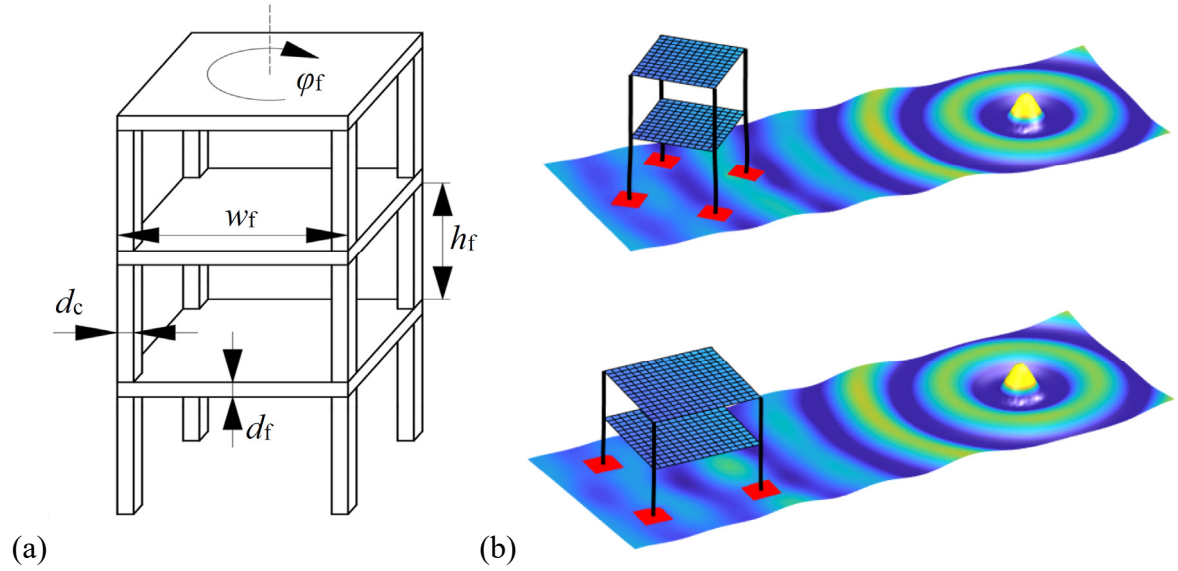

Figure 5.6. Truth model used for calibration of the surrogate models: (a) Varying geometry parameters of the building; (b) examples of randomly generated structures. Parts of the figure are taken from Figures 1 and 2 in Paper S4.

Key points and novelties of the paper:

- A parametric building structure is created, with five parameters describing the geometry. These parameters are used for development of the surrogate model. The structure and the parameters are shown in Figure 5.6. The system is excited by a unit-magnitude vertical time-harmonic load placed on the ground surface, placed at some distance away from the structure. The response of the top floor in the building is investigated.
- The Kriging method is used to create the surrogate model. Surrogate models can only represent a single output value from given input parameters, i.e. a single quantity of interest (QoI). Thus, the root-mean-square value of the top floor node displacement amplitudes is chosen as the representative system response. Analysis is performed in the one-third octave bands, creating a separate surrogate model, i.e. a separate QoI, for each band.
- A sampling plan was created using Latin hypercube sampling, by which the computational model generated the truth model data set. It was determined that 300 data points are needed to obtain a reasonably accurate surrogate model, using a direct fitting method.
- The relative importance of the considered parameters can be evaluated using the Kriging method. It has been determined that the importance of parameters vary through the analysed one-third octave bands. For example, the orientation of the building, given by the parameter φ_f, is important for high frequencies, but not for low frequencies.

Main conclusion of the paper:

Overall, using surrogate models is a viable approach for environmental vibration prediction. However, the method is limited by only one output value and some difficulties with properly calibrating the model. Further, the computational efficiency quickly decreases with increasing number of varying parameters, making the method unsuitable for problems with many design

variables, at least in the present version of the methodology. Future studies could investigate using more advanced machine learning approaches, such as neural networks, which can handle large amounts of input parameters and can predict multiple output values.

5.2.5 Paper S5: Semi-analytical model of soil interacting dynamically with rigid blocks, cavities and piles

P. Bucinskas, L. V. Andersen
Under review in Computers and Geotechnics, initial submission 2019 October 11.

The paper investigates the semi-analytical modelling approach in more detail. Descriptions of modelling three-dimensional rigid blocks, piles and cavities inside the soil are given. The semi-analytical model is validated by a direct comparison with FE and BE methods. Radiation at the artificial boundaries of the FE models is provided, partially, by simple impedance boundary conditions (FE–IBC model), or the FE model is extended by a PML (FE–PML model). The FE–PML model is considered as the most accurate approach, providing the basis to which other methods are compared.

Key points and novelties of the paper:

- Discretization of three-dimensional rigid blocks is discussed in detail. A heuristically obtained discretization parameter is introduced. By using the optimal value of this parameter, extremely accurate results can be obtained with a low computational cost. The optimal value of the parameter has been found to be independent of the discretized shape, and the methodology works well in the entire considered frequency range.
- The proposed rigid block modelling approach is compared to BE–FE, FE–IBC and FE–PML models. The comparison shows very good agreement between the semi-analytical and FE–PML models, while the other methods show some deviation at low frequencies, which can be attributed to partial reflection of waves at the artificial boundaries.
- A pile-modelling approach using rigid discs, as presented in paper S1, is investigated. The semi-analytical model is compared with FE–IBC and FE–PML models. The proposed pile model agrees well with the FE–PML model, especially for vertical loading. Small differences are observed for lateral loading cases, most likely caused by the way in which the interaction forces are represented in the semi-analytical model, i.e. as loads distributed over horizontal areas rather than the vertically oriented surface of the pile–soil interface.
- The cavity modelling approach is investigated, as introduced in Paper S3. In this case, only the cavity is modelled, with no additional stiffness from a tunnel lining, sheet piles or similar structural elements. The model is compared to the FE–IBC and FE–PML models. Again, good agreement is obtained between the semi-analytical approach and the FE–PML model. Selected results obtained with the two approaches can be seen in Figure 5.7. In terms of precision, some issues were observed using the semi-analytical model, caused by the discretization of the cavity. However, the issues are very limited and even then, the semi-analytical model performs better then FE–IBC model which suffers from partial reflection of waves at the artificial boundaries.

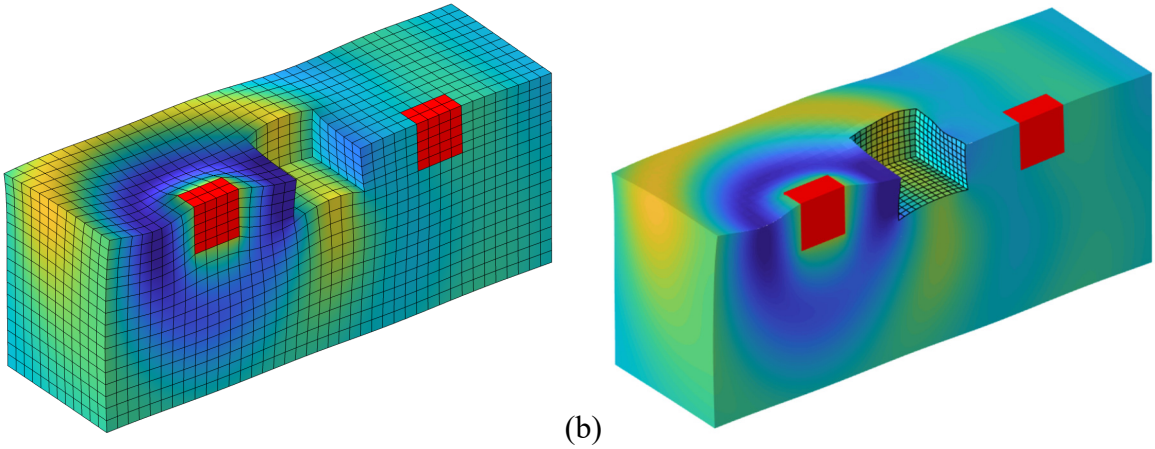

(a) (b)

Figure 5.7. Field response at 30 Hz for two rigid, embedded blocks and with a cavity (an open pit) placed in the middle: (a) FEM-PML model; (b) semi-analytical model. The figure is part of Figure 8 in Paper S5.

Main conclusion of the paper:

The analysis demonstrates that the semi-analytical model is as accurate as the FE–PML model, while requiring much smaller computational effort. Thus, it is a viable alternative to more complex modelling approaches when dynamic SSI is considered. Further, the semi-analytical method combined with the FEM provides a flexible modelling approach, with a wide range of application cases. Additionally, the coupling procedure between approaches is straightforward and does not require any changes to the FE part, making it possible to use commercial FE software.

5.3 Railway vibration modelling

Papers in this group are primarily concerned with surface railway vibration modelling, considering the effects of the moving load associate with a train. Differently from Papers B1–B3, only frequency-domain solution procedures are used to analyse the system. This way the semi-analytical soil modelling approach can be used directly without iterative solution procedures or LPMs.

Further, the intent is to model the full vibration propagation path starting at the moving vehicle and ending inside a building structure. The developed model is also be able to model all the cases described in Papers S1–S5.

5.3.1 Paper R1: Effects of railway track modelling to surrounding soil and structure excitation

P. Bucinskas, L. V. Andersen,
25th International Congress on Sound and Vibration, ICSV 2018.

The paper investigates several railway track modelling approaches and their effects on the observed vibrations. A surface railway line is investigated, with a ballast-less track structure. The whole system is formulated in a stationary frame of reference. The paper still uses the computational model from papers S1–S5, just this time a moving load is introduced.

Key points and novelties of the paper:

- The railway track is modelled using three levels of simplification. The simplest model represents the whole track structure as a single beam coupled to the semi-analytical soil model. Only the translational degrees of freedom are coupled to the soil and the load from each node of the beam is distributed in a circular shape. The second model represents the track slab using a shell, with each rail modelled as a beam. The third and most complex model utilizes three-dimensional solid finite elements to model the track slab, with beam elements for the two rails. It should be noted that the three models have been made to provide, as closely as possible, similar descriptions in terms of the geometry and materials of the track system. Hence, the differences lie mainly in the kinematic constraints implied by the respective approaches.
- The track models are investigated using a stationary time-harmonic unit load, with the response observed in the free-field and in a building structure. It is determined that the beam model is not able to predict the system response accurately, while the other models show very good agreement.
- The computational times required for the solution are compared. The plate model takes around 30 % less time to compute, compared to the solid model. The beam model is almost 80 % faster, but it cannot be used due to the inaccurate results. As in Paper S2, the beam model could likely be improved by using a more advanced SSI coupling approach.
- The three track models are investigated using a constant load moving across the railway track. The system is still modelled in a stationary frame of reference, with forward and inverse Fourier transformation applied to allow a solution in the frequency domain. A comparison between the three models provided similar results as with the stationary load. The beam model results are inaccurate, while the other models agree well.

Main conclusion of the paper:

The shell model can be used, successfully, for environmental vibration prediction, reducing the computational times significantly. However, it is rather difficult to model the moving load in a stationary frame of reference, as the artificial ends of the FE track model can reflect the waves back into the system, especially in cases where the track and embankment are stiff compared to the underlying soil. Further, it is not possible to implement multi-body vehicles into the solution procedure, to account for the dynamic vehicle loads. Therefore, more advanced models are needed.

5.3.2 Paper R2: Modelling train-induced vibration of structures using a mixed-frame-of-reference approach

P. Bucinskas, E. Ntotsios, D. J. Thompson and L. V. Andersen,
Under review in Journal of Sound and Vibration, initial submission 2019 September 17.

The paper proposes a novel computational method for modelling the full vibration propagation path from a vehicle traversing a railway track to a building structure. The semi-analytical approach is utilized in both fixed and moving frames of reference, with additional coupling terms derived between the two frames of reference.

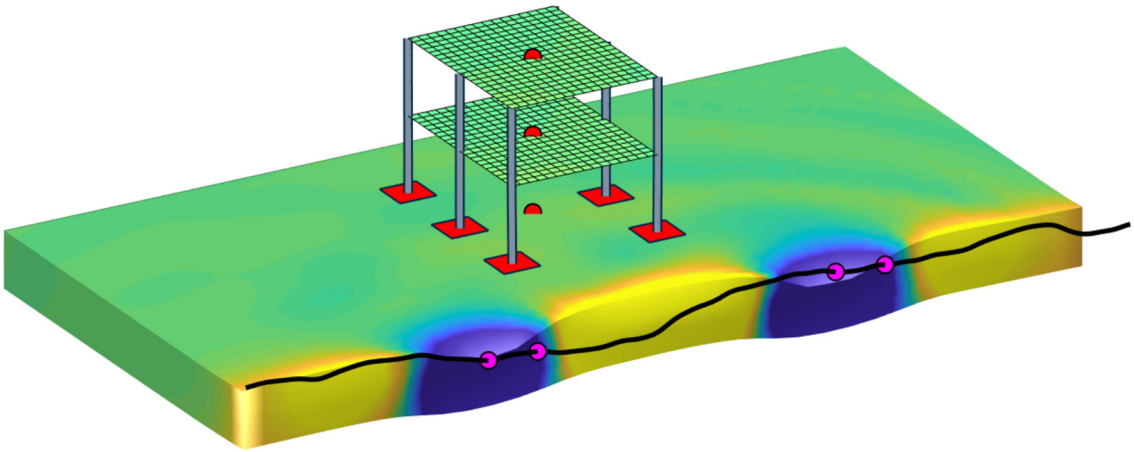

Figure 5.8. Investigated example case using partial coupling solution technique. The figure is an unmodified version of Figure 8 from Paper R2.

Key points and novelties of the paper:

- An analytical track model is utilized as previously described by Sheng et al. [147]. The railway track is modelled in a moving frame of reference, where it is assumed to be infinite. A multi-body vehicle model is coupled to the railway track, with linearized wheel–rail interaction forces that account for the track unevenness.
- Other structures interacting with the soil are modelled in a stationary frame of reference. The structures are introduced a FE structures interacting with the soil via SSI nodes. Any of the previously described methods (Papers S1–S5) can be used to model the structures.
- The full system is assembled in frequency–space domain, combining both moving and fixed frames of reference. Two system interaction techniques are introduced: partial coupling and full coupling. Both techniques allow for a one-step solution procedure for solving the full vibration propagation path.
- The partial coupling technique disregards some of the secondary coupling effects but offers a more efficient calculation. It does not include the frequency-spreading, caused by the Doppler effect, that occurs when waves emanating from a source in one frame of reference are re-scattered by objects in the other frame of reference and then observed again within the first frame of reference.
- The full coupling technique does not disregard any coupling in the system. It is useful for solving systems where back-coupling between the vehicle and the structures in or on the soil is important. However, in this method the system matrices become extremely large, making the method less attractive for problems with many degrees of freedom.
- The capabilities of the proposed model were illustrated with two example cases—one for each coupling technique. A building model with rigid surface footings was modelled using the partial coupling technique, examining the response of the building floors and the ground surface. The created system is shown in Figure 5.8.
- A rigid plate embedded in the soil underneath the rail track was investigated using the full coupling technique. The response of the rigid plate as well as the vehicle was analysed. The track unevenness was not included in the system. Hence, only the effect of parametric

excitation associated with the variation in equivalent subgrade stiffness, caused by the presence of the rigid footing, introduced dynamic loads on the track and the vehicle.

Main conclusion of the paper:

The created computational models offer an interesting solution technique allowing a one-step solution procedure for the whole environmental vibration propagation path. It is easily applicable to a wide range of cases, as adding finite elements is possible in both the moving and the fixed frames of reference with the limitation that objects in the moving frame of reference can, at the present time, only be placed on top of the ground. Embedment is only available in the fixed frame of reference.

6 Conclusion and future work

In this chapter, the main findings and novelties of the thesis are summarised, and the final conclusions are listed. Also, a few proposals for future work are given.

6.1 Main findings of the thesis

The thesis investigated environmental vibrations in an urban environment. As it has been shown, there are a number of international and national standards defining the acceptable vibration limits. However, predicting these effects without in-situ measurements is difficult, and on-site measurements can often be difficult and expensive to perform. Thus, a considerable research effort is concentrated on creating computational tools that can estimate the vibration levels. The literature review showed that there is a multitude of empirical, analytical and numerical methods available for this purpose. Different approaches have different advantages and disadvantages, with, perhaps an unsurprising, overall trend of more precision leading to larger computational difficulty. Unfortunately, the more advanced models, capable of modelling the cases commonly found in the urban environment, are extremely computationally demanding, making their usage rather limited—especially within the early design stages. Thus, the project aimed to investigate using approaches that are in-between the very simple analytical and the extremely complex numerical models.

The work dealt with computational modelling of environmental vibrations, with particular interest in wave propagation through the soil. For that purpose, a variety of computational models were created. These models were used to produce the results presented in ten papers that form the main body of the thesis. As part of the scope of the thesis, the overall aims were defined for the final computational models: computational efficiency (to a reasonable degree), wide application range, and the ability to model the full vibration propagation path. A semi-analytical soil modelling approach based on the Thomson-Haskell transfer matrix was chosen to achieve these aims. The method is advantageous as it automatically ensures radiation into the semi-infinite soil domain, solving one of the biggest difficulties in dynamic soil modelling. Further, the semi-analytical formulation is well suited for modern day computers, as it is easy to parallelize the calculations, and discretization of the full domain is not needed, reducing the required computer memory. However, as determined in the literature review, the original method was rather limited in terms of utilization range and usually constrained to narrow application ranges. Thus, this work aimed to expand the application range of the semi-analytical soil modelling approach and investigate its application to various modelling cases.

Three groups of papers were defined, each dealing with a specific topic: railway bridge excitation (Papers B1–B3), dynamic soil–structure interaction (Papers S1–S5), and railway vibration (Papers R1-R2). However, the overall topic through all of the papers is dynamic SSI and the application of the semi-analytical soil model to the investigated cases.

Papers B1–B3 investigated dynamic railway bridge behaviour, including SSI and non-linear wheel–rail interaction forces. Modelling a finite bridge system is a difficult problem, as a lot of existing numerical methods for surface railways require a frequency-domain solution or assume invariant system geometry along one direction, and, thus, are not applicable to this case. The application of the semi-analytical soil model is difficult too, as it is also formulated in the frequency domain. The frequency-domain solution cannot be used, since the moving vehicle model requires a time-domain solution, due to the changing vehicle position in relation to the bridge and the nonlinear wheel–rail interaction forces. Two solution procedures were investigated, with particular interest in using consistent lumped-parameter models (LPMs) to convert the frequency-domain soil behaviour into the time domain. I was found that, to cover the desired frequency range, extremely high-order polynomial fraction functions were needed, leading to some unexpected numerical stability issues. A novel LPM fitting procedure was introduced, using which the numerical issues can be avoided. The created model was used to run a large number of cases analysing the effects of stochastic rail unevenness, while, at the same time, demonstrating that the obtained model is computationally efficient and can be used for analysing a large number of cases.

Papers S1–S5 investigated using the semi-analytical soil model to analyse dynamic SSI and for modelling the full vibration propagation path from the source to the receiver. The investigated cases were limited to a fixed frame of reference and the frequency domain. Modelling of rigid footings, piled foundations and various FE structures interacting with the soil was investigated, with the coupling between structures and soil achieved through SSI nodes. Modelling of rigid foundations on the soil surface and embedded within the soil was investigated, and a novel discretization technique was proposed. Similarly, a modelling technique was introduced for modelling piled foundations, modelling the pile using beam finite elements coupled to the soil through rigid cross sections. The coupled semi-analytical and FE model was also used to analyse cavities inside the soil. This was achieved by subtracting the dynamic stiffness of the removed material from the dynamic stiffness determined for the soil by utilization of the semi-analytical solution. The flexibility of the created computational model was utilized to compare different modelling approaches, with increasing degree of simplification, of the same structure as shown in Papers S1, S3 and R1. This way, the most computationally efficient and, at the same time, sufficiently accurate modelling approaches were identified for modelling piles, tunnels and surface railway tracks.

The proposed modelling approaches were validated by comparison with other numerical methods in Paper S5. A very good agreement was obtained between the semi-analytical approach and an FE model with transmitting boundaries achieved by using a perfectly matched layer (PML), indicating the high accuracy of the created computational model. At the same time, the semi-analytical model was able to analyse the system significantly faster than the other investigated approaches. For the investigated cases, the largest difficulty of modelling structures interacting with the soil was the appropriate modelling of the SSI nodes. The difficulties are mainly caused by the differences between the FEM and the semi-analytical method. For a computationally efficient solution, the semi-analytical model uses distributed load with polar symmetry, which does not replicate the weight functions used in a typical FE solution. Thus, some discrepancies for the obtained stiffness appear between the two solutions.

This is especially evident when modelling cavities inside the soil, as shown in Papers S3 and S5, where a finely discretized mesh was needed to obtain a reliable solution. Proper modelling of the SSI nodes was investigated in Paper S5, introducing discretization and load distribution methods required for an accurate solution.

An alternative approach, using a surrogate model, was investigated in Paper S4. Here, a simple model is created to directly model the results, instead of recreating the physics of a real system, allowing for almost instantaneous results. To calibrate the surrogate model an initial set of real data is needed, which was created with the semi-analytical soil model coupled to FE structures. The computational model is well suited for this application, due to its efficiency, allowing the creation of large data sets quickly, that are then used to test different surrogate modelling approaches. The surrogate model itself proved to be a viable approach for making quick predictions. However, the investigated approach is somewhat limited.

One of the main environmental vibration sources is railways. Thus, Papers R1–R2 dealt with surface railway lines. Paper R1 investigated a surface railway line using the same semi-analytical model as in Papers S1–S5, modelling the system in a fixed frame of reference with a moving load. However, it was quickly apparent that such a model is not well suited for the analysed case, as only railway tracks of finite lengths can be modelled, and a multi-degree of freedom vehicle model cannot be included. A moving-frame-of-reference solution would solve these issues. However, in that case a finite building structure could not be modelled. Thus, Paper R2 introduced a novel numerical approach coupling the fixed and moving frames of reference. This way, the vehicle and the track can be modelled in a moving frame of reference, while the nearby structures are modelled in a fixed frame of reference. The approach models the full vibration propagation path from a moving source to the receiving structures using a single-step solution procedure. Moreover, the model is not limited to one-way coupling and could be used to model the effects on the moving vehicle from a load applied on a stationary building structure. Two solution procedures accounting for the either the full or partial coupling were introduced, and their capabilities were demonstrated in example cases.

Overall, the thesis expanded the application range of the semi-analytical method by proposing novel foundation modelling approaches, investigating the proper discretization approaches, and proposing new numerical methods utilizing the semi-analytical model. Additionally, an open-access computational model was created during the course of the project, and is included as part of the thesis. The included computational model offers an efficient way of modelling dynamic SSI problems and it could be utilized by other engineers and researchers analysing environmental vibration. The semi-analytical model proved to be a versatile approach, easily applicable to a wide range of modelling cases, commonly encountered in the urban environment. The method offers a computationally efficient and, at the same time, precise way of modelling the environmental vibration. Thus, validating the hypothesis formulated at the beginning of the project.

6.2 Proposals for future research

Future work can be continued in multiple research areas:

- The proposed computational modelling techniques could be validated by comparison with on-site measurement data, or through small-scale experiments. These investigations could determine the needed calibration parameters, and evaluate the naturally occurring uncertainty of the observed vibrations.
- The interaction between the foundations and the soil should be investigated further. In this work, the interaction was assumed perfect. However, this is most likely not true in real structures, as some slippage or imperfect interaction can be expected, which would lead to a different response.
- Further investigation of surrogate models and other data driven approaches would also be interesting. They could combine measurement data with additional computational simulations, where real data is not available. Potentially leading to accurate and computationally efficient models.
- The proposed mixed domain modelling approach could be investigated in more detail. The fully coupled solution procedure is especially interesting. It could enable the usage of the semi-analytical model for a completely new range of cases, dealing with structures very near to the rail track. Currently the approach is limited by the size of obtained matrices, leading to an inefficient solution procedure. This could be improved, using matrix condensation techniques and more advanced linear solvers used for the matrix inverse.
- The created computational model application range could be expanded, by introducing the Green's functions for orthotropic soil or accounting for the poroelasticity. Additionally, fluid, modelling only compressive waves, layers could be introduced to model offshore structures.
- The created modelling approaches can be utilized to investigate various vibration mitigation systems.

References

[1] Urban Europe. Statistics on cities, towns and suburbs., Eurostat, 2016.

[2] EC Transport White Paper: Roadmap to a single European transport area – towards a competitive and resource efficient transport system, (2011).

[3] D.P. Connolly, G.P. Marecki, G. Kouroussis, I. Thalassinakis, P.K. Woodward, The growth of railway ground vibration problems — A review, Science of the Total Environment. 568 (2016) 1276–1282.

[4] C. Sharp, J. Woodcock, G. Sica, E. Peris, A.T. Moorhouse, D.C. Waddington, Exposure-response relationships for annoyance due to freight and passenger railway vibration exposure in residential environments, The Journal of the Acoustical Society of America. 135 (2014) 205–212.

[5] D.C. Waddington, J. Woodcock, M.G. Smith, S. Janssen, K.P. Waye, CargoVibes: Human response to vibration due to freight rail traffic, International Journal of Rail Transportation. 3 (2015) 233–248.

[6] D.J. Thompson, G. Kouroussis, E. Ntotsios, Modelling, simulation and evaluation of ground vibration caused by rail vehicles, Vehicle System Dynamics. 57 (2019) 936–983.

[7] S. Paul de Vos, Railway Induced Vibration - State of the art report, 2017.

[8] ISO 2631-2:2003 Mechanical vibration and shock — Evaluation of human exposure to whole-body vibration — Part 2: Vibration in buildings (1 Hz to 80 Hz), (2003).

[9] M.G. Smith, I. Croy, O. Hammar, M. Ögren, K.P. Waye, Nocturnal vibration and noise from freight trains impacts sleep, Proceedings of Meetings on Acoustics. 19 (2013).

[10] A. Fyhri, G.M. Aasvang, Noise, sleep and poor health: Modeling the relationship between road traffic noise and cardiovascular problems, Science of the Total Environment. 408 (2010) 4935–4942.

[11] ISO 2631-1:1997 Mechanical vibration and shock — Evaluation of human exposure to whole-body vibration — Part 1: General requirements, (1997).

[12] ISO 2631-4:2001 Mechanical vibration and shock — Evaluation of human exposure to whole-body vibration — Part 4: Guidelines for the evaluation of the effects of vibration and rotational motion on passenger and crew comfort in fixed-guideway transport syste, (2001).

[13] ISO 2631-5:2004 Mechanical vibration and shock — Evaluation of human exposure to whole-body vibration — Part 5: Method for evaluation of vibration containing multiple shocks, (2004).

[14] DIN 4150-2: Structural vibrations–Part 2: Human exposure to vibration in buildings., (1999).

[15] DIN 4150-3: Structural vibrations–Part 3: Effects of vibration on structures, (2016).

[16] Transit Noise and Vibration Impact Assessment, (2006) 1–261.

[17] High-Speed Ground Transportation Noise and Vibration Impact Assessment, Federal Railroad Administration, 2012.

[18] BS 6841 Guide to Measurement and Evaluation of Human Exposure to Whole-Body Mechanical Vibration and Repeated Shock, (1987).

[19] BS 6472-1:2008 Guide to evaluation of human exposure to vibration in buildings. Vibration sources other than blasting, (2008).

[20] SN-640312a: Les ébranlements – Effet des ébranlements sur les constructions, (1992).

[21] M. Villot, S. Bailhache, C. Guigou, P. Jean, Prediction of railway induced vibration and ground borne noise exposure in building and associated annoyance, Notes on Numerical Fluid Mechanics and Multidisciplinary Design. 126 (2014) 289–296.

[22] G. Kouroussis, C. Conti, O. Verlinden, Building vibrations induced by human activities: A benchmark of existing standards, Mechanics and Industry. 15 (2014) 345–353.

[23] J. Woodcock, E. Peris, J. Condie, G. Sica, Z. Koziel, T. Evans, A. Moorhouse, A. Steele, D.C. Waddington, Human response to vibration in residential environments (NANR209), Technical Report 6, Determination of exposure-response relationships, (2011) 107.
[24] L. Rayleigh, On waves propagated along the plane surface of an elastic solid, Proceedings of the London Mathematical Society. 1 (1885) 4–11.
[25] K.F. Graff, Wave motion in elastic solids, Courier Corporation, 2012.
[26] J.D. Achenbach, Wave propagation in elastic solids, Elsevier, 2012.
[27] L.V. Andersen, Linear Elastodynamic Analysis, Aalborg University. Department of Civil Engineering, 2006.
[28] H. Lamb, On the propagation of tremors over the surface of an elastic solid, Philosophical Transactions of the Royal Society of London. Series A, Containing Papers of a Mathematical or Physical Character. 203 (1904) 1–42.
[29] W.T. Thomson, Transmission of elastic waves through a stratified solid medium, Journal of Applied Physics. 21 (1950) 89–93.
[30] N.A. Haskell, The dispersion of surface waves on multilayered media, Bulletin of the Seismological Society of America. 43 (1953) 17–43.
[31] M.A. Biot, Theory of Propagation of Elastic Waves in a Fluid-Saturated Porous Solid, Journal of the Acoustical Society of America. 28 (1956) 168–178.
[32] M.A. Biot, Theory of Propagation of Elastic Waves in a Fluid-Saturated Porous Solid II. Higher Frequency Range, Journal of the Acoustical Society of America. 28 (1956) 179–191.
[33] M.A. Biot, Mechanics of deformation and acoustic propagation in porous media, Journal of Applied Physics. 33 (1962) 1482–1498.
[34] M.A. Biot, Generalized Theory of Acoustic Propagation in Porous Dissipative Media, The Journal of the Acoustical Society of America. 34 (1962) 1254–1264.
[35] P. Zheng, B. Ding, S.X. Zhao, D. Ding, 3D dynamic Green's functions in a multilayered poroelastic half-space, Applied Mathematical Modelling. 37 (2013) 10203–10219.
[36] Z. Liu, J. Liang, C. Wu, Dynamic Green's function for a three-dimensional concentrated load in the interior of a poroelastic layered half-space using a modified stiffness matrix method, Engineering Analysis with Boundary Elements. 60 (2015) 51–66.
[37] J.W. Dunkin, Computation of modal solutions in layered, elastic media at high frequencies, Bulletin of the Seismological Society of America. 55 (1965) 335–358.
[38] Watson T. H., A note on fast computation of Rayleigh wave dispersion in the multilayered elastic half-space, Bulletin of the Seismological Society of America. 60 (1970) 161–166.
[39] B.L.N. Kennett, Seismic wave propagation in stratified media, 1983.
[40] C.H. Chapman, Yet another elastic plane-wave, layer-matrix algorithm, Geophysical Journal International. 154 (2003) 212–223.
[41] R. Wang, A simple orthonormalization method for stable and efficient computation of Green's functions, Bulletin of the Seismological Society of America. 89 (1999) 733–741.
[42] E. Kausel, J.M. Roesset, Stiffness matrices for layered soils, Bulletin of the Seismological Society of America. 71 (1981) 1743–1761.
[43] E. Kausel, Generalized stiffness matrix method for layered soils, Soil Dynamics and Earthquake Engineering. 115 (2018) 663–672.
[44] E. Kausel, Fundamental solutions in elastodynamics, a compendium, Cambridge University Press, 2006.
[45] J. Park, A.M. Kaynia, Stiffness matrices for fluid and anisotropic soil layers with applications in soil dynamics, Soil Dynamics and Earthquake Engineering. 115 (2018)

169–182.
[46] G. Waas, Linear two-dimensional analysis of soil dynamics problems in semi-infinite layer media, Ph.D. Thesis, University of California, Berkeley, 1972.
[47] J. Lysmer, G. Waas, Shear waves in plane infinite structures, Journal of Engineering Mechanics Division. ASCE 18 (1972) 85–105.
[48] M. Schevenels, S. François, G. Degrande, EDT: An ElastoDynamics Toolbox for MATLAB, Computers and Geosciences. 35 (2009) 1752–1754.
[49] L.V. Andersen, J. Clausen, Impedance of surface footings on layered ground, Computers and Structures. 86 (2008) 72–87.
[50] L.V. Andersen, J. Clausen, Efficient Modelling of Wind Turbine Foundations, Fundamental and Advanced Topics in Wind Power. (2011).
[51] E. Kausel, Thin-layer method: Formulation in the time domain, International Journal for Numerical Methods in Engineering. 37 (1994) 927–941.
[52] J. Park, E. Kausel, Response of layered half-space obtained directly in the time domain, part I: SH sources, Bulletin of the Seismological Society of America. 96 (2006) 1795–1809.
[53] E. Kausel, J. Park, Response of layered half-space obtained directly in the time domain, part II: SV-P and three-dimensional sources, Bulletin of the Seismological Society of America. 96 (2006) 1810–1826.
[54] J. Virieux, SH-wave propagation in heterogeneous media: Velocity-stress finite-difference method, Geophysics. 49 (1984) 1933–1942.
[55] J. Virieux, P-SV wave propagation in heterogeneous media: Velocity-stress finite-difference method, Geophysics. 51 (1986) 889–901.
[56] R.W. Graves, Simulating seismic wave propagation in 3D elastic media using staggered-grid finite differences, Bulletin of the Seismological Society of America. 86 (1996) 1091–1106.
[57] M. Katou, T. Matsuoka, O. Yoshioka, Y. Sanada, T. Miyoshi, Numerical simulation study of ground vibrations using forces from wheels of a running high-speed train, Journal of Sound and Vibration. 318 (2008) 830–849.
[58] D.P. Connolly, G. Kouroussis, O. Laghrouche, C.L. Ho, M.C. Forde, Benchmarking railway vibrations - Track, vehicle, ground and building effects, Construction and Building Materials. 92 (2015) 64–81.
[59] R.D. Cook, D.S. Malkus, M.E. Plesha, R. j. Witt, Concepts & Appls of Finite Element Analysis, (2002) 733.
[60] D.P. Connolly, A. Giannopoulos, M.C. Forde, Numerical modelling of ground borne vibrations from high speed rail lines on embankments, Soil Dynamics and Earthquake Engineering. 46 (2013) 13–19.
[61] G. Kouroussis, O. Verlinden, C. Conti, Free field vibrations caused by high-speed lines: Measurement and time domain simulation, Soil Dynamics and Earthquake Engineering. 31 (2011) 692–707.
[62] P. Persson, L.V. Andersen, Efficient finite-element analysis of the influence of structural modifications on traffic-induced building vibrations, Numerical Methods in Geotechnical Engineering IX, Proceedings of the 9th European Conference on Numerical Methods in Geotechnical Engineering (NUMGE 2018). (2018) 1557–1564.
[63] G. Kouroussis, O. Verlinden, C. Conti, Ground propagation of vibrations from railway vehicles using a finite/infinite-element model of the soil, Proceedings of the Institution of Mechanical Engineers, Part F: Journal of Rail and Rapid Transit. 223 (2009) 405–413.
[64] COMSOL Multiphysics® v. 5.4. www.comsol.com. COMSOL AB, Stockholm, Sweden., (n.d.).

[65] ABAQUS 6.13, ABAQUS Documentation, Dassault Systèmes, Providence, RI, USA., (n.d.).
[66] J. Lysmer, R.L. Kuhlemeyer, Finite dynamic model for infinite media, Journal of the Engineering Mechanics Division, ASCE. 95 (1969) 859–878.
[67] A. Bamberger, B. Chalindar, P. Joly, J.E. Roberts, J.L. Teron, Absorbing Boundary Conditions for Rayleigh Waves, SIAM Journal on Scientific and Statistical Computing. 9 (1988) 1016–1049.
[68] R.L. Higdon, Absorbing boundary conditions for elastic waves, Geophysics. 56 (1991) 231–241.
[69] S. Krenk, P.H. Kirkegaard, Local tensor radiation conditions for elastic waves, Journal of Sound and Vibration. 247 (2001) 875–896.
[70] P. Bettess, Infinite elements, (1992).
[71] J.P. Berénger, J.P. Berenger, A Perfectly Matched Layer for the Absorption of Electromagnetic Waves, Journal of Computational Physics. 114 (1994) 185–200.
[72] W.C. Chew, Q.H. Liu, Perfectly matched layers for elastodynamics: A new absorbing boundary condition, Journal of Computational Acoustics. 04 (1996) 341–359.
[73] U. Basu, A.K. Chopra, Perfectly matched layers for time-harmonic elastodynamics of unbounded domains: Theory and finite-element implementation, 2003.
[74] U. Basu, Explicit finite element perfectly matched layer for transient three-dimensional elastic waves, International Journal for Numerical Methods in Engineering. 77 (2008) 151–176.
[75] A. Fathi, B. Poursartip, L.F. Kallivokas, Time-domain hybrid formulations for wave simulations in three-dimensional PML-truncated heterogeneous media, International Journal for Numerical Methods in Engineering. 101 (2015) 165–198.
[76] S.S. Madsen, S. Krenk, Asymptotically Matched Layer (AML) for transient wave propagation in a moving frame of reference, Computers and Geotechnics. 82 (2017) 124–133.
[77] P. Lopes, P.A. Costa, M. Ferraz, R. Calçada, A.S. Cardoso, Numerical modeling of vibrations induced by railway traffic in tunnels: From the source to the nearby buildings, Soil Dynamics and Earthquake Engineering. 61–62 (2014) 269–285.
[78] J. Domínguez, Boundary Elements in Dynamics, Computational Mechanics Publications, 1993.
[79] R. Shahi, A. Noorzad, Dynamic Response of Rigid Foundations of Arbitrary Shape Using Half-Space Green's Function, International Journal of Geomechanics. 11 (2011) 391–398.
[80] S.E. Kattis, D. Polyzos, D.. Beskos, Structural vibration isolation by rows of piles, WIT Transactions on The Built Environment. 15 (1970).
[81] D. Clouteau, R. Cottereau, G. Lombaert, Dynamics of structures coupled with elastic media—a review of numerical models and methods, Journal of Sound and Vibration. 332 (2013) 2415–2436.
[82] G. Lombaert, G. Degrande, D. Clouteau, Numerical modelling of free field traffic-induced vibrations, Soil Dynamics and Earthquake Engineering. 19 (2000) 473–488.
[83] D.C. Rizos, Z. Wang, Coupled BEM-FEM solutions for direct time domain soil-structure interaction analysis, Engineering Analysis with Boundary Elements. 26 (2002) 877–888.
[84] P. Galvín, J. Domínguez, Experimental and numerical analyses of vibrations induced by high-speed trains on the Córdoba-Málaga line, Soil Dynamics and Earthquake Engineering. 29 (2009) 641–657.
[85] P. Galvín, A. Romero, J. Domínguez, Fully three-dimensional analysis of high-speed train-track-soil-structure dynamic interaction, Journal of Sound and Vibration. 329

(2010) 5147–5163.
[86] X. Sheng, C.J.C. Jones, D.J. Thompson, Modelling ground vibration from railways using wavenumber finite- and boundary-element methods, Proceedings of the Royal Society A: Mathematical, Physical and Engineering Sciences. 461 (2005) 2043–2070.
[87] L. Andersen, S.R.K. Nielsen, Reduction of ground vibration by means of barriers or soil improvement along a railway track, Soil Dynamics and Earthquake Engineering. 25 (2005) 701–716.
[88] Y. Bin Yang, H.H. Hung, A 2.5D finite/infinite element approach for modelling visco-elastic bodies subjected to moving loads, International Journal for Numerical Methods in Engineering. 51 (2001) 1317–1336.
[89] Y.B. Yang, X. Liang, H.H. Hung, Y. Wu, Comparative study of 2D and 2.5D responses of long underground tunnels to moving train loads, Soil Dynamics and Earthquake Engineering. 97 (2017) 86–100.
[90] G. Degrande, D. Clouteau, R. Othman, M. Arnst, H. Chebli, R. Klein, P. Chatterjee, B. Janssens, A numerical model for ground-borne vibrations from underground railway traffic based on a periodic finite element-boundary element formulation, Journal of Sound and Vibration. 293 (2006) 645–666.
[91] E. Kausel, Early history of soil–structure interaction, Soil Dynamics and Earthquake Engineering. 30 (2010) 822–832.
[92] M. Lou, H. Wang, X. Chen, Y. Zhai, Structure-soil-structure interaction: Literature review, Soil Dynamics and Earthquake Engineering. 31 (2011) 1724–1731.
[93] H.L. Wong, J.E. Luco, Tables of impedance functions for square foundations on layered media, International Journal of Soil Dynamics and Earthquake Engineering. 4 (1985) 64–81.
[94] J.P. Wolf, Foundation vibration analysis using simple physical models, Pearson Education, 1994.
[95] H.L. Wong, J.E. Luco, Dynamic interaction between rigid foundations in a layered half-space, Soil Dynamics and Earthquake Engineering. 5 (1986) 149–158.
[96] J. Fu, J. Liang, B. Han, Impedance functions of three-dimensional rectangular foundations embedded in multi-layered half-space, Soil Dynamics and Earthquake Engineering. 103 (2017) 118–122.
[97] G. Lin, Z. Han, J. Li, An efficient approach for dynamic impedance of surface footing on layered half-space, Soil Dynamics and Earthquake Engineering. 49 (2013) 39–51.
[98] Z. Han, M. Zhou, X. Zhou, L. Yang, Dynamic Response of 3D Surface/Embedded Rigid Foundations of Arbitrary Shapes on Multi-Layered Soils in Time Domain, International Journal of Structural Stability and Dynamics. (2019).
[99] J.P. Wolf, Consistent lumped parameter models for unbounded soil: Physical representation, Earthquake Engineering & Structural Dynamics. 20 (1991) 11–32.
[100] J.P. Wolf, Consistent lumped-parameter models for unbounded soil: Frequency-independent stiffness, damping and mass matrices, Earthquake Engineering & Structural Dynamics. 20 (1991) 33–41.
[101] A.M. Kaynia, Dynamic stiffness and seismic response of pile groups, PhD thesis, Massachusetts Institute of technology, (1982).
[102] A.M. Kaynia, E. Kausel, Dynamics of piles and pile groups in layered soil media, Soil Dynamics and Earthquake Engineering. 10 (1991) 386–401.
[103] K.A. Kuo, H.E.M. Hunt, An efficient model for the dynamic behaviour of a single pile in viscoelastic soil, Journal of Sound and Vibration. 332 (2013) 2549–2561.
[104] L. Auersch, Wave propagation in the elastic half-space due to an interior load and its application to ground vibration problems and buildings on pile foundations, Soil Dynamics and Earthquake Engineering. 30 (2010) 925–936.

[105] G. Kouroussis, I. Anastasopoulos, G. Gazetas, O. Verlinden, Three-dimensional finite element modelling of dynamic pile-soil-pile interaction in time domain, ECCOMAS Thematic Conference - COMPDYN 2013: 4th International Conference on Computational Methods in Structural Dynamics and Earthquake Engineering, Proceedings - An IACM Special Interest Conference. (2013) 4426–4439.
[106] H.R. Masoumi, G. Degrande, G. Lombaert, Prediction of free field vibrations due to pile driving using a dynamic soil-structure interaction formulation, Soil Dynamics and Earthquake Engineering. 27 (2007) 126–143.
[107] C.M. Parente, P.A. Costa, A.S. Cardoso, Ground-borne vibrations induced by pile driving: Prediction based on numerical approach, Proceedings of the 7th International Conference on Structural Engineering, Mechanics and Computation (SEMC 2019). (2019) 97–102.
[108] V. Whenham, Power Transfer and Vibrator-Pile-Soil Interactions within the framework of vibratory pile driving, PhD thesis, Louvain-La-Neuve, Université catholique de Louvain (UCL), 2011.
[109] F. Deckner, Vibration transfer process during vibratory sheet pile driving – from source to soil, PhD thesis, KTH Royal Institute of Technology, 2017.
[110] M.F.M. Hussein, H.E.M. Hunt, A numerical model for calculating vibration from a railway tunnel embedded in a full-space, Journal of Sound and Vibration. 305 (2007) 401–431.
[111] P. Alves Costa, R. Calçada, A. Silva Cardoso, Ballast mats for the reduction of railway traffic vibrations. Numerical study, Soil Dynamics and Earthquake Engineering. 42 (2012) 137–150.
[112] B. Noori, R. Arcos, A. Clot, J. Romeu, Control of ground-borne underground railway-induced vibration from double-deck tunnel infrastructures by means of dynamic vibration absorbers, Journal of Sound and Vibration. 461 (2019) 114914.
[113] J.C.O. Nielsen, A. Mirza, S. Cervello, P. Huber, R. Müller, B. Nelain, P. Ruest, Reducing train-induced ground-borne vibration by vehicle design and maintenance, International Journal of Rail Transportation. 3 (2015) 17–39.
[114] D.J. Thompson, J. Jiang, M.G.R. Toward, M.F.M. Hussein, E. Ntotsios, A. Dijckmans, P. Coulier, G. Lombaert, G. Degrande, Reducing railway-induced ground-borne vibration by using open trenches and soft-filled barriers, Soil Dynamics and Earthquake Engineering. 88 (2016) 45–59.
[115] L.V. Andersen, A. Peplow, P. Bucinskas, Efficiency of nearly periodic structures for mitigation of ground vibration, in: COMPDYN 2017 6th ECCOMAS Thematic Conference on Computational Methods in Structural Dynamics and Earthquake Engineering, 2017: pp. 537-.
[116] L.V. Andersen, A. Peplow, P. Bucinskas, P. Persson, K. Persson, Variation in models for simple dynamic structure-soil-structure interaction problems, Procedia Engineering. 199 (2017) 2306–2311.
[117] V. V. Krylov, Control of traffic-induced ground vibrations by placing heavy masses on the ground surface, Journal of Low Frequency Noise Vibration and Active Control. 26 (2007) 311–320.
[118] A. Dijckmans, P. Coulier, J. Jiang, M.G.R. Toward, D.J. Thompson, G. Degrande, G. Lombaert, Mitigation of railway induced ground vibration by heavy masses next to the track, Soil Dynamics and Earthquake Engineering. 75 (2015) 158–170.
[119] P. Coulier, G. Degrande, A. Dijckmans, J. Houbrechts, G. Lombaert, W. Rucker, L. Auersch, M.. Plaza, V. Cueller, D.J. Thompson, A. Ekbald, A. Smekal, Scope of the parametric study on mitigation measures on the transmission path. RIVAS project., (2011) 1–90.

[120] J.P. Talbot, Base-isolated buildings: Towards performance based design, Proceedings of the Institution of Civil Engineers: Structures and Buildings. 169 (2016) 574–582.
[121] P. Persson, L.V. Andersen, K. Persson, P. Bucinskas, Effect of structural design on traffic-induced building vibrations, Procedia Engineering. 199 (2017) 2711–2716.
[122] G. Lombaert, G. Degrande, S. François, D.J. Thompson, Ground-borne vibration due to railway traffic, International Workshop of Railway Noise. (2013) 266–301.
[123] G. Kouroussis, D.P. Connolly, O. Verlinden, Railway-induced ground vibrations – a review of vehicle effects, International Journal of Rail Transportation. 2 (2014) 69–110.
[124] K. Popp, H. Kruse, I. Kaiser, Vehicle-track dynamics in the mid-frequency range, Vehicle System Dynamics. 31 (1999) 423–464.
[125] D.J. Thompson, Railway noise and vibration mechanisms, modelling and means of control, 2009.
[126] D.R.M. Milne, L.M. Le Pen, D.J. Thompson, W. Powrie, Properties of train load frequencies and their applications, Journal of Sound and Vibration. 397 (2017) 123–140.
[127] A.R.B. Berawi, Improving Railway Track Maintenance Using Power Spectral Density (PSD), Universidade do Porto (Portugal), 2013.
[128] D. Cantero, T. Arvidsson, E. OBrien, R. Karoumi, Train–track–bridge modelling and review of parameters, Structure and Infrastructure Engineering. 12 (2016) 1051–1064.
[129] E. Ntotsios, D.J. Thompson, M.F.M. Hussein, The effect of track load correlation on ground-borne vibration from railways, Journal of Sound and Vibration. 402 (2017) 142–163.
[130] X. Lei, N.A. Noda, Analyses of dynamic response of vehicle and track coupling system with random irregularity of track vertical profile, Journal of Sound and Vibration. 258 (2002) 147–165.
[131] X. Sheng, C.J.C. Jones, D.J. Thompson, A theoretical model for ground vibration from trains generated by vertical track irregularities, Journal of Sound and Vibration. 272 (2004) 937–965.
[132] N. Triepaischajonsak, D.J. Thompson, A hybrid modelling approach for predicting ground vibration from trains, Journal of Sound and Vibration. 335 (2015) 147–173.
[133] G. Kouroussis, D.P. Connolly, G. Alexandrou, K. Vogiatzis, Railway ground vibrations induced by wheel and rail singular defects, Vehicle System Dynamics. 53 (2015) 1500–1519.
[134] G. Kouroussis, B. Olivier, A. Romero, P. Galvín, A FE-BE Model for Predicting Railway Ground Vibration From Discrete Rail Defects, Proceedings of the 15th International Railway Engineering Conference (Railway Engineering 2019). (2019).
[135] D.P. Connolly, P. Galvín, B. Olivier, A. Romero, G. Kouroussis, A 2.5D time-frequency domain model for railway induced soil-building vibration due to railway defects, Soil Dynamics and Earthquake Engineering. 120 (2019) 332–344.
[136] J.C.O. Nielsen, A. Igeland, Vertical dynamic interaction between train and track—influence of wheel and track imperfections, Journal of Sound and Vibration. 187 (1995) 825–839.
[137] J.C.O. Nielsen, G. Lombaert, S. François, A hybrid model for prediction of ground-borne vibration due to discrete wheel/rail irregularities, Journal of Sound and Vibration. 345 (2015) 103–120.
[138] T.X. Wu, D.J. Thompson, A hybrid model for the noise generation due to railway wheel flats, Journal of Sound and Vibration. 251 (2002) 115–139.
[139] A. Pieringer, W. Kropp, J.C.O. Nielsen, The influence of contact modelling on simulated wheel/rail interaction due to wheel flats, Wear. 314 (2014) 273–281.
[140] S.L. Grassie, Rail irregularities, corrugation and acoustic roughness: Characteristics, significance and effects of reprofiling, Proceedings of the Institution of Mechanical

Engineers, Part F: Journal of Rail and Rapid Transit. 226 (2012) 542–557.
[141] V. V. Krylov, On the theory of railway-induced ground vibrations, Journal de Physique IV. 04 (1994) 4–8.
[142] V. V. Krylov, Generation of ground vibrations by superfast trains, Applied Acoustics. 44 (1995) 149–164.
[143] V. V. Krylov, Effects of Track Properties on Ground Vibrations Generated by High-Speed Trains, Acta Acustica. 228 (1998) 78–90.
[144] V. Krylov, C.. Ferguson, Calculations of ground vibrations from heavy-freight trains, Proceedings of the Institute of Acoustics. 15 (1993) 59–68.
[145] G. Degrande, G. Lombaert, An efficient formulation of Krylov's prediction model for train induced vibrations based on the dynamic reciprocity theorem, The Journal of the Acoustical Society of America. 110 (2002) 1379–1390.
[146] X. Sheng, C.J.C. Jones, M. Petyt, Ground vibration generated by a harmonic load acting on a railway track, Journal of Sound and Vibration. 225 (1999) 3–28.
[147] X. Sheng, C.J.C. Jones, M. Petyt, Ground vibration generated by a load moving along a railway track, Journal of Sound and Vibration. 228 (1999) 129–156.
[148] X. Sheng, C.J.C. Jones, D.J. Thompson, A theoretical study on the influence of the track on train-induced ground vibration, Journal of Sound and Vibration. 272 (2004) 909–936.
[149] J.A. Forrest, H.E.M. Hunt, A three-dimensional tunnel model for calculation of train-induced ground vibration, Journal of Sound and Vibration. 294 (2006) 678–705.
[150] E. Ntotsios, S.G. Koroma, W.I. Hamad, D.J. Thompson, H.E.M. Hunt, Modelling of train induced vibration, IMechE: The Stephenson Conference - Research for Railways. (2015).
[151] M.F.M. Hussein, S. Gupta, H.E.M. Hunt, G. Degrande, J.P. Talbot, An efficient model for calculating vibration from a railway tunnel buried in a half-space, 13th International Congress on Sound and Vibration 2006, ICSV 2006. 6 (2006) 4523–4530.
[152] L.V. Andersen, C.J.C. Jones, Coupled boundary and finite element analysis of vibration from railway tunnels-a comparison of two- and three-dimensional models, Journal of Sound and Vibration. 293 (2006) 611–625.
[153] A. Clot, R. Arcos, J. Romeu, T. Pàmies, Dynamic response of a double-deck circular tunnel embedded in a full-space, Tunnelling and Underground Space Technology. 59 (2016) 146–156.
[154] J. O'Brien, D.C. Rizos, A 3D BEM-FEM methodology for simulation of high speed train induced vibrations, Soil Dynamics and Earthquake Engineering. 25 (2005) 289–301.
[155] W. Zhai, Z. He, X. Song, Prediction of high-speed train induced ground vibration based on train-track-ground system model, Earthquake Engineering and Engineering Vibration. 9 (2010) 545–554.
[156] G. Kouroussis, O. Verlinden, Prediction of railway induced ground vibration through multibody and finite element modelling, Mechanical Sciences. 4 (2013) 167–183.
[157] Y.B. Yang, H.H. Hung, D.W. Chang, Train-induced wave propagation in layered soils using finite/infinite element simulation, Soil Dynamics and Earthquake Engineering. 23 (2003) 263–278.
[158] Y.B. Yang, H.H. Hung, Soil vibrations caused by underground moving trains, Journal of Geotechnical and Geoenvironmental Engineering. 134 (2008) 1633–1644.
[159] P. Alves Costa, R. Calçada, A. Silva Cardoso, A. Bodare, Influence of soil non-linearity on the dynamic response of high-speed railway tracks, Soil Dynamics and Earthquake Engineering. 30 (2010) 221–235.
[160] P. Jean, C. Guigou, M. Villot, A 2.5D BEM model for ground-structure interaction,

Building Acoustics. 11 (2004) 157–173.
[161] X. Sheng, C.J.C. Jones, D.J. Thompson, Prediction of ground vibration from trains using the wavenumber finite and boundary element methods, Journal of Sound and Vibration. 293 (2006) 575–586.
[162] S. François, M. Schevenels, P. Galvín, G. Lombaert, G. Degrande, A 2.5D coupled FE-BE methodology for the dynamic interaction between longitudinally invariant structures and a layered halfspace, Computer Methods in Applied Mechanics and Engineering. 199 (2010) 1536–1548.
[163] P. Galvín, S. François, M. Schevenels, E. Bongini, G. Degrande, G. Lombaert, A 2.5D coupled FE-BE model for the prediction of railway induced vibrations, Soil Dynamics and Earthquake Engineering. 30 (2010) 1500–1512.
[164] P. Alves Costa, R. Calçada, A. Silva Cardoso, Track-ground vibrations induced by railway traffic: In-situ measurements and validation of a 2.5D FEM-BEM model, Soil Dynamics and Earthquake Engineering. 32 (2012) 111–128.
[165] S. François, M. Schevenels, G. Lombaert, G. Degrande, A two-and-a-half-dimensional displacement-based PML for elastodynamic wave propagation, International Journal for Numerical Methods in Engineering. 90 (2012) 819–837.
[166] J.F. Ruiz, P.J. Soares, P. Alves Costa, D.P. Connolly, The effect of tunnel construction on future underground railway vibrations, Soil Dynamics and Earthquake Engineering. 125 (2019) 105756.
[167] M.F.M. Hussein, H. Hunt, K. Kuo, P.A. Costa, J. Barbosa, The use of sub-modelling technique to calculate vibration in buildings from underground railways, Proceedings of the Institution of Mechanical Engineers, Part F: Journal of Rail and Rapid Transit. 229 (2015) 303–314.
[168] P. Fiala, G. Degrande, F. Augusztinovicz, Numerical modelling of ground-borne noise and vibration in buildings due to surface rail traffic, Journal of Sound and Vibration. 301 (2007) 718–738.
[169] J.T. Nelson, H.J. Saurenman, A prediction procedure for rail transportation groundborne noise and vibration, Transportation Research Record 1143. In: Proceedings of A1F04 Committee Meetingon the Transportation Research Board. 1143 (1987) 26–35.
[170] H. Kuppelwieser, A. Ziegler, A tool for predicting vibration and structure-borne noise immissions caused by railways, Journal of Sound and Vibration. 193 (1996) 261–267.
[171] C. Madshus, B. Bessason, L. Hårvik, Prediction model for low frequency vibration from high speed railways on soft ground, Publikasjon - Norges Geotekniske Institutt. 195 (1996) 195–203.
[172] F. Rossi, A. Nicolini, A simple model to predict train-induced vibration: Theoretical formulation and experimental validation, Environmental Impact Assessment Review. 23 (2003) 305–322.
[173] M. Bahrekazemi, Train-Induced Ground Vibration and Its Prediction, PhD thesis, Division of Soil and Rock Mechanics, Dept of Civil and Architectural Engineering, Royal Institute of Technology. 1005 (2004) 1650–9501.
[174] D.P. Connolly, G. Kouroussis, A. Giannopoulos, O. Verlinden, P.K. Woodward, M.C. Forde, Assessment of railway vibrations using an efficient scoping model, Soil Dynamics and Earthquake Engineering. 58 (2014) 37–47.
[175] G. Kouroussis, K.E. Vogiatzis, D.P. Connolly, Assessment of railway ground vibration in urban area using in-situ transfer mobilities and simulated vehicle-track interaction, International Journal of Rail Transportation. 6 (2018) 113–130.
[176] E.C. Bovey, Development of an impact method to determine the vibration transfer characteristics of railway installations, Journal of Sound and Vibration. 87 (1983) 357–370.

[177] R. Jones, In-situ measurement of the dynamic properties of soil by vibration methods, Geotechnique. 8 (1958) 1–21.
[178] H.P. Liu, D.M. Boore, W.B. Joyner, D.H. Oppenheimer, R.E. Warrick, W. Zhang, J.C. Hamilton, L.T. Brown, Comparison of phase velocities from array measurements of Rayleigh waves associated with microtremor and results calculated from borehole shear-wave velocity profiles, Bulletin of the Seismological Society of America. 90 (2000) 666–678.
[179] C.G. Lai, G.J. Rix, S. Foti, V. Roma, Simultaneous measurement and inversion of surface wave dispersion and attenuation curves, Soil Dynamics and Earthquake Engineering. 22 (2002) 923–930.
[180] L.F. Kallivokas, A. Fathi, S. Kucukcoban, K.H. Stokoe, J. Bielak, O. Ghattas, Site characterization using full waveform inversion, Soil Dynamics and Earthquake Engineering. 47 (2013) 62–82.
[181] G. Kouroussis, D.P. Connolly, M.C. Forde, O. Verlinden, Train speed calculation using ground vibrations, Proceedings of the Institution of Mechanical Engineers, Part F: Journal of Rail and Rapid Transit. 229 (2015) 466–483.
[182] C. Madshus, A.M. Kaynia, High-speed railway lines on soft ground: dynamic behaviour at critical train speed, Journal of Sound and Vibration. 231 (2000) 689–701.
[183] G. Degrande, L. Schillemans, Free field vibrations during the passage of a thalys high-speed train at variable speed, Journal of Sound and Vibration. 247 (2001) 131–144.
[184] L. Auersch, S. Said, Attenuation of ground vibrations due to different technical sources, Earthquake Engineering and Engineering Vibration. 9 (2010) 337–344.
[185] D.P. Connolly, P. Alves Costa, G. Kouroussis, P. Galvin, P.K. Woodward, O. Laghrouche, Large scale international testing of railway ground vibrations across Europe, Soil Dynamics and Earthquake Engineering. 71 (2015).
[186] P. Bucinskas, L. Agapii, J. Sneideris, L.V. Andersen, Numerical Modelling of the Dynamic Response of High-Speed Railway Bridges Considering Vehicle-Structure and Structure-Soil-Structure Interaction, in: Computational Techniques for Civil and Structural Engineering, Saxe-Coburg Publications, Stirlingshire, UK, 2015: pp. 125–152.

Part II
Papers

Paper B1

Numerical modelling of ground vibration caused by elevated high-speed railway lines considering structure–soil–structure interaction

Full reference:

P. Bucinskas, L.V. Andersen, K. Persson, Numerical modelling of ground vibration caused by elevated high-speed railway lines considering structure–soil–structure interaction, INTER-NOISE and NOISE-CON Congress and Conference Proceedings. 253 (2016) 2119–2130.

Status:

The paper in this chapter has been presented at the international conference INTER-NOISE 2016, August 21–24 in Hamburg, Germany. It has been published in the proceedings of the conference. The contents and typesetting of this chapter are as submitted.

inter.noise
HAMBURG 2016

NUMERICAL MODELLING OF GROUND VIBRATION CAUSED BY ELEVATED HIGH-SPEED RAILWAY LINES CONSIDERING STRUCTURE–SOIL–STRUCTURE INTERACTION

Paulius Bucinskas[1]; Lars Vabbersgaard ANDERSEN[2]; Kent PERSSON[3]

[1, 2] Department of Civil Engineering, Aalborg University, Denmark

[3] Department of Construction Sciences, Lund University, Sweden

ABSTRACT

Construction of high-speed railway lines has been an increasing trend in recent years. Countries like Denmark and Sweden plan to expand and upgrade their railways to accommodate high-speed traffic. To benefit from the full potential of the reduced commuting times, these lines must pass through densely populated urban areas with the collateral effect of increased noise and vibrations levels. This paper aims to quantify the vibrations levels in the area surrounding an elevated railway line built as a multi-span bridge structure. The proposed model employs finite-element analysis to model the bridge structure, including a multi-degree-of-freedom vehicle model and accounting for the track unevenness via a nonlinear contact model. The foundations are implemented as rigid footings resting on the ground surface, while the soil is modelled utilizing Green's function for a horizontally layered half-space. The paper analyses the effects of structure-soil-structure interaction on the dynamic behaviour of the surrounding soil surface. The effects of different soil stratification and material properties as well as different train speeds are assessed. Finally, the drawbacks of simplifying the numerical model, in order to reduce the complexity of the calculations, are determined.

Keywords: Ground Vibration, High-Speed Railways, Finite–Element Analysis, Structure–Soil–Structure Interaction
I–INCE Classification of Subjects Number(s): 43.2.2, 46.3, 75.3

1. INTRODUCTION

High-speed railways are becoming more and more popular, as different countries upgrade the existing lines to handle high speeds or build entirely new infrastructure. Unfortunately, the higher speeds lead to some unwanted effects, namely increased sound and vibration levels in areas near the track. This is an especially big problem in the urban environment, where the surrounding buildings are very close to the tracks. Dynamic excitation of structures and soil is a complex phenomenon, which is hard to predict before actually carrying out measurement on the site. But that is an expensive and time consuming task which is not possible if the structure is only in the planning stage. Therefore numerical models are needed to help estimate these effects. But creating complicated models that take into account a lot of variables is also time consuming and requires a lot of computational power, while very simple models might not provide reliable results. Estimating which modelling factors have a significant effect and which do not is important, when creating computational models and this paper aims to investigate the effects from soil–structure–soil (SSSI) interaction compared to the results of simpler models that do only account for soil–structure interaction (SSI) without dynamic back coupling.

Analytical studies that investigate bridge behaviour from dynamic loading are mostly based on Euler-Bernoulli beam theory, where the bridge is modelled as a simply supported beam. A closed-form solution for a simple moving constant load was formulated by Fryba [1]. Later, simple beam models based on a finite-element-method formulation were used by Thomson [2] and Gry [3] to investigate vertical and lateral vibrations at high frequencies. Wu and Thomson [4, 5] used double Timoshenko beams and continuously supported multi-beam models for dynamic analysis of the track.

[1] pbu@civil.aau.dk
[2] la@civil.aau.dk
[3] kent.persson@construction.lth.se

Currently, more advanced models are used. For example, Lei and Noda [6], Uzzal et al. [7], as well as Zhai and Cai [8] used multi-degree-of-freedom vehicle models running on a layered track. A similar approach to model the track is taken in this paper. More advanced models that account for three-dimensional vehicle–track interaction are also used but are beyond the scope of this study.

To model the dynamic response of soil, often the finite-element method (FEM), the boundary-element method (BEM), or a combination of them, are used. Alternatively, Green's function can be used. A simple case of soil–structure interaction was investigated by Metrikine and Popp [9]. They studied soil vibrations using FEM with a simplified vehicle model coupled with an infinite beam resting on a half-space. Similar work was done by Lombaert et al. [10] using the BEM. The Green's function approach was utilized by Andersen and Clausen [11] to investigate dynamic soil–structure interaction with rigid foundations. This approach has also been used in the current work.

The investigated case considers a multi-support bridge structure excited by a passing single locomotive. A computational model including a three-dimensional (3D) bridge structure, soil coupled with bridge foundations, and non-linear wheel–rail interaction emerges. The effects to the bridge structure itself and the surround soil surface are analysed.

2. COMPUTATIONAL MODEL

The computational model is composed of several parts: the vehicle model, the bridge model and the soil model. Each of these parts are described in the following subchapters, as well as interaction between them. The description of the model in this paper is not full. A more detailed look at all components and the solution procedure can be found in the work by Bucinskas et al. [12].

The FEM is used to model the bridge structure and the vehicle traversing it. For the FEM, the governing equations are discretized using the standard Galerkin approach with cubic interpolation functions for transverse displacements and linear interpolation for longitudinal displacements and torsion. Damping is introduced as Rayleigh damping.

The soil is modelled utilizing a semi-analytical approach that utilizes Green's function in frequency–wave number domain. The solution is based on the work by Andersen and Clausen [11], and only a short introduction is given in the present paper.

2.1 Computational Model of the Bridge

The bridge is modelled using FEM and has several different parts for which different elements are used. The bridge deck is modelled as a layered structure, which accounts for rails, rail pads, sleepers, ballast and deck. The simplified deck system used for calculations is illustrated in Figure 1. It is assumed that only one railway line is present, and therefore the deck is only loaded along the centre

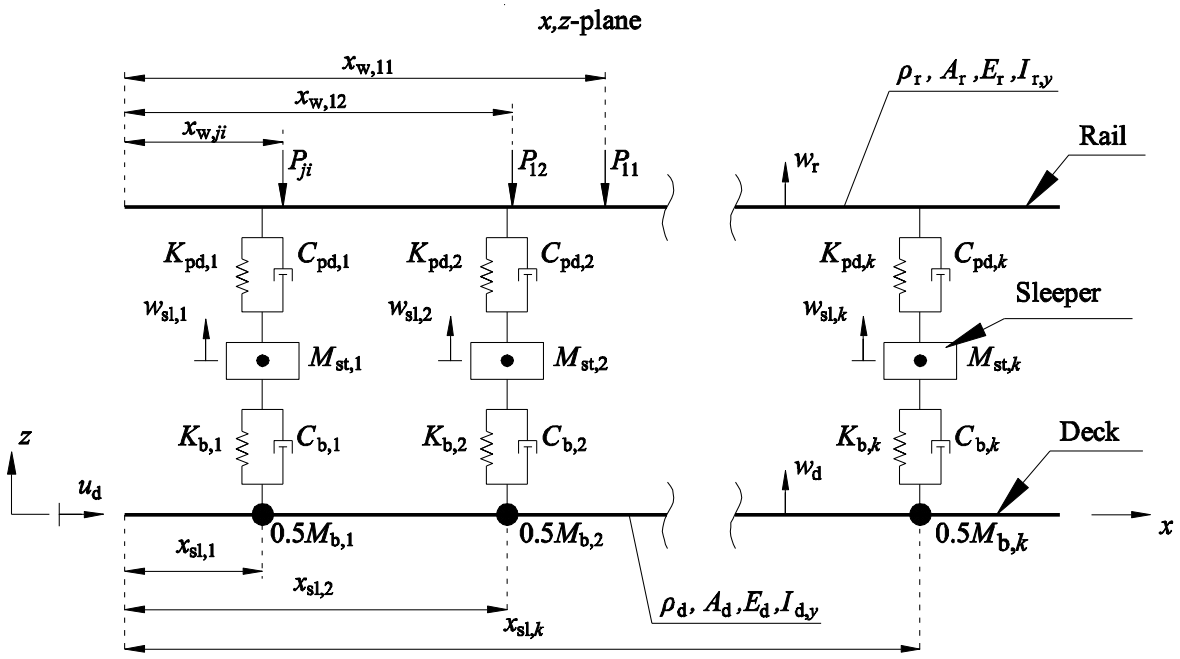

Figure 1 – Bridge deck computational model.

line, i.e. along the x-axis.

The rail is loaded by a number of forces P_{ji} at distances $x_{\mathrm{w},ji}$, where $i = 1{,}2$, $j = 1{,}2$, and each force corresponds to a wheel set of the vehicle. The two rails are simplified to one two-dimensional Euler-Bernoulli beam in the x,z-plane. It is discretely supported by a number, N_{sl}, of spring–dashpot systems at distances $x_{\mathrm{sl},k}$ that account for rail pads and are connected to the sleepers. The rail has the following parameters: mass density ρ_{r}, cross-sectional area A_{r}, Young's modulus E_{r}, moment of inertia around the y-axis $I_{\mathrm{r},y}$ and displacement in z-direction w_{r}. The spring–dashpot system used to model the rail pads is described by stiffness $K_{\mathrm{pd},k}$ and damping $C_{\mathrm{pd},k}$, where $k = 1{,}2, \dots, N_{\mathrm{sl}}$. The effects from concentrated forces and sleepers are introduced by using the Dirac delta function $\delta(x)$, thus the equation of motion for the rail is:

$$\rho_{\mathrm{r}}A_{\mathrm{r}}\frac{\partial^2 w_{\mathrm{r}}(x,t)}{\partial t^2} + E_{\mathrm{r}}I_{\mathrm{r},y}\frac{\partial^4 w_{\mathrm{r}}(x,t)}{\partial x^4} + \sum_{k=1}^{N_{\mathrm{sl}}}\delta\big(x - x_{\mathrm{sl},k}\big)\,K_{\mathrm{pd},k}\left(w_{\mathrm{r}}(x,t) - w_{\mathrm{sl},k}(t)\right)$$

$$+\sum_{k=1}^{N_{\mathrm{sl}}}\delta\big(x - x_{\mathrm{sl},k}\big)\,C_{\mathrm{pd},k}\left(\frac{w_{\mathrm{r}}(x,t)}{\partial t} - \frac{w_{\mathrm{sl},k}(t)}{\mathrm{d}t}\right) = \sum_{j=1}^{2}\sum_{i=1}^{2}\delta\left(x - x_{\mathrm{w},ji}(t)\right)P_{ji}(t). \qquad (1)$$

Further each rail pad is connected to a sleeper that has one degree of freedom $w_{\mathrm{sl},k}$ in z-direction, and there are N_{sl} sleepers in the system. Each sleeper has a mass $M_{\mathrm{sl},k}$ and is connected to the deck through another spring dashpot system, which accounts for the ballast stiffness $K_{\mathrm{b},k}$ and damping $C_{\mathrm{b},k}$. It assumed that half of the ballast mass $M_{\mathrm{b},k}$ moves together with the sleeper, while the other half moves together with the bridge deck. Therefore, the total mass moving with the sleeper becomes $M_{\mathrm{st},k} = M_{\mathrm{sl},k}+0.5M_{\mathrm{b},k}$. The equation of motion for one sleeper becomes:

$$(K_{\mathrm{pd},k} + K_{\mathrm{b},k})w_{\mathrm{sl},k}(t) - K_{\mathrm{pd},k}w_{\mathrm{r}}\big(x_{\mathrm{sl},k},t\big) - K_{\mathrm{b},k}w_{\mathrm{d}}\big(x_{\mathrm{sl},k},t\big) + (C_{\mathrm{pd},k} + C_{\mathrm{b},k})\frac{\mathrm{d}w_{\mathrm{sl},k}(t)}{\mathrm{d}t}$$

$$-C_{\mathrm{pd},k}\frac{\partial w_{\mathrm{r}}\big(x_{\mathrm{sl},k},t\big)}{\partial t} - C_{\mathrm{b},k}\frac{\partial w_{\mathrm{d}}\big(x_{\mathrm{sl},k},t\big)}{\partial t} + M_{\mathrm{st},k}\frac{\mathrm{d}^2 w_{\mathrm{sl},k}(t)}{\mathrm{d}t^2} = 0. \qquad (2)$$

The deck of the structure is modelled in the x,z-plane and for the bending Euler–Bernoulli beam theory is employed. To account for the deck displacements in z-direction w_{r}, the following parameters are used: mass density ρ_{d}, cross-sectional area A_{d}, Young's modulus E_{d}, moment of inertia around y-axis $I_{\mathrm{d},y}$. Half of the ballast mass $M_{\mathrm{b},k}$ and the effects from the sleepers are accounted for by using the Dirac delta function $\delta(x)$:

$$\rho_{\mathrm{d}}A_{\mathrm{d}}\frac{\partial^2 w_{\mathrm{d}}(x,t)}{\partial t^2} + E_{\mathrm{d}}I_{\mathrm{d},y}\frac{\partial^4 w_{\mathrm{d}}(x,t)}{\partial x^4} + \sum_{k=1}^{N_{\mathrm{sl}}}\delta\big(x - x_{\mathrm{sl},k}\big)\,K_{\mathrm{b},k}\left(w_{\mathrm{d}}(x,t) - w_{\mathrm{sl},j}(t)\right)$$

$$+\sum_{k=1}^{N_{\mathrm{sl}}}\delta\big(x - x_{\mathrm{sl},k}\big)\,C_{\mathrm{b},k}\left(\frac{\partial w_{\mathrm{d}}(x,t)}{\partial t} - \frac{\mathrm{d}w_{\mathrm{sl},k}(t)}{\mathrm{d}t}\right) + \sum_{k=1}^{N_{\mathrm{sl}}}\delta\big(x - x_{\mathrm{sl},k}\big)\frac{1}{2}\,M_{\mathrm{b},k}\frac{\partial^2 w_{\mathrm{d}}(x,t)}{\partial t^2} = 0. \qquad (3)$$

Further, for the axial deformation of the deck u_{d}, the equation of motion becomes:

$$E_{\mathrm{d}}A_{\mathrm{d}}\frac{\partial^2 u_{\mathrm{d}}(x,t)}{\partial x^2} + \rho_{\mathrm{d}}A_{\mathrm{d}}\frac{\partial^4 u_{\mathrm{d}}(x,t)}{\partial t^2} + \sum_{k=1}^{N_{\mathrm{sl}}}\delta\big(x - x_{\mathrm{sl},k}\big)\,0.5\,M_{\mathrm{b},k}\frac{\partial^2 u_{\mathrm{d}}(x,t)}{\partial t^2} = 0. \qquad (4)$$

The bridge pylons are again modelled in two dimensions in the x,z-plane and connected to rigid footings that rest on the soil surface, see Figure 2. Each pylon has the following properties: mass density ρ_{p}, cross-sectional area A_{p}, Young's modulus E_{p}, moment of inertia around the y-axis $I_{\mathrm{p},y}$, and displacements u_{p} and w_{p} in the x and z-directions, respectively. The equations of motion for bending and axial deformation then become:

$$\rho_{\mathrm{p}}A_{\mathrm{p}}\frac{\partial^2 u_{\mathrm{p}}(z,t)}{\partial t^2} + E_{\mathrm{p}}I_{\mathrm{p},y}\frac{\partial^4 u_{\mathrm{p}}(z,t)}{\partial z^4} = 0, \qquad E_{\mathrm{p}}A_{\mathrm{p}}\frac{\partial^2 w_{\mathrm{p}}(z,t)}{\partial z^2} + \rho_{\mathrm{p}}A_{\mathrm{p}}\frac{\partial^4 w_{\mathrm{p}}(z,t)}{\partial t^2} = 0. \qquad (5)$$

The foundations are assumed to be rigid and they are placed on the soil surface. Each foundation has mass M_{f} and moment of inertia for pitch $J_{\mathrm{f},y}$. Pylons are connected to the foundations through connecting nodes placed at each foundation centre.

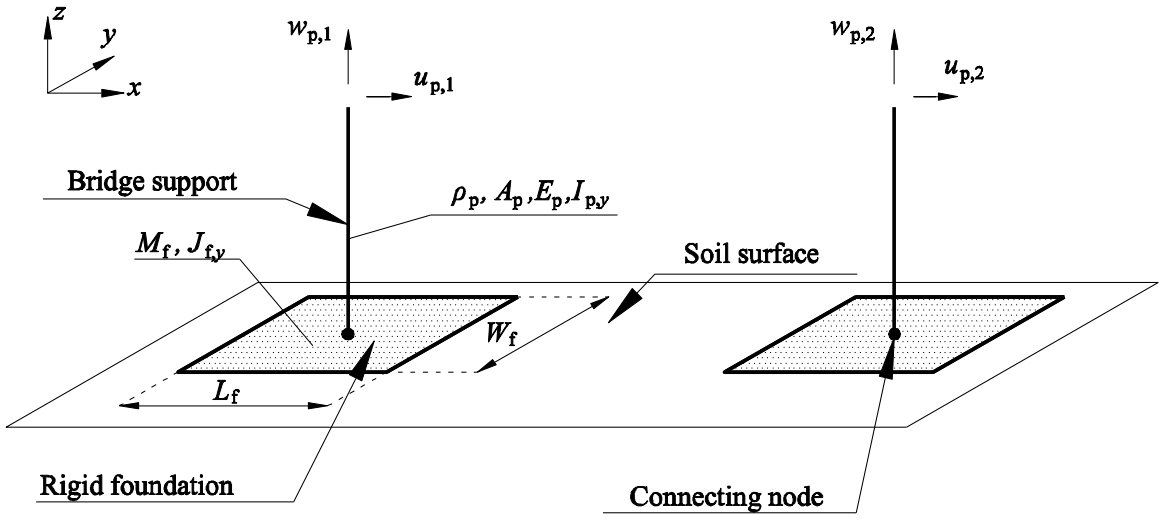

Figure 2 – Pylons and foundations on the soil surface

2.2 Computational Model of the Vehicle

The bridge is loaded by a single passing locomotive. The locomotive is simplified into a two-dimensional ten-degrees-of-freedom system, which involves two layers of spring–dashpot suspension systems in which vertical translation and pitch rotation of the bogie and vehicle body are included. The system is illustrated in Figure 3.

The vehicle body has a mass, M_c, and pitch moment of inertia, J_c, and it has two degrees of freedom: vertical displacement w_c and pitch angle φ_c. It is connected to the bogies through secondary suspension with stiffness $K_{su,2}$ and damping $C_{su,2}$, at distances L_2 from the vehicle centre line. The equation of motion for the vehicle body vertical displacement reads:

$$2K_{su,2}w_c(t) - K_{su,2}w_{t,1}(t) - K_{su,2}w_{t,2}(t) + 2C_{su,2}\frac{dw_c(t)}{dt} - C_{su,2}\frac{dw_{t,1}(t)}{dt}$$

$$-C_{su,2}\frac{dw_{t,2}(t)}{dt} - M_c\frac{d^2w_c(t)}{dt^2} = 0, \tag{6}$$

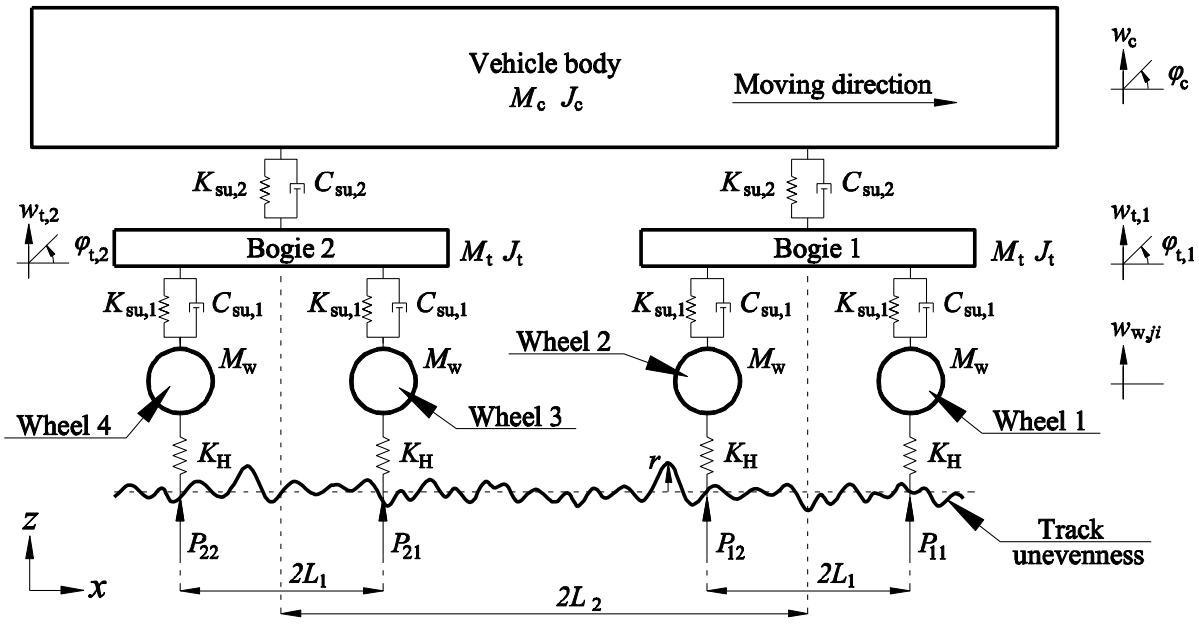

Figure 3 – Multi-degree of freedom vehicle model

and for the rotation, the equation has the form:

$$2L_2^2 K_{\mathrm{su},2}\varphi_{\mathrm{c}}(t) - L_2 K_{\mathrm{su},2} w_{\mathrm{t},1}(t) - L_2 K_{\mathrm{su},2} w_{\mathrm{t},2}(t) + 2C_{\mathrm{su},2}\frac{\mathrm{d}w_{\mathrm{c}}(t)}{\mathrm{d}t} - C_{\mathrm{su},2}\frac{\mathrm{d}w_{\mathrm{t},1}(t)}{\mathrm{d}t}$$

$$-C_{\mathrm{su},2}\frac{\mathrm{d}w_{\mathrm{t},2}(t)}{\mathrm{d}t} - M_{\mathrm{c}}\frac{\mathrm{d}^2 w_{\mathrm{c}}(t)}{\mathrm{d}t^2} = 0. \tag{7}$$

Further, the first and the second bogies are effected by the primary and secondary suspensions, with primary suspension having stiffness $K_{\mathrm{su},1}$ and damping $C_{\mathrm{su},1}$. Each bogie has a mass M_{t}, pitch moment of inertia J_{t}, vertical displacement $w_{\mathrm{t},j}$ and pitch angle $\varphi_{\mathrm{t,j}}$, where $j = 1{,}2$. The vertical displacements are governed by:

$$(2K_{\mathrm{su},1} + K_{\mathrm{su},2})w_{\mathrm{t},j}(t) - K_{\mathrm{su},1} w_{\mathrm{w},j1}(t) - K_{\mathrm{su},1} w_{\mathrm{w},j2}(t) + (2C_{\mathrm{su},1} + C_{\mathrm{su},2})\frac{\mathrm{d}w_{\mathrm{t},j}(t)}{\mathrm{d}t}$$

$$-C_{\mathrm{su},1}\frac{\mathrm{d}w_{\mathrm{w},j1}(t)}{\mathrm{d}t} - C_{\mathrm{su},1}\frac{\mathrm{d}w_{\mathrm{w},j2}(t)}{\mathrm{d}t} - M_{\mathrm{t}}\frac{\mathrm{d}^2 w_{\mathrm{c}}(t)}{\mathrm{d}t^2} = 0, \qquad j = 1{,}2. \tag{8}$$

The rotations $\varphi_{\mathrm{t,j}}$ of both bogies are also effected by primary and secondary suspensions. The primary suspensions are attached at distances L_1 from the boogies centre lines, and the secondary suspension at the centre line. The equations of motion are:

$$2L_1^2 K_{\mathrm{su},1}\varphi_{\mathrm{t},j}(t) - L_1 K_{\mathrm{su,j1}} w_{\mathrm{w},j}(t) + L_1 K_{\mathrm{su},1} w_{\mathrm{w},j2}(t) + 2L_1^2 C_{\mathrm{su},1}\frac{\mathrm{d}\varphi_{\mathrm{t},j}(t)}{\mathrm{d}t}$$

$$-L_1 C_{\mathrm{su},1}\frac{\mathrm{d}w_{\mathrm{w},j1}(t)}{\mathrm{d}t} + L_1 C_{\mathrm{su},1}\frac{\mathrm{d}w_{\mathrm{w},j2}(t)}{\mathrm{d}t} - J_{\mathrm{t}}\frac{\mathrm{d}^2\varphi_{\mathrm{t},j}(t)}{\mathrm{d}t^2} = 0, \qquad j = 1{,}2. \tag{9}$$

Each wheel is attached to the primary suspension and has a vertical degree of freedom $w_{\mathrm{w},ji}$ and mass M_{w}, where $i = 1, 2$ and $j = 1, 2$. Each wheel is also effected by the wheel–rail interaction force P_{ji} and one quarter of the force $F_{\mathrm{total}} = M_{\mathrm{total}} g$, where M_{total} is the total mass of the vehicle and g is the gravitational constant. Thus, the equations of motions for the wheels become:

$$K_{\mathrm{su},1} w_{\mathrm{w},ji}(t) - K_{\mathrm{su},1} w_{\mathrm{t},j}(t) + (-1)^i L_1 K_{\mathrm{su},1}\varphi_{\mathrm{t},j}(t) + C_{\mathrm{su},1}\frac{\mathrm{d}w_{\mathrm{w},ji}(t)}{\mathrm{d}t} - C_{\mathrm{su},1}\frac{w_{\mathrm{t},j}(t)}{\mathrm{d}t}$$

$$+(-1)^i L_1 C_{\mathrm{su},1}\frac{\varphi_{\mathrm{t},j}(t)}{\mathrm{d}t} - M_{\mathrm{w},ji}\frac{\mathrm{d}^2 w_{\mathrm{w},ji}(t)}{\mathrm{d}t^2} = P_{ji}(t) + \frac{1}{4}F_{\mathrm{total}}, \qquad j = 1{,}2\,, i = 1{,}2. \tag{10}$$

The interaction between the wheels and rail track are accounted for by forces P_{ji}. While the wheel is in contact with the track they are modelled using non-linear Hertzian springs, and when the wheel lifts off from the track the forces are equal to zero:

$$P_{ji} = \begin{cases} K_H\left(\left|w_{\mathrm{rel},ji}\right|\right)^{\frac{3}{2}} & \text{for } w_{\mathrm{rel},ji} \le 0 \\ 0 & \text{for } w_{\mathrm{rel},ji} > 0 \end{cases} \tag{11}$$

where $w_{\mathrm{rel},ji}(t) = w_{\mathrm{w},ji}(t) - w_{\mathrm{r}}(x_{\mathrm{w},ji}(t), t) - r(x_{\mathrm{w},ji}(t))$ and K_H is the Hertzian spring constant.

The wheels are affected by the irregularities of the track $r(x_{\mathrm{w},ji})$, which excite high-frequency vibrations. Only vertical track irregularities along the x-axis are considered. They are modelled as a stationary stochastic process and are described from the one–sided power spectral density function:

$$S(k_x) = A_{\mathrm{low}}\frac{k_{\mathrm{c}}^2}{(k_{\mathrm{r}}^2 + k_{\mathrm{x}}^2)(k_{\mathrm{c}}^2 + k_{\mathrm{x}}^2)}, \tag{12}$$

where S is the one sided power spectral density, k_x is the horizontal wavenumber, and A_{low}, k_{r} and k_{c} are constants describing the track unevenness. The function is only defined for $k_x > 0$.

2.3 Computational Model of Soil

Soil is modelled utilizing a semi-analytical approach for a layered half-space, based on the work by Andersen and Clausen [11]. The method utilizes Green's function describing the relation between displacements on the soil surface $u_{\mathrm{s},i}(x, y, t)$ and traction applied at another point, $p_{\mathrm{s},j}(x', y', t')$:

$$u_{s,i}(x,y,t) = \int_{-\infty}^{t}\int_{-\infty}^{\infty}\int_{-\infty}^{\infty} g_{s,ij}(x-x', y-y', t-t')\, p_{s,j}(x',y',t')\, dx'dy'dt', \qquad (1)$$

where $g_{s,ij}(x-x', y-y', t-t')$ is the Green's function tensor. A closed form solution for Equation 13 is not possible, but it can be established in frequency–wavenumber domain, assuming the response of the soil is linear:

$$\overline{U}_{s,i}(k_x, k_y, \omega) = \overline{G}_{s,ij}(k_x, k_y, \omega)\overline{P}_{s,j}(k_x, k_y, \omega) \qquad (2)$$

where $\overline{U}_{s,i}$, $\overline{G}_{s,ij}, \overline{P}_{s,j}$ are triple Fourier transforms of $u_{s,i}, g_{s,ij}, p_{s,j}$. The angular frequency is denoted as ω, and k_x, k_y are horizontal wavenumbers. The solution is valid for a horizontally layered stratum with linear viscoelastic behaviour. The equations of motion for the soil are described by the Navier equations in frequency–wavenumber domain with hysteric material damping introduced through complex Lamé constants.

The Green's function provides the displacement field from a known stress distribution. To obtain the impedance matrix for a set of rigid footings, the following approach is taken:

Step 1. The displacement matrix $[\mathbf{U}_s]$ corresponding to each rigid body motion is prescribed at a number of points N_f, uniformly distributed across the boundary between a number N_F of surface footings and the soil.

Step 2. The Green's function is evaluated in the wavenumber domain.

Step 3. The wave–number spectrum for a simple distributed load with unit magnitude and rotational symmetry around a point on the soil surface is computed.

Step 4. The response at a point n to a load centred at a point m is calculated for all combinations of $n, m = 1,2,3 \ldots, N_f$ and stored in matrix $[\mathbf{G}_s]$.

Step 5. The unknown magnitudes of the loads applied around each of the points are computed:

$$[\mathbf{P}_s] = [\mathbf{G}_s]^{-1}[\mathbf{U}_s]. \qquad (3)$$

Integration of $[\mathbf{P}_s]$ over the contact area provides the impedance matrix $[\mathbf{Z}_s]$, in frequency domain.

In this paper, a number of points on the soil surface are also investigated. It is assumed that points that are not part of the foundations are not loaded, and are only effected by the displacements of the foundations. The response $[\mathbf{G}_{sp}]$ between soil surface points that are analysed and the foundation points is found by again utilizing Green's function. A unit load is applied to the foundation points, and the response found at a number of points on the ground surface. As mentioned before, Green's function provides the displacement field for a known stress distribution. Therefore, the loads $[\mathbf{P}_s]$ found in Step 5 are employed, as they represent the loads caused by unit displacement or rotation related to a rigid body mode. By multiplying the two matrices, surface displacements are found, based on unit displacement of a footing:

$$[\mathbf{U}_{sp,0}] = [\mathbf{G}_{sp}][\mathbf{P}_s]. \qquad (4)$$

Finally, the real soil displacements are obtained after the computations for the bridge structure itself are complete, by multiplying real foundations displacements with the matrix $[\mathbf{U}_{sp,0}]$.

2.4 Structure–Soil Interaction and Structure–Soil–Structure Interaction

To couple the bridge structure with soil, the FEM matrices for the bridge stiffness $[\mathbf{K}_B]$, damping $[\mathbf{C}_B]$, and mass $[\mathbf{M}_B]$ are converted into the complex impedance matrix $[\mathbf{Z}_B]$:

$$[\mathbf{Z}_B] = [\mathbf{K}_B] + i\omega[\mathbf{C}_B] - \omega^2[\mathbf{M}_B]. \qquad (5)$$

Further, the soil impedance matrix is added to the structure impedance matrix at the nodes connecting the foundations and pylons, see Figure 2. Defining $[\mathbf{Z}_{B,11}]$ as the impedance submatrix for nodes not connected to the soil, $[\mathbf{Z}_{B,22}]$ as the impedance submatrix for nodes connected to the soil, and the coupling terms as submatrices $[\mathbf{Z}_{B,12}] = [\mathbf{Z}_{B,12}]^T$, the resulting impedance matrix for the system consisting of the bridge structure (including the track), the footings and the subsoil then becomes:

$$[\mathbf{Z}] = \begin{bmatrix} [\mathbf{Z}_{B,11}] & [\mathbf{Z}_{B,12}] \\ [\mathbf{Z}_{B,21}] & [\mathbf{Z}_{B,22}] + [\mathbf{Z}_{B,sf}] \end{bmatrix}. \qquad (6)$$

The matrix $[\mathbf{Z}_{\mathrm{sf}}]$ is the impedance matrix for all foundations. In this paper it is calculated utilizing two different approaches. One of the approaches considers structure–soil–structure interaction (SSSI), thus the behaviour of one footing can affect the behaviour of other footings through the soil stratum. In this case, the procedure to obtain the impedance matrix $[\mathbf{Z}_{\mathrm{s}}]$, described in Subsection 2.3, is carried out for all foundations at once and $[\mathbf{Z}_{\mathrm{sf}}]$ becomes:

$$[\mathbf{Z}_{\mathrm{sf}}] = [\mathbf{Z}_{\mathrm{s}}]. \tag{7}$$

The resulting matrix is symmetric, fully populated and the size is $6N_{\mathrm{F}} \times 6N_{\mathrm{F}}$, because each foundation has six rigid-body modes.

Another approach only considers structure–soil interaction (SSI) so in this case there is no coupling between foundations through the soil. The impedance matrix is calculated for one foundation on a free field and then applied to all foundations, assuming that all foundations have the same shape and dimensions. The advantage of this approach is significantly lower computation times, but the results are not as precise. To compute the impedance matrix the procedure described in Subsection 2.3 is only carried out for one foundation at a time. Thus the dimensions of $[\boldsymbol{Z}_{\mathrm{s}}]$ are 6×6, as it is only for one foundation with six rigid-body modes. The impedance matrix for all foundations becomes:

$$[\mathbf{Z}_{\mathrm{sf}}] = \begin{bmatrix} [\mathbf{Z}_{\mathrm{s}}] & \mathbf{0} & \cdots & \mathbf{0} \\ \mathbf{0} & [\mathbf{Z}_{\mathrm{s}}] & \cdots & \mathbf{0} \\ \vdots & \vdots & \ddots & \vdots \\ \mathbf{0} & \mathbf{0} & \cdots & [\mathbf{Z}_{\mathrm{s}}] \end{bmatrix}. \tag{20}$$

The resulting matrix $[\mathbf{Z}_{\mathrm{sf}}]$ has the size $6N_{\mathrm{F}} \times 6N_{\mathrm{F}}$, i.e. the same size as in the case of SSSI, but it is only populated in 6×6 blocks along the diagonal. To calculate the soil displacements when only accounting for SSI, the ground-surface displacements caused by each foundation are calculated separately and then all the contributions are added together, assuming superposition.

2.5 Solution Procedure

To solve the previously described system, an iterative procedure is required. The wheel–rail interaction force is modelled using a nonlinear force, and therefore a time-domain solution is needed. However, the impedance matrix for the layered half-space is obtained in the frequency domain. A solution involving two iterative procedures is used. In this paper, only a brief overview for it is given. For a more detailed explanation, see Bucinskas et al. [12].

Step 1. Firstly, for iteration step number k, the vehicle system is solved in time domain. This step calculates the nonlinear forces P_{ji} acting at the wheels, cf. Equation 11. For this purpose, a Newmark second-order time-integration scheme is modified to include an iterative procedure to find the forces acting at each time step. When this step is carried out for the first time, it is assumed that rail displacements are equal to zero. Otherwise the bridge displacements $\{\mathbf{d}_{\mathrm{B}}^{k-1}(t)\}$ from the previous step are used. The determined forces acting on the vehicle wheels are stored as a vector $\{\mathbf{f}_{\mathrm{V}}^{k}(t)\}$, where k denotes iteration number. Such a vector, containing the displacements of the vehicle, is found for each time step.

Step 2. The obtained forces $\{\mathbf{f}_{\mathrm{V}}^{k}(t)\}$ are applied to the bridge, thus obtaining the bridge load vector $\{\mathbf{f}_{\mathrm{B}}^{k}(t)\}$ for each time step. Further, the loads are Fourier transformed to frequency domain. This results in load vector $\{\mathbf{F}_{\mathrm{B}}^{k}(\omega)\}$ for each analysed frequency.

Step 3. The coupled bridge–soil system is solved in frequency domain:

$$\{\mathbf{D}_{\mathrm{B}}^{k}(\omega)\} = [\mathbf{Z}_{\mathrm{B}}]^{-1}\{\mathbf{F}_{\mathrm{B}}^{k}(\omega)\}. \tag{21}$$

Step 4. The obtained displacements $\{\mathbf{D}_{\mathrm{B}}^{k}(\omega)\}$ are inverse Fourier transformed to time domain, to obtain bridge displacements $\{\mathbf{d}_{\mathrm{B}}^{k}(t)\}$ for iteration step k.

Step 5. Convergence of the solution is checked by comparing the displacement matrix $\{\mathbf{d}_{\mathrm{B}}^{k}(t)\}$ with the displacements for previous iteration $\{\mathbf{d}_{\mathrm{B}}^{k-1}(t)\}$. If convergence is reached, iteration is stopped, and if no convergence has been obtained, iteration continues, repeating the procedure from Step 1.

3. BRIDGE GEOMETRY AND PROPERTIES

The geometry of the considered multi-span bridge structure is given in Figure 4. The total bridge length is 200m, it is supported by seven pylons, and the deck has a span of 25 metres between pylons. The sleepers are spaced 0.6m apart. From each side of the bridge, an additional 25m of track are added, where the sleepers are connected to a rigid surface, instead of the deck. Each pylon is 6m tall and connected to a surface footing.

Points from which data were obtained for further analysis are also shown in Figure 4. There are two points in the bridge structure named Deck point and Pylon point from which the acting normal stresses are obtained. Another point used for analysis is named Connecting point. Here the connecting node between foundation number 6 and the soil surface is located. Further, two points on the soil surface farther away from the bridge structure are also analysed.

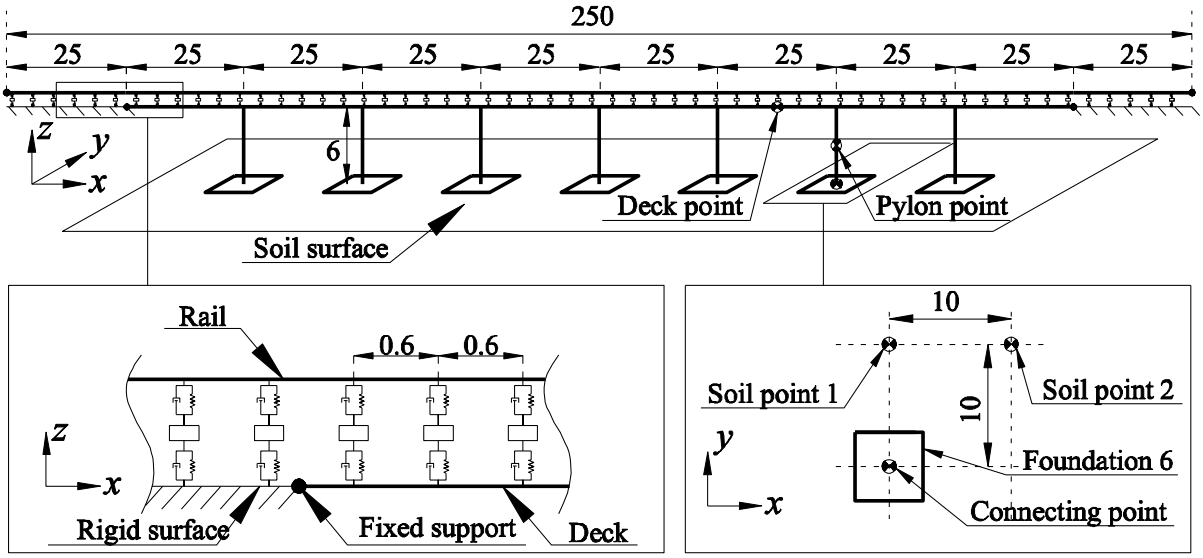

Figure 4 – Investigated bridge model geometry

Table 1 – Properties of the vehicle.

Vehicle properties			
Total force	F_{total}	$-6.8 \cdot 10^5$	N
Primary stiffness	$K_{\text{s},1}$	$3.28 \cdot 10^6$	N/m
Secondary stiffness	$K_{\text{s},2}$	$1.31 \cdot 10^6$	N/m
Primary damping	$C_{\text{s},1}$	$9.00 \cdot 10^4$	$\text{N} \cdot \text{s/m}$
Secondary damping	$C_{\text{s},2}$	$3.00 \cdot 10^4$	$\text{N} \cdot \text{s/m}$
Hertzian constant	K_{H}	$8.70 \cdot 10^{10}$	$\text{N/m}^{3/2}$
Mass car body	M_{c}	$5.35 \cdot 10^4$	kg
Mass boogie	M_{t}	3260	kg
Mass wheel set	M_{w}	2000	kg
Pitch moment body	J_{c}	$2.24 \cdot 10^6$	$\text{kg} \cdot \text{m}^2$
Pitch moment bogie	J_{t}	$2.45 \cdot 10^3$	$\text{kg} \cdot \text{m}^2$
Half-length	L_1	1.5	m
Half-length	L_2	7	m

Table 2 – Properties of the track structure.

Rail properties			
Young's modulus	E_{r}	$210 \cdot 10^9$	Pa
Density	ρ_{r}	8050	kg/m^3
Inertia	$I_{\text{r},y}$	$2.0 \cdot 10^{-5}$	m^4
Area	A_{r}	0.0064	m^2
Rail pad properties			
Stiffness	$K_{\text{pd},i}$	$1.2 \cdot 10^8$	N/m
Damping	$C_{\text{pd},i}$	$1.24 \cdot 10^5$	$\text{N} \cdot \text{s/m}$
Sleeper properties			
Mass	$M_{\text{sl},j}$	237	kg
Spacing	L_{sl}	0.6	m
Ballast properties			
Stiffness	$K_{\text{b},j}$	$2.4 \cdot 10^8$	N/m
Damping	$C_{\text{b},j}$	$5.88 \cdot 10^4$	$\text{N} \cdot \text{s/m}$
Mass	$M_{\text{b},j}$	683	kg

Table 3 – Properties of bridge deck and pylons.

Deck properties			
Young's modulus	E_d	$34 \cdot 10^9$	Pa
Shear modulus	G_d	$13 \cdot 10^9$	Pa
Density	ρ_d	2400	$\mathrm{kg/m^3}$
Inertia	$I_{\mathrm{d},y}$	4.07	$\mathrm{m^4}$
Area	A_d	7.52	$\mathrm{m^2}$
Pylon properties			
Young's	E_p	$34 \cdot 10^9$	Pa
Shear	G_p	$13 \cdot 10^9$	Pa
Density	ρ_p	2400	$\mathrm{kg/m^3}$
Inertia	$I_{\mathrm{p},y}$	4.57	$\mathrm{m^4}$
Area	A_p	5.00	$\mathrm{m^2}$
Surface footing properties			
Mass	M_f	$3.84 \cdot 10^4$	kg
Inertia	$J_{\mathrm{f},y}$	$1.032 \cdot 10^5$	$\mathrm{kg \cdot m^2}$
Length	L_f	5.60	m
Width	W_f	5.60	m

Table 4 – Properties of different soil types.

		Clay	Sand	
Poisson's ratio	υ	0.30	0.40	–
Mass density	ρ	2000	2000	$\mathrm{kg/m^3}$
Hysteric damping	η	0.045	0.040	–
Young's modulus	E	20	160	MPa
P-wave speed	c_P	116.0	414.0	m/s
S-wave speed	c_S	62.0	169.0	m/s
R-wave speed	c_R	57.5	159.0	m/s

The track parameters are given in Table 2 and the properties of the bridge deck and pylons are listed in Table 3. The properties of the multi-degree-of-freedom vehicle are given in Table 1. The unevenness parameters used are: $A_\mathrm{low} = 0.8246 \cdot 10^{-6}\ \mathrm{rad \cdot m}$, $k_\mathrm{r} = 0.8246\ \mathrm{rad/m}$, $k_\mathrm{c} = 0.0206\ \mathrm{rad/m}$.

Two different soil types are used: a relatively soft soil (clay), and a stiffer soil (sand). The parameters for these types of soil are given in Table 4. Four different soil stratification cases are tested:

Case 1: A homogenous half-space of clay;

Case 2: A homogenous half-space of sand;

Case 3: A 7m deep layer of clay over a half-space of sand;

Case 4: A 3.5m deep layer of clay over a half-space of sand.

4. EFFECTS ON THE BRIDGE STRUCTURE

Firstly, the effects from different vehicle speeds to the bridge–soil system are investigated. For this case, the bridge model was simplified to model only the vehicle as four constant forces moving across the deck. This was done in order to isolate the effects of the soil stratification to the structure. It should be noted that further analysis, which included the vehicle and track unevenness, showed similar behaviour, only the effects ware harder to analyse due to the stochastic nature of rail unevenness.

Four different soil stratification cases were tested, as described in Section 3. The same calculations were performed for both models: one considering SSSI and another considering only SSI. The results are presented in Figure 5, where the dependency of the vehicle speed on the maximum absolute displacement of the Connecting point (i.e. the node connecting pylon and foundation number 6, counting from the left), are displayed. The blue line shows the behaviour of the SSSI model, while the red and yellow lines show the behaviour of the SSI model. For the SSI model, there are two lines, as the node on the pylon (blue line) and the soil surface displacement (yellow line) at exactly the same position are different. This is due to how the soil displacements are calculated, where the effect from each foundation is calculated separately and then added together.

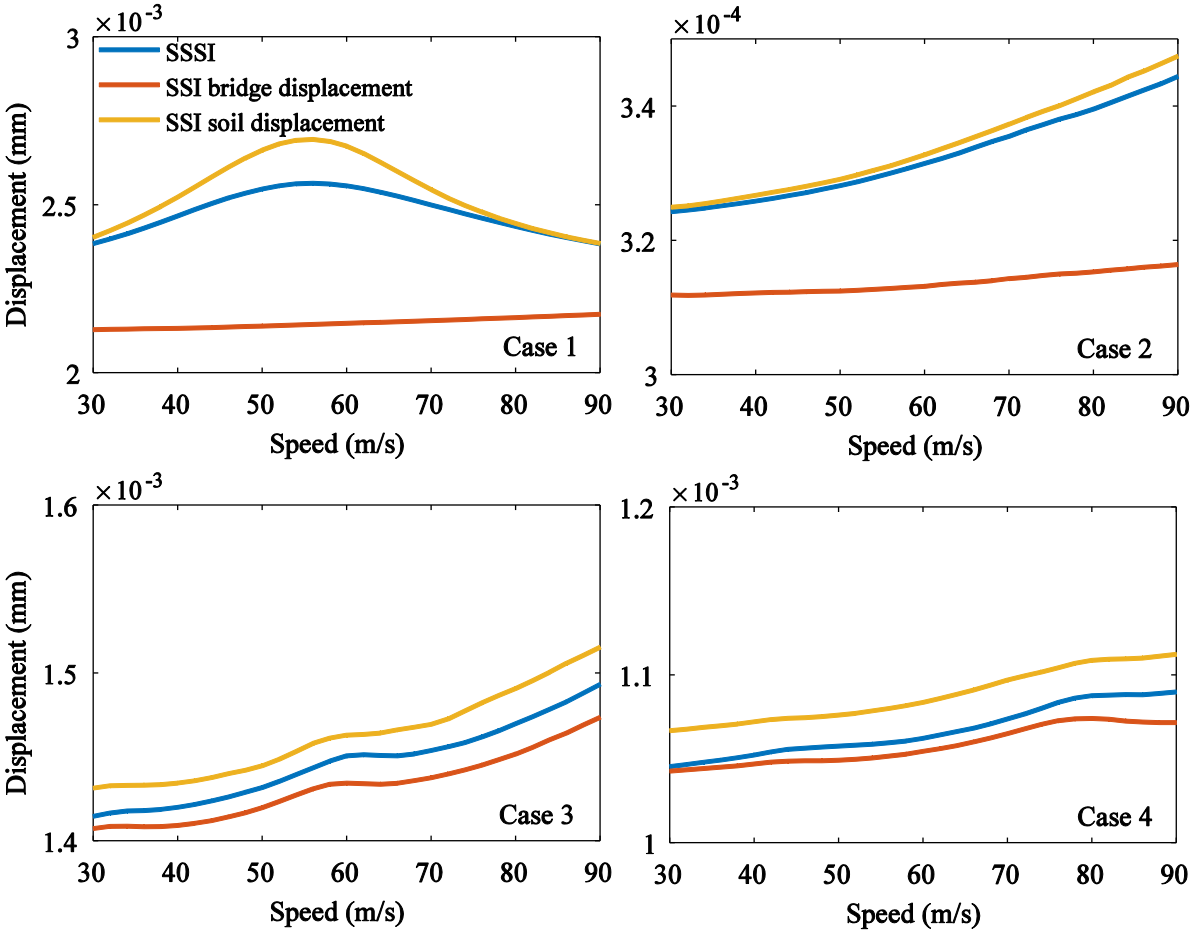

Figure 5 – Maximum absolute bridge displacement dependency on vehicle speed for different soil cases. Results are obtained at the connecting node between pylon and foundation number 6, as well as the soil surface at the same location.

In Figure 5, it can be seen that with the stratification Case 1 there is a critical speed, where the displacements reach critical values. The critical speed is around 56.0m/s, which is very close to the Rayleigh wave speed in clay. However, the bridge model that only considers SSI does not predict a critical speed and the difference between the models reaches up to 25%, which is rather significant. For Cases 2, 3, 4, the maximum displacements are increasing with increasing speed, and no other analysed case showed a critical speed—at least within the used speed limits. All cases show that the

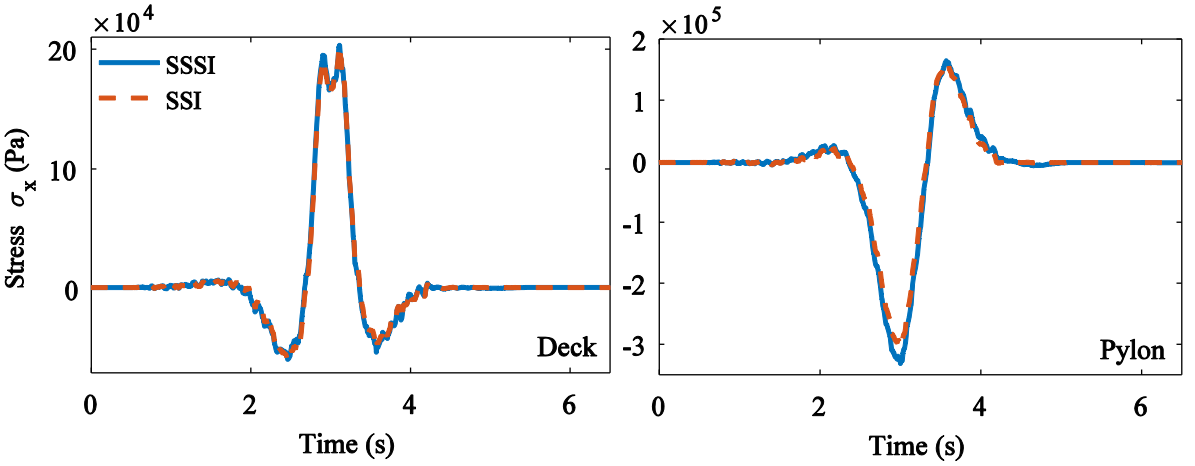

Figure 6 – Stress σ_x acting on a point on the deck and on a point in a pylon. For both cases it is assumed that the distance from the neutral axis is $y = -0.5$m. The vehicle speed is 56 m/s, soil Case 1.

SSI model tends to under-predict the bridge displacement, while the soil displacements are over–predicted. The cases with layered soil generally show a better agreement between the two different approaches, with the difference not exceeding 3%.

Further the stresses acting in the bridge structure were analysed. This time the full model with the multi-degree-of-freedom vehicle and track unevenness was considered. For both SSSI and SSI models the vertical track profiles were the same. Two points were chosen: one in the middle of deck between pylons number 5 and 6, and another one in the middle of pylon number 6. For both points it is assumed that the local normal stress σ_x is analysed at a distance $y = -0.5\text{m}$ from the neutral axis of the cross section. Analysis of different speeds and soil cases showed no significant difference between the stresses obtained from the two different approaches. There is a general trend of increasing stress with increasing vehicle speed due to track unevenness. Figure 6 shows the stresses for soil case 1 with a vehicle speed of 56m/s. This combination provided the biggest differences between the two approaches, but it is still only around 8%. With the other soil cases, there is no significant difference, which leads to the conclusion that SSI models should be adequate for most cases.

5. VIBRATION LEVELS IN THE SURROUNDING SOIL

The displacement caused to the soil that is near the bridge structure are also important, especially in densely populated urban environments, where structures can be very close to railway lines. Two points on the soil surface are investigated, as shown in Figure 4. The vertical displacements were analysed in the frequency domain, by using the SSSI and SSI computational models. Once again, a number of simulations was performed by testing different vehicle speeds and soil stratification cases.

Generally, the SSI model tends to over-predict the soil displacements when compared to the more precise SSSI model. The difference between the models increases with increasing speed, but still the biggest difference arises with soil case 1 (half-space of clay) at the speed of 56m/s. Figure 7 shows the vertical displacements of soil points 1 and 2 in frequency domain, as well as the phase angle. It can be seen that the displacements from the SSI model are higher at both points, while the phase angles are the same.

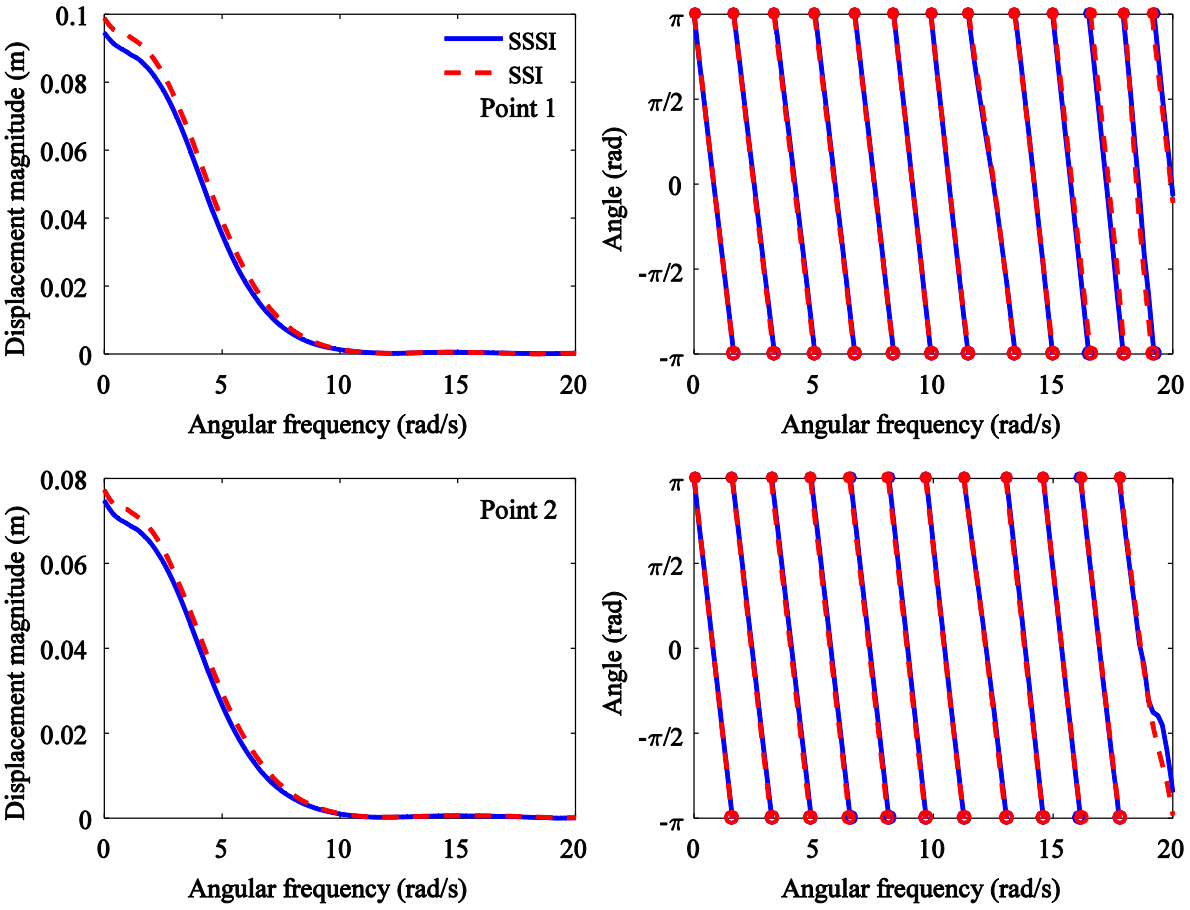

Figure 7 – Displacements in *z*-direction for two points on the soil surface.

6. CONCLUSIONS

A dynamic analysis of an elevated railway track with surface foundations has been carried out. The model includes a simplified vehicle model, vertical railway track unevenness, a FEM-based bridge structure and a soil body. The soil was modelled using two different approaches: one considering only structure–soil interaction (SSI) and another with structure–soil–structure interaction (SSSI). Analyses show that the coupling between the foundations of the bridge through the soil might become an important factor when considering soft soils. In that case, the simpler SSI model is not able to predict the effects caused on the system by the Rayleigh wave. Further, it was observed that the simpler model tends to under-predict the bridge displacements while over-predicting the soil surface displacements. When considering the stresses acting in the bridge structure, which could be important for fatigue calculations, the difference between the models is not very high, even for the worst cases.

The work may be expanded by creating models that are more sophisticated. Introducing a three-dimensional vehicle model, together with vertical and horizontal track unevenness, would allow a more realistic modelling of high frequency vibrations. Further, the bridge structure could also be modelled in three–dimensions, using FEM shell of solid elements. Modelling of the soil response could be expanded by analysing other types of foundations and introducing a simplified model of the structures near the railway track.

To conclude, the SSSI phenomenon is important for this type of structure behaviour, especially when the structure lies on a soft soil. The proposed computational model offers a simplified approach, which could be used for preliminary calculations, while still accounting for the most important factors.

ACKNOWLEDGEMENTS

The authors of the paper would like to show their gratitude to the European Union for financial support via the Interreg V project “Urban Tranquility”.

REFERENCES

1. Frýba L. Vibration of solids and structures under moving loads. Springer Science & Business Media; 2013 Apr 18.
2. Thompson DJ. Wheel-rail noise generation, part III: rail vibration. Journal of sound and vibration. 1993 Mar 8;161(3):421-46.
3. Gry L. Dynamic modelling of railway track based on wave propagation. Journal of Sound and Vibration. 1996 Aug 22;195(3):477-505.
4. Wu TX, Thompson DJ. A double Timoshenko beam model for vertical vibration analysis of railway track at high frequencies. Journal of Sound and Vibration. 1999 Jul 8;224(2):329-48.
5. Wu TX, Thompson DJ. Analysis of lateral vibration behavior of railway track at high frequencies using a continuously supported multiple beam model. The Journal of the Acoustical Society of America. 1999 Sep 1;106(3):1369-76.
6. Lei X, Noda NA. Analyses of dynamic response of vehicle and track coupling system with random irregularity of track vertical profile. Journal of Sound and Vibration. 2002 Nov 14;258(1):147-65.
7. Uzzal RU, Ahmed W, Rakheja S. Dynamic analysis of railway vehicle-track interactions due to wheel flat with a pitch-plane vehicle model. Journal of Mechanical Engineering. 2008;39(2):86-94.
8. Zhai W, Cai Z. Dynamic interaction between a lumped mass vehicle and a discretely supported continuous rail track. Computers & structures. 1997 Jun 30;63(5):987-97.
9. Metrikine AV, Popp K. Instability of vibrations of an oscillator moving along a beam on an elastic half-space. European Journal of Mechanics-A/Solids. 1999 Apr 30;18(2):331-49.
10. Lombaert G, Degrande G, Kogut J, François S. The experimental validation of a numerical model for the prediction of railway induced vibrations. Journal of Sound and Vibration. 2006 Nov 6;297(3):512-35.
11. Andersen L, Clausen J. Efficient modelling of wind turbine foundations. INTECH Open Access Publisher; 2011.
12. Bucinskas P, Agapii L, Sneideris J, Andersen LV. Numerical Modelling of the Dynamic Response of High-Speed Railway Bridges Considering Vehicle-Structure and Structure-Soil-Structure Interaction. In Computational Techniques for Civil and Structural Engineering 2015. Saxe-Coburg Publications.

Paper B2

Lumped-parameter models for structure–soil interaction of multi-span railway bridges

Full reference:

P. Bucinskas, L.V. Andersen, Lumped-parameter models for structure–soil interaction of multi-span railway bridges, Proceedings of the 30th Nordic Seminar on Computational Mechanics (NSCM-30). (2017) 50–53.

Status:

The paper in this chapter has been presented at the international conference NSCM-30, 2017 October 25–27 in Lyngby, Denmark. It has been published in the proceedings of the conference. The contents and typesetting of this chapter are as submitted.

30th Nordic Seminar on Computational Mechanics
NSCM-30
J Høgsberg. N.L. Pedersen (Eds.)
2017

LUMPED-PARAMETER MODELS FOR STRUCTURE–SOIL INTERACTION OF MULTI-SPAN RAILWAY BRIDGES

PAULIUS BUCINSKAS[*] AND LARS V. ANDERSEN[†]

[*] Department of Civil Engineering
Aalborg University
Thomas Manns Vej 23, 9220 Aalborg Ø, Denmark
e-mail: pbu@civil.aau.dk

[†] Department of Engineering
Aarhus University
Inge Lehmanns Gade 10, 8000 Aarhus C, Denmark
e-mail: lva@eng.au.dk

Key words: Structure–soil interaction, railway, dynamic, bridge, lumped-parameter model.

1 INTRODUCTION

High-speed rails are an efficient and fast way of passenger transportation. For medium-distance transportation, a well-developed high-speed railway system can rival transportation by airplane, both by travel time and cost. Due to these reasons, high-speed rails are seeing an increased surge of development across the globe. Unfortunately, increased speeds lead to higher excitations of the exposed infrastructure, which in turn requires better numerical models for proper understanding of its dynamic behaviour.

The dynamic behaviour of systems excited by passing trains is a problem that has been investigated by a large number of researchers. Various analytical solutions and computational models have been created with varying complexity, starting from the most basic analytical solutions for a simply supported beam traversed by a mass to full three-dimensional finite element solutions. However, currently existing methods are often too simplified, disregarding such phenomena as structure–soil–structure interaction, or on the other end—are extremely computationally demanding. This work aims to produce a computational model that considers the most important phenomena such as structure–soil interaction (SSI), stochastic railway track unevenness, vehicle suspension system, etc.

A multi-span bridge structure with surface footings resting on soil is considered. Similar models, modelling the railway track placed directly on the soil surface, have been used by Nielsen et al. [1] and Koroma et al. [2]. However, in this case a bridge structure is introduced. It is modelled using a finite-element (FE) approach using beam elements, with a layered deck structure. Further, the soil is modelled with a semi-analytical approach, as originally proposed by Thomson [3] and Haskell [4]. To transform the solution into time domain, consistent lumped-parameter models (LPMs) are used as described by Wolf [5] and Andersen [6]. The vehicle is modelled as a simplified two-dimensional spring and dashpot system. Further, non-linear Hertzian springs are used to account for wheel–rail interaction including random railway track unevenness.

2 COMPUTATIONAL MODEL

The computational model used is very similar as already presented in previous work [7]. Therefore, only a general description of the model is given.

The vehicle is modelled as a two dimensional system with 10 degrees-of-freedom. This way the model accounts for both primary and secondary suspension of a railway locomotive. Only a single passing vehicle is considered. The railway track and the vehicle interact only through vertical forces and the vehicle travels along the centre line of the bridge.

The bridge structure is modelled using the FE method. Three-dimensional Euler-Bernoulli beam elements with three translational and three rotational degrees of freedom per node are used to model both the bridge deck and the pylons. The railway track is modelled as a layered structure with rails modelled as a single beam discretely connected to single-degree-of-freedom sleepers and further connected to the bridge deck. The rail pads and ballast are modelled as spring/dashpot systems with appropriate stiffness and damping values.

The footings are modelled as rigid slabs resting on the ground surface, and the soil is modelled by a semi-analytical approach employing Green's function in frequency-wavenumber domain to obtain a flexibility matrix for the soil–foundation interface. The flexibility matrix is then inverted and integrated over the interface area to obtain a dynamic stiffness matrix for the foundation system. The bridge structure and the soil interact through structure–soil interaction (SSI) nodes, as shown in Figure 1. However, this approach provides only a frequency domain solution. Thus, LPMs are used as described in Subsection 2.3.

The rail track unevenness is generated from a power density spectrum by assigning random phase angles to each wavenumber. Only vertical track unevenness is considered. Describing the interaction force through a non-linear Hertzian spring requires a time-domain solution as the force needs to be determined by iteration at every time step. Therefore, the whole system needs to be solved in time domain.

To transform the obtained dynamic stiffness matrix of soil to time domain consistent LPM are used. This way, the standard stiffness, damping and mass matrices for soil are obtained, which then can be coupled to the FE bridge structure. Consistent LPMs use a polynomial-fraction approximation to recreate the system behaviour. Curve fitting is performed by changing the polynomial coefficients and polynomial order. This can be done by a least-squares minimization of the error, or in Matlab using the function *invfreqs*.

The obtained solution can then be represented by a combination of linear, first order and second order systems, for which the stiffness, mass and damping matrices are readily available. The approach does introduce some additional degrees-of-freedom in the system, especially when using high order polynomials. However, the number of additional degrees of freedom is low when compared with FE or boundary element solutions.

3 TEST CASE

To test the performance and the solution procedure of the proposed computational model, a test case was created. A bridge structure with three pylons is analysed, as shown in Figure 1. The material and cross-sectional parameters of the bridge are the same as in [7]. The distance between footings is 30 m. The footings are resting on a 5 m layer of soft soil (the primary wave

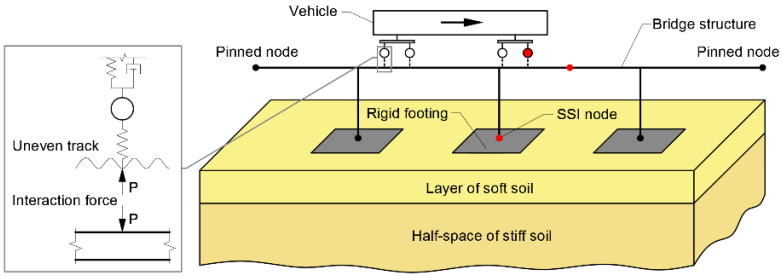

Figure 1: Analysed case: bridge structure supported by three pylons, with rigid footings resting on the soil surface. Red dots indicate positions from which results were extracted.

speed is $c_P = 116$ m/s and the secondary wave speed $c_s = 62$ m/s) with an underlying half-space of stiffer soil ($c_P = 414$ m/s and $c_s = 169$ m/s). Three different speeds of the vehicle are tested: 30 m/s, 60 m/s and 90 m/s. For each speed, 100 simulations are performed, each time generating new random rail profile. The wavelengths used for the rail-profile generation are between 0.2 m and 100 m. Three points of interest are checked: the first wheel of the vehicle, the rail in the middle between second and third pylon and the SSI node of the second footing.

4 RESULTS AND DISCUSSION

The Fourier transform of the wheel–rail interaction forces, as experienced by the first wheel of the vehicle, is shown in Figure 2. The coloured area represents the maximum and minimum values, while the darker lines show the mean values from all simulations. It can be seen that with increasing vehicle speeds, the interaction forces become higher and, furthermore, a wider frequency range is excited. Some peaks are at the same frequencies no matter the vehicle speed. This is due to excitation of eigenmodes of various parts of the vehicle and the structure. Other peaks are only observed at certain speeds and are caused by wheels passing certain parts of the structure, such as the wheel passing the discrete sleepers—at 60 Hz for vehicle speed of 30m/s, 100 Hz for 60 m/s, and 150 Hz for 90 m/s.

Further, Figure 3 shows the acceleration of the rail in the middle of a span and at the SSI node of the second footing. The same trend can be seen as for the wheel–rail interaction forces, with higher vehicle speeds leading to higher excitation. However, especially for the rail, the excited frequency range is spread out through a wider frequency range. Comparing the response at the rail and SSI node, it is evident that the response is reduced significantly closer to the soil,

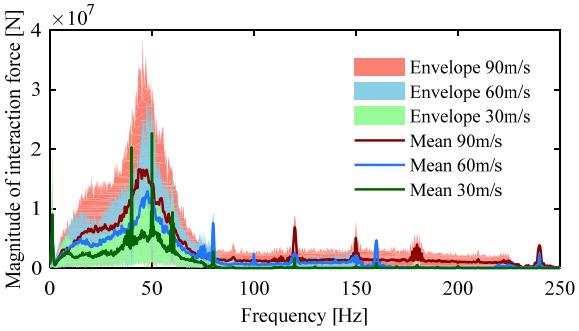

Figure 2: Fourier coefficients for wheel–rail interaction force for the first wheel of the vehicle.

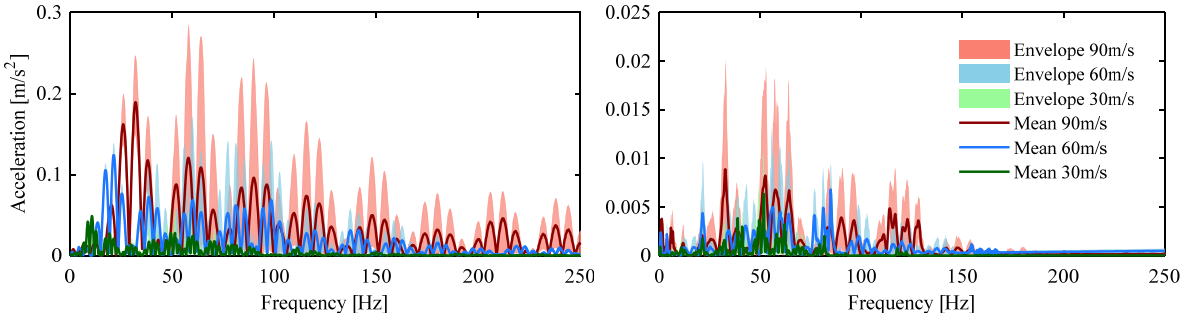

Figure 3: System excitation. On the left—rail, on the right—SSI node.

with high-frequency response (above 150 Hz) disappearing almost completely. Finally, the response at the SSI node shows that at some frequencies the excitations at 60 m/s and 90 m/s are almost equal. This can be caused by the Rayleigh wave travelling in the soft top layer of soil, when the wave speed is close to the vehicle speed.

4 CONCLUSION

- The proposed model of a railway bridge interacting with soil offers an approach that can be used in early design phases, when considering elevated railway tracks.
- Stochastic railway track unevenness, vehicle speed and structure–soil interaction all have an effect of the system behavior and must be considered when modelling such systems.

ACKNOWLEDGMENTS

The research was carried out in the framework of the project “Urban Tranquility. The authors of this work gratefully acknowledge the Interreg V European Regional Development Fund for the financial support.

REFERENCES

[1] J.C. Nielsen, G. Lombaert, S. François, “A hybrid model for prediction of ground-borne vibration due to discrete wheel/rail irregularities”, *Journal of Sound and Vibration*, **345**, 103-20 (2015).

[2] S.G. Koroma, D.J. Thompson, M.F. Hussein, E. Ntotsios, “A mixed space-time and wavenumber-frequency domain procedure for modelling ground vibration from surface railway tracks”, *Journal of Sound and Vibration*, **32**, 400–508 (2017).

[3] W. T. Thomson, “Transmission of elastic waves through a stratified solid medium”, *Journal of applied Physics*, **21.2**, 89–93 (1950).

[4] N. A. Haskell, “The dispersion of surface waves on multilayered media”, *Journal of Sound and Vibration*, **43.1**, 17–34 (1953).

[5] J. P. Wolf, “Consistent lumped-parameter models for unbounded soil: Frequency-independent stiffness, damping and mass matrices”, *Earthquake Engineering & Structural Dynamics*, **20(1)**, 33–41 (1991).

[6] L. Andersen, “Assessment of lumped-parameter models for rigid footings”, *Computers & structures*, **88(23)**, 1333-1347 (2010).

[7] P. Bucinskas, L. Agapii, J. Sneideris, L.V. Andersen, “Numerical modelling of the dynamic response of high-speed railway bridges considering vehicle-structure and structure-soil-structure interaction”, *Computational Techniques for Civil and Structural Engineering,* 125-152 (2015).

Paper B3

Dynamic response of vehicle–bridge–soil system using lumped-parameter models for structure–soil interaction

Full reference:

P. Bucinskas, L.V. Andersen, Dynamic response of vehicle–bridge–soil system using lumped-parameter models for structure–soil interaction. Under review in Computers and Structures, initial submission 2019 April 30, revised submission 2019 September 18.

Status:

This chapter presents the manuscript submitted to Computers and Structures journal on 2019 April 30. A revised version of the manuscript has been resubmitted on 2019 September 18 and is currently under review. The contents of this chapter are as revised submission, with minor typesetting changes.

Dynamic response of vehicle–bridge–soil system using lumped-parameter models for structure–soil interaction

Paulius Bucinskas[1] and Lars Vabbersgaard Andersen[1]

[1]Department of Engineering, Aarhus University, Aarhus, Denmark

Abstract

Prediction of vibrations generated by railway traffic experiences an increasing interest, as new lines are being constructed and planned in many countries. The paper proposes a numerical model to analyse a coupled vehicle–bridge–soil system, taking into account the most important phenomena affecting the structure, while at the same time being comparatively computationally efficient. Such model is useful in the early design phases of a project, when analysing a range of possible configurations or conducting parametric analysis is required.

A simplified vehicle model, nonlinear wheel–rail interaction, a bridge structure modelled using the finite-element method and a semi-analytical model for layered soil are all introduced in the model. A pure time-domain solution procedure is used, utilizing lumped-parameter models (LPMs) for the soil–foundation system. Representation of the dynamic stiffness matrix using LPMs is investigated by analysing the cross-coupling between footings and a novel procedure necessary for computationally stable LPMs is introduced and utilized. Further, pure time-domain solution is compared with an iterative mixed-domain solution. Finally, to illustrate the capabilities of the model, analyses are carried out to determine the resulting maximum and minimum excitation limits resulting from wheel–rail interaction on a number of randomly generated uneven track profiles.

Keywords: high-speed railways, railway bridge, multi-degree-of-freedom vehicle, wheel–rail interaction, soil–structure interaction, lumped-parameter models.

1 Introduction

Environmental vibrations and resulting reradiated noise lead to annoyance and even possible health concerns to the exposed population [1, 2]. One of the main sources of

these vibrations is railway lines. Therefore, train-induced ground vibrations must be considered when designing or upgrading new railway lines—especially the development of new high-speed lines, railway stations and metro lines close to already existing urban centres. Close proximity to existing structures does not allow the vibrations to properly dissipate, thus resulting in high vibration levels at the structures. An analysis of multiple technical reports, performed by Connolly et al. [3], showed that in around half of the projects additional mitigation measures had to be implemented. Computational models can be used in such cases to identify the problematic areas and alter the project design pro-actively, which saves both funds and time.

Environmental vibrations have been studied extensively and a large number of numerical models already exist. Sheng et al. [4] proposed a model combining a layered railway track with the underlying soil. The solution was obtained in a moving frame of reference, where the rails are represented as a single Euler-Bernoulli beam supported by a continuous layered track structure. The soil was modelled using a semi-analytical approach proposed by Thomson [5] and Haskell [6]. The model was further expanded to include wheel–rail interaction [7]. Thus, various multi-degree-of-freedom vehicle models together with an uneven track profile can be included in the analysis. The created approach was then used for development of a TGV (train-induced ground vibration) model [8]. More complex models, with less simplifications, are also used. Kouroussis et al. [9, 10] modeled a similar vehicle, track and soil system, where the soil is modelled using the finite-element method (FEM) combined with infinite elements. Infinite elements are used to avoid wave reflection from the artificial boundaries of the finite-element (FE) model. Further, Koroma et al. [11] modelled the railway track with nonlinear track parameters. The semi-analytical soil model is used to obtain the dynamic soil behaviour, to which lumped-parameter models (LPMs) are fitted. The use of LPMs allows a time-domain solution, which is needed to analyse the nonlinear track behaviour. A more detailed overview of models for predicting ground vibration from railways can be found in the work by Kouroussis et al. [12].

Including a bridge structure into the system changes the system behaviour. The dynamic response of railway bridges traversed by vehicles, has been studied extensively. For example a simple two-dimensional system with a layered track structure has been developed by Cheng et al. [13]. A more complex model involving a three-dimensional bridge structure modelled with shell elements, traversed by a three-dimensional vehicle, has been used by Song et al. [14]. A detailed literature review of the problem has been conducted by Cantero et al. [15]. However, most of the studies do not include the underlying soil, often assuming the soil to be completely rigid. Computational models that include the structure–soil interaction are much less frequent. Ülker-Kaustell et al. [16] analysed the structure–soil interaction for a single-span railway bridge. The soil was modelled with a three-dimensional FE model from which the dynamic stiffness for the foundations was obtained. The bridge structure was modelled as a simple Euler-Bernoulli beam with added dynamic stiffness of the foundations. Only point loads were used to represent the vehicle; thus a frequency domain solution was sufficient. Romero et al. [17] have studied a similar single span bridge structure. However, their model includes a full three-dimensional FE shell-element model of the bridge

coupled with boundary elements (BEs) to model the soil. Further, the structure is excited by a traversing multi-degree-of-freedom vehicle model. Takemiya and Bian [18] analyse a multi-span railway bridge structure. Their model accounts for the vehicle with point loads at the wheel possitions, and the bridge structure is simplified to Euler-Bernoulli beam elements. To model the soil, a similar approach to Ülker-Kaustell et al. [16] was taken, where a single foundation is modelled in a three-dimensional FE model from which, assuming rigid footing movement, a dynamic stiffness matrix for a single footing is obtained.

Overall, reaserchers often choose the FEM combined with special boundary conditions to model the soil. The FEM is advantageous, since time-domain solution of the system is possible, allowing analysis of nonlinear behaviour, such as the nonlinear wheel rail interactions. Further, the method is very flexible making it ideal when modelling systems with complex geometry. However, using the FEM to model the soil unavoidably requires large computational effort. This is due to the unbounded nature of the soil, which requires special non-reflecting boundary conditions or large computational domains to be properly accounted for, as described by Andersen et al. [19]. An alternative to this is the semi-analytical approach derived by Thomson [5] and Haskell [6]. The approach can be implemented using the originally proposed flexibility-based layer-transfer-matrix method (as implemented by Sheng et al. [4]) or a stiffness approach proposed by Kausel and Roesset [20]. The computational effort needed for the semi-analytical is much smaller when compared to FE or BE approaches. However, the solution is only available in frequency domain. This problem is often overcome by implementing a two-step solution in which the computational domain is split into two parts. Usually, the structure interacting directly with the wheels is analysed in time domain, assuming the soil to be rigid. Then, the obtained interaction loads are applied to the soil [9, 10, 21, 22]. The approach disregards some interactions present in the real system. However, it is assumed to be acceptable for stiff soil conditions.

Another way of solving the system in time domain is to use LPMs as proposed by Wolf [23, 24]. This way the soil behaviour is represented by a system of springs, dashpots and masses. This approach is advantageous because the obtained model can easily be added to already established FE matrices for the structure. As already discussed, this approach has been utilized by Koroma et al. [11] to analyse a railway track placed on the soil surface. The work uses LPMs to represent the behaviour of the sleepers resting on the soil, including the coupling between the sleepers through soil. Similarly the LPMs have been utilized for a multi-span bridge structure by Carbonari et al. [25]. However, the work analyses the seismic structure behaviour and does not consider vehicle excitation. An alternative approach to using two-step solutions and LPM could be the hybrid approaches. A hybrid-frequency-time-domain (HFTD) formulation for structure–soil interaction problems has been demonstrated by Darbre and Wolf [26] and Nimtaj and Bagheripour [27]. Alternatively, a hybrid-time-frequency-domain (HTFD) approach was introduced by Bernal and Youssef [28]. In practise both approaches are similar with the nonlinear behaviour being approximated through linear mass, damping and stiffness matrices. The differences between the ap-

proximate linear and real nonlinear behaviours are accounted for by corrective forces, and iteration is performed until convergence is reached.

From the overview of previous works, it can be seen that modelling a bridge–soil system traversed by a vehicle is a rather difficult task. The bridge structure is naturally finite, not allowing the usage of periodic or movement-direction-invariant solutions. And, if the vehicle is represented by any sort of multi-degree-of-freedom system, the system becomes time dependent, making the use of frequency domain solutions difficult. Thus, using approaches formulated in the time domain is preferable. However, both FE and BE formulations require long computation times making their use rather limited, especially in cases where nonlinear system response requires multiple iterations for every time step. The aim of this work is to create an efficient computational model for modelling such systems. The model could be used for predicting vibration levels in both the bridge and other nearby structures, excited by the passing vehicle. Prediction of small amplitude 'annoying' vibrations is the main objective, and therefore linear system behaviour for both the soil and bridge are assumed. The model uses a number of previously available methods that are combined together to model a rather complex system response over a wide frequency range. An efficient semi-analytical soil model is utilized, that is commonly used for environmental vibration prediction from surface rail lines. However, the semi-analytical solution is only available in the frequency domain, thus requiring special handling. LPMs are used to convert the frequency-domain solution to time-domain, allowing the system to be solved. However, it has been found, that the system can become unstable due to LPMs being fitted over a wide frequency range, even when ensuring that no poles with positive real part exist and an unconditionally stable time integration scheme is used. Thus, an additional procedure is created and described that is needed to establish stable LPMs. Further, the solution procedure is compared with a mixed-domain solution, previously developed by the authors in [29]. The final model is a coupled vehicle–bridge–soil system, that includes a multi-degree-of-freedom vehicle model, nonlinear wheel–rail interaction, FE bridge structure with layered deck and semi-analytical soil model. The system is excited by a passing vehicle, including both quasi-static and dynamic effects, due to the rail unevenness. Nonlinear wheel–rail interaction was included in the model to better represent the real system behaviour and to expand the capabilities of the model, for modelling cases such as: large faults on the rails or hanging sleepers. The created model is used to analyse a multi-span railway bridge structure traversed by a single vehicle. However, the methodology presented can be easily applied to other similar structures where time domain solution is needed.

Section 2 introduces the separate parts of the model: the vehicle, the bridge structure and the soil. Further, Section 3 describes the different computational approaches used to solve the system including the vehicle–track interaction model. Finally, Section 4 uses the described computational model to analyse illustrative examples.

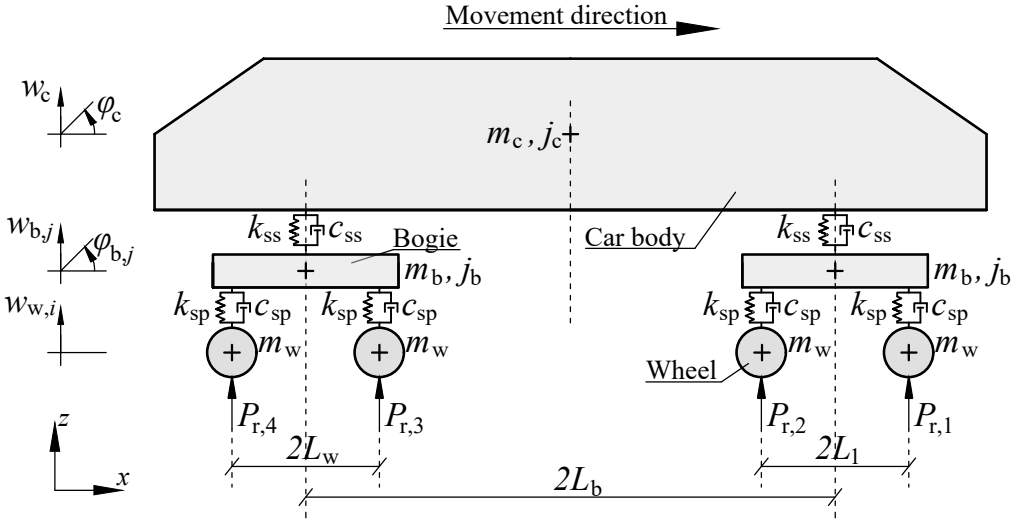

Figure 1: Multi-degree of freedom vehicle model.

2 Modelling approach

To model an elevated railway line the problem can be split into three separate parts: the vehicle, the bridge structure (including the track system) and the soil body (including the foundations). Each of these parts need to be considered and properly accounted for in order to obtain realistic dynamic behaviour of the total system. The three parts of the system are described in more detail in this section.

2.1 Vehicle, bridge and railway track models

The vehicle travelling across the bridge deck introduces dynamic excitation to the system. The acting loads depend on a number of factors, such as the vehicle weight, travel speed, track construction and unevenness characteristics, vehicle suspension system, etc. To model the vehicle, a 10-degree-of-freedom system is introduced, as shown in Figure 1 and and decribed in [7, 30, 31]. The system is modelled in two dimensions and only considers vertical interaction between the rails and the wheel. However, it is still able to model the most important contributions from a vehicle, moving on a straight track. This configuration represents a two-layered suspension system, with primary suspension connecting the four wheels to two bogies and secondary suspension systems connecting the bogies to the main car body. Each wheel represents a wheel set of a real train. The mass, damping and stiffness properties needed to model the vehicle are illustrated in Figure 1. The equation of motion for the vehicle can be

written as:

$$[\mathbf{M}_\mathrm{V}]\{\ddot{\mathbf{u}}_\mathrm{V}\} + [\mathbf{C}_\mathrm{V}]\{\dot{\mathbf{u}}_\mathrm{V}\} + [\mathbf{K}_\mathrm{V}]\{\mathbf{u}_\mathrm{V}\} = \{\mathbf{f}_\mathrm{V}\}, \tag{1}$$

where $[\mathbf{M}_\mathrm{V}]$, $[\mathbf{C}_\mathrm{V}]$, $[\mathbf{K}_\mathrm{V}]$ are the mass, damping and stiffness matrices, respectively. Further, $\{\mathbf{u}_\mathrm{V}\}$ is the displacement vector, while $\{\dot{\mathbf{u}}_\mathrm{V}\}$ and $\{\ddot{\mathbf{u}}_\mathrm{V}\}$ denote the first and second time derivatives.

The bridge structure is modelled using the FEM. Beam elements are used to model the bridge deck and the pylons. The pylons are fixed to the deck through shared nodes, where both the translational and rotational degrees of freedom are coupled. Each element has two nodes, with three degrees-of-freedom in each node. The structure is placed in the (x,z) plane and beam bending around the y-axis is accounted for by using Euler-Bernoulli beam theory. Further, axial deformation is assumed to be uncoupled from the other degrees of freedom.

The properties of the bridge deck are: Young's modulus E_d, moment of inertia I_d, mass density ρ_d and cross-sectional area A_d. Similarly, the same properties are needed for the bridge pylons, they are denoted with subscript 'p'. The mass, damping and stiffness matrices, $[\mathbf{M}_\mathrm{B}]$, $[\mathbf{C}_\mathrm{B}]$ and $[\mathbf{K}_\mathrm{B}]$, for the FE model are obtained by the standard Galerkin approach. Cubic interpolation functions are used for bending and linear interpolation functions are employed for axial deformation. The equation of motion for the bridge structure can then be written as:

$$[\mathbf{M}_\mathrm{B}]\{\ddot{\mathbf{u}}_\mathrm{B}\} + [\mathbf{C}_\mathrm{B}]\{\dot{\mathbf{u}}_\mathrm{B}\} + [\mathbf{K}_\mathrm{B}]\{\mathbf{u}_\mathrm{B}\} = \{\mathbf{f}_\mathrm{B}\}, \tag{2}$$

where $\{\mathbf{u}_\mathrm{B}\}$ is the displacement vector of the bridge, with $\{\dot{\mathbf{u}}_\mathrm{B}\}$ and $\{\ddot{\mathbf{u}}_\mathrm{B}\}$ indicating first and second time derivatives (velocity and acceleration), respectively. Both dynamic wheel–rail interaction forces and the

In this work, a ballasted railway track on the bridge deck is modelled. Therefore, a layered bridge structure is introduced, as illustrated in Figure 2. The track structure is then composed of: rail, rail pads, sleepers, ballast, and the bridge deck. The two rails of a track are modelled as a single Euler-Bernoulli beam in two-dimensions (i.e. (x,z) plane in the global coordinate system, see Figure 2. No axial deformation of the rail is considered, thus the used rail properties are: Young's modulus E_r, moment of inertia I_r, mass density per unit length μ_r. The forces $P_{\mathrm{w},i}$, resulting from the vehicle wheels including both the dynamic and quasi-static effects, are stored in the force vector $\{\mathbf{f}_\mathrm{B}\}$. Further, the rail is discretely supported by rail pads which are modelled as springs and a dashpots connected in parallel, with stiffness k_rp and damping c_rp. Further, the dashpots are connected to the sleepers. Each sleeper has just one degree of freedom, i.e. translation in the z-direction, and the associated mass m_sl. Further, the sleepers are placed on the ballast of the track. The ballast is once again modelled as a spring and dashpot system, with stiffness k_bl and damping c_bl, that is then connected to the bridge deck. It is assumed that one quarter of the ballast mass m_bl is moving with the sleepers and the rest is moving with the deck.

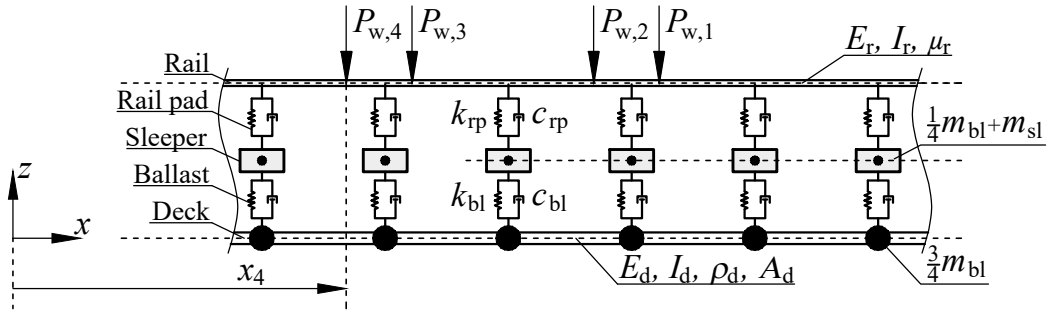

Figure 2: Simplified bridge structure for a single span. The deck and pylons of the bridge are modelled as three-dimensional beam elements. The track is modelled as a layered structure connected through spring and dashpot systems.

2.2 Soil–structure interaction in frequency domain

The soil is modelled using a semi-analytical approach. The approach uses the Green's function to evaluate the soil response in the frequency–wavenumber domain. The frequency–wavenumber domain is used, since the analytical solution employed to evaluate the Green's function is only available in this domain. The Green's function relates the displacements and traction applied in the soil stratum:

$$[\bar{\mathbf{G}}_S]\{\bar{\mathbf{P}}_S\} = \{\bar{\mathbf{U}}_S\}, \tag{3}$$

where $[\bar{\mathbf{G}}_S]$ is the Green's function, $\{\bar{\mathbf{P}}_S\}$ is the traction vector and $\{\bar{\mathbf{U}}_S\}$ is the displacement vector. All these terms are in the frequency–wavenumber domain.

To obtain the Green's function, the transfer-matrix method is used, originally developed by Thomson [5] and Haskell [6]. According to this method, the state at the top of a soil layer, including the displacements and tractions applied, is related to the state at the bottom of the same layer through the transfer matrix. Using these transfer matrices, a soil stratum containing multiple layers can be assembled and, after applying the boundary conditions, an analytical expression for the Green's function is obtained. The applied boundary conditions can account for either an underlying half-space of soil or fixed displacements at a certain depth. The originally proposed flexibility based approach is sufficient when considering relatively low frequencies or cases where only a half-space of soil is present. However, when high frequencies or very deep layers are considered the approach does encounter numerical stability problems, caused by limited precision of computers. In those cases, different layer assembly methods can be used that include additional numerical stabilization procedures. The present implementation is based on the approach described by Wang [32].

After the Green's function has been found, the solution needs to be converted into stiffness expression in spatial domain in order to couple it to the structures. This is established through a number of steps. Firstly, the frequency–wavenumber domain

solution is transformed into frequency-spatial domain solution, using double discrete inverse Fourier transformation. Here, a bell shaped load (two-dimensional Gaussian distribution) with a unit magnitude is applied to obtain the flexibility (receptacle) of the soil. The bell shape is beneficial for the computations, as in the wavenumber domain it approaches zero monotonically with increasing wavenumber. The analysed rigid footings are discretized into a number of discretization nodes, as illustrated in Figure 3 for single a footing. Through these nodes the structure (in this case a pylon) interacts with the soil stratum. A global flexibility matrix is constructed, by placing a load on a discretization node and then checking the displacements in all nodes in the soil–foundation interface of all footings. This is repeated for all of the nodes to establish the relation between all of the considered points. Further, the flexibility matrix in inverted to obtain the corresponding dynamic stiffness matrix. When considering rigid bodies, such as the rigid surface footings for the analysed case, an integration over the area of each footing is also needed, which results in a reduction of the matrix size corresponding to six degrees of freedom per rigid footing. Finally, the dynamic stiffness matrix for the soil $[\mathbf{D}_\mathrm{S}]$ is obtained. A detailed explanation of the methodology used, including modelling of rigid objects can be found in works by Andersen and Clausen [33, 34].

The described semi-analytical model is an attractive approach to modelling the soil due to the low computational effort needed. It can be easily expanded to include additional rigid objects or FE structures interacting with the bridge through the soil. However, in cases when a more detailed soil model is necessary, different approaches, such as FE and BE methods or even experimental measurements, can be used, as long as the dynamic flexibility or stiffness matrix of the soil $[\mathbf{D}_\mathrm{S}]$ can be obtained.

In order, to couple to the soil the bridge FE matrices are converted to the dynamic stiffness matrix needed for the frequency-domain solution:

$$[\mathbf{D}_\mathrm{B}] = [\mathbf{K}_\mathrm{B}] + \mathrm{i}\omega[\mathbf{C}_\mathrm{B}] - \omega^2[\mathbf{M}_\mathrm{B}]. \tag{4}$$

Further, the matrix is rearranged and split into sub-matrices:

$$[\mathbf{D}_\mathrm{BS}] = \begin{bmatrix} [\mathbf{D}_\mathrm{B}^\mathrm{bb}] & [\mathbf{D}_\mathrm{B}^\mathrm{fb}] \\ [\mathbf{D}_\mathrm{B}^\mathrm{bf}] & [\mathbf{D}_\mathrm{B}^\mathrm{ff}] \end{bmatrix}. \tag{5}$$

For foundation nodes that are directly interacting with the soil, the sub-matrix is denoted with superscript “ff”, while nodes above the soil (no direct interaction with soil) are denoted with “bb”. Coupling terms are denoted as “bf” and “fb”, and it is noted that $[\mathbf{D}_\mathrm{B}^\mathrm{fb}] = [\mathbf{D}_\mathrm{B}^\mathrm{bf}]^\mathrm{T}$.

Now the soil can be coupled to the bridge structure above. The bridge and soil share the same structure–soil interaction (SSI) nodes, where the pylons meet the rigid footings. Both translational and rotational degrees of freedom are coupled between lower ends of the pylons and the corresponding footings, resulting in a fixed connection between them. An SSI node is illustrated in Figure 3. The equation of motion of the bridge–soil system becomes:

$$[\mathbf{D}_\mathrm{BS}]\{\mathbf{U}_\mathrm{BS}\} = \{\mathbf{F}_\mathrm{BS}\} \tag{6}$$

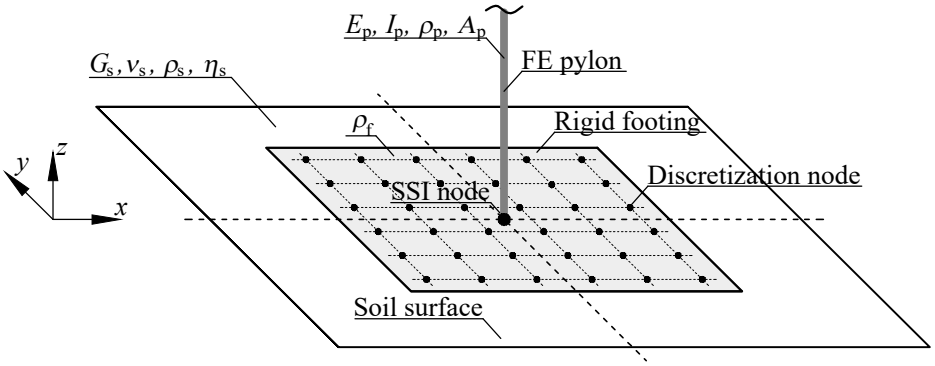

Figure 3: Single rigid footing discretization

where $[\mathbf{D}_{BS}]$ is the dynamic stiffness matrix for the bridge–soil system, $\{\mathbf{U}_{BS}\}$ is the nodal displacement vector, and $\{\mathbf{F}_{BS}\}$ is the nodal force vector in frequency domain:

$$[\mathbf{D}_{BS}] = \begin{bmatrix} [\mathbf{D}_B^{bb}] & [\mathbf{D}_B^{fb}] \\ [\mathbf{D}_B^{bf}] & [\mathbf{D}_B^{ff}] + [\mathbf{D}_S] \end{bmatrix}, \tag{7a}$$

$$\{\mathbf{U}_{BS}\} = \left\{ \{\mathbf{U}^{bb}\}^T \quad \{\mathbf{U}^{ff}\}^T \right\}^T, \tag{7b}$$

$$\{\mathbf{F}_{BS}\} = \left\{ \{\mathbf{F}^{bb}\}^T \quad \{\mathbf{F}^{ff}\}^T \right\}^T. \tag{7c}$$

2.3 Soil–structure interaction in time domain

To obtain a time-domain solution, the same steps as in the previous section are taken to obtain the dynamic stiffness matrix of the soil $[\mathbf{D}_S]$. Then, instead of converting the bridge FE solution into frequency domain, the soil solution is converted into time domain. However, transforming the dynamic stiffness matrix $\mathbf{D}_S$ into separate stiffness, damping and mass matrices is not a straightforward task. For that LPMs are utilized. LPMs were proposed by Wolf in [23, 24].

An LPM works by reproducing the real system behaviour with an artificial system of springs, dashpots and masses. This way a large domain with a high number of degrees of freedom can be reduced into a much simpler system with fewer degrees of freedom. Another advantage of an LPM is that a frequency-domain behaviour can be recreated by a relatively simple system, for which separate stiffness, damping and mass matrices are readily available. This work uses consistent LPMs which allow better representation of the real system behaviour. Using this approach, higher-order systems with multiple degrees of freedom are fitted, which can include linear, first-order and second-order terms, or a combination of such terms. A detailed description of consistent LPMs can be found in [33].

Soil behaviour in frequency domain can be reproduced as:

$$[\mathbf{D}_{\mathrm{S}}(\omega)]\{\mathbf{U}_{\mathrm{S}}(\omega)\} = \{\mathbf{F}_{\mathrm{S}}(\omega)\}, \tag{8}$$

where the dynamic stiffness matrix $[\mathbf{D}_{\mathrm{S}}(\omega)]$ relates the displacements $\{\mathbf{U}_{\mathrm{S}}(\omega)\}$ and forces $\{\mathbf{F}_{\mathrm{S}}(\omega)\}$. A non-dimensional frequency is introduced:

$$a_0 = \frac{\omega R_0}{c_0}, \tag{9}$$

where R_0 is the characteristic size of the footing and c_0 is a characteristic wave speed. For example, when considering a square footing, R_0 could be the length of one side and c_0 the shear wave velocity in soil. Using the non-dimensional frequency, a dynamic stiffness component of the soil–foundation system is put in the form:

$$Z(a_0) = Z(\omega c_0/R_0) = D_{\mathrm{S}}(\omega). \tag{10}$$

where $D_{\mathrm{S}}(\omega)$ is a single element of matrix $[\mathbf{D}_{\mathrm{S}}(\omega)]$, e.g. $[\mathbf{D}_{\mathrm{S},11}(\omega)]$. A normalized frequency-dependent dynamic stiffness coefficient $S(a_0)$ is introduced as:

$$Z(a_0) = K_{\mathrm{s}} S(a_0), \tag{11}$$

where K_{s} is the corresponding static stiffness component. The stiffness coefficient is approximated as:

$$S(a_0) \approx k^{\infty} + \mathrm{i}a_0 c^{\infty} + \frac{1 - k^{\infty} + p_1(\mathrm{i}a_0) + p_1(\mathrm{i}a_0)^2 + ... + p_{M-1}(\mathrm{i}a_0)^{M-1}}{q_0 + q_1(\mathrm{i}a_0) + q_1(\mathrm{i}a_0)^2 + ... + q_M(\mathrm{i}a_0)^M}. \tag{12}$$

The term q_0 could be conveniently chosen to be equal to 1, thus ensuring double a asymptotic solution. However, it is not possible when using some inbuilt functions in programming languages, such as *invfreqs* in MATLAB [35]. In that case, precise solution at $a_0 = 0$ can be ensured by using an additional weight function, with high weights for low frequencies. Further, parameters p_i and q_i should always be real and no poles should appear along the positive real axis. This way the filter is physically meaningful and in theory should not cause instability issues in time domain. However, this is not the case when high order filters fitted over a wide frequency range are used. In those cases, a procedure introduced in Section 6.2 is needed.

Equations 10–12 describe the force–displacement relation for a single degree of freedom. Thus, the described procedure needs to be repeated for every degree of freedom interacting with soil. Further, coupling terms might also need to be represented to obtain realistic behaviour of the structure.

After approximating the chosen terms of the dynamic stiffness matrix, the stiffness matrix $[\mathbf{K}_{\mathrm{LPM}}]$, mass matrix $[\mathbf{M}_{\mathrm{LPM}}]$ and damping matrix $[\mathbf{C}_{\mathrm{LPM}}]$ of the LPM are obtained. The bridge–soil system matrices can then be assembled:

$$[\mathbf{K}_{\mathrm{BS}}] = \begin{bmatrix} [\mathbf{K}_{\mathrm{B}}^{\mathrm{bb}}] & [\mathbf{K}_{\mathrm{B}}^{\mathrm{bf}}] & \mathbf{0} \\ [\mathbf{K}_{\mathrm{B}}^{\mathrm{fb}}] & [\mathbf{K}_{\mathrm{B}}^{\mathrm{ff}}] + [\mathbf{K}_{\mathrm{LPM}}^{\mathrm{ff}}] & [\mathbf{K}_{\mathrm{LPM}}^{\mathrm{fi}}] \\ \mathbf{0} & [\mathbf{K}_{\mathrm{LPM}}^{\mathrm{if}}] & [\mathbf{K}_{\mathrm{LPM}}^{\mathrm{ii}}] \end{bmatrix}, \tag{13}$$

where the degrees of freedom of the foundation are indicated with the superscript “ff”, internal degrees of freedom in the LPM—“ii” and of the bridge—“bb”. Combinations of superscripts are used for coupling terms. Further, in a similar way, the system mass matrix$[\mathbf{M}_{\mathrm{BS}}]$ and damping matrix $[\mathbf{C}_{\mathrm{BS}}]$ are assembled. The equation of motion for the bridge–soil system becomes:

$$[\mathbf{M}_{\mathrm{BS}}]\{\ddot{\mathbf{u}}_{\mathrm{BS}}\} + [\mathbf{C}_{\mathrm{BS}}]\{\dot{\mathbf{u}}_{\mathrm{BS}}\} + [\mathbf{K}_{\mathrm{BS}}]\{\mathbf{u}_{\mathrm{BS}}\} = \{\mathbf{f}_{\mathrm{BS}}\}. \tag{14}$$

3 Method of analysis

3.1 Track irregularities and wheel–rail interaction

A vehicle wheel travelling along the rail is exposed to track irregularities, which introduce additional excitation to the system. Railway track unevenness is a stochastic property and depends on a number on factors. It is described using power spectral density functions which describe the unevenness distribution through wavenumbers. The functions are generally determined empirically. A number of formulations exist, however the most widely used are the FRA (Federal Railway Administration), the German, the SNCF (Socit Nationale des Chemins de Fer Franais) and the Chinese power spectral density function standards, as described in [12, 15, 36]. Comparison between different standards is difficult due to different definitions used for each spectrum. For example, some are only valid for specific wavenumber ranges or vehicle speeds. In this work the German track spectrum is used, as found in [15]:

$$S(k) = \frac{A_{\mathrm{p}} k_{\mathrm{c}}}{(k^2 + k_{\mathrm{r}}^2)(k^2 + k_{\mathrm{c}}^2)}, \tag{15}$$

with coefficients $k_{\mathrm{c}} = 0.8246$ rad/m and $k_{\mathrm{r}} = 0.0206$ rad/m. For a medium quality track, $A_{\mathrm{p}} = 5.9233 \times 10^{-7}$ rad·m. From the power spectral density function, the track profile can be generated by assigning random phase angles to the wavenumbers and performing inverse Fourier transformation into spatial domain. In this work only vertical track irregularities are considered, as usually done in the literature [7, 9, 10].

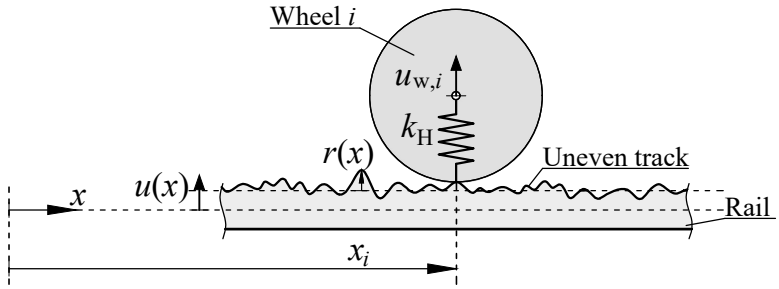

Figure 4: Wheel-rail interaction through nonlinear Hertzian spring

With reference to Figures 1 and 2, the wheels interact with the rail through forces $P_i = -P_{\mathrm{w},i} = P_{\mathrm{r},i}$. Additional force $P_{\mathrm{stat},i}$ from the weight of the vehicle is applied to each wheel. The interaction forces for each wheel depend on the relative displacement between the wheel $u_{\mathrm{w},i} = u_{\mathrm{w}}(x_i(t))$ and the rail $u_{\mathrm{r},i} = u_{\mathrm{r}}(x_i(t))$. It is further influenced by the track unevenness $r_i = r(x_i(t))$. The system is sketched in Figure 4. Due to the circular wheel shape, the stiffness of the wheel is not linear. Therefore, a nonlinear Hertzian spring is introduced to model the wheel behaviour. Further, if the wheel loses contact with the track, the interaction force disappears. The wheel–rail interaction force, for wheel i, can be found:

$$P_i = -P_{\mathrm{w},i} = P_{\mathrm{r},i} = \begin{cases} k_{\mathrm{H}}(|u_{\mathrm{w},i} - u_{\mathrm{r},i} - r_i|)^{3/2} & \text{for} \quad (u_{\mathrm{w},i} - u_{\mathrm{r},i} - r_i) \leq 0 \\ 0 & \text{for} \quad (u_{\mathrm{w},i} - u_{\mathrm{r},i} - r_i) > 0 \end{cases}. \tag{16}$$

The Hertzian spring is often linearised when frequency domain solutions are used, for example in [7]. However, using nonlinear wheel–rail interaction increases the application range of the model, for modelling larger local defects in the railway track structure.

3.2 Time-domain solution

To determine the wheel–rail interaction force time-domain solution is needed, as an iteration needs to be performed in every time step. The iteration scheme used is very similar to the one proposed by Lei [30]. It is based on the Newmark-beta time integration algorithm, with integration constants $\gamma = 0.5$ and $\beta = 0.25$ to obtain an unconditionally stable solution. Assuming the displacements and velocities of time step $j-1$ to be known and employing the time step Δt, the iterative scheme has the following steps:

Step 1. Predict values of velocities $\{\dot{\mathbf{u}}^j_{\mathrm{V},*}\}$ and displacements $\{\mathbf{u}^j_{\mathrm{V},*}\}$ at time step j for the vehicle:

$$\{\dot{\mathbf{u}}^j_{\mathrm{V},*}\} = \{\dot{\mathbf{u}}^{j-1}_{\mathrm{V}}\} + \{\ddot{\mathbf{u}}^{j-1}_{\mathrm{V}}\}\Delta t, \tag{17a}$$

$$\{\mathbf{u}^j_{\mathrm{V},*}\} = \{\mathbf{u}^{j-1}_{\mathrm{V}}\} + \{\dot{\mathbf{u}}^{j-1}_{\mathrm{V}}\}\Delta t + \frac{1}{2}\{\ddot{\mathbf{u}}^{j-1}_{\mathrm{V}}\}\Delta t^2. \tag{17b}$$

An equivalent procedure is carried out to find the predicted values $\{\dot{\mathbf{u}}^j_{\mathrm{BS},*}\}$, $\{\mathbf{u}^{j+1}_{\mathrm{BS},*}\}$ for the bridge–soil system. To begin the iteration inside time step j, an initial guess for the displacements in iteration $k = 0$ is made:

$$\{\mathbf{u}^{j,0}_{\mathrm{V}}\} = \{\mathbf{u}^j_{\mathrm{V},*}\}, \quad \{\mathbf{u}^{j,0}_{\mathrm{BS}}\} = \{\mathbf{u}^j_{\mathrm{BS},*}\}. \tag{18}$$

Using these values, a first guess for the wheel interaction forces $P^{j,0}_i$ can be found using Equation 16. The obtained forces are then placed in the force vector for the vehicle $\{\mathbf{f}^{j,0}_{\mathrm{V}}\}$.

Step 2. Determine acceleration, velocity and displacement vectors of the vehicle for time step j and iteration k:

$$\{\ddot{\mathbf{u}}_{\mathrm{V}}^{j,k}\} = \{\ddot{\mathbf{u}}_{\mathrm{V}}^{j-1}\} + [\hat{\mathbf{M}}_{\mathrm{V}}]^{-1}\big(\{\mathbf{f}_{\mathrm{V}}^{j,k}\} - [\mathbf{M}_{\mathrm{V}}]\{\ddot{\mathbf{u}}_{\mathrm{V}}^{j-1}\} - [\mathbf{C}_{\mathrm{V}}]\{\dot{\mathbf{u}}_{\mathrm{V},*}^{j}\} - [\mathbf{K}_{\mathrm{V}}]\{\mathbf{u}_{\mathrm{V},*}^{j}\}\big), \tag{19a}$$

$$\{\dot{\mathbf{u}}_{\mathrm{V}}^{j,k}\} = \{\dot{\mathbf{u}}_{\mathrm{V},*}^{j}\} + \gamma\big(\{\ddot{\mathbf{u}}_{\mathrm{V}}^{j,k}\} - \{\ddot{\mathbf{u}}_{\mathrm{V}}^{j-1}\}\big)\Delta t, \tag{19b}$$

$$\{\mathbf{u}_{\mathrm{V}}^{j,k}\} = \{\mathbf{u}_{\mathrm{V},*}^{j}\} + \beta\big(\{\ddot{\mathbf{u}}_{\mathrm{V}}^{j,k}\} - \{\ddot{\mathbf{u}}_{\mathrm{V}}^{j-1}\}\big)\Delta t^2, \tag{19c}$$

where $[\hat{\mathbf{M}}_{\mathrm{V}}] = [\mathbf{M}_{\mathrm{V}}] + \gamma[\mathbf{C}_{\mathrm{V}}]\Delta t + \beta[\mathbf{K}_{\mathrm{V}}]\Delta t^2$.

Step 3. Update interaction forces $P_i^{j,k}$ using Equation 16. The obtained forces are then placed to the coupled bridge–soil system force vector $\{\mathbf{f}_{\mathrm{BS}}^{j,k}\}$.

Step 4. Calculate bridge–soil displacements $\{\mathbf{u}_{\mathrm{BS}}^{j,k}\}$, velocities$\{\dot{\mathbf{u}}_{\mathrm{BS}}^{j,k}\}$ and accelerations $\{\ddot{\mathbf{u}}_{\mathrm{BS}}^{j,k}\}$. The procedure is equivalent to Step 2, just in this case coupled bridge-soil matrices and vectors with subscript BS are used.

Step 5. Recalculate the interaction forces $P_i^{j,k}$ for iteration k and place them in the force vector for the vehicle $\{\mathbf{f}_{\mathrm{V}}^{j,k}\}$.

Step 6. Check for convergence:

$$\frac{\|\mathbf{u}_{\mathrm{V}}^{j,k-1} - \mathbf{u}_{\mathrm{V}}^{j,k}\|}{\|\mathbf{u}_{\mathrm{V}}^{j,k-1}\|} < \epsilon_{\mathrm{t}}, \tag{20}$$

where ϵ_{t} is the iteration tolerance. Similarly the convergence of the solution can be determined by comparing the interaction forces $P_i^{j,k}$ or bridge–soil displacements $\{\mathbf{u}_{\mathrm{BS}}^{j,k}\}$. If convergence is reached—continue to the next time step $j := j + 1$, from Step 1. If convergence is not reached—continue to the next iteration step $k = k + 1$, from Step 2. Further, if the last time step is reached, computation is stopped and the vehicle displacements $[\mathbf{u}_{\mathrm{V}}(t)]$ and bridge–soil displacements $[\mathbf{u}_{\mathrm{BS}}(t)]$ for the whole considered time period are obtained.

3.3 Mixed-domain solution

An alternative approach to solving the whole system in time domain is to used the so-called mixed-domain solution. Using this approach, an approximation of the soil behaviour is avoided as the soil solution obtained directly from the semi-analytical soil model is used. However, the iterative process is somewhat more complicated. The procedure has already been described in a previous work by the authors [29], thus only a general overview is given here.

The procedure involves double iteration with some steps being the same as in the time-domain solution. However, in this case only the vehicle is solved in time domain, while the bridge–soil system is solved in the frequency domain, assuming periodicity with the period T. To start the iteration, rail displacements $u_{r,i}^{l-1}(t)$ are estimated through all times $t \in [0, T]$. Practice shows that assuming no rail displacements as a first estimate is a fair assumption. The procedure for iteration step number l is:

Step 1. Vehicle displacements $\{\mathbf{u}_{\mathrm{V}}^{l}(t)\}$, velocities $\{\dot{\mathbf{u}}_{\mathrm{V}}^{l}(t)\}$ and accelerations $\{\ddot{\mathbf{u}}_{\mathrm{V}}^{l}(t)\}$ are found using rail displacements $r_i^{l-1}(t)$. This is carried out the same way as in Subsection 3.2, just Steps 4 and 5 are skipped. This way only the vehicle response is calculated without updating the bridge–soil system response, or the rail displacements $r_i^l(t)$.

Step 2. Wheel–rail interaction forces $P_i^l(t)$ obtained in the previous step are Fourier transformed into frequency domain and placed in the bridge–soil interaction force vector $\{\mathbf{F}_{\mathrm{BS}}^{l}(\omega)\}$.

Step 3 The bridge–soil system can now be solved using the obtained $\{\mathbf{F}_{\mathrm{BS}}^{l}(\omega)\}$ as input. The system displacements $\{\mathbf{U}_{\mathrm{BS}}^{l}(\omega)\}$ in frequency domain are obtained.

Step 4 The obtained displacements are inverse Fourier transformed into time domain, thus providing $\{\mathbf{u}_{\mathrm{BS}}^{l}(t)\}$, and the rail displacements $u_{\mathrm{r},i}^{l}(t)$ are extracted.

Step 5 To check the convergence of the solution, the bridge–soil displacements $\{\mathbf{u}_{\mathrm{BS}}^{l}(t)\}$ are compared to those obtained in the previous iteration step:

$$\frac{\|\{\mathbf{u}_{\mathrm{BS}}^{l-1}(t)\} - \{\mathbf{u}_{\mathrm{BS}}^{l}(t)\}\|}{\|\{\mathbf{u}_{\mathrm{BS}}^{l-1}(t)\}\|} < \epsilon_{\mathrm{m}}. \tag{21}$$

If convergence is reached, the iteration is terminated and results extracted. If convergence is not reached, the computation continues to the next mixed-domain solution iteration step $l := l + 1$, from Step 1.

4 Definition of the computational model

4.1 Parameters of the soil, structure and vehicle

A model of a multi-span railway bridge is considered. The total length of the bridge deck is 210 m, and it is supported by six pylons. The pylons are evenly spaced with a distance of 30 m, centre to centre. Each pylon is 8 m tall. The structure interacts with the soil through rigid square surface footings with one side length equal to 5.66 m. The footing is roughly estimated to be sufficient for static bridge load. To account for additional mass of the surface footings, their thickness is set to 1.0 m thick with the mass density $\rho_{\mathrm{f}} = 2400$, representative for reinforced concrete. An additional 30 m of track is added to each side of the structure to allow the wheel–rail interaction forces to reach an equilibrium, before the vehicle reaches the bridge. The stretches of additional track are assumed to be connected to a rigid surface instead of the bridge deck. Their stiffness is decreasing linearly from a factor 10 of the given track properties at the ends, to a factor of 1 where the additional track stretches connect to the bridge. The gradually changing stiffness reduces the wheel excitation at the very beginning and end of simulations when the wheels transfer from an interaction with a completely rigid surface to interaction with a layered track structure and vice versa. The model is illustrated in Figure 5.

Material and cross-sectional properties of the bridge structure are given in Table 1 and properties of the vehicle are given in Table 2. Rayleigh damping is employed

for the bridge structure. It is calibrated with damping ratios of 0.03 and 0.04, for eigenmodes 1 and 2, respectively, of the bridge structure fixed at the base. Track irregularities are generated for 2048 discrete wavelengths in the range from 0.3 m to 70 m, using the track spectrum described in Subsection 3.1.

The structure was discretized using FE elemets. The convergence analysis was performed up to 100 Hz, ensuring that the eigenfrequencies around this limit are within 2% accuracy. The resulting model has around 4000 degrees of freedom. The mesh size in the rails and deck is set to be equal to the distance between the sleepers, leading to a model where sleepers are connected directly to the nodes of the FE model of the rail and deck. Thus, the stiffness and damping of the rail pads and ballast are not distributed between multiple nodes, leading to a more accurate model.

The structure is placed on an 4 m thick layer of clay over a half-space of hard till. The clay properties are: Shear modulus $G_\mathrm{s} = 80$ GPa, Poisson's ratio $\nu_\mathrm{s} = 0.498$, mass density $\rho_\mathrm{s} = 2000$ kg/m^3 and hysteric damping ratio $\eta_\mathrm{s} = 0.02$. That corresponds to a compression wave speed of 3200 m/s, shear wave speed of 200 m/s and Rayleigh wave speed of 191 m/s. The hard till properties are: Shear modulus $G_\mathrm{s} = 2000$ GPa, Poisson's ratio $\nu_\mathrm{s} = 0.333$, mass density $\rho_\mathrm{s} = 2000$ kg/m^3, hysteric damping ratio $\eta_\mathrm{s} = 0.02$, compression wave speed of 2000 m/s, shear wave speed of 1000 m/s, and Rayleigh wave speed of 933 m/s. The analysed case corresponds to medium–stiff soil conditions with the vehicle travelling much slower than the Rayleigh wave in the top soil layer. Hence, the vehicle does not reach the critical speed for the analysed system. However, the secondary effects, such as footing coupling through soil, could still lead to significant effects on the overall results.

Three investigation points are chosen on the structure, as seen in Figure 5. Point A is placed on the connecting node between the surface footing and the soil, Point B is placed in the middle of the span between columns 5 and 6, and Point 3 is placed in the middle of the span between columns 2 and 3. Points B and C refer to the rail as well as the deck. The specified points are later used to extract data and apply loads.

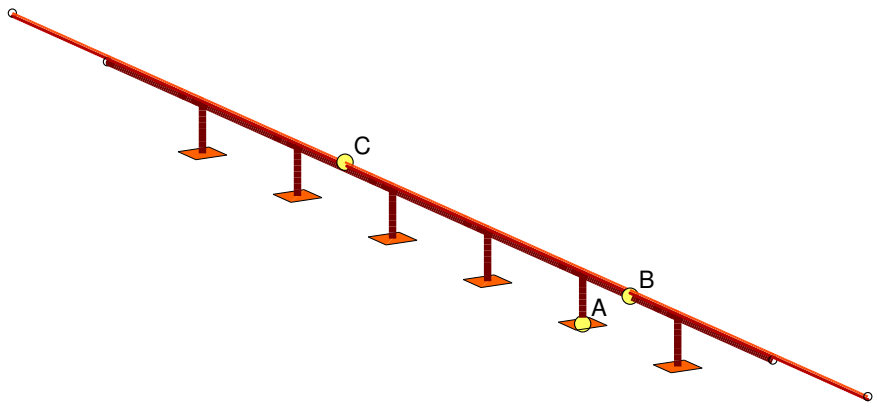

Figure 5: Full bridge model with the positions of investigation points. The ends of the rail track and the bridge structure are fixed, and shown as black hollow dots.

Table 1: Material and cross-sectional properties of bridge structure

Rail properties			
Young's modulus	E_{r}	$2.1 \cdot 10^{11}$	Pa
Moment of inertia	I_{r}	$3.055 \cdot 10^{-5}$	m^4
Mass per unit length	μ_{r}	60.3	kg/m
Rail pad properties			
Stiffness	k_{rp}	$5.0 \cdot 10^{8}$	N/m
Damping	c_{rp}	$2.0 \cdot 10^{5}$	N· s/m
Sleeper properties			
Mass	m_{sl}	290.0	kg
Spacing	l_{sl}	0.6	m
Ballast properties			
Stiffness	k_{bl}	$5.38 \cdot 10^{8}$	N/m
Damping	c_{bl}	$1.20 \cdot 10^{5}$	N·s/m
Mass per sleeper	m_{bl}	1000.0	kg
Deck properties			
Moment of inertia	I_{d}	4.07	m^4
Cross-sectional area	A_{d}	7.52	m^2
Young's modulus	E_{d}	$3.4 \cdot 10^{10}$	Pa
Mass density	ρ_{d}	2400	$\mathrm{kg/m}^3$
Pylon properties			
Moment of inertia	I_{p}	0.42	m^4
Cross-sectional area	A_{p}	5.00	m^2
Young's modulus	E_{p}	$3.4 \cdot 10^{10}$	Pa
Mass density	ρ_{p}	2400	$\mathrm{kg/m}^3$

Table 2: Properties of the vehicle

Primary suspension stiffness	k_{sp}	$3.28 \cdot 10^{6}$	N/m
Secondary suspension stiffness	k_{ss}	$1.31 \cdot 10^{6}$	N/m
Primary suspension damping	c_{sp}	$9.00 \cdot 10^{4}$	N·s/m
Secondary suspension damping	c_{ss}	$3.00 \cdot 10^{4}$	N·s/m
Hertzian spring constant	h_{H}	$8.70 \cdot 10^{10}$	$\mathrm{N/m}^{3/2}$
Mass of car body	m_{c}	$5.35 \cdot 10^{4}$	kg
Mass of bogie	m_{b}	3260.0	kg
Mass of wheel set	m_{w}	2000.0	kg
Pitch moment of inertia for car body	j_{c}	$2.24 \cdot 10^{6}$	$\mathrm{kg \cdot m}^2$
Pitch moment of inertia for bogie	j_{b}	$2.45 \cdot 10^{3}$	$\mathrm{kg \cdot m}^2$
Static force per wheel set	$P_{\mathrm{stat},i}$	$1.70 \cdot 10^{5}$	N
Half length between two axles of one bogie	$L_{\mathrm{v},1}$	1.5	m
Half length between two bogies centre lines	$L_{\mathrm{v},2}$	7.0	m

5 Comparison between solution procedures

Two different approaches of solving the system have been presented: the pure time-domain solution in Subsection 3.2 and the mixed-domain solution in Subsection 3.3. To compare the performance of the proposed solution procedures, a smaller section of the full bridge model is analysed. The section contains 60 m of bridge deck supported by a single pylon in the centre. The pylon is 8 m in height and it rests on a circular rigid footing with a radius of 4 m. Similarly to the full bridge model, 15 m additional track stretches are added to either end of the deck. The soil is modelled as a half-space of clay. All other properties of the system are exactly the same as for the full bridge model. The reduced bridge model is shown in Figure 6. The system is excited by a passing vehicle at 30 m/s, 60 m/s and 90 m/s, and the resulting wheel–rail interaction forces and structure accelerations are analysed.

The differences stemming from the mismatch between the real frequency dependent soil behaviour and the fitted LPM are not investigated in this subsection. Therefore, a standard LPM is used, as described by Wolf [37]. The standard LPM offers relatively simple expressions for rigid surface footings on an elastic half-space. The mass, damping and stiffness matrices provided by the standard LPM are then used to represent the soil–footing system identically in the time-domain and frequency-domain analysis.

While analysing the two approaches, it has been found that for simple analysis cases, such as a simply supported beam traversed by a vehicle exposed to an uneven track, both approaches provide identical results. However, when the layered track structure and structure–soil interaction is introduced into the system, the mixed-domain approach converges extremely slowly or stops converging all together. Therefore, for the mixed-domain computation procedure to achieve a sufficient degree of convergence, an additional high-frequency filtering is needed. A low-pass filter is therefore introduced in Step 1 of the procedure described in Subsection 3.2, such that

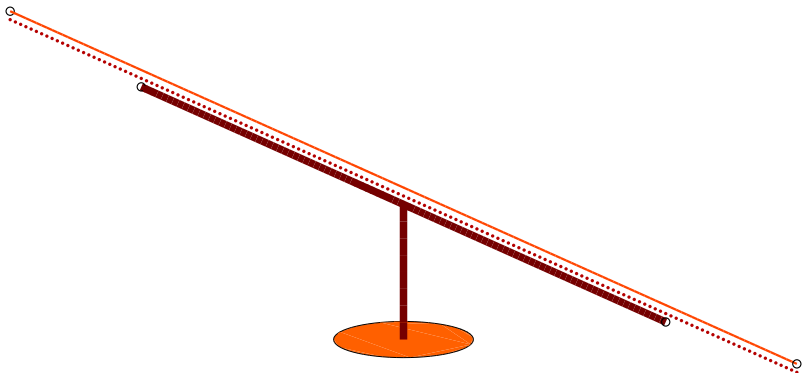

Figure 6: Reduced bridge model used to for comparison of solution procedures. The ends of the rail track and the bridge structure are fixed, and shown as black hollow dots.

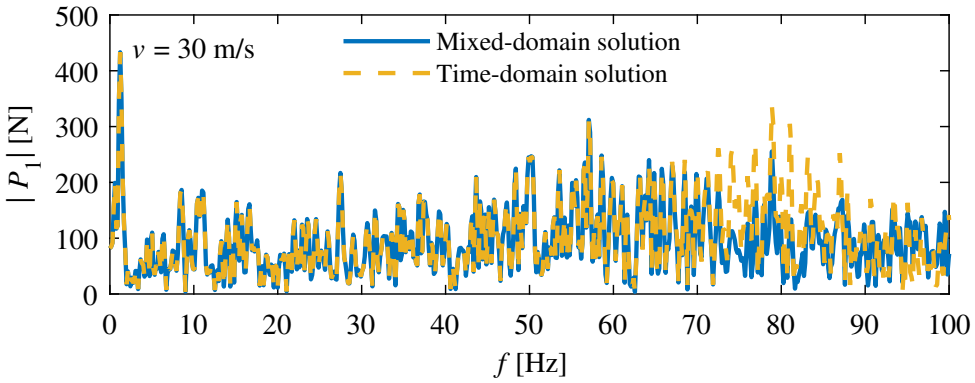

Figure 7: Wheel–rail interaction force for the front vehicle wheel.

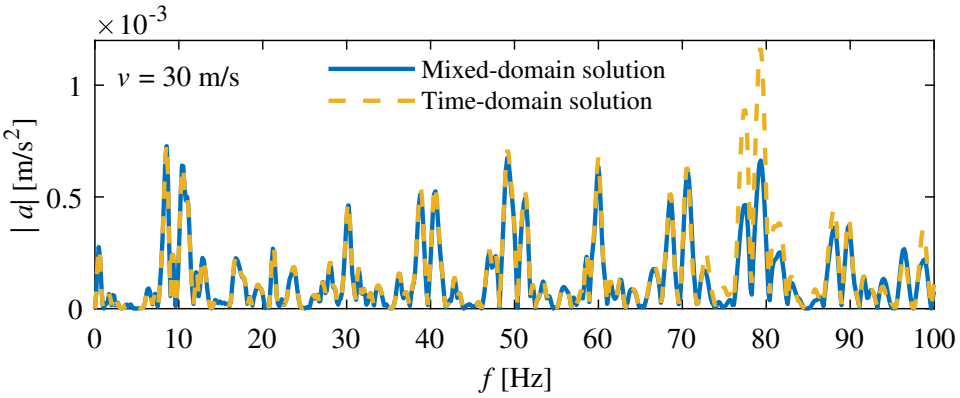

Figure 8: Vertical accelerations of the footing.

the high-frequency contents of the rail displacements experienced by the vehicle wheel $u_{\mathrm{r},i}$ are filtered out. In this case, it has been found that low-pass filter with a cut-off frequency of 70 Hz was needed.

Figure 7 shows the wheel–rail interaction forces for the first vehicle wheel. It can be seen that the agreement between the two solution procedures is acceptable. The agreement is good up to 70 Hz and then the two solutions begin to diverge. This is due to the additional filtering applied in the mixed–domain solution. However, the differences are not very large and are mostly limited to the 72–88 Hz range. For frequencies above 88 Hz, the absolute values obtained are similar; however, the positions of the peaks are different. The same behaviour was also observed for 60 m/s and 90 m/s vehicle speeds, indicating that the problem is not dependent on the vehicle speed. Figure 8 shows the accelerations of the SSI node connecting the bridge pylon to the soil. The results here are very similar to Figure 7. The accelerations observed show very good agreement up to 70 Hz and then start to differ. However, they are mostly limited to the 68–92 Hz range. Interestingly, even with the higher frequencies filtered out, the mixed-domain approach predicts almost the same positions and absolute values of the peaks at the higher frequencies. Once again, the same behaviour

have been observed for other vehicle speeds. Overall, the agreement between the two approaches is better when analysing the accelerations of the structure, when compared to the wheel–rail interaction forces.

To conclude, both approaches are able to predict the system behaviour to at least 70 Hz, with some differences at higher frequencies. The higher frequency range is important when analysing the behaviour of the vehicle or the track underneath, and in those cases using the pure time domain solution is preferable. However, when analysing the ground vibrations generated by a passing train, frequency ranges up to 70 Hz might be fully sufficient. In those cases using the mixed-domain approach could be beneficial as it uses the directly calculated soil behaviour and does not require fitting of an LPM. For further analysis the pure time-domain solution is used, as higher frequencies are of interest for the investigated case.

6 Modelling structure–soil interaction with lumped parameter models

6.1 Quantification of cross-coupling via the soil

Consistent LPMs are used to obtain stiffness, mass and damping matrices needed to recreate the behaviour of the soil in the time domain. The quality of the recreated system depends on a number of factors. Firstly, each member of the stiffness matrix needs

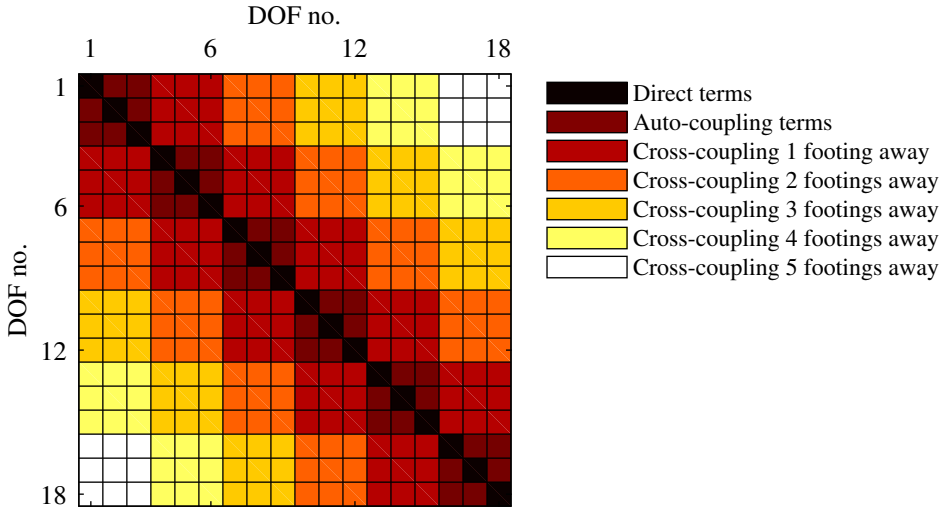

Figure 9: Dynamic stiffness matrix for soil. Axes show the positions of degrees of freedom in the matrix. The colors indicate different levels of coupling between the foundations included in simulations.

to be recreated using separate LPMs. This includes the direct terms located along the diagonal of the stiffness matrix, the auto-coupling terms defining the coupling between the internal degrees of freedom of a single footing and the cross-coupling terms connecting the degrees of freedom from separate footings. Practice shows that recreating all terms of the dynamic stiffness matrix is not always the best approach, as it often leads to an unnecessarily large systems without adding additional precision. Further, cross-coupling terms for degrees of freedom that are separated by multiple footings often display extremely complex behaviour in the frequency domain. Therefore, high order polynomial-fraction functions are needed, thus adding a large amount of internal degrees of freedom to the system. Otherwise, using badly-fitting lower order functions leads to a decrease of the overall quality of the solution. Thus, the influence of direct, auto-coupling and cross-coupling terms should be quantified, see Andersen [38]. The structure of the dynamic stiffness matrix obtained from the semi-analytical soil model is shown in Figure 9, where different colors indicate different levels of cross-coupling between the footings.

To determine the level of cross-coupling needed to recreate the system behaviour, an analysis was carried out. For that purpose, a harmonic load was placed on the rail at Point C (see Figure 5) and the whole system solved in the frequency domain. The

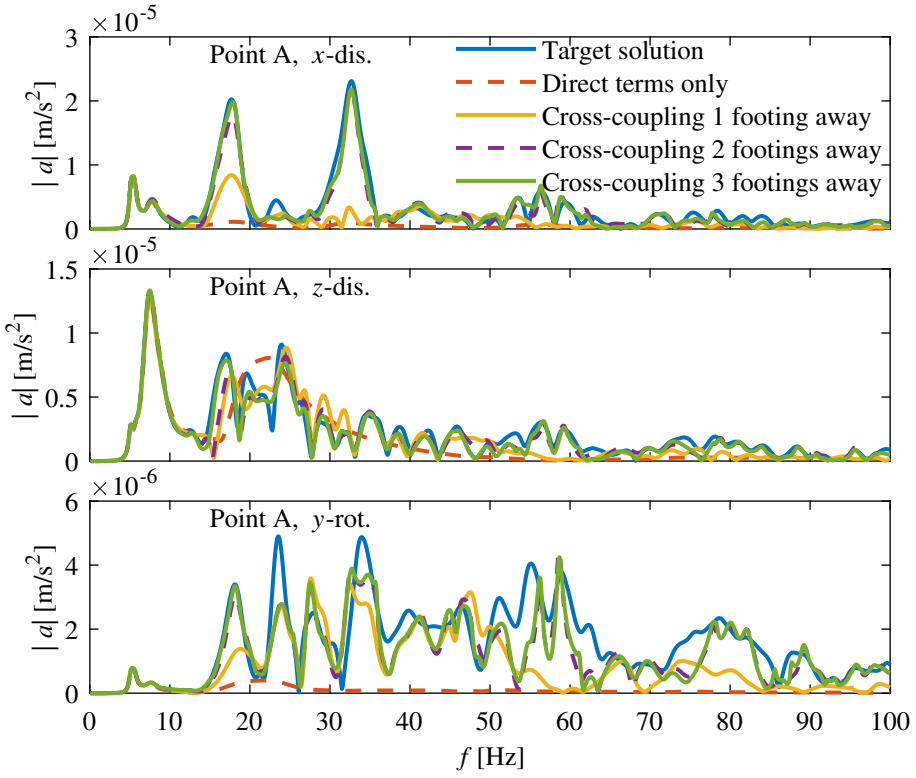

Figure 10: Bridge response at Point A with different levels of coupling. From top down: x-axis displacement, z-axis displacement and rotation around y-axis.

system is excited in a (x,z) plane. Thus, only three degrees of freedom are excited: displacements in the x and z directions, and rotation around the y-axis. The load is applied as blue noise , that is the load magnitude is proportional to the excitation frequency. This way, the high frequency response is amplified, as it is important for the high frequency wheel-rail excitation loads. The vehicle is not included into the system, thus the system does not require an iterative solution procedure. Due to the standard frequency domain solution, it is also possible to directly couple the bridge structure and the soil to obtain the target solution, without utilizing LPMs. The obtained results for the fifth footing displacements (Point A in Figure 5) are presented in Figure 10. The fifth footing was chosen, as it is sufficiently far away from the excitation point of the system for the coupling terms via the ground to have a significant contribution. Further, the effects from the underlying soil are evident for the footings,

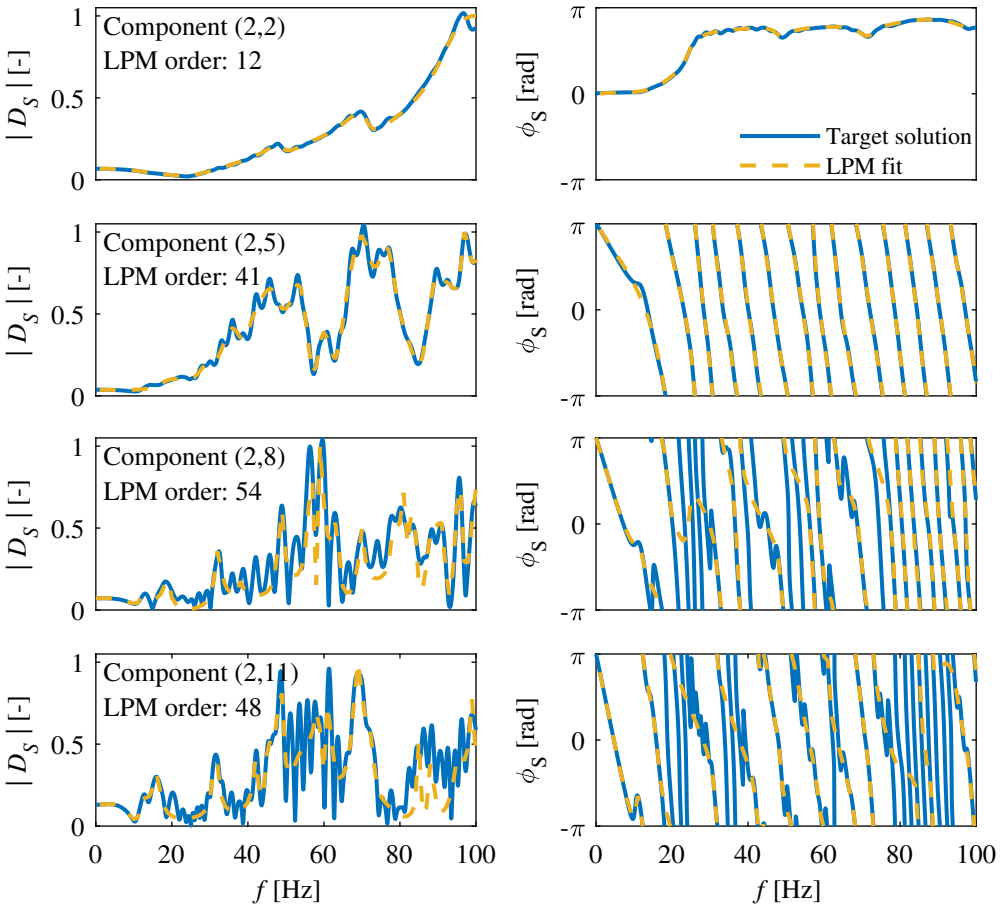

Figure 11: Examples of LPMs fitted to members of the dynamic stiffness matrix for the soil. The stiffness values are normalized by the maximum absolute stiffness of the LPM fit. Top to bottom: direct, cross-coupling 1 footing away, cross-coupling 2 footings away and cross-coupling 3 footings away terms.

while the behaviour of the bridge deck, sleepers or the rails is effected to a lesser degree. Analysing Figure 10, it can be seen that the low frequency behaviour up to 15 Hz is dominated by the direct terms of the dynamic stiffness matrix. Here, including additional coupling terms does not improve the solution. However, for higher frequencies the direct terms are not able to reproduce the system behaviour. It is not shown in the figure, but additionally including auto-coupling terms does not improve the solution, indicating that the higher frequency behaviour is dominated by the interactions between separate footings. Further, including cross-coupling terms one footing away drastically improves the higher-frequency match to the target solution. However, the match is still not very good, especially for frequencies higher that 50 Hz. Adding additional coupling terms to the system further improves the solution, up to cross-coupling terms three footings away. However, coupling terms four and five footings away do not further improve the fit. Therefore, for further analysis, LPMs are created for terms up to three footings away. Looking at the overall fit, it can be seen that the rotational degree of freedom is associated with the higher inaccuracy, and that the fit is poor around 22 Hz for all three considered degrees of freedom.

Further, the overall quality of the created system depends on the quality of the individual LPMs. As already mentioned, coupling terms separated by multiple footings tend to have a behaviour that is more complex compared to the coupling terms for nearby footings or auto-coupling terms. Thus, while the overall effects of the far-away coupling terms might be limited, they still require high-order polynomial-fraction functions. Figure 11 shows the fitted LPMs created for terms related to the vertical displacement of the first footing of the system (degree of freedom number 2). It can be seen that a relatively low order polynomial is needed for the direct terms to represent the system well in the whole frequency range. However, the complexity increases with increasing distance from the first footing. The cross-coupling terms two and three footings away require rational approximations of orders around 50 and even then the fit at higher frequencies is not recreated well. However, as seen in Figure 10, inclusion of these terms still improves the overall quality of the system.

6.2 Improving the stability of the lumped-parameter models

Another important factor when creating an LPM is the overall time-domain stability of the system. In this work, an inbuilt MATLAB function *invfreqs* is used. The function utilizes a damped Gauss-Newton iterative scheme [35], which ensures the obtained poles will only have negative real parts. In theory that should be enough to ensure a stable time-domain solution. However, the dynamic stiffness matrix of the soil proves to be difficult to fit and the obtained LPMs are often numerically unstable. Even using unconditionally stable time integration schemes like the Newmark-beta approach, with integration constants $\gamma = 0.5$ and $\beta = 0.25$, generalized alpha method [39] or a fourth-order accurate algorithm developed by Krenk [40] still produces unstable time domain behaviour. It is difficult to pinpoint the exact reasons for the instabilities. A possible explanation is the finite computational precision errors associated

with fitting high order polynomials. As the order increases, the results obtained will contain numbers that are extremely small as well as numbers that are extremely large, leading to computational instabilities. The problem is especially pronounced when fitting a wide frequency range. One way to limit the instabilities is to use a low-order rational approximation function, limiting the solution up to orders 3 or 4. Another approach is to use larger time steps in the time integration scheme or to limit the overall computed time period. Increasing the time step size limits the excitation of unstable high frequencies, while calculating a shorter time period does not allow the computational errors to build up. However, neither of these approaches are useful for the case considered in this study. The considered frequency range is large and the wheel–rail interaction forces require small time steps. Further, low-order approximations are not able to recreate the system behaviour, and the bridge structure is long, therefore requiring a long time period for the vehicle to pass.

A fitting scheme was developed to determine the best fitting and at the same time stable LPMs. The fitting procedure is shown in Figure 12. The fitting is performed for a range of orders of the rational approximations using the MATLAB function $invfreqs$. For the direct terms, orders 12–40 were tested, for the auto-coupling terms 17–48, and for the cross-coupling terms 33–64. The used orders are high as the analysed soil contains an interface between two soil layers which produces some wave reflections and a complex frequency-domain behaviour. When fitting, a weight function is applied to prioritize the lower frequencies.

$$w_{\text{LPM}} = \frac{1}{(1 + (\zeta_1 a_0)^{\zeta_2})^{\zeta_3}}, \tag{22}$$

where parameters ζ_1, ζ_2 and ζ_3 define the shape of the weight function. Initially, values $\zeta_1 = 2$, $\zeta_2 = 3$ and $\zeta_3 = 4$ were used. The best-fitting function order is then determined by taking the root mean square of the differences between the obtained frequency response and the target solution. Two tolerance values $\epsilon_{\text{tol},1}$ and $\epsilon_{\text{tol},2}$ are used to determine best fitting LPM, as shown in Figure 12. For the case considered, the tolerance values are set to $\epsilon_{\text{tol},1} = 0.04$ and $\epsilon_{\text{tol},1} = 0.2$. After the best fitting LPM is determined, three tests are performed to ensure stability:

Test 1. If a direct term of the dynamic stiffness matrix is analysed, the obtained LPM frequency response function should only contain positive phase angles. Negative phase angles imply negative damping, which should not exist for the direct stiffness terms. Naturally, the target solution obtained from the semi-analytical soil model does not have negative phase angles. However, when the LPMs are fitted, the resulting function might have negative phase angle in a narrow frequency range. This is especially problematic at very low frequencies, as at frequency 0 the phase angle is also equal to 0. Thus, there is a high risk of the LPM's having negative phase angle at low frequencies. Hence, if a negative phase angle has been detected, the LPM is discarded.

Test 2. If the real part of a pole vanishes, the imaginary part of the same pole will combine with the imaginary part of it's complex conjugate to form a real positive

pole, which results in instability in the time domain. Limited precision of a computer dictates that the real part of a complex pole should not be too small when compared to the imaginary part. To account for this, the ratio of the real to the imaginary part of the complex poles is checked. If the smallest ratio is smaller than 10^{-4}, the whole LPM is discarded.

Test 3. Fitting of the polynomial-fraction filter is performed in the frequency range of 0–100 Hz. However, additional peaks can appear at frequencies beyond the fitting range. These peaks often have values exceeding the target solution by several orders of magnitude, causing instabilities and non-physical behaviour in the system. There are various approaches to check for this behaviour. In this study, the obtained stiffness and mass matrices of the LPM are used to solve the eigenvalue problem. The stiffness matrices of the LPM model might have zeros in the diagonal of the matrix; thus some of the obtained eigenfrequencies are infinite and should be discarded. The remaining eigenfrequecies can then be used to identify peaks at high frequencies. Further, the LPM response is analysed in an extended frequency range looking for uncharacteristically large values. If the tested LPM contains peaks above 1.5 times the maximum fitted frequency and, at the same time, has absolute values higher than 100 times the highest absolute target value, the LPM is discarded.

If an LPM fails one or more of the tests, the next best fitting order of the polynomial-fraction function is used to create a new LPM model and the procedure is repeated. If none of the initially crated LPMs pass the tests, a new set of LPMs is fitted using a different weight function. The new weight function is obtained by randomizing the parameters ζ_1, ζ_2 and ζ_3. Each initial parameter is multiplied by a random factor, which is evenly distributed in the $0.67 - 1.33$ range. Small changes in the fitting procedure often lead to significantly different results, thus the randomization procedure can be repeated until an LPM with satisfactory accuracy and stability has been established.

The proposed procedure produces stable LPMs that can be coupled to the bridge structure. The approach is also stable for different soil stratification cases or bridge layouts. However, the parameters used might need to be adjusted for some configurations. Naturally, the additional steps needed increase the difficulty in finding the correct fit and randomization of the weight function means that there is some uncertainty in the procedure. Overall, the stability of the system is highly dependent on the time step size and the total simulated time period, with longer time steps and shorter total time periods resulting in more stable systems. Therefore, the case analysed in this work is a 'worst case scenario', where the nonlinear wheel–rail interaction forces require very short time steps, while the bridge itself is rather long, in turn requiring long total time period for the vehicle to pass.

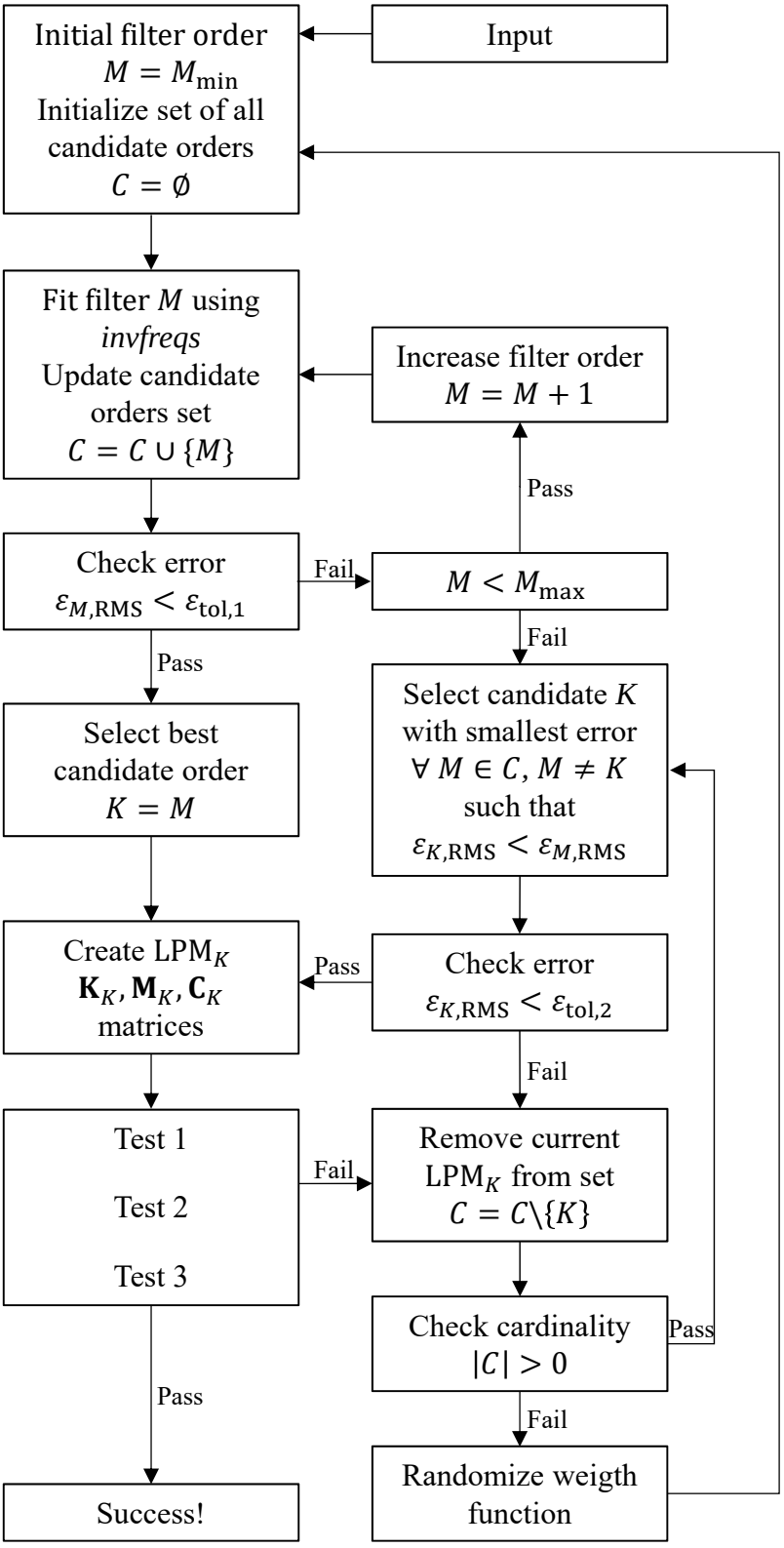

Figure 12: LPM fitting procedure used to obtain stable time domain solution. Note that the set theory notation is used.

7 Time-domain analysis of vehicles passing the bridge at different speeds

The model is used to analyse the system behaviour when the track is excited by a passing vehicle. The time-domain solution approach is used, with an LPM including cross-coupling up to four footings away. In total, 100 randomly generated uneven track profiles are created and each profile is then tested for three vehicle speeds: 30 m/s, 60 m/s and 90 m/s. The spectrum defined in Section 3.1 has been used, and uniformly distributed phase angles have been generated for each case. Figure 13 shows the wheel–rail interaction forces as experienced by the leading vehicle wheel converted into frequency domain. The solid lines show the overall average values from all simulations, the dashed lines are 10% and 90% quantiles and the shaded area indicates the limits of observed results. It can be seen that the amplitude of the interaction forces corresponds to the vehicle speed. With increasing speeds higher amplitudes of the force are excited. Further, it is evident that most of the excitation is due to the unevenness of the track profiles. The amplitude of the interaction force increases with frequency for all vehicle speeds, until an overall peak is reached in the 60–80 Hz range, after which the accelerations start to decrease. A distinct peak is present at 50 Hz for the vehicle speed of 30 m/s, which contains no variation of the results. The peak corresponds to the vehicle wheels passing over discrete sleepers supporting the rail, which are placed 0.6 m apart. A similar peak can be observed for the vehicle speed of 60 m/s at 100 Hz and is also present for the vehicle speed of 90 m/s at 150 Hz (beyond the limits of the figure). Other distinct peaks are present for all speeds at the very low 1–2 Hz frequency range. It is most likely caused by low frequency vibrations caused by bouncing of the vehicle body combined with the vehicle passing over the

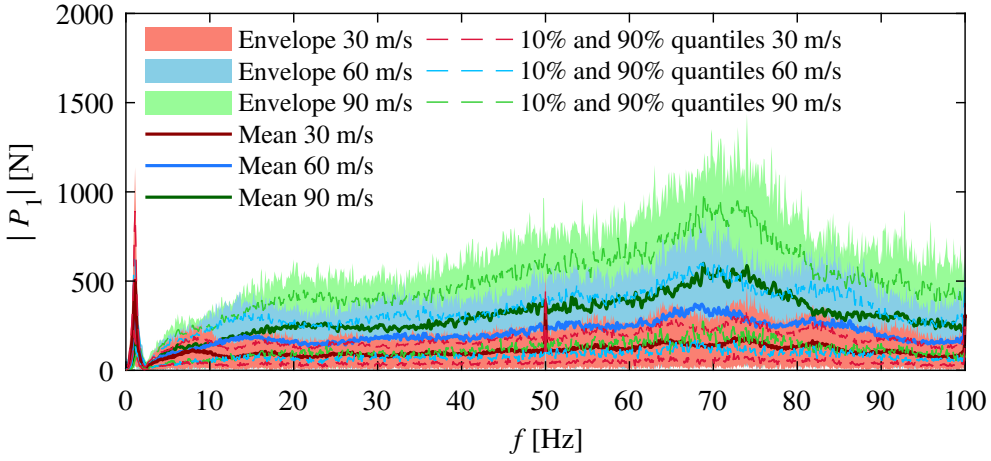

Figure 13: Fourier coefficients of wheel-rail interaction force for different vehicle speeds. Each simulation was performed for 100 randomly generated rail unevenness profiles.

pylons supporting the bridge deck.

Further, the accelerations of the bridge structure are analysed. Figure 14 shows the accelerations obtained for Points A and B (see Figure 5). Overall, the excited frequency ranges are very similar to those in Figure 13. The rail response at Point B shows that the generated accelerations in the frequency range up to 30 Hz have very low variation and are almost independent of the track profile. There are three distinct peaks cantered around 10 Hz for the 30 m/s case, that correspond to time period needed for two wheels of a single bogie to pass over the analysed point. The peaks are spread through frequencies due to the Doppler effect. Similar peaks can be also observed at 20 Hz for the 60 m/s and 30 Hz for the 90 m/s cases. Further, with increasing frequency, the variation of the accelerations increases, especially for

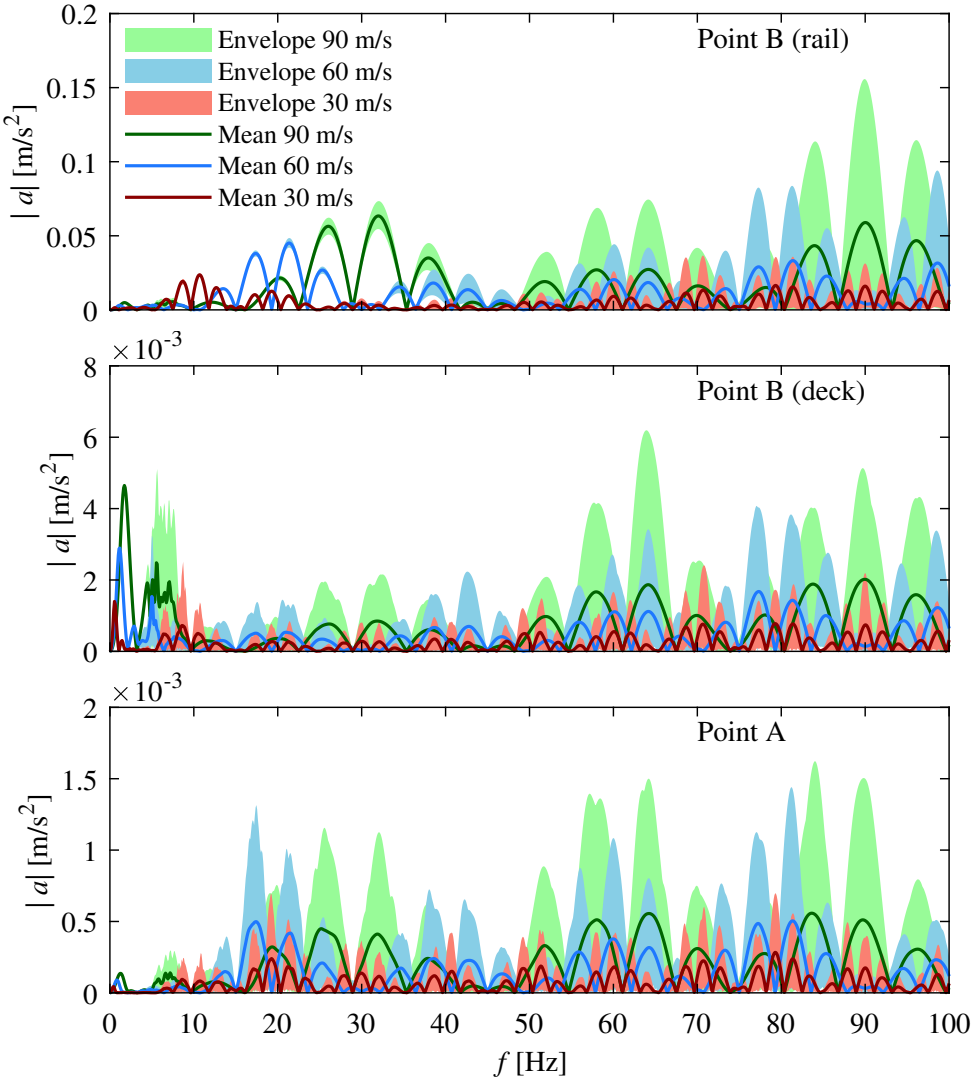

Figure 14: Accelerations for rail, deck and pylon for different vehicle speeds. Simulations performed for 100 random rail unevenness profiles.

vehicle speeds of 60 m/ and 90 m/s. The vehicle speed 30 m/s produces vibrations that show much smaller variation in the whole analysed frequency range. Further, the deck accelerations at Point A are analysed. Here, the overall obtained accelerations are much smaller, when compared to the rail. However, the variation of accelerations is higher and is present over a wider frequency range. Almost no variation of accelerations is observed in the very low 0–2 Hz frequency range. This is especially evident when analysing the deck displacements, as shown in Figure 15. Here the bridge displacements are dominated by the semi-static bridge displacements caused by the passing deadweight of the vehicle. It can be seen that with increasing speed higher frequencies are excited, with decreasing contribution from the static displacements. The effects of the track unevenness are more evident when analysing rail displacements in the wavenumber domain at one instant of time, as shown in Figure 16. Here the highest displacements are observed at very low wavenumbers that are outside the

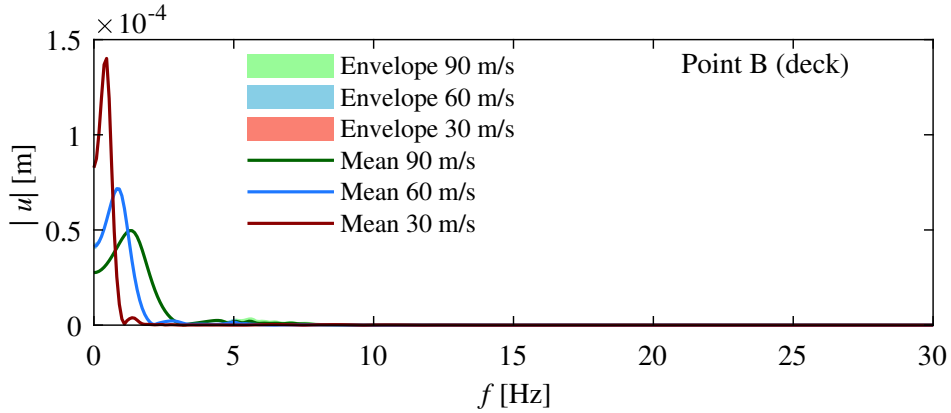

Figure 15: Displacements of the bridge deck for different vehicle speeds. Each simulation was performed for 100 randomly generated rail unevenness profiles.

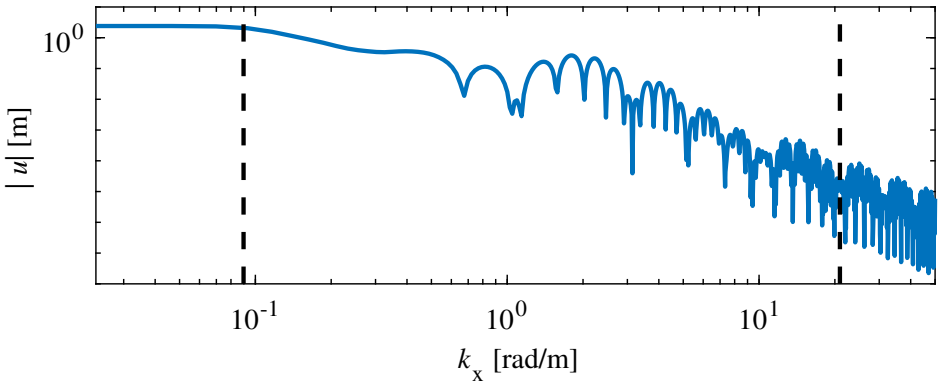

Figure 16: Displacements of the rail in the wavenumber domain, at one instant of time for the vehicle travelling at 30 m/s. Dashed lines indicate the upper and lover limits of the generated rail unevenness.

generated rail unevenness range, and are caused by the semi-static bridge displacements. The displacements observed for wavenumbers inside the unevenness range are lower and are constantly decreasing with increasing wavenumber. Coming back to Figure 14, the bottom sub-figure shows the accelerations of the bridge footing at Point A. Here, the accelerations are once again lower. However, the overall results are very similar to the deck behaviour, with large variations in the whole frequency range and semi-static behaviour at very low frequencies.

8 Conclusions

A computational model for a coupled vehicle–bridge–soil system has been presented. The model utilizes a multi-degree-of-freedom vehicle model, a bridge structure modelled using beam finite elements combined with a layered track structure and a soil modelled using the semi-analytical approach. Two solution procedures have been presented. They are needed in order to combine the semi-analytical soil approach and vehicle–rail interaction. One of the solution procedures is the time-domain approach. It is based on the use of a lumped-parameter-model (LPM) to recreate the soil behaviour in frequency domain, using a system of springs, dashpots and masses. The approach is advantageous as the obtained solution can be directly added to already existing finite-element matrices and the system solved in time domain. An alternative mixed-domain approach has also been introduced. Here the bridge–soil system is solved in frequency domain, thus eliminating the need of an LPM. However, the approach requires an additional convergence procedure. Further, it has been found that for the solution to converge, additional high-frequency filtering is needed, making the system behaviour for high-frequencies imprecise. Overall, it can be concluded that using pure time-domain solution approach is advantageous when high frequency range analysis is needed, provided a proper fit of LPM can be obtained. However, when only the lower frequency range is of interest, the mixed-domain solution is sufficient.

Recreating the frequency domain behaviour of the soil using consistent LPMs requires proper fit of the polynomial-fraction function. Further, to recreate the interactions between separate footings and even between degrees-of-freedom of a single footing, the structure of the dynamic stiffness matrix also needs to be recreated. Thus, LPMs are used to model the direct and cross-coupling terms of the matrix. An analysis investigating the effects of including additional coupling terms was performed. It has been determined that modelling the cross-coupling terms is necessary for an accurate solution. Including the cross-coupling up to three footings away significantly improves the solution, with inclusion of terms further away becoming less important. However, the overall improvements are limited and often modelling only the direct terms of the system might be sufficient. Further, special care should be taken when fitting LPMs over a wide frequency range requiring high order polynomial functions. It has been found, that just ensuring the commonly used condition of no poles existing with positive real parts is not sufficient, even when using unconditionally stable time integrations schemes or schemes with additional numerical damping. Therefore,

additional LPM fitting procedure has been introduced, that, when calibrated correctly, ensures a stable solution.

The effects of railway track unevenness to a multi-support railway structure was analysed. For this purpose, 100 random track unevenness profiles were generated and each of them tested for three vehicle speeds: 30 m/s, 60 m/s and 90 m/s. From the obtained results, upper and lower limits of expected interaction forces and resulting accelerations were determined in the frequency domain. It was found that most of the observed vibrations in the 2–100 Hz range are generated by the wheel–rail interactions. Another distinct peak in the interaction forces is generated by the vehicle wheel passing over sleepers. Further, the effects of the moving vehicle mass can be observed in the very low 0–2 Hz frequency range.

The created model offers a relatively fast computation times, especially when compared to FE or BE solutions. The model could be useful in the early design stages of a project, to quickly estimate the levels of predicted environmental vibrations, allowing the testing of a wide array of configurations. It can be easily further expanded to evaluate the vibration levels of the surrounding soil and, in turn, structures close to the modelled bridge structure. Further, the methodology introduced is not limited to the investigated cases and can be easily applied to similar systems involving structures excited by traversing vehicles that are solved in time domain. The usage of time domain solution is beneficial, as nonlinearities can be easily introduced into the system, e.g. to account for nonlinear ballast behaviour.

Acknowledgement

The research was carried out in the framework of the project “Urban Tranquillity” under the Interreg V programme. The authors of this work gratefully acknowledge the European Regional Development Fund for the financial support.

References

[1] C. Sharp, J. Woodcock, G. Sica, E. Peris, A.T. Moorhouse, D.C. Waddington, Exposure-response relationships for annoyance due to freight and passenger railway vibration exposure in residential environments, The J. Acoust. Soc. Am. 135 (2014) 205-212.

[2] D. Waddington, J. Woodcock, M.G. Smith, S. Janssen, K.P. Waye, CargoVibes: Human response to vibration due to freight rail traffic, Int. J. Rail Transp. 3 (2015) 233-248.

[3] D.P. Connolly, G.P. Marecki, G. Kouroussis, I. Thalassinakis, P.K. Woodward, The growth of railway ground vibration problems A review, Sci. Total Environ. 568 (2016) 1276-1282.

[4] X. Sheng, C.J.C. Jones, M. Petyt, Ground vibration generated by a load moving along a railway track, J. Sound Vib. 228 (1999) 129-156.

[5] W.T. Thomson, Transmission of elastic waves through a stratified solid medium, J. Appl. Phys. 21 (1950) 89-93.

[6] N.A. Haskell, The dispersion of surface waves on multilayered media, Bull. Seismol. Soc. Am. 43 (1953) 17-43.
[7] X. Sheng, C.J.C. Jones, D. Thomson, A theoretical model for ground vibration from trains generated by vertical track irregularities, J. Sound Vib. 272 (2004) 937-965.
[8] E. Ntotsios, S.G. Koroma, W.I. Hamad, D. Thomson, H.E.M. Hunt, Modelling of train induced vibration, IMechE Stephenson Conf. - Res. Railw. (2015).
[9] G. Kouroussis, O. Verlinden, C. Conti, On the interest of integrating vehicle dynamics for the ground propagation of vibrations: The case of urban railway traffic, Veh. Syst. Dyn. 48 (2010) 1553-1571.
[10] G. Kouroussis, O. Verlinden, C. Conti, A two-step time simulation of ground vibrations induced by the railway traffic, Proc. Inst. Mech. Eng. Part C J. Mech. Eng. Sci. 226 (2012) 454-472.
[11] S.G. Koroma, D. Thomson, M.F.M. Hussein, E. Ntotsios, A mixed space-time and wavenumber-frequency domain procedure for modelling ground vibration from surface railway tracks, J. Sound Vib. 400 (2017) 508-532.
[12] G. Kouroussis, D.P. Connolly, O. Verlinden, Railway-induced ground vibrations a review of vehicle effects, Int. J. Rail Transp. 2 (2014) 69-110.
[13] Y.S. Cheng, F.T.K. Au, Y.K. Cheung, Vibration of railway bridges under a moving train by using bridge-track-vehicle element, Eng. Struct. 23 (2001) 1597-1606.
[14] M.K. Song, H.C. Noh, C.K. Choi, A new three-dimensional finite element analysis model of high-speed train-bridge interactions, Eng. Struct. 25 (2003) 1611-1626.
[15] D. Cantero, T. Arvidsson, E. OBrien, R. Karoumi, Traintrackbridge modelling and review of parameters, Struct. Infrastruct. Eng. 12 (2016) 10511064.
[16] M. Ülker-Kaustell, R. Karoumi, C. Pacoste, Simplified analysis of the dynamic soil-structure interaction of a portal frame railway bridge, Eng. Struct. 32 (2010) 3692-3698.
[17] A. Romero, M. Sols, J. Domnguez, P. Galvn, Soil-structure interaction in resonant railway bridges, Soil Dyn. Earthq. Eng. 47 (2013) 108-116.
[18] H. Takemiya, X.C. Bian, Shinkansen high-speed train induced ground vibrations in view of viaduct-ground interaction, Soil Dyn. Earthq. Eng. 27 (2007) 506-520.
[19] L. Andersen, S.R.K. Nielsen, S. Krenk, Numerical methods for analysis of structure and ground vibration from moving loads, Comput. Struct. 85 (2007) 43-58.
[20] E. Kausel, J.M. Roesset, Stiffness matrices for layered soils, Bull. Seismol. Soc. Am. 71 (1981) 1743-1761.
[21] J.C.O. Nielsen, G. Lombaert, S. Franois, A hybrid model for prediction of ground-borne vibration due to discrete wheel/rail irregularities, J. Sound Vib. 345 (2015) 103-120.
[22] N. Triepaischajonsak, D.J. Thompson, A hybrid modelling approach for predicting ground vibration from trains, J. Sound Vib. 335 (2015) 147-173.
[23] J.P. Wolf, Consistent lumped parameter models for unbounded soil: Physical representation, Earthq. Eng. Struct. Dyn. 20 (1991) 11-32.

[24] J.P. Wolf, Consistent lumpedparameter models for unbounded soil: Frequencyindependent stiffness, damping and mass matrices, Earthq. Eng. Struct. Dyn. 20 (1991) 33-41.
[25] S. Carbonari, F. Dezi, G. Leoni, Seismic soilstructure interaction in multi-span bridges: Application to a railway bridge, Earthq. Eng. Struct. Dyn. (2011) 1219-1239.
[26] G.R. Darbre, J.P. Wolf, Criterion of stability and implementation issues of hybrid frequency-time-domain procedure for non-linear dynamic analysis, Earthq. Eng. Struct. Dyn. 16 (1988) 569-581.
[27] A. Nimtaj, M.H. Bagheripour, Non-linear seismic response analysis of the layered soil deposit using hybrid frequency-time domain (HFTD) approach, Eur. J. Environ. Civ. Eng. 17 (2013) 1039-1056.
[28] D. Bernal, A. Youssef, A hybrid time frequency domain formulation for non-linear soil-structure interaction, Earthq. Eng. Struct. Dyn. 27 (1998) 673-685.
[29] P. Bucinskas, L. Agapii, J. Sneideris, L.V. Andersen, Numerical Modelling of the Dynamic Response of High-Speed Railway Bridges Considering Vehicle-Structure and Structure-Soil-Structure Interaction, in: Comput. Tech. Civ. Struct. Eng., Saxe-Coburg Publications, Stirlingshire, UK, 2015: pp. 125-152.
[30] X. Lei, N.A. Noda, Analyses of dynamic response of vehicle and track coupling system with random irregularity of track vertical profile, J. Sound Vib. 258 (2002) 147-165.
[31] R. Ferrara, G. Leonardi, F. Jourdan, A contact-area model for rail-pads connections in 2-D simulations: Sensitivity analysis of train-induced vibrations, Veh. Syst. Dyn. 51 (2013) 1342-1362.
[32] R. Wang, A simple orthonormalization method for stable and efficient computation of Greens functions, Bull. Seismol. Soc. Am. 89 (1999) 733-741.
[33] L. Andersen, J. Clausen, Efficient Modelling of Wind Turbine Foundations, Fundamental and Advanced Topics in Wind Power. (2011).
[34] L.V. Andersen, J. Clausen, Impedance of surface footings on layered ground, Comput. Struct. 86 (2008) 72-87.
[35] MATLAB 2017b and Signal Processing Toolbox 7.5, The MathWorks, Inc., Natick, Massachusetts, United States.
[36] A.R.B. Berawi, Improving Railway Track Maintenance Using Power Spectral Density (PSD), PhD thesis, Universidade do Porto (Portugal), 2013.
[37] J.P. Wolf, Spring-dashpot-mass models for foundation vibrations, Earthq. Eng. Struct. Dyn. 26 (1997) 931-949.
[38] L.V. Andersen, Dynamic soilstructure interaction of polypod foundations, Computers & Structures, 2018 Oct 30.
[39] J. Chung, G.M. Hulbert, Chung J, Hulbert GM. A time integration algorithm for structural dynamics with improved numerical dissipation: the generalized-α method, J. Appl. Mech. 60 (1993) 371.
[40] S. Krenk, State-space time integration with energy control and fourth-order accuracy for linear dynamic systems, Int. J. Numer. Methods Eng. 65 (2006) 595-619.

Paper S1

Semi-analytical approach to modelling the dynamic behaviour of soil excited by embedded foundations

Full reference:

P. Bucinskas, L.V. Andersen, Semi-analytical approach to modelling the dynamic behaviour of soil excited by embedded foundations, Procedia Engineering, X International Conference on Structural Dynamics, EURODYN 2017. 199 (2017) 2621–2626

Status:

The paper in this chapter has been presented at the international conference EURODYN 2017, September 10–13 in Rome, Italy. It has been published in the proceedings of the conference. The contents and typesetting of this chapter are as published.

Available online at www.sciencedirect.com

ScienceDirect

Procedia Engineering 199 (2017) 2621–2626

Procedia Engineering

www.elsevier.com/locate/procedia

X International Conference on Structural Dynamics, EURODYN 2017

Semi-analytical approach to modelling the dynamic behaviour of soil excited by embedded foundations

Paulius Bucinskas[a,*], Lars Vabbersgaard Andersen[a]

[a] *Departament of Civil Engineering, Aalborg University, Thomas Manns Vej 23, Aalborg 9220, Denmark*

Abstract

The underlying soil has a significant effect on the dynamic behaviour of structures. The paper proposes a semi-analytical approach based on a Green's function solution in frequency–wavenumber domain. The procedure allows calculating the dynamic stiffness for points on the soil surface as well as for points inside the soil body. Different cases of soil stratification can be considered, with soil layers with different properties overlying a half-space of soil or bedrock. In this paper, the soil is coupled with piles and surface foundations. The effects of different foundation modelling configurations are analysed. It is determined how simplification of the numerical model affects the overall dynamic behaviour.

Peer-review under responsibility of the organizing committee of EURODYN 2017.

Keywords: Ground vibration; Green's function; foundation modelling.

1. Introduction

Proper evaluation of vibrations is a complex problem, which is especially hard to reproduce numerically. Vibration propagation through soil can be modelled using the Finite Element Method (FEM), but this approach requires modelling of large soil domains and special boundary conditions, and this leads to high computation times and cumbersome calculation procedures. For computational tools to be useful in practice—especially in the early design phase—when a large number of different cases need to be analysed, they have to be relatively fast. Therefore, more computationally efficient approaches are needed.

One way of modelling the response of the soil is by using a semi-analytical approach, based on the Green's function. The semi-analytical solution provides an analytical solution for the Green's function if frequency–wavenumber

* Corresponding author. Tel.: +45 50123118.
E-mail address: pbu@civil.aau.dk

1877-7058
Peer-review under responsibility of the organizing committee of EURODYN 2017.
10.1016/j.proeng.2017.09.396

domain and afterwards a numerical inverse Fourier transform is performed. For the formulation used in this paper, a layer transfer matrix is used. The transfer matrix describes the displacements and traction relation between the top and the bottom of a single layer. The layer transfer matrix was developed by Thomson [1] and further expanded by Haskell [2]. The Green's function approach has been commonly used for various problems concerning the vibrations of soil. Sheng and Jones [3] used it to model the vibrations propagating from a railway track placed on the soil surface. Further solutions for rigid surface footings were provided by Andersen and Clausen [4] and Lin *et al.* [5]. An alternative formulation to the Green's function approach is the stiffness matrix approach by Kausel and Roesset [6]. This method still uses the same layer transfer matrix, however the solution is formulated in terms of stiffness not flexibility.

While the Green's function based model is well known, it is most commonly used to model structure–interaction through the soil surface. This work aims to provide an approach to finding the Green's function between points not only on the soil surface, but also embedded inside the soil body. The obtained system can be modified in order to couple the soil with structures modelled using the FEM. The formulation of the solution is given in Section 2. Further, in Section 3, to illustrate the described approach, some analyses are carried out to evaluate how different foundation-modelling approaches affect the surrounding soil behaviour. Finally, Section 4 list the main conclusions.

Semi-analytical soil model

1.1. Transfer matrix for layered soil based on Green's function

Consider two points: in or on a horizontally stratified half-space Point 1 placed at the coordinates (x_1, y_1, z_1) and Point 2 placed at (x_2, y_2, z_2). The traction p_1 is applied at Point 1 and at time t_1, while the displacement resulting from the load are investigated at Point 2 at time t_2. The relation between the traction and displacement can be expressed using Green's function, provided in time–space domain:

$$\mathbf{u}_2(x_2, y_2, z_2, t_2) = \int_{-\infty}^{t_2} \int_{-\infty}^{\infty} \int_{-\infty}^{\infty} \int_{-\infty}^{0} \mathbf{g}_{12}(x_2 - x_1, y_2 - y_1, z_1, z_2, t_2 - t_1)\mathbf{p}_1(x_1, y_1, z_1, t_1)\mathrm{d}z_1\, \mathrm{d}y_1\, \mathrm{d}x_1\, \mathrm{d}t_1. \quad (1)$$

Unfortunately, an analytical expression for $\mathbf{g}_{12}$ cannot be found. To overcome this problem, a triple Fourier transformation is performed over two spatial coordinates (x, y) and time. The resulting equation is:

$$\mathbf{U}_2\big(k_x, k_y, z_2, \omega\big) = \mathbf{G}_{12}\big(k_x, k_y, z_1, z_2, \omega\big)\mathbf{P}_1\big(k_\mathrm{x}, k_\mathrm{y}, z_1, \omega\big), \quad (2)$$

where $\mathbf{U}_2, \mathbf{P}_1, \mathbf{G}_{12}$ are the triple Fourier transforms of displacement, traction and Green's function, respectively. Further, k_x and k_y are the wavenumbers in the respective horizontal coordinate directions and ω is the circular frequency. The displacement and traction acting on the interface of a layer are combined in the state vector $\mathbf{S}^{j,i}$:

$$\mathbf{S}^{j,i} = [(\mathbf{U}^{j,i})^\mathrm{T} \quad (\mathbf{P}^{j,i})^\mathrm{T}]^\mathrm{T}. \quad (3)$$

The layer number is denoted by the first superscript, j, while the second superscript, i, denotes the top interface of the layer, when equal to 0, or the bottom interface, when equal to 1.

The expression for the Green's function is obtained by solving the Navier equations in frequency–wavenumber domain. After some manipulation, the following expression is obtained, as described by Thomson [1] and Haskell [2]:

$$\mathbf{S}^{j,1} = \mathbf{B}^j\mathbf{S}^{j,0} = \mathbf{S}^{j-1,0}. \quad (4)$$

Matrix $\mathbf{B}^j$ is the transfer matrix and describes the relationship between displacements and tractions at the top and bottom of layer j. A detailed description of the procedure to obtain the transfer matrix can also be found in the work by Sheng *et al.* [3] as well as Andersen and Clausen [4]. The second reformulation in Eq. (4) prescribes continuity of displacements and equilibrium of traction, between adjacent layers at interfaces.

Following the same procedure, a relation between the soil surface $\mathbf{S}^{1,0}$ and the bottommost interface $\mathbf{S}^{J,1}$ can be found. Starting from Layer J and going upwards through the layers, the following is obtained:

$$\mathbf{S}^{J,1} = \mathbf{B}^J\mathbf{B}^{J-1}\mathbf{B}^{J-2}\cdots\,\mathbf{B}^1\mathbf{S}^{1,0}. \quad (5)$$

Now assume that a forced discontinuity in the displacement and/or traction occurs at an interface via the incremental state vector $\Delta\mathbf{S}^{n,0}$ as illustrated in Fig. 1. This results in the following state at the bottom of Layer J:

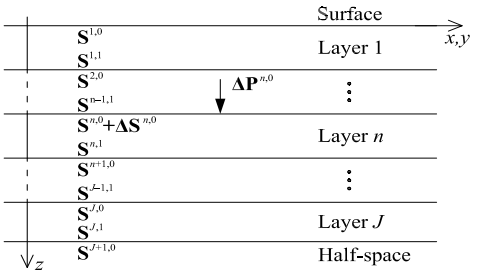

Fig. 1. Assembly of multiple soil layers over a half-space.

$$\mathbf{S}^{J,1} = \mathbf{B}^{J}\mathbf{B}^{J-1}\mathbf{B}^{J-2}\cdots\,\mathbf{B}^{n}(\mathbf{S}^{n,0} + \Delta\mathbf{S}^{n,0}). \tag{6}$$

Including all the layers up to the soil surface, Eq. (7) can be reformulated into

$$\mathbf{S}^{J,1} = \mathbf{T}^{1}\mathbf{S}^{1,0} + \mathbf{T}^{n}\Delta\mathbf{S}^{n,0}; \qquad \mathbf{T}^{n} = \mathbf{B}^{J}\mathbf{B}^{J-1}\mathbf{B}^{J-2}\cdots\,\mathbf{B}^{n+1}\mathbf{B}^{n}. \tag{7}$$

The stratum is assumed to a homogeneous half-space of soil. The relationship between the soil displacement and traction acting at the top of the half-space can be defined as:

$$\mathbf{U}^{J+1,0} = \mathbf{G}_{\mathrm{hh}}\mathbf{P}^{J+1,0}. \tag{8}$$

The half-space is denoted as Layer $J+1$, and $\mathbf{G}_{\mathrm{hh}}$ is the Green's function for the half-space defining a relation between displacement and traction acting on the surface. The derivation of this expression can be found in Ref. [4].

The traction and displacements at the bottom of Layer J have to be equal to the traction and displacement at the top of Layer $J+1$, as shown by Eq. (5). Combining Eq. (8) and Eq. (9), and further assuming that the traction applied to the soil surface and displacement discontinuity applied at Layer n are both equal to zero, the following is obtained:

$$\begin{bmatrix}\mathbf{U}^{J+1,0}\\ \mathbf{P}^{J+1,0}\end{bmatrix} = \begin{bmatrix}\mathbf{U}^{J,1}\\ \mathbf{P}^{J,1}\end{bmatrix} = \begin{bmatrix}\mathbf{G}_{\mathrm{hh}}\mathbf{P}^{J,1}\\ \mathbf{P}^{J,1}\end{bmatrix} = \begin{bmatrix}\mathbf{T}_{11}^{1} & \mathbf{T}_{12}^{1}\\ \mathbf{T}_{21}^{1} & \mathbf{T}_{22}^{1}\end{bmatrix}\begin{bmatrix}\mathbf{U}^{1,0}\\ \mathbf{0}\end{bmatrix} + \begin{bmatrix}\mathbf{T}_{11}^{n} & \mathbf{T}_{12}^{n}\\ \mathbf{T}_{21}^{n} & \mathbf{T}_{22}^{n}\end{bmatrix}\begin{bmatrix}\mathbf{0}\\ \Delta\mathbf{P}^{n,0}\end{bmatrix}. \tag{9}$$

This results in a relationship between the traction applied at the top of Layer n and the displacement on the soil surface:

$$\mathbf{U}^{1,0} = \mathbf{G}_{\mathrm{lh}}\Delta\mathbf{P}^{n,1}; \qquad \mathbf{G}_{\mathrm{lh}} = (\mathbf{G}_{\mathrm{hh}}\mathbf{T}_{21}^{1} - \mathbf{T}_{11}^{1})^{-1}(\mathbf{T}_{12}^{n} - \mathbf{G}_{\mathrm{hh}}\mathbf{T}_{22}^{n}). \tag{10}$$

The matrix $\mathbf{G}_{\mathrm{lh}}$ is the Green's function for displacements on the soil surface caused by a traction applied at the top of the Layer n. To calculate the displacements at lower layers, the original Eq. (4) is used. Further, similar relations can be established for a layered stratum over rigid bedrock.

1.2. Coupling of the layered soil model to a finite element model

The obtained Green's function describes a relation between two points for traction and displacements in three directions (k_x, k_y, z). Calculating a dynamic stiffness matrix for the soil that can be coupled with an FEM model to analyse soil–structure interaction (SSI) involves a number of steps:

1. The Green's function needs to be established for a sufficient number of wavenumbers k_x and k_y to ensure good coverage of the analysed soil body. This can be achieved by evaluating the Green's function along a single axis in the wavenumber domain and rotating the result according to the needed combinations of k_x and k_y.
2. The displacement at a point caused by a distributed load of unit magnitude centred on another point is found in frequency–wavenumber domain and converted to frequency–space domain by inverse Fourier transformation. This is carried out for every combination of two nodal points in which the FEM model interacts with the soil.
3. The obtained 3×3 matrices, describing the relations between two points in three directions, are placed in a single matrix $\mathbf{G}$ with dimensions $3m \times 3m$, when m is the total number of SSI nodes in the system.
4. Unit displacements are prescribed for each degree of freedom in the system and stored in matrix $\mathbf{U_0}$. If n SSI nodes move together as a rigid body, the number of degrees of freedom associated with these points is reduced from $3n$ to 6. The unit displacement matrix size is $3m \times l$, where l is the number of degrees of freedom in the system, and $l \leq 3m$.
5. The Green's function describes the displacements due to the applied loads. Thus:

$$\mathbf{G}\mathbf{P_0} = \mathbf{U_0}. \tag{11}$$

The matrix $\mathbf{P_0}$ containing the acting forces from unit displacement can then be found. It is further integrated over the contact area between rigid bodies and soil (if any rigid bodies are present) to obtain the dynamic stiffness matrix $\mathbf{D}_{\text{soil}}$. This can be achieved by pre-multiplying matrix $\mathbf{P_0}$ with the transposed unit displacement matrix:

$$\mathbf{D}_{\text{soil}} = \mathbf{U_0}^{\text{T}}\mathbf{P_0}. \tag{12}$$

The final obtained dynamic stiffness matrix has the dimensions $l \times l$. To couple the soil with finite elements using the standard stiffness matrix $\mathbf{K}_{\text{FE}}$, damping matrix $\mathbf{C}_{\text{FE}}$ and mass matrix $\mathbf{M}_{\text{FE}}$, the dynamic stiffness matrix for SSI is defined as:

$$\mathbf{D}_{\text{full}} = \mathbf{D}_{\text{FE}} + \mathbf{D}_{\text{soil}}; \quad \mathbf{D}_{\text{FE}} = \mathbf{K}_{\text{FE}} + \mathrm{i}\omega\mathbf{C}_{\text{FE}} - \omega^2\mathbf{M}_{\text{FE}}. \tag{13}$$

Further coupling with a structure above ground level can be obtained by classical FEM assembly. The final model is a computationally efficient solution that still considers fully coupled structure–soil system.

2. Foundation modelling using the semi-analytical soil model

2.1. Rigid and flexible surface footings

A soil body excited by a surface footing is analysed. The surface footing is square, with a length of 2 m. The height of the footing is 0.6 m. It is constructed from concrete, for which the material properties are given in Table 1. The surface footing is modelled using two approaches.

The first approach is to model the footing as a rigid body. In this case, the local deformations of the footing are not considered. Therefore, only the mass density is utilized, whereas the remaining material properties (Young's modulus, Poisson's ratio and damping ratio) are not used. In this case, the footing contact area is discretized into a number of points on the soil surface and, by using the procedure described in Section 2.2, an impedance matrix for 6 degrees of freedom is obtained. The six degrees of freedom include three translational and three rotational degrees of freedom. The footing mass and rotational mass moment of inertia are added to the corresponding degrees of freedom.

The second approach is to model the footing using Mindlin shell finite elements with quadratic interpolation and selective integration. A description of the elements can be found in Ref. [7]. The interface between the soil and the footing is once again discretized into the same number of points. In this case each point has only three translational (or displacement) degrees of freedom, which are coupled with the nodes of the shell elements.

Two different soil cases are tested. The first case considers a half-space of clay material (all the material properties are given in Table 1), while in the second case a half-space of sand is overlaid by a 3 m thick layer of clay. The

Table 1. Materials used in the calculations.

Material	Young's modulus (MPa)	Poisson's ratio (-)	Mass density (kg/m^3)	Damping ratio (-)
Clay	100	0.48	2000	0.045
Sand	250	0.30	2000	0.050
Concrete	34000	0.15	2400	0.010

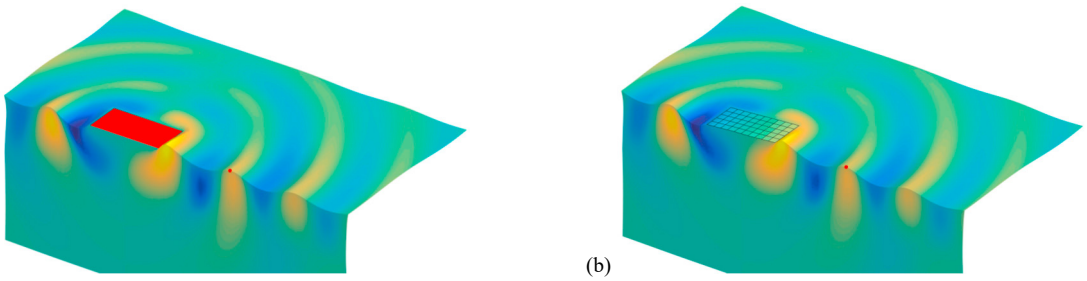

(a) (b)

Fig. 2. Surface footing modelled as rigid (Case a) and flexible body (Case b), excited at 35 Hz. Soil stratification: 3 m layer of clay overlaying half-space of sand. Blue/yellow shades indicate positive/negative displacements in the z-direction. The red dot is the observation point for soil displacement analysis.

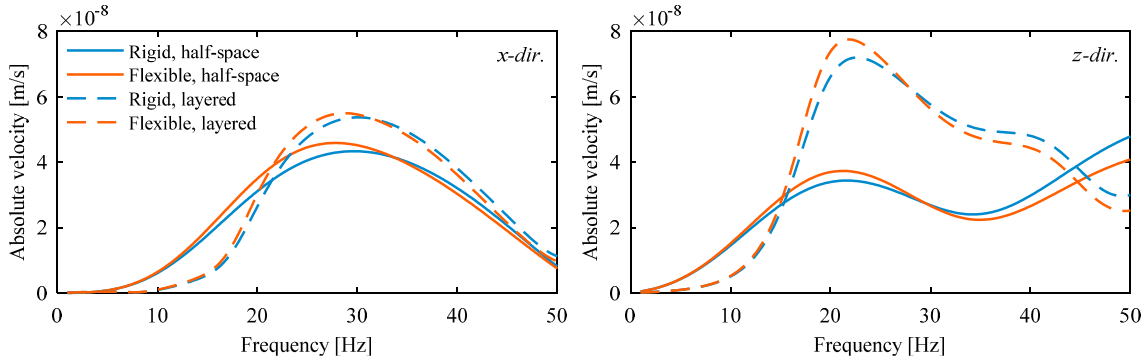

Fig. 3. Velocity dependency on frequency for a point placed 4m from the footing. The footing is modelled as a rigid or flexible plate.

footings are excited by applying a unit moment around the *y*-axis, at every frequency. The behaviour of the footings and soil for one frequency is illustrated in Fig. 2. Further, the soil displacements are analysed at a point placed 4 m from the edge of the footing, on the *x*-axis (position shown in Fig. 2). The results are illustrated in Fig. 3.

From Fig. 2 and Fig. 3 it can be seen that the two approaches provide very similar results. The flexible foundation produces somewhat higher excitation for lower frequencies, but the difference is not significant. Representing the surface footing as a completely stiff plate can be concluded to be a fair assumption in the considered frequency range. However, care should be taken as thinner footings might provide different results.

2.2. Pile foundations

A single pile foundation is analysed. A 5 m long pile is embedded 3 m into the soil body. The pile is modelled using three-dimensional beam elements with six degrees of freedom in each node. A detailed description of the elements is available in Ref. [8]. To couple with soil, the embedded part of the pile is discretized into SSI nodes for which the soil dynamic stiffness matrix is found. The connecting SSI nodes are modelled in three different ways:

1. Each connecting node is a single point in the soil. It has three degrees of freedom which are later coupled to the pile. Therefore, rotational degrees of freedom of the pile are not coupled to the soil.
2. For each connecting node, a horizontal rigid disc with the same diameter as the pile is created, illustrated in Fig. 4a. The disc is discretized into a number of points and the dynamic stiffness is obtained. In this case, the rigid disc has 6 degrees of freedom that are coupled to the translational and rotational degrees of freedom of the pile.
3. Instead of the disk, a ring with same the diameter as the pile is created, see Fig. 4b. The ring is assumed rigid and later coupled to the six degrees of freedom of the pile.

The same two soil-stratification cases as in previous subsection are used. The system is excited by placing a unit moment around the *y*-axis at the very top of the pile. The behaviour of the system with rigid discs and rings, excited at 45 Hz, can be seen in Fig. 4. Further, the displacements of the soil surface 3 metres from the pile are investigated (see Fig. 5). It is observed that different approaches produce significant differences in the behaviour of the system. The peaks, corresponding to the first eigenmode of the pile, are at 5.4 Hz, 10.8 Hz and 11.4 Hz, respectively. This could lead to dramatically different behaviour if used for a bigger system. The first approach, while computationally

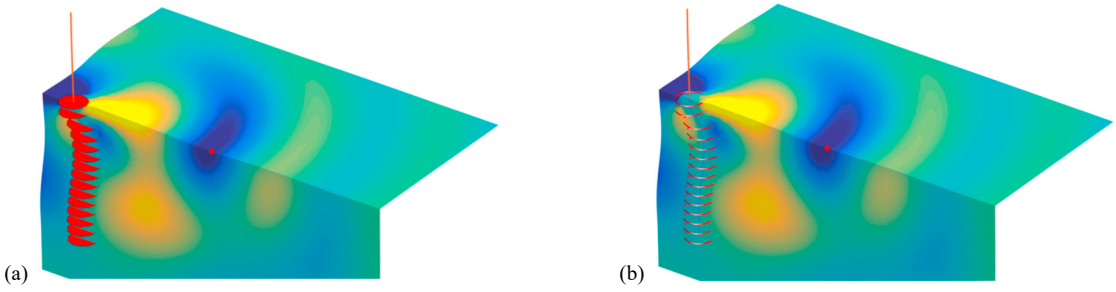

Fig. 4. Pile modelled with rigid disks (Case a) and rings (Case b), excited at 45 Hz. Soil stratification: half-space of clay. Blue/yellow shades indicate positive/negative displacements in the *z*-direction. The red dot is the observation point for soil displacement analysis.

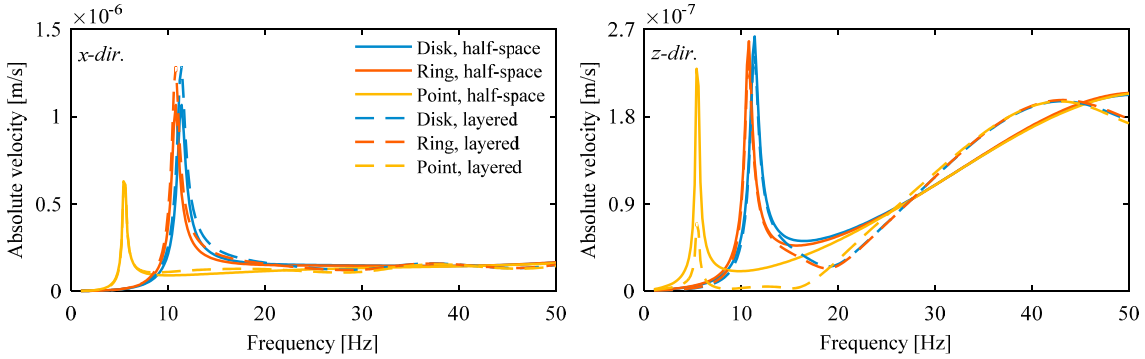

Fig. 5. Velocity dependency on frequency for a point placed 3m from the pile. The interaction points between the soil and pile modelled with three different approaches.

faster compared the other two, underestimates the stiffness added to the pile by the soil. This is caused by the lack of rotational stiffness added from the soil. The second and third approaches produce results much closer to each other. However, to determine the most suitable approach, further validation should be carried out. Most likely, the exact choice of pile modelling approach should be determined depending on the particular modelling case.

3. Conclusions

A semi-analytical soil model is described in this work. A formulation for obtaining Green's function between two points embedded at different depths in the stratum is provided. The semi-analytical model has some advantages when compared to modelling the same problem using an FEM based approach. This approach does not require complicated boundary conditions as infinite boundaries are already assumed in the formulation. Therefore, when optimized correctly, the semi-analytical approach is faster for a wide range of analyses. This formulation could be useful when considering various embedded foundation types or underground structures.

Further, some cases of modelling foundations using the described numerical approach are presented. Surface footings are modelled assuming the footing to be rigid or flexible, modelling the footing using shell finite elements. It was found that the difference between the two approaches is not significant. However, caution should be taken when considering thinner and more flexible surface footings, as investigated by Iguchi and Luco [9].

Finally, pile foundations were analysed. Three different approaches of coupling the pile to the soil were considered. It was found that the coupling between the pile and the soil has a significant effect and that a proper model of the pile cross section interacting with the soil must be used.

Acknowledgements

The research was carried out in the framework of the project "Urban Tranquility" under the Interreg V programme. The authors of this work gratefully acknowledge the European Regional Development Fund for the financial support.

References

[1] W. T. Thomson, "Transmission of elastic waves through a stratified solid medium", Journal of applied Physics 21.2 (1950) 89–93.
[2] N. A. Haskell, "The dispersion of surface waves on multilayered media", Bulletin of the seismological Society of America 43.1 (1953) 17–34.
[3] X. Sheng, C. J. C. Jones, and m. Petyt, "Ground vibration generated by a harmonic load acting on a railway track", Journal of sound and vibration 225.1 (1999) 3–28.
[4] L. Andersen and J. Clausen, "Impedance of surface footings on layered ground", Computers & structures 86.1 (2008) 72–87.
[5] G. Lin, Z. Han, and J. Li, "An efficient approach for dynamic impedance of surface footing on layered half-space", Soil Dynamics and Earthquake Engineering 49 (2013) 39–51.
[6] E. Kausel and J. M. Roësset. "Stiffness matrices for layered soils", Bulletin of the Seismological Society of America 71.6 (1981) 1743-1761.
[7] O. C. Zienkiewicz and R. L. Taylor, "The finite element method for solid and structural mechanics", Butterworth-heinemann, 2005.
[8] M. Paz, "Structural dynamics: theory and computation", Springer Science & Business Media, 2012.
[9] M. Iguchi and J. E. Luco, "Dynamic response of flexible rectangular foundations on an elastic half-space.", Earthquake Engineering & Structural Dynamics 9.3 (1981) 239-249.

Paper S2

Excitation of structures near railway tracks — analysis of the wave propagation path

Full reference:

P. Bucinskas, L.V. Andersen, Excitation of structures near railway tracks — analysis of the wave propagation path, Proceedings of the 6th International Conference on Computational Methods in Structural Dynamics and Earthquake Engineering, COMPDYN 2017. (2017).

Status:

The paper in this chapter has been presented at the international conference COMPDYN 2017, June 15–17 in Rhodes, Greece. It has been published in the proceedings of the conference. The contents and typesetting of this chapter are as submitted.

COMPDYN 2017
6th ECCOMAS Thematic Conference on
Computational Methods in Structural Dynamics and Earthquake Engineering
M. Papadrakakis, m. Fragiadakis (eds.)
Rhodes Island, Greece, 15–17 June 2017

EXCITATION OF STRUCTURES NEAR RAILWAY TRACKS—ANALYSIS OF THE WAVE PROPAGATION PATH

Paulius Bucinskas[1] **and Lars V. Andersen**[1]

[1] Department of Civil Engineering, Aalborg University
Thomas Manns Vej 23, Aalborg 9220, Denmark
{pbu, la}@civil.aau.dk

Keywords: Soil vibration, wave propagation path, structure-soil interaction, railway vibrations.

Abstract. *High-speed rails are an attractive alternative to other forms of intercity transportation. It is a fast, cost-efficient and environmentally friendly solution, which is being developed in various countries across the world. However, in order to be successful, high-speed rails need to transport the passengers as close as possible to the city centres. Therefore, railway tracks have to go through densely populated urban areas, which causes a number of issues. One of the biggest complaints from the inhabitants living near such infrastructures is the high vibration and noise levels caused by the passing trains.*

Unfortunately, the prediction of vibrations in nearby structures is difficult, as wave propagation from the vibration source to the structure is a complex phenomenon. The behaviour of the structure is highly dependent on the path along which the vibrations travel between their source and the building itself. Especially in the densely built urban environment, the wave propagation path can have different features, such as underground infrastructure, roads, pavements or even other nearby buildings. Such features might have a significant effect on the final excitation of the structure in question.

This work aims to analyse how different features in the wave propagation path affect the excitation of a structure. A numerical model is constructed to account for the track structure and the underlying soil. The model utilizes a finite-element model for the structures together with a semi-analytical model of the underlying soil. Different features in the wave-propagation path are introduced, and their effects are compared regarding the behaviour of the structure and the free-field.

1 INTRODUCTION

Continued development of railway infrastructure causes some issues related to vibrations in nearby structures. To make the railways an effective form of passenger transportation the railway stations need to be as close as possible to urban centres. This means that railway tracks need to go through densely built urban environments, causing unwanted vibrations in nearby structures. However, in situ testing of these cases is an expensive and time-consuming task which is sometimes even impossible to carry out. Therefore, computational prediction tools are needed to evaluate the effect on nearby structures. It is not an easy job as wave propagation through soil is a complex phenomenon that depends on a large number of unknowns. The ground between the source of vibrations and receiver point might often contain various obstructions. These obstructions might be on the ground surface or embedded inside the soil body, for example roads, footpaths, demolished building foundations, or sewer lines. This is especially true in a tightly built urban environment.

One of the most commonly used approaches to model the soil body is the finite-element (FE) method. Using this method it is possible to model both the structures interacting with the ground and the ground itself. However, to avoid reflections from the boundaries, absorbing boundary conditions must be used, as in the work by Connolly et al. [1], or the FE model must be coupled to a boundary-element formulation, as in the work by Andersen and Nielsen [2], Nielsen et al. [3] or Andersen [4]. Hence, a semi-analytical soil model can be beneficial to use, especially if the modelled geometry is not very complicated. The semi-analytical approach requires less computational resources and is faster to compute, and infinite boundaries are already included in the formulation. The method is based on analytical evaluation of the Green's function in frequency–wavenumber domain. The original layer-transfer matrix, used in the model, was developed by Thomson [5] and Haskell [6]. Further, the semi-analytical model is commonly used for problems involving wave propagation through soil. For example, Sheng et al. [7] used this method to analyse the vibrations from a simplified railway track placed on the soil surface.

This work also uses the semi-analytical model to model the ground, which is later coupled to structures modelled using an FE approach. The aim is to analyse the effects of various obstructions in the wave propagation path. The effects of these obstructions in the wave path might be an important factor to consider when analysing the ground-borne vibrations, and often they are completely dismissed in this type of analysis. For this, a computational model was constructed that considers a railway track coupled to the underlying ground as described in Section 2. Further, the analysed cases and parameters used are introduced in Section 3. Finally, the obtained results are presented in Section 4, and Section 5 contains the main conclusions.

2 COMPUTATIONAL MODEL

Problems regarding wave propagation through soil can be split into three main components: the vibration source, the propagation path and the receiver. Each of these elements has an effect on the overall system behaviour. In this paper, the vibration source is a railway track, which is introduced in Subsection 2.2. Further, the vibrations propagate through a layered soil for which a semi-analytical model is used as explained in Subsection 2.1. To reduce the number of variables, the receiver is only modelled as a rigid footing on the soil surface.

2.1 Soil model and coupling to finite elements

A semi-analytical approach is used to model the ground. In this case it is more advantageous compared to FE-based approaches due to lower computation times, which allows testing a wider variety of cases. The method is based on an analytical expression for the Green's function in horizontal wavenumber–frequency domain:

$$\mathbf{U}_2(k_x, k_y, z_2, \omega) = \mathbf{G}_{12}(k_x, k_y, z_1, z_2, \omega)\mathbf{P}_1(k_x, k_y, z_1, \omega). \quad (1)$$

Equation (1) provides a relation between a load $\mathbf{P}_1$ applied at point 1 and the corresponding displacements $\mathbf{U}_2$ at point 2. The Green's function $\mathbf{G}_{12}$ is dependent on the horizontal wave-numbers k_x, k_y the vertical coordinates z_1, z_2 of both points, and the circular frequency ω.

After establishing the solution, a numerical inverse Fourier transform is performed to obtain a solution in space–frequency domain. The method assumes that the soil is linear viscoelastic, composed of layers with perfectly horizontal interfaces and with a horizontal ground surface.

To couple the semi-analytical model to the FE formulation of other parts, soil–structure-interaction (SSI) nodes are used. By establishing Green's function relations between these nodes, a flexibility matrix for the soil is obtained. Inverting the flexibility matrix provides the dynamic stiffness matrix for the soil, $\mathbf{D}_{\text{soil}}$, which can then be added to the dynamic stiffness matrix of the FE-based parts, $\mathbf{D}_{\text{FE}}$, to obtain an expression for the whole system:

$$\mathbf{D}_{\text{full}} = \mathbf{D}_{\text{FE}} + \mathbf{D}_{\text{soil}}, \quad \mathbf{D}_{\text{FE}} = \mathbf{K}_{\text{FE}} + \mathrm{i}\omega\mathbf{C}_{\text{FE}} - \omega^2\mathbf{M}_{\text{FE}}, \quad (2)$$

where $\mathbf{K}_{\text{FE}}$ is the stiffness matrix, $\mathbf{C}_{\text{FE}}$ is the damping matrix, $\mathbf{M}_{\text{FE}}$ is the mass matrix, and i is the imaginary unit: $\mathrm{i} = \sqrt{-1}$. The calculations are then performed for the fully coupled system in frequency domain. A more detailed description of the soil model is available in the work by Andersen and Clausen [8], and coupling of multiple structures via the soil was discussed by Andersen [9] and Bucinskas et al. [10].

2.2 Railway track and embankment model

The structure of the railway track has a great impact on how the vibrations are transferred to the soil body. Further, the presence of the track introduces secondary effects to the system such as waves travelling through the embankment and back coupling to the surrounding structures. Therefore, proper modelling of the track structure is important.

To reduce the computational requirements of the model and decrease the computation time, shell elements were used to model the railway track and embankment. A cross-section of an embankment can be seen in Figure 1. A single plate was constructed to model the whole embankment. Mindlin-Reissner shell finite elements were used with four nodes and linear Lagrangian interpolation of the displacements and bending rotations. Two types of elements were used: an element type with three layers to model the three-layered embankment, and an element type with four layers to model the sleepers together with the embankment. Using these element types, the embankment plate is assembled to model the sleepers and all layers of the embankment.

Two rails are connected separately to the embankment. The rails are modelled as Euler-Bernoulli beam elements with two nodes and cubic displacement interpolation. The rails and sleepers are connected through rail pads, which are modelled as a spring and damper system. Thus, the rails are discretely supported only at the positions where the sleepers are located.

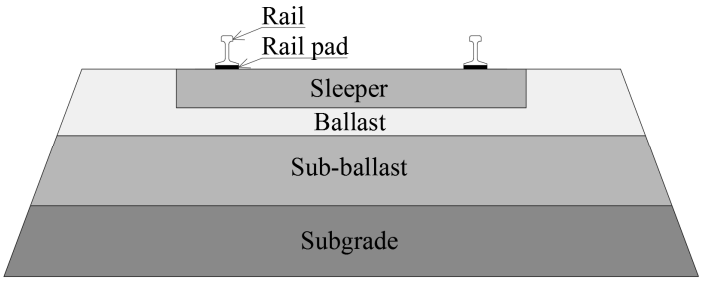

Figure 1: Railway track and embankment cross-section.

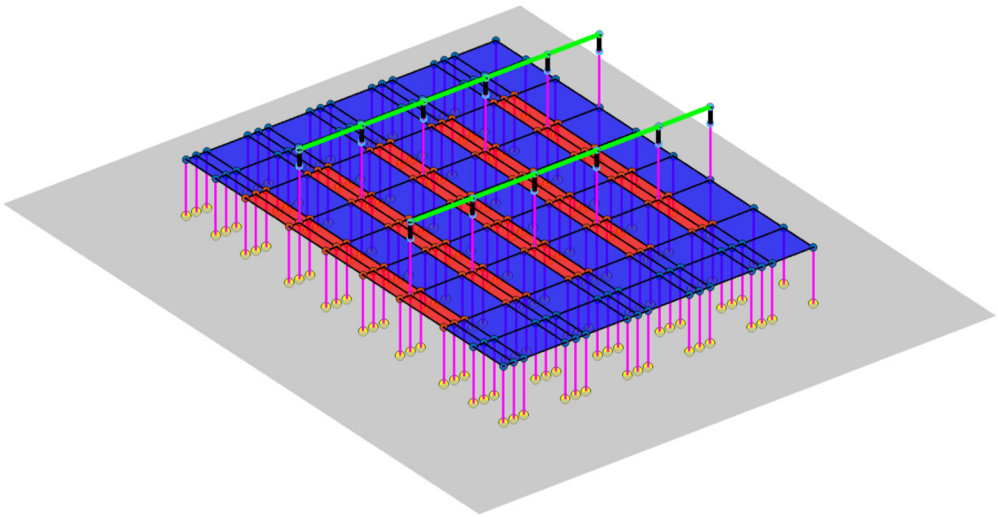

Figure 2: Parts of the track structure. In blue: three layered embankment shell elements; in red: four layered (including sleepers) embankment shell elements; in green: rail beam elements; in grey: soil surface; in yellow: SSI nodes; in magenta: rigid links between soil–embankment and embankment–rail.

The railway embankment is a three-dimensional structure with a considerable thickness. Therefore, modelling the whole embankment as a single flat plate might not be sufficient. To obtain a more realistic model, the plate was placed at the mid-plane of the embankment and then connected to the soil through rigid links. The rigid link length is equal half of the thickness of the embankment. This way the lateral displacements and rotations of the embankment nodes were coupled to lateral displacements of the SSI nodes. The same approach was then used to connect the embankment and the rail pads. The rigid links were introduced into the FE matrices using Lagrange multipliers. This approach was not difficult to implement, as the FE matrix structure stayed unchanged. An example of the FE model of the track can be seen in Figure 2.

Introducing rigid links to the system better represents the real structure, but this kind of formulation also has some disadvantages. The plate representing the embankment does not share nodes with the soil, and thus the number of degrees of freedom in the system increases significantly. Further, Lagrange multipliers also introduce additional constraints to the system, which leads to further increase of FE matrix sizes.

3 ANALYSED CASE

A rail track of 30.0 m length was modelled as described in the previous section. The embankment has a width of 4.0 m and is composed of three layers: a 0.5 m thick subgrade layer, a 0.2 m thick sub-ballast layer, and a 0.3 m thick ballast layer. The material properties for these and other materials used are given in Table 1. The sleepers are embedded in the ballast layer, and they are placed at 0.6 m intervals along the track. The sleepers are constructed from concrete with dimensions $0.2\times0.2\times2.5$ m^3. The rails are made from steel and modelled with a rectangular 0.15×0.08 m cross-section, and the gauge is 1.4 m. The rails are connected to the sleepers via rail pads with stiffness $1.2\cdot10^8$ N/m and damping $1.24\cdot10^5$ Ns/m.

Vibrations are measured on a rigid surface footing placed 20.0 m from the track structure. The rigid footing has a square shape with a side length of 3.0 m. The footing is assumed to be 0.8 m thick and made from concrete. Therefore, the mass density of concrete is used to calculate the mass and mass moments of inertia, which are then added to the corresponding degrees of freedom of the rigid footing.

Material	Young's modulus (MPa)	Poisson's ration (-)	Mass density (kg/m^3)	Damping ratio (-)
Concrete	30000	0.15	2400	0.040
Steel	210000	0.25	7900	0.040
Ballast	100	0.35	1800	0.040
Sub-ballast	300	0.35	2200	0.040
Subgrade	120	0.35	2100	0.040
Clay	80	0.48	2000	0.045
Sand	250	0.30	2000	0.050

Table 1: Materials and their properties used in the analysis

The whole rail track structure and the receiver footing are placed on a 4.0 m thick layer of clay which lies on top of a half-space of sand. This stratification was chosen because the relatively soft layer of clay over the stiffer material (sand) "traps" the propagating vibrations in the upper soil layer, leading to higher excitation at the receiver position.

The system is excited by placing a vertical unit load on one of the rails. It is placed in three different positions along the rail: Position 1—at the centre of the track in the longitudinal direction; Position 2—6.0 m along the track from the centre; Position 3—12.0 m from the centre. In all of the positions, the load is acting on a node that is also connected to a sleeper through the rail pad. Using different positions allows analysis of the system response for cases in which the obstructions in the soil are not in the direct path of the propagating waves.

Four different cases were investigated:

- Free-field conditions. Nothing is placed between the rail track and the receiver footing. This case is used for comparison with other cases.
- A rigid box is embedded between the track and the footing, 10.0 m from the track. The box dimensions are 3.0×3.0×3.0 m^3. The top of the box is embedded 1.0 m from the ground surface. It is assumed that the box is filled with soil and that the density of the walls is close to the density of the surrounding soil. Therefore, the additional mass is not considered.
- A single-lane road is placed on the ground surface between the source and the receiver, 10.0 m from the track. The road is placed alongside the track and has the same length (30.0 m) as the rail track. It is constructed from concrete. The dimensions are: width 4.0 m and thickness 0.3 m. The road structure is modelled using Mindlin-Reissner shell finite elements coupled to soil through SSI nodes.
- A concrete pipe is placed alongside the rail track, 10.0 m from the track and embedded 1.5 m into the soil. As in the previous case, the pipe runs alongside the track and has the same length. The pipe is modelled as a cylindrical tube with an outer diameter of 1.0 m and an inner diameter of 0.75 m. It is modelled as a finite Euler-Bernoulli beam coupled to the soil through SSI nodes.
- Same as previous case, just this time the pipe is oriented at 45° angle to the rail track. The pipe centre is 10 m from the track.
- Once again the same embedded pipe is used. In this case, the pipe is at 90° angle to the track, that is the pipe goes under the rail track and extends towards the receiver footing.

4 THE EFFECT OF OBSTRUCTIONS IN THE WAVE PROPAGATION PATH

The wave propagation path was analysed for the previously described six cases. The analysis was performed from 1 Hz up to 50 Hz, with 1 Hz intervals. The results are presented in Figures 3 and 4.

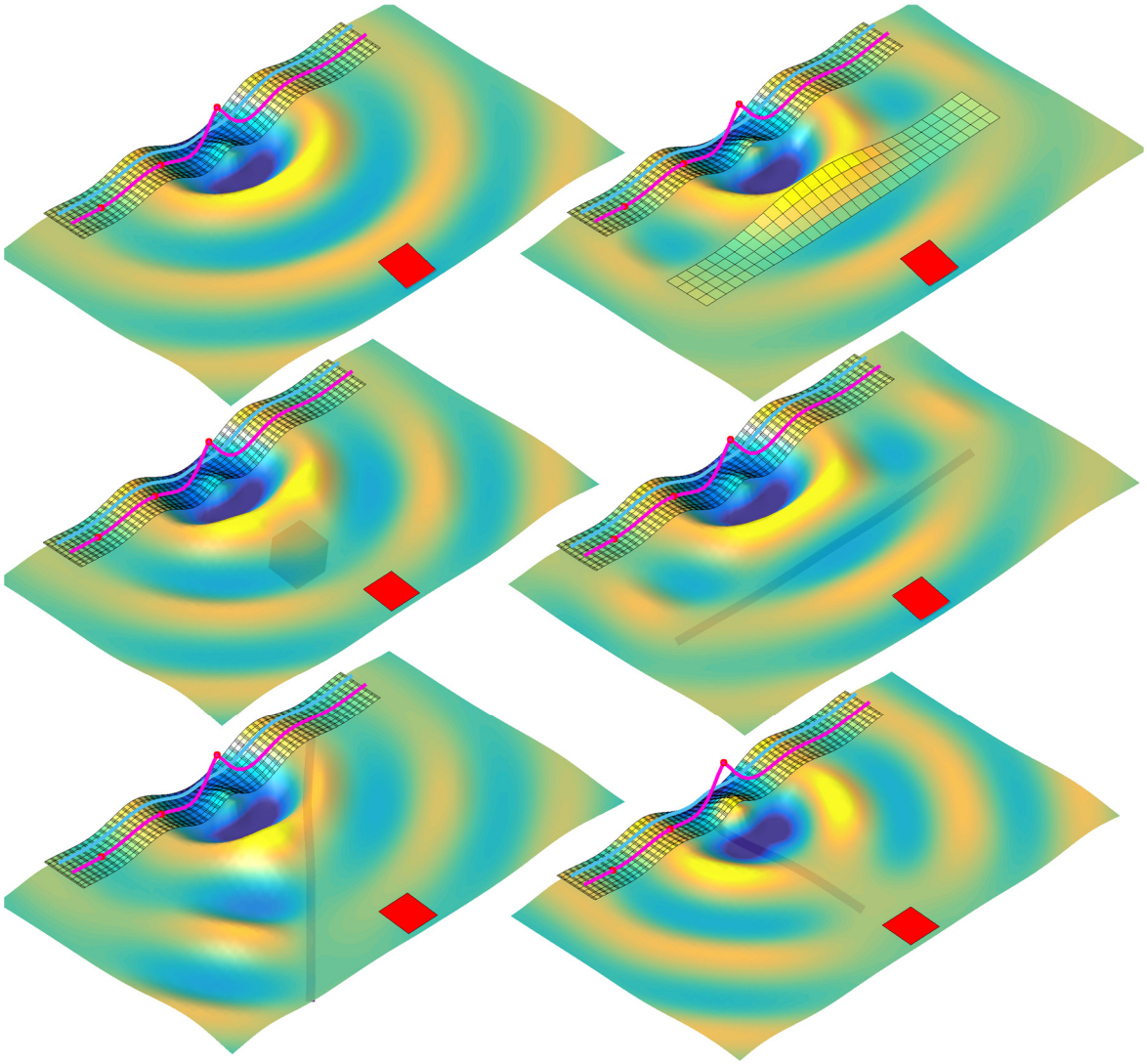

Figure 3: Steady state soil surface response for a load applied on the rail at the centre of the track, excited at 25 Hz. Blue/yellow shades indicate positive/negative displacement in vertical direction. The red dots on the rail show the three positions in which the load is applied within the analysis. In this case, the load is only applied in the first point. Top left: free-field; top right: road placed between the track and receiver; middle left: embedded rigid box; middle right: embedded pipe along the track; bottom left: embedded pipe at 45° angle to the track; bottom right: embedded pipe at orthogonal to the track.

Figure 3 shows the response of the soil surface excited at 15 Hz. All cases are shown for the load placed on the rail at Position 1. It is evident that the displacements of the soil are effected significantly by obstructions in the wave propagation path. The road surface forms a wave-impeding barrier for the propagating surface waves, thus decreasing the displacement field over a large area. However, the effect at the receiver footing is rather small. Further, the embedded rigid box has a larger effect for the receiver footing, however it is localized to a small shadow area behind the box. The overall effect to the displacement is much smaller when compared to the road case. Further, all three cases of embedded pipes cause very different behaviour of the system. For the pipe laid along the track, the effects are very similar to the road case—the displacement field is reduced in a large area, but the effects at the receiver footing are small. It can be seen that obstructions have less impact when the obstructions are laid orthogonally to the propagating waves. This is illustrated in the next case—embedded pipe at 45° angle. In this

case there is a significant reduction of displacements at the receiver footing, while the displacements are increased directly in front of the embedded pipe. Finally, the last case, the embedded pipe orthogonal to the track, provides the most significant reduction of displacements for the receiver footing. However, similar to the embedded box, the effects are localized to a smaller area and the surrounding displacement field is largely unaffected.

Further, Figure 4 shows the absolute velocities at the receiver position for all cases. Overall it can be seen that introducing obstructions in the wave propagation field have the highest effect in frequency ranges between 7–40 Hz, while frequencies up to 7 Hz are almost unaffected. In the 7–30 Hz range, the obstructions tend to reduce the velocities at the receiver position when compared to the free-field case. However, in the 30–40 Hz range the effects are not as evident. In this range, some cases—especially the road—tend to increase the velocities significantly.

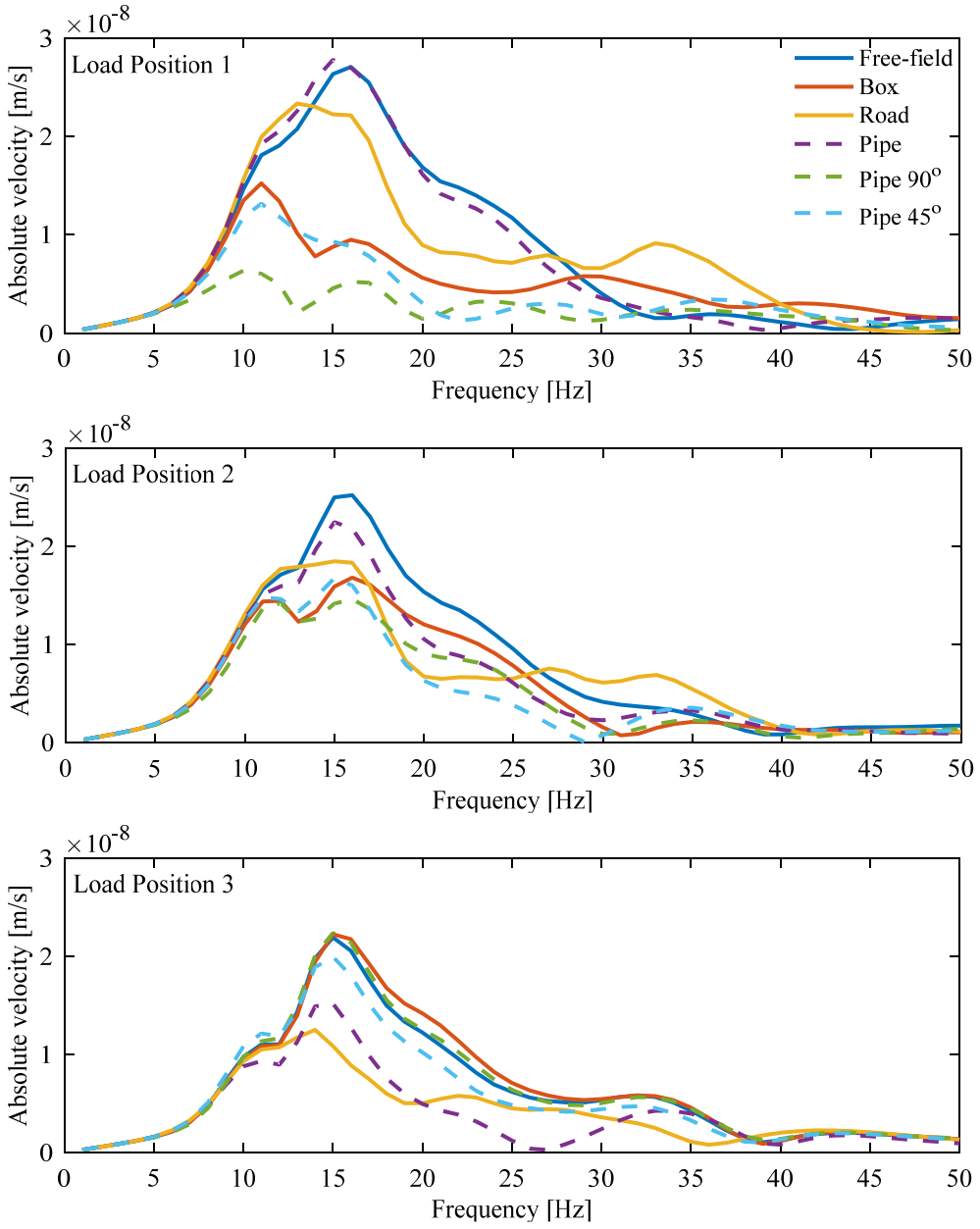

Figure 4: Response at the receiver for obstructions in the wave propagation path: a) load Position 1, applied on a rail at the centre of track; b) load Position 2, applied on a rail 6.0 m from the centre of the track; c) load Position 3, applied on a rail 12.0 m from the centre of the track.

Further, Figure 4 shows that pipe running along the rail track has a very small effect when the load is placed at Position 1. However, this effect increases when the load is placed further from the track centre. A completely opposite behaviour is observed with the pipe placed orthogonally to the track—the effects become smaller when the centre the load is placed further away from the track. This shows that the angle at which the waves reach the obstruction is a very important factor in the analysed system. The road case has a similar effect as the pipe placed along the track, but the overall effects across all loading positions are higher. This is due to larger stiffness and mass introduced to the system by the road, when compared to an embedded pipe. However, in the 30–40 Hz frequency range, the changes in absolute velocity relative to the reference case become positive, that is the velocities at the receiver increase when compared to the free-field case. Finally, the rigid box has a more localized effect. For loading in Positions 1 and 2, the effects are positive and rather large, but as soon as the box is not in the direct wave path between source and receiver (loading at Position 3) these effects disappear almost completely.

5 CONCLUSIONS

A presentation has been given of ground vibration due to harmonic excitation. Analysis was performed to investigate the effects of obstacles placed inside the soil body or on the ground surface between the source and the receiver. The load was applied on a railway track and the response was checked on a surface footing. Five different cases were tested: an embedded rigid box (simulating an infilled tank or former cellar), a segment of a single-lane road (or a large footpath) running parallel to the rail track on the soil surface, and three different orientations of an embedded pipe in the wave propagation path. The cases were compared to the free-field response with no obstacles in or on the ground. A computational model was created using an FE formulation to model the rail track structure and the obstructions, while the soil was modelled using a semi-analytical approach.

The results show that obstruction in the wave propagation field does cause significant changes in the overall system behaviour. In most cases, the obstacles have a mitigation effect, thus reducing the absolute velocities, especially within the 7–30 Hz frequency range. However, in some cases, the response increases within the 30–40 Hz frequency range. The effects of the structures considered in this paper are mostly seen at higher frequencies. This can be explained by the relatively small size of the considered structures, where at lower frequencies the wavelength in the soil body is much longer than the dimensions of the structures. Therefore, the effects at low frequencies are very small.

Future work could investigate these effects for a wider frequency range together with different soil-stratification cases. Further, analysis could be performed for different obstructions to the propagating waves that are commonly present, such as: tree roots, large boulders, underground cables, etc. Also more in-depth analysis of different orientations of the structures considered might reveal different effects caused to the system.

ACKNOWLEDGMENTS

The research was carried out in the framework of the project “Urban Tranquility” under the Interreg V programme. The authors of this work gratefully acknowledge the European Regional Development Fund for the financial support.

REFERENCES

[1] D. Connolly, A. Giannopoulos, and M. C. Forde. Numerical modelling of ground borne vibrations from high speed rail lines on embankments. *Soil Dynamics and Earthquake Engineering* **46**: 13–19, 2013.

[2] L. Andersen and S. R. K. Nielsen, Reduction of ground vibration by means of barriers or soil improvement along a railway track, *Soil Dyn. Earthq. Eng.*, **25**(7–10), 701–716, 2005.

[3] J.C.O. Nielsen, G. Lombaert, and S. François. A hybrid model for prediction of ground-borne vibration due to discrete wheel/rail irregularities. *Journal of Sound and Vibration* **345**: 103–120, 2015.

[4] L.V. Andersen, Influence of dynamic soil-structure interaction on building response to ground vibration, in Numerical Methods in Geotechnical Engineering—Proceedings of the 8th European Conference on Numerical Methods in Geotechnical Engineering, NUMGE 2014, 2014, vol. 2.

[5] W.T. Thomson, Transmission of elastic waves through a stratified solid medium, Journal of applied Physics **21.2:** 89–93, 1950.

[6] N.A. Haskell, The dispersion of surface waves on multilayered media, *Bulletin of the seismological Society of America* **43.1:** 17–34. 1953.

[7] X. Sheng, C. J. C. Jones, and M. Petyt, Ground vibration generated by a harmonic load acting on a railway track, *Journal of sound and vibration* **225.1**: 3–28, 1999.

[8] L. Andersen and J. Clausen, Impedance of surface footings on layered ground, *Computers & structures* **86.1**: 72–87, 2008.

[9] L. V. Andersen, "Dynamic soil–structure interaction of monopod and polypod foundations," in *Insights and Innovations in Structural Engineering, Mechanics and Computation, Proceedings of the Sixth International Conference on Structural Engineering, Mechanics and Computation, 5–7 September 2016, Cape Town, South Africa*, 2016, pp. 2036–2041.

[10] P. Bucinskas, L. V. Andersen, and K. Persson, "Numerical modelling of ground vibration caused by elevated high-speed railway lines considering structure-soil-structure interaction," in *Proceedings of the INTER-NOISE 2016 - 45th International Congress and Exposition on Noise Control Engineering: Towards a Quieter Future*, 2016.

Paper S3

Dynamic soil excitation from railway tunnels

Full reference:

P. Bucinskas, L.V. Andersen, Dynamic soil excitation from railway tunnels, Numerical Methods in Geotechnical Engineering IX, Proceedings of the 9th European Conference on Numerical Methods in Geotechnical Engineering, NUMGE 2018. Volume 2 (2018) 1551–1556.

Status:

The paper in this chapter has been presented at the international conference NUMGE 2018, June 25–27 in Porto, Portugal. It has been published in the proceedings of the conference. The contents and typesetting of this chapter are as submitted.

Dynamic soil excitation from railway tunnels

P. Bucinskas & L. V. Andersen
Department of Engineering, Aarhus University, Aarhus, Denmark

ABSTRACT: Underground railway lines generate a large amount of ground-borne vibrations, which has negative effects to the inhabitants and structures nearby. However, due to the large number of variables affecting the generation and propagation of vibrations, numerically predicting these effects is a complex task. When accounting for all factors, the numerical models become complicated to produce and take long time to compute. Alternatively, severely simplified models do not provide satisfactory precision. The aim of the paper is identification of the most important factors when modelling the propagation of vibrations from railway tunnels. Identifying the most important parameters allows creation of computational models that account for the most significant phenomena, while reducing the computational complexity as much as possible. For this task a number of different embedded railway tunnel models are created. To account for soil–tunnel interactions a semi-analytical soil model is used, which is based on the transfer matrix method. The tunnel structure is modelled using finite elements which are coupled to the semi-analytical soil solution, thus achieving a fully coupled structure–soil model.

1 INTRODUCTION

Underground metro lines are an essential part large urban centres, as they allow fast and efficient transportation for a large number of passengers. Therefore, new lines are constantly being constructed and old ones upgraded across the world. However, rail lines underneath a densely built city environment can lead to serious problems caused by ground borne vibrations. Hence, numerical models capable of predicting these effects are needed. This becomes especially important in the early project design phases, where the uncertainty regarding the soil conditions and specifications of the structure are high. Thus, computationally efficient models are required that can be used to evaluate larger number of cases.

Over the years, several models have been proposed to analyse railway tunnels. The most commonly used approaches are the finite element (FE) and the boundary element (BE) methods. These methods offer great flexibility to model different conditions and structure geometries, they can also be combined to create coupled FE-BE solutions. An example of coupled FE-BE model can be found in the work by Andersen & Jones (2006). However, these approaches can be extremely time consuming.

To reduce the computation times, so-called 2.5-dimensional models are often used, in which Fourier transformation is carried out in the spatial direction along the tunnel. François *et al.* (2010) as well as Rieckh *et al.* (2012) introduced 2.5-dimensional BE tunnel models in horizontally layered soil. The work assumed a straight tunnel with infinite extent in one direction. Thus, the soil response can be split between separate wavenumbers, allowing efficient parallel computations.

Alternatively, modelling the soil using a semi-analytical approach can also greatly reduce the computational times. The pipe-in-pipe model by Forrest & Hunt (2006) uses a full-space Green's function to model the soil behaviour. The obtained solution is computationally efficient and reproduces the most important phenomena in the system. However, for shallow cut-and-cover type tunnels, the full-space assumption might not be sufficient.

This work uses a Green's function calculated for a half-space as described by Andersen & Clausen (2008), this way taking into account the effect of soil surface. The semi-analytical solution is then coupled with FE, which models the tunnel structure, similar to the models of railways and surface structures previously proposed by the authors (Persson *et al.* 2017; Bucinskas *et al.* 2016; Bucinskas & Andersen 2017).

The modelling approach is described in detail in Section 2. Using the described approach, a number of tunnel models are created and presented in Section 3. These models have varying degree of complexity to investigate the most important modelling

parameters of the system. Results obtained are then presented in Section 4. Finally, the conclusions are given in Section 5.

2 MODELLING APPROACH

2.1 *Semi-analytical soil model*

A semi-analytical model based on the Green's function is used to model the soil. The soil stratum is assumed to be homogeneous and visco-elastic with hysteric damping. Further, the surface and the interfaces between layers are perfectly horizontal. To assemble multiple soil layers and obtain the Green's function, the transfer matrix method is used, as originally proposed by Thompson (1950) and Haskell (1953).

An analytical expression for the Green's function is only obtained after transforming the solution into frequency and wavenumber domain over the two horizontal directions, while keeping the vertical coordinates in spatial domain. Due to the approach used, it is only possible to apply external forces on the interfaces between two layers or on the soil surface. Therefore, additional interfaces need to be created for every depth where the structure and soil interact. The Green's function is then calculated for all combinations of created interfaces. After obtaining the Green's function, a unit load is applied at the origin of the coordinate system and the corresponding displacements calculated for a range of wavenumbers. A so-called bell-shaped unit load is created using a two-dimensional Gaussian distribution. This shape of unit load is advantageous as it approaches zero for high wavenumbers, compared to a point force which provides a constant Fourier coefficient in the whole wavenumber domain. This results in a solution where the response of the system at high wavenumbers is also approaching zero, thus acting as a filter. Two bell-shaped loads applied on nearby nodes and the overlap of the loaded areas are shown in Figure 1. It should be noted that the loads can only be distributed over the horizontal coordinates, even when a horizontal load is applied.

Further, double inverse Fourier transformation is applied to transform the solution into frequency-spatial domain. The domain itself is discretized into a number of structure-soil interaction (SSI) nodes, where the response is of interest. To obtain the flexibility matrix, a unit load is placed on a single node and the resulting response is investigated at all nodes. After repeating the process for all SSI nodes a flexibility matrix of the system is obtained. Finally, inverting the flexibility matrix the dynamic stiffness matrix $\mathbf{D}_s$ of the soil is obtained.

2.2 *Sub-structuring approach to model cavities*

The semi-analytical soil model offers an efficient approach when modelling the soil behaviour. However, a tunnel is a rather complex structure that among other things involves excavation of a substantial amount of material from the continuous stratum. That could significantly influence the overall system behaviour. Unfortunately, directly modelling cavities inside the soil is not possible with the used semi-analytical soil model.

Therefore, the soil–tunnel system is divided into sub-structures. The continuous soil stratum is modelled using the semi-analytical approach, while the volume of the cavity inside the soil is discretized using solid FEs with the material properties of the soil. The cavity inside the soil can then be recreated by subtracting the FE substructure from the continuous stratum. Further, additional shell FEs are added to the exterior of the cavity to model the tunnel lining. The approach is illustrated in Figure 2.

The dynamic stiffness matrix of the system becomes:

$$\mathbf{D}_{\text{full}} = \begin{bmatrix} \mathbf{D}_s^{11} & \mathbf{D}_s^{12} \\ \mathbf{D}_s^{21} & \mathbf{D}_s^{22} \end{bmatrix} - \begin{bmatrix} \mathbf{D}_c^{11} & \mathbf{D}_c^{12} \\ \mathbf{D}_c^{21} & \mathbf{D}_c^{22} \end{bmatrix} + \begin{bmatrix} \mathbf{D}_l & 0 \\ 0 & 0 \end{bmatrix}, \tag{1}$$

where $\mathbf{D}_s$ and $\mathbf{D}_l$ is the dynamic stiffness matrices of the cavity and tunnel lining respectively. The superscript 11 denotes nodes on the outer boundary of the tunnel, 22 are nodes inside the tunnel, and 21/12 are the coupling terms. The dynamic stiffness matrices of the FE parts are calculated from standard stiffness, $\mathbf{K}$, damping, $\mathbf{C}$, and mass, $\mathbf{M}$, matrices. The dynamic stiffness matrix for the tunnel lining includes linear viscous damping:

$$\mathbf{D}_l = \mathbf{K}_l - \omega^2 \mathbf{M}_l + \mathrm{i}\omega \mathbf{C}_l, \tag{2}$$

where ω is the circular frequency and i is the unit imaginary number. A hysteric damping model is used for the soil, where damping is independent of the frequency. Therefore, the dynamic stiffness matrix for the cavity becomes:

$$\mathbf{D}_c = \mathbf{K}_c - \omega^2 \mathbf{M}_c + \mathrm{i}\mathbf{C}_c. \tag{3}$$

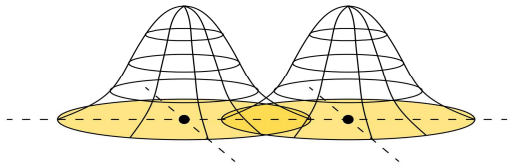

Figure 1. Two bell-shaped loads applied on nearby SSI nodes

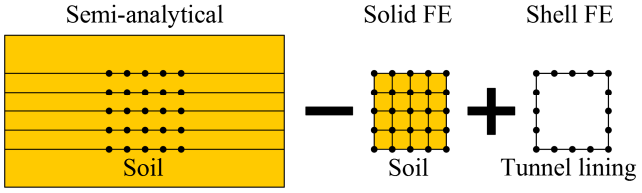

Figure 2. Sub-structuring approach to model a tunnel.

To properly couple both approaches, additional considerations are needed. Firstly, the SSI nodes inside the stratum are placed in the exact same positions as the nodes in the FE sub-model. Further, the bell-shaped load radiuses are directly related to the element size of the FE, such that the area loaded by the SSI nodes in an interface would be equal to the interaction area between the two sub-models. Eight-node solid FEs are used to model the soil inside the cavity and four-node Mindlin shell elements are utilized to model the tunnel lining. Practice showed that elements with linear interpolation work better with the semi-analytical soil model, compared to elements with quadratic interpolation, as all nodes inside an equal-sided element distribute the stiffness evenly, without additional weighting depending on the position of the node inside the element. This way the obtained dynamic stiffness matrices better represent the results from the semi-analytical soil model.

The sub-structuring approach encounters some problems when modelling cavities inside the soil, without the additional stiffness from the tunnel lining. Most likely the problems arise due to the differences in the two modelling approaches. The two approaches are especially different when dealing with horizontal forces. As already mentioned, the semi-analytical model distributes the loads over horizontal interfaces, thus leading to somewhat different behaviour in vertical and horizontal directions, while in the FE method all directions are handled in the same manner. Further, the convergence between the two approaches also differs—poor discretization tends to underestimate the stiffness in the semi-analytical approach, while it is generally overestimated in the FE method. To an extent these problems can be avoided by properly discretizing the modelled structure.

Further, the damping values obtained in the stratum are often very close to the damping of the FE cavity part. Thus, when subtracting the two sub-structures, the damping can become extremely small or even negative for direct terms. That leads to unphysical behaviour of the system. To avoid these problems, the damping term $\mathbf{C}_c$ in Equation 3 was not used in the computations. The accuracy of the obtained results is somewhat reduced. However, it is assumed to be insignificant, especially when investigating the excitation on the soil surface.

3 ANALYSED CASE

A cut-and-cover type tunnel is investigated in this paper. Construction of this type of tunnel involves digging a trench in which the structure is constructed and then covered back with soil. Cut-and-cover tunnels are easy to construct and are commonly encountered in the urban environment. Further, due to the relatively shallow depth, the excitation of the tunnel can lead to high vibrations on the soil surface.

The modelled tunnel structure has a square profile, with the width and the height both equal to 4.9 m. The tunnel lining is 0.5 m thick and constructed from concrete (material properties used are given in Table 1). The total length of the modelled structure is 49.7 m to minimize the effects of the ends of the structure. It is embedded by 3.1 m from the soil surface to the tunnel crown or 8.0 m from the soil surface to the tunnel floor. The structure is excited by a unit vertical force applied on the tunnel floor in the centre of the structure.

Analysis is performed within the frequency range 1–50 Hz. To ensure a sufficient number of elements to model wave propagation accurately, all FEs are created with a mesh size of 0.7 m, which ensures at least nine elements per S-wavelength at 50 Hz. Four different cases are tested:

- Full model—the tunnel is modelled as described in Section 2. The system is divided into three sub-structures: the continuous soil stratum modelled with the semi-analytical soil model, cavity discretized into solid FEs and tunnel lining modelled with shell FEs. The unit force is equally divided over 4 nodes, loading a 0.7×0.7 m^2 square in the middle of the tunnel.
- Tunnel lining—the full model is simplified by removing the solid FEs that model the cavity. In this case only the tunnel lining is modelled with shell FEs and coupled to the semi-analytical stratum solution.
- Beam—the tunnel-lining model is further simplified by replacing the shell elements with three-dimensional beam elements. In this case a single beam is placed along the centre line of the tunnel, with the corresponding cross-sectional properties. The excitation force is placed on a single node at the centre of the beam.
- Only soil—reference case. No structure is coupled to the semi-analytical soil model. The load is distributed the same way as in the full case.

The soil is modelled as a half-space of drained stiff sand, with a P-wave speed of 580 m/s and an S-wave speed of 310 m/s.

Two dispersion diagrams for these soil conditions are shown in Figure 3. The dispersion diagram on the left shows the vertical soil response from a vertical load applied on the soil surface, while the dispersion diagram on the right is the soil surface response from a vertical load applied at 8.0 m depth, i.e. where the tunnel floor will be placed.

Comparing the two diagrams it can be seen that in both cases the response is dominated by Rayleigh waves (R-waves). Thus, a strong response of the

Table 1. Material properties

Material	Young's modulus (MPa)	Poisson's ratio (-)	Mass density (kg/m3)	Damping ratio (-)
Sand	250	0.30	2000	0.045
Concrete	30000	0.15	2400	0.040

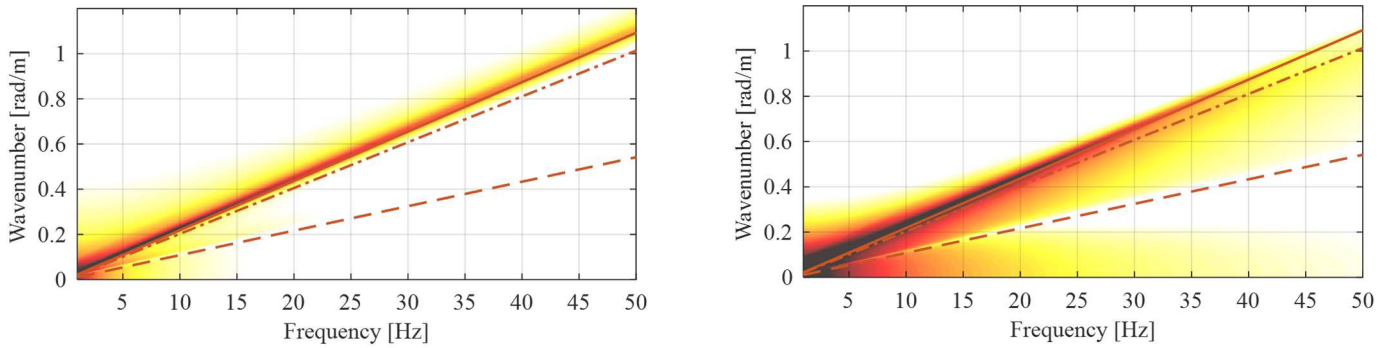

Figure 3. Dispersion diagrams for vertical soil surface displacement. On the left—from a vertical load applied at the soil surface, on the right— from a vertical load applied at 8.0 m depth. Lines indicate P-waves (— —), S-waves (— · —) and R-waves (——). Darker colors indicate higher response. Colors in both plots are not on the same scale.

ground surface can be seen at combinations of the wavenumber and frequency corresponding to the dispersion line of the R-wave. However, when the force is embedded, the response is spread out through a wider wavenumber range.

4 RESULTS

4.1 *Soil surface response over frequencies*

The response of the soil is investigated at four points on the soil surface. The most complex model, i.e. the full tunnel model, is used as the reference for the correct system behaviour, investigating how different simplifications affect the soil response. Figure 4 shows the soil surface response at four observation points. The positions of the points can be seen in Figures 5 and 6.

Figure 4a shows the absolute vertical displacements on the soil surface directly above the excitation point inside the tunnel (the positions of observation nodes can be also seen in Figures 5 and 6). It can be seen that introducing a tunnel structure inside the soil significantly influences the response, when comparing with the only soil case.

Further, modelling the tunnel with or without the cavity does not influence the results significantly. Especially, the responses observed in the different models are similar at higher frequencies. However, the differences between the simple beam model and more complex models that model the tunnel lining with shell elements are quite significant. The beam model predicts a distinct peek at around 28 Hz, which is not predicted in the other cases. This could lead to an overestimation of the response in the middle frequency range, when the simplified tunnel model is utilized.

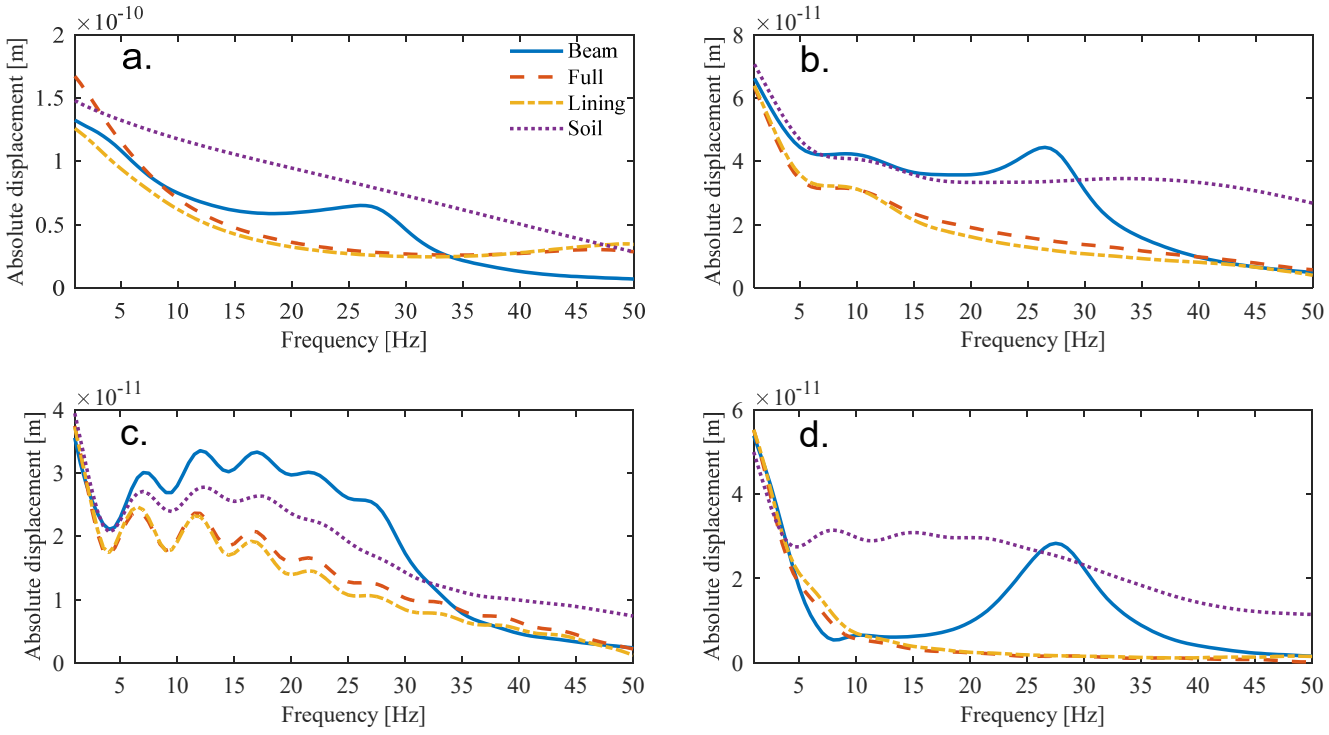

Figure 4. Absolute vertical soil surface displacements at selected observation points: a—directly above the excitation point in the tunnel, b—12.5 m away orthogonally to the tunnel, c—25.0 m away orthogonally to the tunnel, d—20.0 m along the centre line of the tunnel. The point positions are illustrated in Figures 5 and 6.

Further, Figure 4b shows the soil surface response 12.5 m away from the tunnel perpendicularly. The overall behaviour is very similar to that in Figure 4a, with both the full model and the tunnel-lining model showing very similar overall behaviour. In this case, the beam model shows better agreement in very low (up to 5 Hz) and high (above 40 Hz) frequency ranges. However, at middle frequencies the differences are still large. This trend continues with distance increased up to 25.0 m away from the tunnel, as shown in Figure 4c. The simple beam model shows even better agreement with the more complex models. However, the middle frequency range is still represented poorly.

Figure 4d shows the vertical soil surface displacements 20.0 m away from the excitation point along the direction of the tunnel. It is evident that in this direction the tunnel model is very important in the frequency range above 5 Hz, when compared with the only-soil case. Once again, the beam model has a significant peak at around 28 Hz, with poor results in the middle frequency range.

When comparing all four observation points, it can be seen that both the full and lining-only models provide very similar results for all cases. The beam model is not able to reproduce the same behaviour, especially at medium frequency ranges, indicating that modelling the tunnel as a single beam is an oversimplification of the system. However, excluding the cavity inside the tunnel does not have a significant influence. This could be used to simplify the computational model.

4.2 *Displacement field of surrounding soil*

To investigate the effects of the cavity inside the soil, full and just tunnel lining cases are investigated in more detail. The soil displacements are observed on a 30×30×18 m^3 box is placed around the tunnel structure and the response calculated at two frequencies: 10 Hz and 50 Hz.

Figure 5 shows the absolute vertical soil displacements at 10 Hz. The displacement fields for the investigated cases are almost identical, except the zone around the tunnel excitation point. Here the full model predicts somewhat higher overall displacements, while the zone with large displacements is more localized within the tunnel-lining-only model. Further, the waves are quickly attenuated by the tunnel structure and mostly propagate away from the structure. Similar behaviour is seen in Figure 6, where the displacement field is illustrated at 50 Hz.

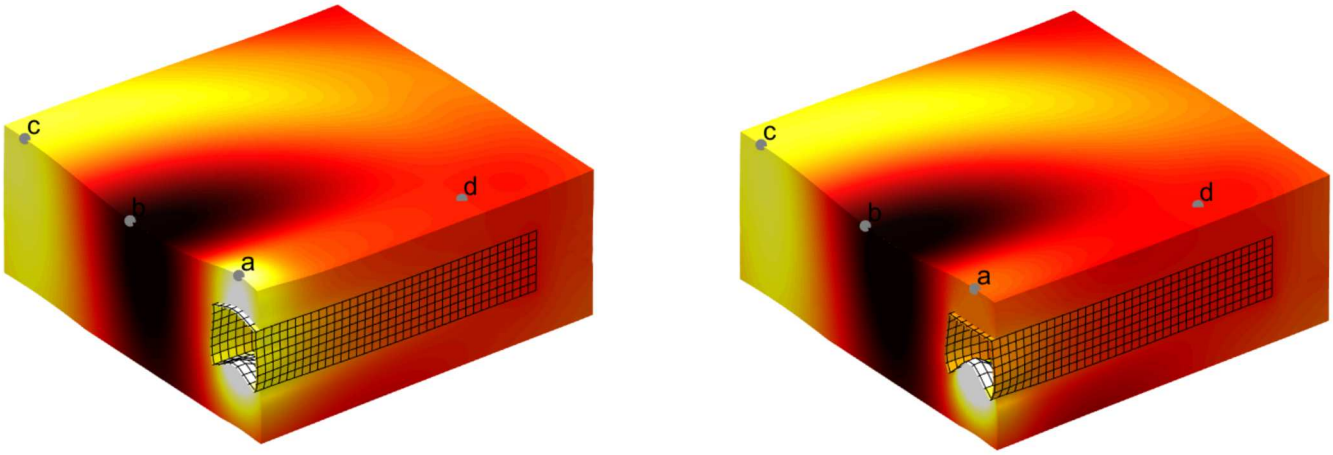

Figure 5. Field response at 10 Hz. On the left—full model; on the right—model with only tunnel lining present. Dark and light shades indicate negative and positive displacement in the vertical direction. Nodes show the positions of observation points used in Figure 4.

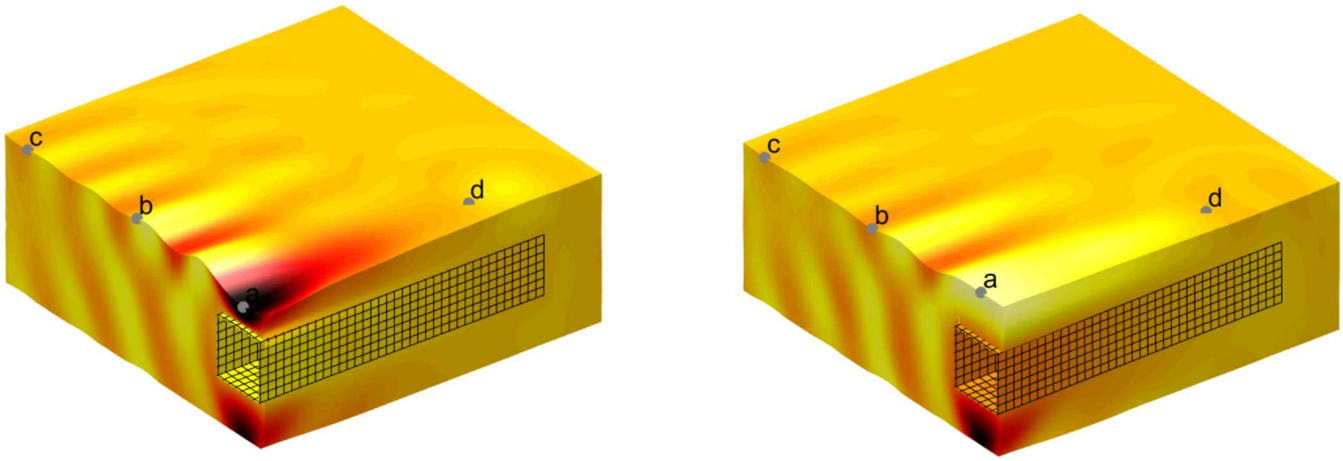

Figure 6. Field response at 50 Hz. On the left—full model; on the right—model with only tunnel lining present. Dark and light shades indicate negative and positive displacement in the vertical direction. Nodes show the positions of observation points used in Figure 4.

Once again, the two approaches provide very similar displacement fields further away from the zone around the excitation point. In this case the soil displacements above the tunnel have completely opposite phase angles. This illustrates that the effects from the cavity are present in the nearfield and quickly disappear further away from the structure.

5 DISCUSSION AND CONCLUSION

A computational model to simulate the behaviour of a tunnel structure and the surrounding soil was presented. The proposed method combines a semi-analytical soil model with the FE method which is used to model the cavity inside the tunnel as well as the tunnel lining. A computationally efficient system that can be used to analyse large numbers of cases is obtained. Due to the differences in the two modelling approaches, i.e. the semi-analytical method and the FE method, some difficulties can arise when modelling cavities without the supporting structure. Therefore, further investigation of the proposed methodology is needed. However, adding the supporting structure (in this case the tunnel lining) stabilizes the system and provides satisfactory results.

Using the described methodology, a cut-and-cover type tunnel was modelled. Several different models of the tunnel structure were investigated, with varying degree of simplifications, focus of the analysis being the vertical response of the soil surface. It was determined that modelling the cavity inside the soil is not essential, as the model with only the tunnel lining provides similar results with significantly lower computational effort. However, when considering the displacements close to the excitation point, or when a bigger cavity is present in the soil, the effects from the cavity might become more important. Further, a very simple model that models the whole tunnel as a single beam did not provide satisfactory results. Especially, it overestimates the response in the middle frequency range around 25 Hz. Thus, the beam model provides poorer results than a model with no tunnel at all, i.e. with soil only.

ACKNOWLEDGMENT

The research was carried out in the framework of the project “Urban Tranquility” under the Interreg V programme. The authors of this work gratefully acknowledge the European Regional Development Fund for the financial support.

REFERENCES

Andersen, L. and Clausen, J., 2008. Impedance of surface footings on layered ground. *Computers & Structures*, 86(1), 72–87.

Andersen, L. and Jones, C.J.C., 2006. Coupled boundary and finite element analysis of vibration from railway tunnels—a comparison of two-and three-dimensional models. *Journal of Sound and Vibration*, 293(3), 611–625.

Bucinskas, P., Andersen, L.V., Persson, K., 2016. Numerical modelling of ground vibration caused by elevated high-speed railway lines considering structure-soil-structure interaction, in: Proceedings of the INTER-NOISE 2016—45th International Congress and Exposition on Noise Control Engineering: Towards a Quieter Future.

Bucinskas, P., Andersen, L.V., 2017. Semi-analytical approach to modelling the dynamic behaviour of soil excited by embedded foundations. *Procedia Engineering*, 199, 2621–2626.

Forrest, J.A. and Hunt, H.E.M., 2006. A three-dimensional tunnel model for calculation of train-induced ground vibration. *Journal of Sound and Vibration*, 294(4), 678–705.

François, S., Schevenels, M., Galvín, P., Lombaert, G., Degrande, G., 2010. A 2.5D coupled FE-BE methodology for the dynamic interaction between longitudinally invariant structures and a layered halfspace. *Comput. Methods Appl. Mech. Eng.* 199, 1536–1548.

Haskell, N.A., 1953. The dispersion of surface waves on multilayered media. *Bulletin of the seismological Society of America*, 43(1), pp.17–34.

Persson, P., Andersen, L. V., Persson, K., Bucinskas, P., 2017. Effect of structural design on traffic-induced building vibrations. *Procedia Engineering*, 199, 2711–2716.

Rieckh, G., Kreuzer, W., Waubke, H., Balazs, P., 2012. A 2.5D-Fourier-BEM model for vibrations in a tunnel running through layered anisotropic soil. *Eng. Anal. Bound. Elem.* 36, 960–967.

Thomson, W.T., 1950. Transmission of elastic waves through a stratified solid medium. *Journal of applied Physics*, 21(2), 89–93.

Paper S4

Dynamic structure response using surrogate models

Full reference:

P. Bucinskas, L.V. Andersen, Dynamic structure response using surrogate models, Advances in Engineering Materials, Structures and Systems: Innovations, Mechanics and Applications, Proceedings of the 7th International Conference on Structural Engineering, Mechanics and Computation, SEMC 2019. (2019) 109–114.

Status:

The paper in this chapter has been presented at the international conference SEMC 2019, September 2–4 in Cape Town, South Africa. It has been published in the proceedings of the conference. The contents and typesetting of this chapter are as submitted.

Dynamic structure response using surrogate models

P. Bucinskas & L. V. Andersen
Department of Engineering, Aarhus University, Aarhus, Denmark

ABSTRACT: Environmental vibrations are a well-known problem that can cause annoyance and even have negative health effects to the exposed population. Using surrogate models for the estimation of vibrations is an attractive alternative to costly numerical modelling or on-site measurements. They can provide almost instantaneous results, which are needed for the early design phases of a construction project. In this paper, a surrogate model is developed for the response of a simplified building structure coupled to the underlying soil. To obtain the data needed to fit the surrogate model, a numerical approach is used. In it, the structure is modelled using finite elements, while the soil is modelled using a semi-analytical approach based on the Green's function. The surrogate models are created to estimate the changes to the vibration level from the changes in the building internal structure, e.g. spacing between the columns, floor height and building footprint.

1 INTRODUCTION

Computational modelling of ground-borne vibration is a complex and time-consuming task. Various computational approaches are available, from very simple analytical approaches to complex three-dimensional model based on the finite element (FE) method. The analytical approaches simplify the modelled systems to a large degree, making their use rather limited, while the more complex models are limited by the large computational effort needed. Therefore, if an estimation of the environmental vibrations is required, the computational models are most often only used in the later design stages. Surrogate models allow representing the complex computational model through a relatively simple and quick-to-compute emulator of the results, making them suitable for use in the early project design stages.

To create the surrogate model, a data set of high quality is needed, provided by the so-called 'truth model'. In this paper, the truth model combines a semi-analytical soil model with an FE model of the structure. The soil is modelled using the transfer-matrix method as described by Thompson (1950) and Haskell (1953). To combine the FE structure with the soil, the approach previously described by Bucinskas & Andersen (2017) is used. Further, the rigid surface footings of the building are modelled as described by Andersen & Clausen (2008). The obtained computational model is relatively quick to compute, allowing easy testing of different surrogate modelling approaches.

The Kriging method is used to create the surrogate model, as originally described by Krige (1951). The method allows individually adjusting the behaviour of each variable of the modelled parameter space, leading to a more precise surrogate model. Further, the used data set has a large effect in the overall precision of the surrogate model. Data can be obtained from experimental measurements or from previously performed numerical simulations. In any case, the most accurate surrogate models are achieved by creating a data-sampling plan, for which the computational model is used. This way, the obtained surrogate model can fill the parameter space well. That is, the behaviour of the system is represented accurately through the modelled parameter space. Creation of a space-filling sampling plan and fitting of the surrogate model is described by Forrester et al. (2008). The described methodology is also used in this paper.

2 METHODOLOGY

2.1 *Coupled soil–structure model*

A surrogate model requires a data set, which can be used to fit the model. In this case, a coupled soil-structure computational model is used to obtain the truth model that generates this data set.

The soil is modelled using a semi-analytical approach, utilizing the Green's function. The soil body is assumed to behave elastically, with perfectly horizontal interfaces between the soil layers and perfectly horizontal soil surface. The analytical solution to the

Green's function is obtained in the frequency–wavenumber domain. Here, only the horizontal coordinates (x and y-coordinates) are transformed into wavenumbers, while the vertical coordinate (the z-coordinate) is left in the spatial domain. The expressions for the Green's function tensor $\mathbf{G}$ in the frequency wavenumber domain is:

$$\mathbf{U}(k_x, k_y, z_r) = \mathbf{G}(k_x, k_y, z_s, z_r)\mathbf{P}(k_x, k_y, z_s), \quad (1)$$

where $\mathbf{U}$ is the displacement vector for the receiver point, $\mathbf{P}$ is the load applied at a source point, k_x and k_y are the horizontal wavenumbers, and z_s and z_r are the source and receiver depths, respectively. To obtain the Green's function, the layer-transfer matrix method is utilized, assembling the layers using a flexibility-based approach. Hysteric damping is used, making the Young's modulus E of the soil complex:

$$E = E(1 + \mathrm{i}\,\mathrm{sign}(\omega)\,\eta), \quad (2)$$

where η is the loss factor and $\mathrm{sign}(\omega)$ is the sign of the angular frequency. After the Green's function has been obtained, it is transformed back into frequency–space domain by discrete inverse Fourier transformation.

To couple the structure to the soil, the dynamic stiffness matrix for the soil is needed. Therefore, the interface between the structure and the soil is discretized into a number of structure–soil interaction (SSI) nodes. Then, a load is applied at each node and the resulting displacements observed at all nodes, using the previously obtained Green's function. Placing these results into a matrix form, the global flexibility matrix $\bar{\mathbf{G}}_\mathrm{s}$ of the system is obtained. Then, the global stiffness matrix of the soil can then be obtained by simply inverting the flexibility matrix:

$$\bar{\mathbf{K}}_\mathrm{s} = \bar{\mathbf{G}}_\mathrm{s}^{-1}. \quad (3)$$

Further, if rigid objects interacting with the soil are modelled, the stiffness matrix is concentrated by adding the contributions of discrete nodes together for each degree of freedom of the rigid body.

The structure interacting with the soil is modelled using finite elements. In this case, two types of elements are used: Euler-Bernoulli beam elements and Mindlin-Reissner shell elements. The beam elements have six degrees of freedom per node (three translational and three rotational), while the shell elements have five degrees of freedom per node (three translational and two rotational around local x and y-axes). Since the soil is modelled in the frequency domain, stiffness $\mathbf{K}$, mass $\mathbf{M}$, and damping $\mathbf{C}$ matrices are transformed into the dynamic stiffness matrix $\bar{\mathbf{K}}_\mathrm{b}$:

$$\bar{\mathbf{K}}_\mathrm{b} = \mathbf{K} + \mathrm{i}\omega\mathbf{C} - \omega^2\mathbf{M}. \quad (4)$$

The dynamic stiffness matrix $\bar{\mathbf{K}}_\mathrm{sb}$ of the coupled soil-structure system can now be assembled as:

$$\bar{\mathbf{K}}_\mathrm{sb} = \begin{bmatrix} \bar{\mathbf{K}}_\mathrm{b,nn} & \bar{\mathbf{K}}_\mathrm{b,na} \\ \bar{\mathbf{K}}_\mathrm{b,an} & \bar{\mathbf{K}}_\mathrm{b,aa} + \bar{\mathbf{K}}_\mathrm{s} \end{bmatrix}, \quad (5)$$

where subscript 'a' indicates the degrees of freedom of the structure 'attached' to the soil and subscript 'n' the degrees of freedom "not attached" the soil stratum. After the dynamic stiffness matrix has been assembled, the system can be solved using standard FE method approach in the frequency domain.

Due to the semi-analytical approach used to account for the soil, the proposed computational model offers relatively short computation times. This is useful when testing surrogate models. A faster computational model can be used to determine the best approach of fitting the surrogate model, before carrying out expensive and time-consuming detailed FE analysis or carrying out on-site measurements.

2.2 *Surrogate model*

A surrogate model recreates the behaviour of a modelled system utilising a number of data points where the real system behaviour is known. Intuitively, more data points should lead to a more precise surrogate model. However, the distribution of the data points throughout the design space is also extremely important. Ideally, the design space could be filled creating an n-dimensional grid of points, but this approach quickly becomes impractical with increasing number of variables (dimensions of design space). In this paper, the sampling plan is created using Latin Hypercube sampling. Firstly, a number of random samples are created which are then tested to determine the most space filling sampling plan, as described by Forrester et al. (2008).

To create the surrogate model, the Kriging method is used. Firstly, the Quantity of Interest (QoI) Y at a number k of sampling points (according to the sampling plan) is found using the computational model:

$$\mathbf{Y} = \{Y(\mathbf{x}_1), Y(\mathbf{x}_2), \ldots, Y(\mathbf{x}_k)\}^\mathrm{T}, \quad (6)$$

where each input variable $\mathbf{x}$ is an n-dimensional vector. The Kriging method utilizes the correlation of points according to the basis function:

$$\mathrm{cor}(\mathbf{x}_i, \mathbf{x}_j) = \exp\left(-\sum_{l=1}^{n} \theta_l \left|x_{i,l} - x_{j,l}\right|^{p_l}\right). \quad (7)$$

By changing the fit factors θ_l and p_l, the surrogate model can be adjusted to fit the data. In this work, the factor p_l is constant and equal to 2, leading to a smooth correlation between data points. However, the factor θ_l is adjusted to fit the surrogate model to the truth model. This factor can be interpreted as a measure of how 'active' a variable is in the model. Thus, properties that have a high effect on the system behaviour will have a higher θ_l factor. The correlation matrix is then assembled as:

$$\boldsymbol{\Psi} = \begin{bmatrix} \mathrm{cor}(\mathbf{x}_1, \mathbf{x}_1) & \ldots & \mathrm{cor}(\mathbf{x}_1, \mathbf{x}_k) \\ \vdots & \ddots & \vdots \\ \mathrm{cor}(\mathbf{x}_k, \mathbf{x}_1) & \ldots & \mathrm{cor}(\mathbf{x}_k, \mathbf{x}_k) \end{bmatrix}. \quad (8)$$

To find the best fit, the concentrated ln-likelihood function is used:

$$\ln(L) \approx -\frac{k}{2}\ln(\sigma^2) - \frac{1}{2}\ln(|\boldsymbol{\psi}|), \quad (9)$$

where σ^2 is found as:

$$\sigma^2 = \frac{(\mathbf{Y} - \mathbf{1}\mu)^{\mathrm{T}}\boldsymbol{\psi}^{-1}(\mathbf{Y} - \mathbf{1}\mu)}{k}, \quad \mu = \frac{\mathbf{1}^{\mathrm{T}}\boldsymbol{\psi}^{-1}\mathbf{Y}}{\mathbf{1}^{\mathrm{T}}\boldsymbol{\psi}^{-1}\mathbf{1}}. \quad (10)$$

Equation 9 is maximized by changing the θ_l factor to fit the surrogate model. It is not possible to differentiate this equation analytically, thus a numerical procedure is needed. In Matlab, it is achieved by using an inbuilt function '*ba*', which utilizes a genetic algorithm to find the minimum of a function. Since the algorithm searches for the minimum of a function, Equation 9 is modified by multiplication with –1.

After the surrogate model has been made, it can be used for prediction of new function values $\hat{Y}(\hat{\mathbf{x}})$. A correlation vector between the new input value $\hat{\mathbf{x}}$ and the input values used to create the surrogate model $\mathbf{x}$ is constructed, as described in Equation 7:

$$\hat{\boldsymbol{\psi}} = \{\mathrm{cor}(\mathbf{x}_1, \hat{\mathbf{x}}) \quad \ldots \quad \mathrm{cor}(\mathbf{x}_k, \hat{\mathbf{x}})\}^{\mathrm{T}}. \quad (12)$$

Using the created vector, a new prediction can be made as:

$$\hat{Y}(\hat{\mathbf{x}}) = \mu + \hat{\boldsymbol{\psi}}^{\mathrm{T}}\boldsymbol{\psi}^{-1}(\mathbf{Y} - \mathbf{1}\mu). \quad (13)$$

The correlation matrix size increases with increasing number of points used for fitting, and the computational times needed to calculate new data points increase correspondingly. This is usually not a problem if the initial data set is not too large. However, when high precession is needed or the number of variables is large, the correlation matrix size can become problematic. This leads to long computation times and in some cases difficulties searching for the maximum of Equation 9. Therefore, the size of the data set should be considered when creating the surrogate model.

3 ANALYSED CASE

3.1 *System geometry and varying parameters*

The response of a simplified building structure is analysed. The building is composed of two square floors supported by four columns. The floors are modelled using shell elements with constant thickness across the whole floor. The columns are modelled using beam elements with a square cross-section. The building structure is made of concrete with the material properties given in Table 1.

Building foundations are modelled as rigid footings, resting on the soil surface. The footings are 2 m wide squares. Each rigid footing has six degrees of freedom that are directly attached to the columns. The structure is resting on a two-layered soil stratum. The first layer is a 4 m thick sand layer, and the second layer is a half-space of hard till. Material properties for the soil layers are also given in Table 1. The system is excited by a vertical unit load placed 25 m from the centre of the structure. The load is distributed as a two-dimensional Gaussian distribution, creating a 'bell-shaped' load, with a standard deviation of 0.5 m.

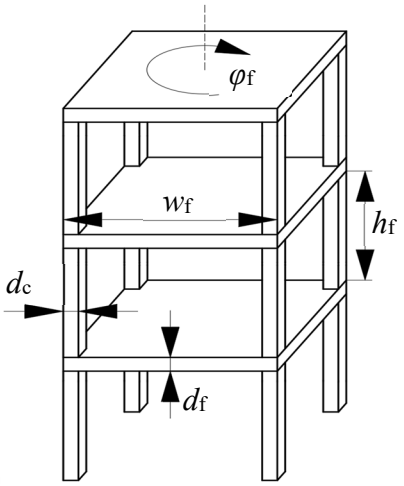

Figure 1. Varying parameters of the building model

Five geometry parameters of the building structure are assumed to be varying: floor height h_f, floor width w_f, floor thickness d_f, column cross-section width d_c and the rotation of the whole structure φ_f. The varying building geometry properties are illustrated in Figure 1. Further, the minimum and maximum values for these properties are given in Table 2. All other parameters, including the properties of the soil, are constant. Examples of some realizations of the created building structure, by assigning random values to the varying parameters, are shown in Figure 2.

One of the biggest limitations of the surrogate model is that it is only able to produce one output value for a given set of input parameters. This is a significant limitation when the dynamic behaviour of the structure is of interest, as the structural response is dependent on the frequency. Therefore, choosing a single QoI to represent the structural response is a non-trivial task. In this case, it has been decided to analyse the response of the top floor of the building.

Table 1. Material properties.

	Young's modulus	Poisson's ratio	Mass density	Loss Factor
	[MPa]	[-]	[kg/m^3]	[-]
Concrete	30,000	0.150	2400	0.030
Sand	161.2	0.465	1650	0.030
Hard till	1800	0.350	2140	0.013

Table 2. Varying building geometry parameters.

			min	max	mean
Floor height	h_f	[m]	2.5	7.0	4.75
Floor width	w_f	[m]	4.0	8.0	6.0
Floor thickness	d_f	[m]	0.15	1.0	0.575
Column width	d_c	[m]	0.15	1.0	0.575
Structure rotation	φ_f	[rad]	0	0.5π	0.25π

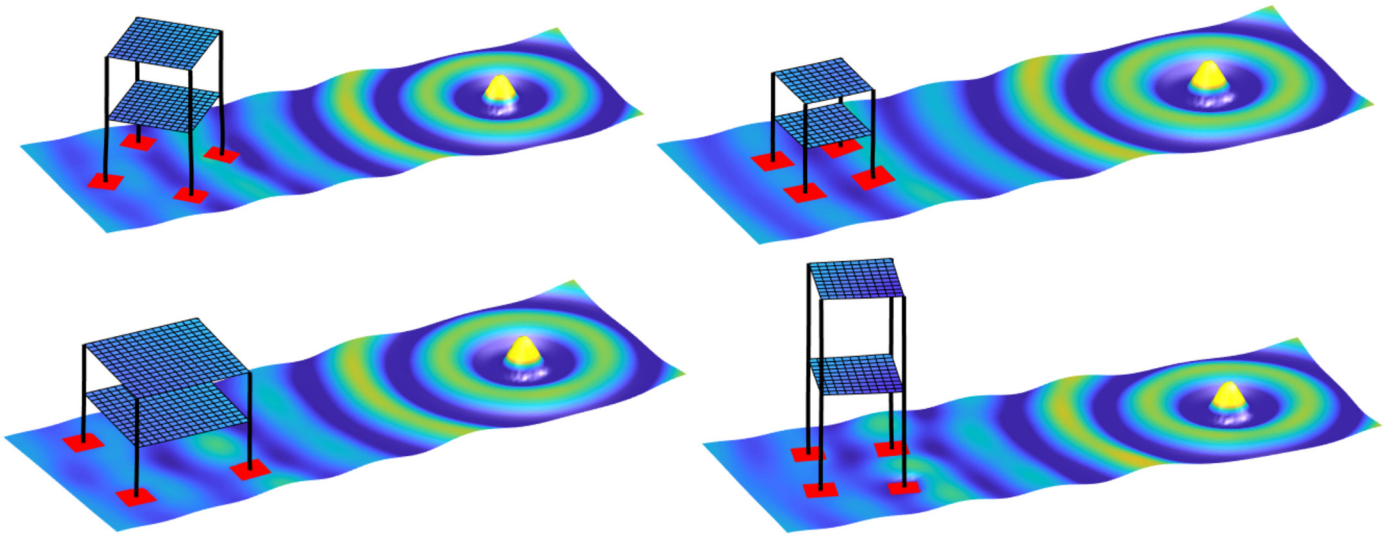

Figure 2. Examples of the created building structures by assigning random geometry parameters. The shown system is excited at 31.6 Hz. Note that the column cross-section size and floor thickness are not illustrated.

However, choosing just a single point on the floor as an observation point might disregard some eigenmodes of the structure. Thus, the vertical displacements of all nodes of the top floor are considered, taking the root-mean-square (RMS) level to obtain a single number. Further, the narrow band response is concentrated into one-third octave bands. For each band, the response at 10 equally spaced discrete frequencies are calculated and the RMS value taken to obtain the QoI. This is done for all one-third octave bands with central frequencies in the range from 6.3 Hz to 80 Hz, i.e. 12 one-third octave bands are analysed. This way, the system response in frequency domain can be recreated based on 12 QoIs based on 12 separate surrogate models. Another approach could be to assume the frequency as one of the varying parameters in the surrogate model. However, in that case, fitting the surrogate model might prove to be challenging and would require a large amount of points, further complicating the fitting procedure.

3.2 *Fitting of the surrogate model*

The fitting procedure is very important when creating a surrogate model. Larger sets of data used to fit the surrogate model will generally lead to more precise representations. However, as discussed previously, more data points will also lead to a model that is slower and harder to use. Therefore, a compromise between the data set size and the precision of the model needs to be found. This is only possible when a computational model is used and it is possible get the response anywhere in the parameter space. This might not be the case when experimental results are needed to create the surrogate model.

Two strategies of fitting the surrogate model were considered. The first approach is to calculate a large data set and fit the surrogate model directly. The second approach is to create a smaller data set and then selectively add additional points, while continuously updating the surrogate model. To find the best fitting approach, three cases were tested. Using the first approach two cases were created by fitting the surrogate model to data sets of 150 and 300 points. The locations of the data points were determined by searching for the most space filling set of locations from a set of randomly generated Latin Hyper cubes. For the second approach, a smaller data set of 50 points was used initially, and then an additional 100 points selectively added. The selective point positions in the parameter space where determined by searching for maximum expected improvement, cf. Forrester et al. (2008). Due to constant updating of the surrogate model, the second approach is rather computationally demanding. For the analysed case, a surrogate model created with 150 points by infilling 100 points requires more computational effort than calculating 300 data points and fitting the model directly. Of course, this will not be true for more demanding computational models. To test how well the created models perform, the root mean square error (RMSE) was calculated:

$$\varepsilon_{\mathrm{RMS}} = \sqrt{\frac{1}{n}\sum_{j=1}^{n}\left(Y(\mathbf{x_j}) - \hat{Y}(\mathbf{x_j})\right)^2}, \tag{14}$$

where $Y(\mathbf{x_j})$ are values obtained from the computational model and $\hat{Y}(\mathbf{x_j})$ are the values from the tested surrogate model. To obtain the error, $n = 100$ realizations of the computational were used, computed independently of the tested surrogate models.

The obtained RMSEs for one-third octave bands are given in Figure 3. It can be observed that the first approach of creating the surrogate model provides more accurate results within most of the tested frequency range. Even when comparing surrogate models that use 150 data points, the first approach provides a more precise result. This can be expected, as the function used to find the positions of the infill points tends to $\mathbf{x}$ close to the extremes of the parameter space. Hence, the resulting surrogate model may predict the results better at the extreme values, but the overall fit may be worse. Since the overall behaviour

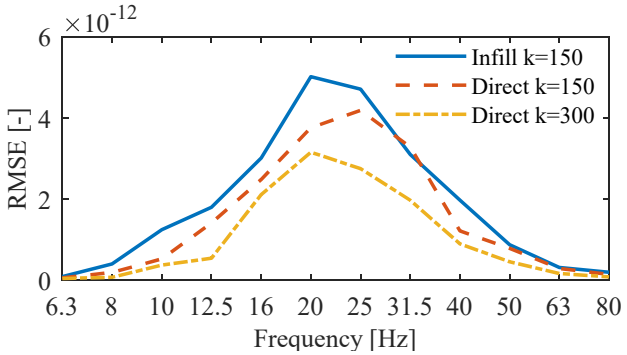

Figure 3. RMSE for different surrogate-model-fitting methods.

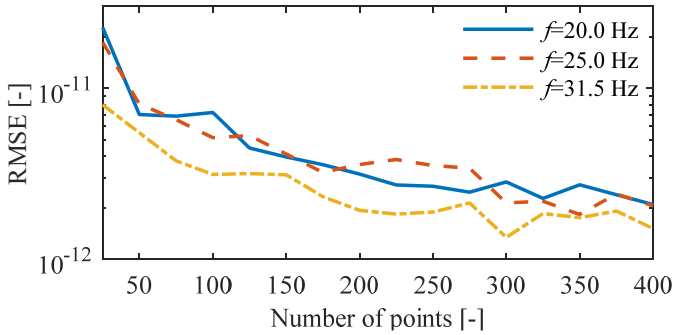

Figure 4. RMSE dependency on the number of points used to fit the surrogate model.

of the system is more important in the considered problem, the first approach is preferred.

Another important aspect to consider when creating a surrogate model is the number of data points produced by the truth model. Thus, additional analysis was carried out to determine the optimum number of such points needed to obtain a precise model. The three one-third octave bands that produced the largest RMSE in Figure 3 were chosen for this analysis. The analysis was performed starting with 25 and ending with 400 data points from the truth model, with a step of 25. For each case, the positions of the points were determined by choosing the most space-filling Latin Hypercube and calculating the computational model results at those positions. The results are shown in Figure 4. As expected, the precision of the surrogate model increases with larger data set. However, the improvement rate decreases quickly with increasing data set size. For further analysis, the surrogate model data set size is chosen as 300 points.

3.3 *Using the surrogate model*

Using the Kriging approach to create the model is advantageous as the obtained fitting factor θ (see Equation 7) can be used to estimate the importance of the varying parameters. As a separate surrogate model was created for each investigated one-third octave band, it is possible to compare the values of this factor through frequencies. Larger θ values correspond to higher importance of the parameter. While the exact values can change, depending on the distribution of the fitting data and the optimization algorithm used, the overall trends remain the same.

The obtained results are shown in Figure 5. It can be observed that the height of the floor is effecting the system the least. It can be expected, as the system is excited by a vertical load and only the vertical displacements are investigated, leading to a low importance of the building height. Similarly, the effects of the floor thickness are also limited and mostly constant though frequencies. Further, the rotation of the whole structure has almost no effect at low frequencies, but with increasing frequency, it increases, becoming one of the most important parameters at the highest investigated frequencies. This is most likely due to the wavelength of the waves propagating through the soil. At low frequencies, the wavelengths are large and the structural response is governed by large-scale displacements. At higher frequencies, the waves are shorter, and the response is governed by higher modes with more localized displacements, leading to higher importance of the building rotation. Column width demonstrates an opposite behaviour with high importance at low frequencies and low importance at higher frequencies. This behaviour may likely have a similar reason as the varying influence of the building rotation. Column stiffness has a larger effect on the overall building behaviour and smaller effect on more localized floor displacements. Finally, the floor width, which governs the overall footprint of the building, is very importance within the whole frequency range, with some gradual increase for higher frequencies. Interestingly, a distinct peak is present at the centre frequency of 25 Hz. The peak is within a frequency range where most of the first eigenfrequencies for the floors of the building are present.

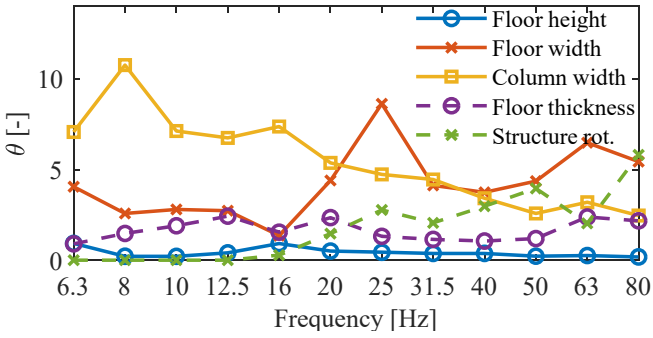

Figure 5. Kriging surrogate model fitting parameter θ.

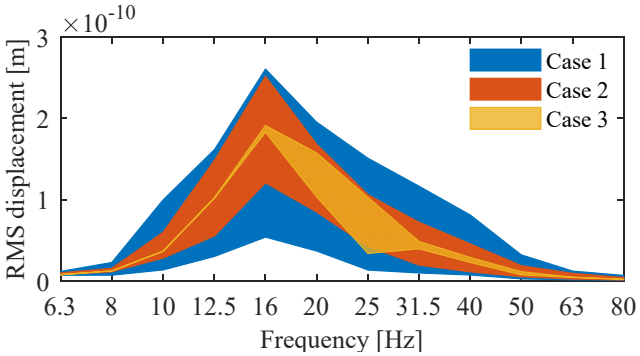

Figure 6. Building response envelope indicating the maximum and minimum values given the input limits of Cases 1 to 3.

With the surrogate model, it is possible to obtain the envelope defining the maximum and minimum values of the function, within a limited parameter space. To illustrate this, some cases of limited parameter spaces were tested:

- Case 1. All five parameters are allowed to vary through the whole parameter space. This case shows the absolute maximum and minimum values possible in the analysed system.
- Case 2. The floor height, floor width and structure rotation are fixed and equal to the mean values given in Table 2. While, the column width and floor thickness are allowed to vary. The case illustrates a perhaps more real world scenario, where the building geometry is fixed, but the cross-section size of the structural elements can still be optimized.
- Case 3. Only the structure rotation is varying. All other parameters have the mean values as defined in Table 2.

The results can be seen in Figure 6. Case 1 shows the overall minimum and maximum values of the created surrogate model, all results, from more limited parameter spaces, should fit within this envelope. The highest response is observed at 16 Hz octave band. It is most likely the frequency band where the first eigenfrequencies of the structure fall for most realizations of input parameters. Looking further, at the lower and higher frequencies, the response of the structure is lower, for both minimum and maximum limits. Case 2 shows the effects of limiting the design space to only two parameters. It can be seen that the maximum values of the response are reduced starting at the centre frequency of 20 Hz and going onwards. However, the maximum values observed at the 16 Hz one-third octave band are barely effected, indicating that the extreme values of the floor height, floor width and structure rotation are not needed to obtain an extreme value in the response of the structure. Further, Case 3 shows the effects of varying only the structure rotation. Here, the spread is almost exclusively limited to the 20 Hz and 25 Hz one-third octave bands. For all other bands, the effects of the structure rotation are negligible. This illustrates that while the importance of rotation is high at high frequencies, as seen in Figure 5, the overall effect of the parameter might be limited. Of course, changing the constant parameter values will affect the location and the response range of the observed response envelope.

4 CONCLUSIONS AND DISCUSSION

The paper deals with creating and utilizing a surrogate model of a building structure. The structural response to vibrations propagating through the soil is investigated. A short introduction into the computational truth model, used to gather the needed data set, and the surrogate model, that uses the created data set to represent the system, is given. Several approaches of fitting the surrogate model were investigated, together with a convergence analysis to investigate the size of the data set needed. Further, the created surrogate model was used to find the most important geometry parameters to the behaviour of the system and to show the envelope within which the structure response falls for a given parameter space.

The created surrogate model can be used to obtain the system response from any combination of input parameters as long as they are within the limits of the parameter space. The results can be obtained without much computational effort. Thus, it is easy to explore the surrogate model to find the maximum or the minimum values, given available limits of the modelled structure. Further, the obtained model is fast enough to provide real-time results during the design process. This could prove to be a useful tool, for example, giving the designer of the structure an indication that a certain threshold is exceeded, during the design process itself. This way, the problematic areas of the design space could be easily identified and further investigated—or avoided in a design.

Using surrogate models to predict dynamic structural behaviour does have drawbacks. The surrogate model is limited to one output variable (Quantity of Interest), making it difficult to approximate complex system behaviour. Further, the surrogate model precision is somewhat limited, especially at the extreme boundaries of the modelled parameter space. Thus, the surrogate model is better suited to observe the general trends of the system, while the exact values should be validated using the truth model. Some of these problems might be mitigated using different data selection and surrogate model optimization techniques. Further, it might be beneficial to utilize other machine-learning techniques, such as creating artificial neural network that would allow multiple output values to be modelled with a single model.

REFERENCES

Thomson, W.T. 1950. Transmission of elastic waves through a stratified solid medium, *J. Appl. Phys*. 21(2): 89-93.

Haskell, N.A. 1953. The dispersion of surface waves on multilayered media, *Bull. Seismol. Soc. Am*. 43: 17-43.

Bucinskas, P. & Andersen, L.V 2017. Excitation of structures near railway tracks - analysis of the wave propagation path, *COMPDYN 2017 - Proc. 6th Int. Conf. Comput. Methods Struct. Dyn. Earthq. Eng*. 2: 15-17.

Andersen, L.V. & Clausen, J. 2008. Impedance of surface footings on layered ground, *Comput. Struct*. 86: 72-87.

Krige, D.G. 1951. A statistical approach to some basic mine valuation problems on the Witwatersrand. *Journal of the Southern African Institute of Mining and Metallurgy*, 52(6): 119-139.

Forrester, A., Sobester, A. & Keane, A. 2008. *Engineering design via surrogate modelling: a practical guide*. John Wiley & Son.

Paper S5

Semi-analytical model of soil interacting dynamically with rigid blocks, cavities and piles

Full reference:

P. Bucinskas, L.V. Andersen, Semi-analytical model of soil interacting dynamically with rigid blocks, cavities and piles. Under review in Computers and Geotechnics, initial submission 2019 October 11.

Status:

This chapter presents the manuscript submitted to Computers and Geotechnics journal on 2019 October 11. The contents and typesetting of this chapter are as submitted.

Semi-analytical model of soil interacting dynamically with rigid blocks, cavities and piles

Paulius Bucinskas* and Lars Vabbersgaard Andersen

Department of Engineering, Aarhus University, Aarhus, Denmark
** Corresponding author, e-mail address pb@eng.au.dk*

Abstract

The paper proses a computationally efficient approach for modelling soil–structure interaction, including the coupling through the soil. The method utilizes a semi-analytical model for the soil, based on an analytical solution for the Green's function in the frequency–wavenumber domain. Structures are modelled as rigid blocks or by coupling with a finite-element model. Modelling of rigid footings and flexible piles is described. Further, an approach to including cavities inside the soil domain is introduced by utilizing finite elements with negative dynamic stiffness. The proposed methodology is validated by comparison with other well-known methodologies. The comparison is carried out by modelling the same systems with the semi-analytical approach, the boundary-element method and the finite-element method. In the finite-element models, non-reflecting boundaries are introduced in the form of either impedance boundary conditions or perfectly matched layers. The proposed semi-analytical modelling technique offers very good agreement to much more complex and computationally demanding finite-element models. Further, the obtained dynamic stiffness matrix of the foundations is compatible with the finite-element-method matrices. Therefore, the proposed methodology is useful for structural analysis, as a quick and precise way to account for the dynamic soil–structure interaction.

Keywords: semi-analytical soil model; soil–structure interaction; rigid footing; pile foundation; cavity; ground vibration.

1. Introduction

Modelling dynamic soil response, especially including soil–structure interaction, is a complex task. However, it is often necessary when analysing the dynamic excitation from railway lines, pile driving, vibrating equipment, and in other similar cases. The problem is difficult to model, as the waves propagating through the soil stratum are usually only bounded by the soil surface, while the propagation in both horizontal directions, as well as downwards, is unbounded. Further, reflection from interfaces between the layers and the surface quickly creates a very complex system behaviour. Additionally, introducing structures interacting with the soil complicates the problem. In turn, this leads to computational models that are hard to implement and take long time to compute. Therefore, when considering dynamic structural response, the underlying soil is often neglected, modelling the foundations as completely fixed.

Various methods for accounting for the underlying soil exist, usually dependent on the type of foundation used. They can be as simple as the standard lumped-parameter models proposed by Wolf [1], where rigid footings are represented by spring, dashpot and mass systems with properties that can be obtained from the available soil properties. Alternatively, tables expressing the dynamic stiffness of rigid square footings on layered half-space have been described by Wong and Luco [2]. However, their usage is limited to simple cases, and some effects—such as foundations coupling through soil or embedded in the ground—are not accounted for. More advanced models for rigid footing modelling also exist. For example, the work by Wong and Luco [3] includes the dynamic interaction between multiple footings, which was achieved through boundary integral equations and an iterative solution procedure. Another work by Wong and Luco [4] models embedded foundations using a hybrid approach, combining finite elements and the Green's function to account for the infinite boundaries.

An overview of the early methods developed for modelling embedded foundation's coupled horizontal–rocking response can be found in [5]. Another overview of simplified approaches to modelling the structure–soil interaction was provided by Dutta and Roy [6]. Similarly, simplified approaches to modelling pile foundations are described in, for example, [7–9].

For more advanced cases, numerical methods such as the finite-element method (FEM) and the boundary-element method (BEM) are often used. Finite-element (FE) analysis requires special boundaries to model the infinite domain of the soil. The problem may be handled by creating a large domain, allowing the waves to dissipate by material damping before re-entering into the domain of interest. However, this is infeasible. Instead, non-reflecting boundaries can be accounted for by, for example, local impedance boundary conditions (IBC) [10,11] or, as a more recent development, the perfectly matched layers (PML) that were originally developed by Berenger [12] for electromagnetic waves. As discussed by Kausel and Tassoulas [13], the accuracy of the solution is strongly dependent on the quality of the transmitting boundary conditions. Hence, for accurate results, long computational times are required for solution. However, the FEM is versatile and widely available in commercial software, and thus widely used. Alternatively, boundary-element (BE) formulations are used, in which the wave radiation into a (semi) infinite domain is an inherent part of the formulation. The methods are often combined into FE–BE models, where the FEM is used to model the structures and the BEM accounts for the soil. However, similarly to the FEM, long computation times and difficult formulations are the limiting factors of the BEM. A literature review by Clouteau et al. [14] gives a good overview of the various methodologies used to model structures coupled to elastic media, especially regarding the FEM and the BEM. As an example, the BEM is used to analyse the impedance of rigid footings in [15,16], while coupled FE–BE models are used to model pile foundations in [17,18].

This paper utilizes a semi-analytical method for modelling the soil, while the interacting structures are modelled as completely rigid, or they are discretized using the FEM. The used semi-analytical model was originally proposed by Thomson [19] and Haskell [20]. It is a well-known approach that has been applied to various problems, e.g., railway track modelling by Sheng et al. [21,22]. Andersen and Clausen [23] proposed an efficient computation procedure for the semi-analytical model, exploiting the polar symmetry of the Green's function, to analyse arbitrarily shaped rigid surface footings. Using the proposed computation technique, the methodology offers very short computation times, making the approach useful when analysing structure–soil interaction. In this work, the modelling technique is expanded to a much wider range of applications.

Firstly, Section 2 gives an introduction to the computation of the Green's function with numerical stabilization. Further, modelling of arbitrarily shaped three-dimensional rigid blocks, including a discretization technique, is introduced in Section 3.1. Additionally, the semi-analytical model is coupled to the FEM to analyse flexible piles and cavities within the soil, as described in Sections 3.2 and 3.3, respectively. One of the main aims of the work is to benchmark the performance of the proposed methodology by a comparison with other well-established techniques. Thus, in Section 4, the introduced modelling approaches for rigid blocks, piles and cavities are validated by comparison with BE and FE models,. Finally, conclusions are given in Section 5.

2. Semi-analytical soil model

The work utilizes a semi-analytical soil model based on the Green's function for a horizontally layered linear elastic half-space. The method is well known and widely used, thus only a general overview is given here. A more detailed explanation of the methodology used can be found, for example, in [23,24].

The Green's function matrix, $\mathbf{G}$, is defined analytically as the relation between the applied harmonic load $\mathbf{P}$ and the resulting harmonic displacement $\mathbf{U}$, both given as vectors in the horizontal wavenumber–frequency domain:

$$\mathbf{U}(k_x, k_y, z_\mathrm{r}, \omega) = \mathbf{G}(k_x, k_y, z_\mathrm{r}, z_\mathrm{s}, \omega)\mathbf{P}(k_x, k_y, z_\mathrm{s}, \omega). \tag{1}$$

Thus, the Cartesian coordinates in the horizontal directions are Fourier transformed into wavenumbers. Here k_x and k_y refer to the wavenumbers in the x and y-directions, and z_s is the vertical position of the load (i.e. the *source*), while z_r is the vertical coordinate at which the displacement is observed (the *receiver*). Finally, ω is the circular frequency. As already mentioned, the analytical solution for the used Green's function was developed by Thomson [19] and Haskell [20]. They introduced a transfer matrix which propagates displacements and traction through a single soil layer. This layer transfer matrix is then used to assemble multiple layers and, after applying boundary conditions, the resulting global transfer matrix is utilized to obtain the Green's function matrix $\mathbf{G}$. The method is based on the flexibility of the system, and the considered matrices are never bigger than six by six, making the solution procedure very quick. Unfortunately, the method suffers from computational instability issues when considering high frequencies or thick soil layers.

To overcome the numerical instability problems, the stiffness matrix approach could be used [25]. Here the layer transfer matrices are reorganised into stiffness matrices that are assembled similarly to the FEM. Using approximate solutions over a single layer, the method is known as the thin-layer method [25,26]. Another approach is to introduce additional stabilization techniques into the flexibility approach. In the present work, the orthonormalization method, proposed by Wang [27] for geophysical applications, is used. Here, before the traction and displacement values are propagated through a layer, they are rotated to remove the coupling terms between the primary (P) and the vertically polarized secondary (SV) waves. In essence, the approach is similar to obtaining the principal stresses from a stress tensor. The method was originally described for two-dimensional cases that only contain P and SV waves, but it can easily be generalized to three-dimensional cases by introducing the horizontally polarized secondary wave (SH). The SH wave is naturally uncoupled from the other two waves; however, this should be enforced in computational codes, since rotating the other waves might introduce weak coupling due to numerical precision errors. Further, the transfer matrices contain exponential terms that grow with increasing layer depth and frequency. Thus, very thick layers should be split into multiple smaller layers with the same material properties in order to avoid exceeding the limits of floating-point numbers. Using these techniques, very efficient computer calculations can be achieved, as all the computations are still based on interaction between layer transfer matrices not bigger than six by six.

After the Green's function has been obtained in the frequency–wavenumber domain, it is transformed into the frequency–space domain, where it can be coupled to external structures. The Green's function is axi-symmetric; thus, it is enough to evaluate it along a single wavenumber axis. Care should be taken to choose a correct sampling rate, as too few discrete wavenumbers will not represent the Green's function well, while too many points will lead to long computation times. In this work, a varying sampling rate has been chosen, where 70% of the discrete wavenumbers are concentrated in the zone around the peak corresponding to the slowest S-wave. This way, most of the points are located where the largest variation of the Green's function is present, while parts of the spectrum with less variation are represented with fewer points. A double semi-discrete inverse Fourier transformation in polar coordinates is used to transform the Green's function into spatial domain. Applying an axisymmetric load, the inverse Fourier transformation in the azimuthal direction can be done analytically [23]. Using the obtained solution, a global flexibility matrix is constructed. It stores the reacceptances between all points of interest in the soil domain. Inverting the global flexibility matrix produces the dynamic stiffness matrix of the soil $\mathbf{D}_\mathrm{S}$.

The points of interest can be treated as nodes through which the interaction with the soil domain is possible, for applying the load and observing the displacements. In the following, they are referred to as structure–soil–interaction (SSI) nodes. It is noted that the Green's function requires an interface in the soil at every depth where SSI nodes are present. This is ensure by splitting the soil layers at the required vertical coordinates. Then, the Green's function defining the relation between each soil interface and all other interfaces is found.

To obtain the receptances between the SSI nodes, a unit load is applied in each node, and the corresponding displacements are obtained. This procedure is performed in the frequency–wavenumber domain before the

double inverse Fourier transformation. Therefore, it is beneficial to model the unit-magnitude load as a 'bell-shaped' two-dimensional Gaussian distribution with a standard deviation equal to one half of the parameter r_{c0} that represents the radius of the circular area over which the main part of the load is applied. In the Cartesian wavenumber domain, this load distribution transforms into

$$P(k_x, k_y) = \exp\left(-\frac{(k_x^2 + k_y^2) r_{c0}^2}{4}\right). \tag{2}$$

As opposed to a rectangular or square distribution, the 'bell shape' maintains the polar symmetry of the Green's function, and the monotonous decrease with increasing wavenumbers entails the computational advantage that an overall smaller wavenumber domain needs to be evaluated.

However, it must be emphasized that the behaviour of rigid objects coupled to the soil via SSI nodes is effected significantly by the value of r_{c0}, and it must therefore be chosen carefully. Further, the loads are only distributed over the horizontal coordinates and not over the vertical coordinate. This leads to different discretization approaches for vertical and horizontal directions, as further discussed in Subsection 3.1.

3. Modelling structures interacting with the soil

Structures can be coupled with the soil via the SSI nodes. The following subsections present the main steps in coupling the soil with rigid blocks (Subsection 3.1), flexible piles (Subsection 3.2) and pits or cavities (Subsection 3.3), where the two latter cases involve the coupling with a finite-element model.

3.1 Rigid blocks

Often structures interacting with the soil are much stiffer compared to the surrounding soil and can be modelled as being completely rigid. This way, a very efficient system can be created, in which the rigid object motion is represented using only a few degrees of freedom. To model a rigid object interacting with the soil, it must be discretized into SSI nodes serving as slave nodes to a reference master node used for condensation of the stiffness of the rigid object. Due to the semi-analytical modelling approach, the discretization of rigid objects is handled differently in vertical and horizontal directions.

Firstly, the cross-sectional discretization over the horizontal coordinates is performed. Here, the unit load, used to obtain the global flexibility matrix, is distributed over an area defined by the load distribution parameter r_{c0}, as shown in Eq. (2). The most straightforward approach, named Approach A, is to split the total area of the rigid block's cross-section equally between all the SSI discretization nodes. This discretization approach is shown in Figure 1a. The distance, d_{s0}, between two nodes can then be found as

$$d_{s0} = \frac{d_R}{n}, \tag{3}$$

where d_R is the characteristic length of the cross-section (e.g., the diameter or side length) and n is the number of nodes used in the discretization in each horizontal direction. The corresponding load distribution parameter for a square cross-section can then be found as

$$r_{c0} = \frac{d_{s0}}{2}\sqrt{\frac{4}{\pi}}. \tag{4}$$

The multiplication factor provides an area scaling from a circle into a square. Due to the nature of the semi-analytical model, the assigned rigid body displacements are only guaranteed at the exact positions of the loaded nodes, and not over the full loaded area. This leads to 'soft' edges of a rigid object, and therefore the displacements obtained by discretization Approach A are generally too large.

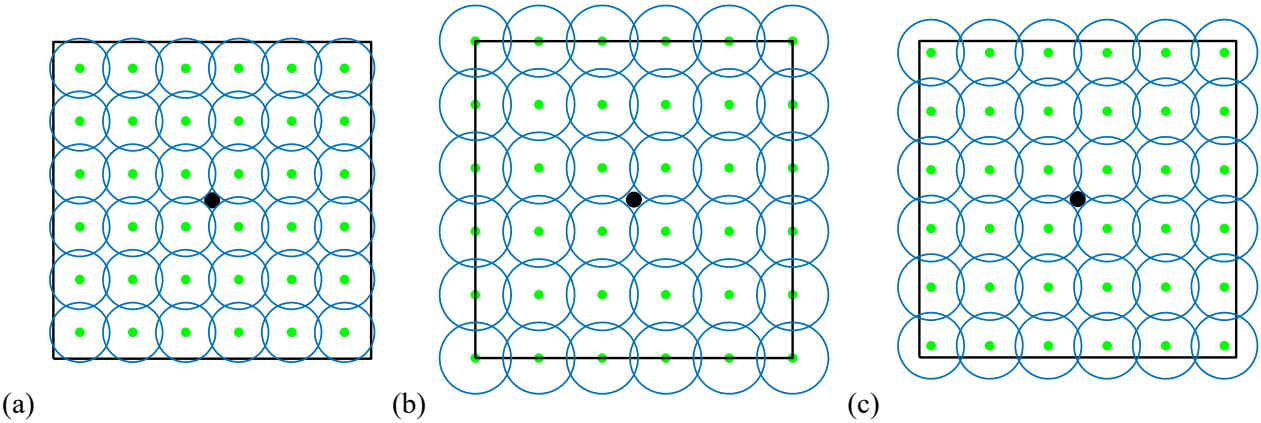

Figure 1. Discretization in the horizontal plane of a rigid object using the semi-analytical soil model: (a) Approach A; (b) Approach B; (c) Approach C. The black outlines show the perimeter of the object, while the green dots are the SSI slave nodes with the blue circles indicating the loaded areas, and the black dots at the centres of the objects are the reference master nodes.

Alternatively, discretization Approach B can be used, as shown in Fig. 1b. Here the outer SSI slave nodes are placed on the perimeter of the rigid object. This implies an increase in the distance between the slave nodes compared to discretization Approach A, such that d_{s0} is now defined as

$$d_{s0} = \frac{d_R}{n-1}. \tag{5}$$

However, this approach tends to overestimate the stiffness of the rigid objects and produce displacements that are too small due to the overall increased loading area.

It is evident that the correct behaviour of the system can be obtained by placing the discretization nodes somewhere between the limits provided by Approaches A and B. Then, the distance between two adjacent discretization nodes is defined as

$$d_{s0} = \frac{d_R}{n-n_0,} \tag{6}$$

where n_0 is a parameter influencing the spacing between the discretization nodes. From Eqs. (3) and (5) it can be seen that Approaches A and B are special cases of Eq. (6) evaluated for $n_0 = 0$ and $n_0 = 1$, respectively.

The optimal position of the SSI nodes has been obtained heuristically by comparing with the results obtained by modelling the same system with high-fidelity finite-element models. It has been found that $n_0 = 0.6$ (coined Approach C), produces highly accurate results. The discretization of a cross-section using the approach is shown in Fig. 1c. Validation shows that this factor works well, independently on how many discretization nodes are used and does not need to be adjusted for different frequencies. Further, discretizing different rigid shapes, such as circles, or using a different load distribution shapes, such a cylindrical distribution, works equally well with the same factor. Thus, the discretization Approach C is used for all further calculations.

Discretization in the vertical direction is less complicated, as the used unit loads are not distributed vertically. Therefore, horizontally discretized cross-sections are created for the top and the bottom of the rigid blocks, adding additional cross-sections in between, with vertical spacing as close as possible to d_{s0}.

As mentioned previously, the SSI discretization nodes created for a rigid object move together in reference to a master node assigned to the rigid object. In this work, the master node is placed at the top centre of the created rigid blocks. However, it is not a requirement, and the master node could be placed anywhere. In order to perform condensation of the stiffness related to the original degrees of freedom of the SSI slave nodes to the

degrees of freedom of the reference master nodes of the rigid blocks, the transformation matrix $\mathbf{T}_0$ is introduced. Considering a three-dimensional case, where a single rigid object composed of M SSI nodes is modelled, the transformation matrix $\mathbf{T}_{0,i}$ is created in the format

$$\mathbf{T}_{0,i} = \begin{bmatrix} 1 & 0 & 0 & 0 & (z_1 - z_0) & -(y_1 - y_0) \\ 0 & 1 & 0 & -(z_1 - z_0) & 0 & (x_1 - x_0) \\ 0 & 0 & 1 & (y_1 - y_0) & -(x_1 - x_0) & 0 \\ 1 & 0 & 0 & 0 & (z_2 - z_0) & -(y_2 - y_0) \\ 0 & 1 & 0 & -(z_2 - z_0) & 0 & (x_2 - x_0) \\ \vdots & \vdots & \vdots & \vdots & \vdots & \vdots \\ 0 & 0 & 1 & (y_M - y_0) & -(x_M - x_0) & 0 \end{bmatrix}. \tag{7}$$

Here it is assumed that the degrees of freedom of the SSI nodes are ordered as lateral displacements in the x, y and z-directions, whereas the rigid block degrees of freedom are ordered as the displacements in the x, y and z-directions followed by the rotations around the local x, y and z-axes, with the master node placed at coordinates (x_0, y_0, z_0). Each SSI slave node has the coordinates (x_m, y_m, z_m), $m = 1,2, \dots, M$, which is used to obtain the distance to the reference master node for the rotational degrees of freedom. The transformation matrix is formulated in a righthanded coordinate system with the z-axis facing upwards. If multiple rigid blocks are present in the system, the global transformation matrix $\mathbf{T}_0$ is assembled as a block diagonal matrix:

$$\mathbf{T}_0 = \mathrm{diag}[\mathbf{T}_{0,1} \quad \mathbf{T}_{0,2} \quad \dots \quad \mathbf{T}_{0,I}], \tag{8}$$

where the total number of rigid blocks is I. The system could also include independent SSI nodes that are not part of rigid blocks. In that case, the corresponding local transformation matrix $\mathbf{T}_{0,i}$ is replaced by the identity matrix of dimensions (3×3) for a three-dimensional case. The stiffness matrix including the rigid objects and independent nodes can then be obtained as

$$\mathbf{D}_\mathrm{R}(\omega) = \mathbf{T}_\mathbf{0}^\mathrm{T} \mathbf{D}_\mathrm{S}(\omega) \mathbf{T}_0. \tag{9}$$

The obtained stiffness matrix is used to obtain the system response in frequency domain:

$$\mathbf{D}_\mathrm{R}(\omega) \mathbf{u}_\mathrm{R}(\omega) = \mathbf{f}_\mathrm{R}(\omega), \tag{10}$$

where $\mathbf{u}_\mathrm{R}$ is the nodal displacement vector and $\mathbf{f}_\mathrm{R}$ is the corresponding nodal load vector.

After the system response has been calculated, the response of the soil stratum, which is not interacting directly with structures, can be found by utilizing the Green's function to evaluate the influence of the the obtained displacements. This calculation is computationally inexpensive, since it is enough to establish the flexibility matrix and use it directly, without the need for a matrix inversion to obtain the stiffness matrix.

3.2 Piles

Pile foundations are a commonly used foundation type, often utilized for poor soil conditions. However, modelling piles as rigid objects is not a suitable approach, as the piles can deform locally together with the soil. A pile-modelling approach using a coupled semi-analytical and finite-element formulation has been presented in a previous work by the authors in [28]. Therefore, only a general overview of the modelling approach is given here.

To model the pile behaviour, the semi-analytical soil model is combined with the FEM. The piles are modelled using Euler-Bernoulli beam elements enriched by degrees of freedom to account for axial and torsional behaviour. It is assumed that the axial deformation and torsional rotation are uncoupled from the bending of the beam. The resulting elements have six degrees of freedom per node: three translational and three rotational. The elements are assigned the cross-sectional properties of the piles, while the material properties are modified by subtracting the soil stiffness and density from the stiffness and density of the piles. This way the stiffness of the soil is only accounted for once. The dynamic stiffness matrix for the FE piles is found as

$$\mathbf{D}_{\mathrm{P}}(\omega) = \mathbf{K}_{\mathrm{P}} - \omega^2\mathbf{M}_{\mathrm{P}} + \mathrm{i}\mathbf{C}_{\mathrm{P}}, \tag{11}$$

where $\mathbf{K}_{\mathrm{P}}$, $\mathbf{M}_{\mathrm{P}}$ and $\mathbf{C}_{\mathrm{P}}$ are the static stiffness, the mass and the damping matrices. Hysteric damping is used; thus, damping is frequency independent.

The nodes of FE pile model are coupled to SSI master nodes in the soil model, created at the positions of the FE nodes. It has been found that creating single SSI nodes to couple to FE beam nodes does not properly account for the rotational stiffness of the pile. Therefore, rigid two-dimensional discs are created with the same diameter as the modelled pile. The discs are discretized using the discretization Approach C, as described in Section 3.1, where the diameter of the pile is used in Eq. (6) for parameter d_{R}. The rigid discs have six degrees of freedom in the three-dimensional case, and they are coupled to the translational as well as the rotational degrees of freedom of the FE nodes. The stiffness matrix for the full system is then obtained by adding the stiffness matrix of rigid disks $\mathbf{D}_{\mathrm{R}}$ to the stiffness matrix of the piles $\mathbf{D}_{\mathrm{P}}$:

$$\mathbf{D}_{\mathrm{PR}}(\omega) = \begin{bmatrix} \mathbf{D}_{\mathrm{P}}^{\mathrm{uu}}(\omega) & \mathbf{D}_{\mathrm{P}}^{\mathrm{us}}(\omega) \\ \mathbf{D}_{\mathrm{P}}^{\mathrm{su}}(\omega) & \mathbf{D}_{\mathrm{P}}^{\mathrm{ss}}(\omega) + \mathbf{D}_{\mathrm{R}}(\omega) \end{bmatrix}, \tag{12}$$

where the superscript ‘s’ refers to the degrees of freedom coupled to the soil, and ‘u’ refers to all other degrees of freedom. If only the embedded part of the piles is analysed, the stiffness matrix reduces to $\mathbf{D}_{\mathrm{P}}^{\mathrm{ss}}(\omega) + \mathbf{D}_{\mathrm{R}}(\omega)$.

3.3. Cavities

The semi-analytical model assumes homogeneous soil layers with perfectly horizontal interfaces between them. Thus, analytically it is not possible to model pits or cavities. However, utilizing three-dimensional solid finite elements it is possible to ‘remove’ the material from the system. The approach was previously applied by the authors for modelling a tunnel structure [29]. However, in the previous study, additional stiffness was added to account for the tunnel lining, significantly reducing the effect of the cavity. In this work, a system is analysed, in which the cavity is unsupported by additional structures. This amplifies the effects of the cavity and can lead to modelling difficulties as further discussed below.

The cavity is discretized using solid finite elements and assigned the properties of the soil. At the same time, at set of single SSI nodes are created in the locations corresponding to the discretized cavity using the semi-analytical soil model. Subtracting the stiffness of FE system from the dynamic stiffness matrix of the soil recreates the effects of the cavity in the system. The whole three-dimensional cavity is discretized, and thus some internal nodes in the newly created system will have extremely low stiffness. However, these nodes are still left in the system and no condensation is performed. Further, the quality of the solution relies on good agreement between the two approaches, including the overall structure of the created stiffness matrices. Linear FE elements are used, since they provide a stiffness matrix structure that is closer to the structure of the dynamic stiffness matrix provided by the semi-analytical soil model. Quadratic interpolation elements are not suited for this application, because the stiffness is distributed unevenly between the nodes, depending on the local position of a node in an element, i.e. mid-side nodes contribute more than edge and corner nodes. Therefore, quadratic elements can lead to local stiffness variation across nearby nodes in the final system, leading to unphysical system behaviour.

Some of the systems modelled in this paper contain both rigid objects interacting through the soil and a cavity placed in the wave propagation path between them. Therefore, the dynamic stiffness matrix of the soil $\mathbf{D}_{\mathrm{R}}$ is split into different parts: The degrees of freedom for rigid blocks are denoted with superscript ‘r’, and the degrees of freedom for the cavity are assigned the superscript ‘c’. Finally, the discretized cavity dynamic stiffness matrix, denoted $\mathbf{D}_{\mathrm{C}}$, is found similarly to Eq. (11). The dynamic stiffness matrix for the full system is then assembled as

$$\mathbf{D}_{\mathrm{RC}}(\omega) = \begin{bmatrix} \mathbf{D}_{\mathrm{R}}^{\mathrm{rr}}(\omega) & \mathbf{D}_{\mathrm{R}}^{\mathrm{rc}}(\omega) \\ \mathbf{D}_{\mathrm{R}}^{\mathrm{cr}}(\omega) & \mathbf{D}_{\mathrm{R}}^{\mathrm{cc}}(\omega) - \mathbf{D}_{\mathrm{C}}(\omega) \end{bmatrix}. \tag{13}$$

As the SSI node positions are controlled by the discretization of the FE model, the discretization procedure described in Section 3.1 is not applicable for this case. It has been found heuristically that setting the load distribution parameter r_{c0} to a value around 60 % of the shortest distance between two nodes in the FE cavity model provides accurate results. More details about the system discretization are given in Section 4.3.

4. Validation of modelling approach

4.1 Rigid structure interaction with soil

To validate the proposed methodology of modelling rigid blocks, it was compared to other commonly used modelling approaches. Two rigid 3D blocks were modelled, both being cubes with a side length of 2 m. The blocks were placed with a distance of 6 m (centre-to-centre) along the x-axis. The soil was modelled as a homogeneous half-space with a Young's modulus of 250 MPa, a Poisson's ratio of 0.25, a mass density of 2000 kg/m^3 and a loss factor of 0.05. Two cases were considered: Case A with both blocks embedded in the soil, so that the top of the cubes were at the same level as the ground surface (see Figs. 2a and 2b), and Case B with the top of the blocks buried 2 m below the ground surface (Figs. 2c and 2d). For both cases, one block was loaded by placing a unit force, either in the vertical (z) direction or in the horizontal (x) direction, observing the resulting displacements of both blocks in both directions.

For the semi-analytical modelling approach, an in-house computer code was developed in FORTRAN and used for the main analysis, with MATLAB used for user input and result visualisation. The Green's function in the frequency–wavenumber domain was evaluated along a single axis up to 15 rad/m, with 12 000 discrete wavenumbers. The wavenumber domain discretization was varied according to the analysed frequency and the phase velocity of the shear waves, c_s. In each case, 70 % of the discrete wavenumbers were placed in the range from $0.75\omega/c_s$ to $1.25\omega/c_s$, 20 % were placed below $0.75\omega/c_s$, and 10 % were placed above $1.25\omega/c_s$, distributed uniformly in each subrange. The discretization was truncated at a wavenumber of $25\omega/c_s$ or when the largest set wavenumber is reached (in this case 15 rad/m), by choosing the largest value of the two. With the 'bell-shaped' load, this provided an accurate discrete inverse Fourier transformation. In this context, it is noted that the inverse Fourier transformation was carried out by numerical integration over the radial wavenumber direction in terms of the Simpson rule. Combined with the refinement of the wavenumber discretization around ω/c_s, this has been found (by a preliminary study, not fully reported in the paper) to provide a superior convergence compared to Fast Fourier Transformation with linear or logarithmic stepping. The inverse Fourier transform of the Green's function was evaluated for 500 discrete distances, spaced uniformly from zero up to the largest horizontal distance between two SSI nodes in the analysed system. The results for intermediate distances were then found by interpolation. Each cross-section of the rigid blocks was discretised into a 10×10 grid, with a spacing between the nodes of $d_{s0} = 0.212\,8$ m, resulting in around 12 SSI nodes per Rayleigh wavelength at 80 Hz. The load distribution parameter was then determined to be $r_{c0} = 0.12$ m. Further, 12 layers of the created cross-sections were used for the vertical discretization of the system. A visualisation of the model can be seen in Figs. 2b and 2d. It should be noted that only half of the created model is shown, due to system symmetry around the x-axis. The surrounding soil displacements, illustrated with shaded colours, are calculated after the displacements of the rigid blocks have been found, utilizing the Green's function directly.

For comparison, a BE–FE model was created using the in-house modelling software BEASTS [30,31]. Further, an FE model was created in COMSOL Multiphysics [32]. The analyses were carried out in the frequency domain for the discrete frequencies 5, 10, …, 80 Hz. As discussed in the introduction, the FE method requires special boundary conditions in order to account for the radiation of waves into a half-space. These boundary conditions have a significant effect on the system behaviour, especially when analysing the secondary coupling effects caused by through-soil coupling between the two rigid blocks. Two types of low-reflecting or non-reflecting boundaries were considered: impedance boundary conditions (FE–IBC) as first suggested by Lysmer

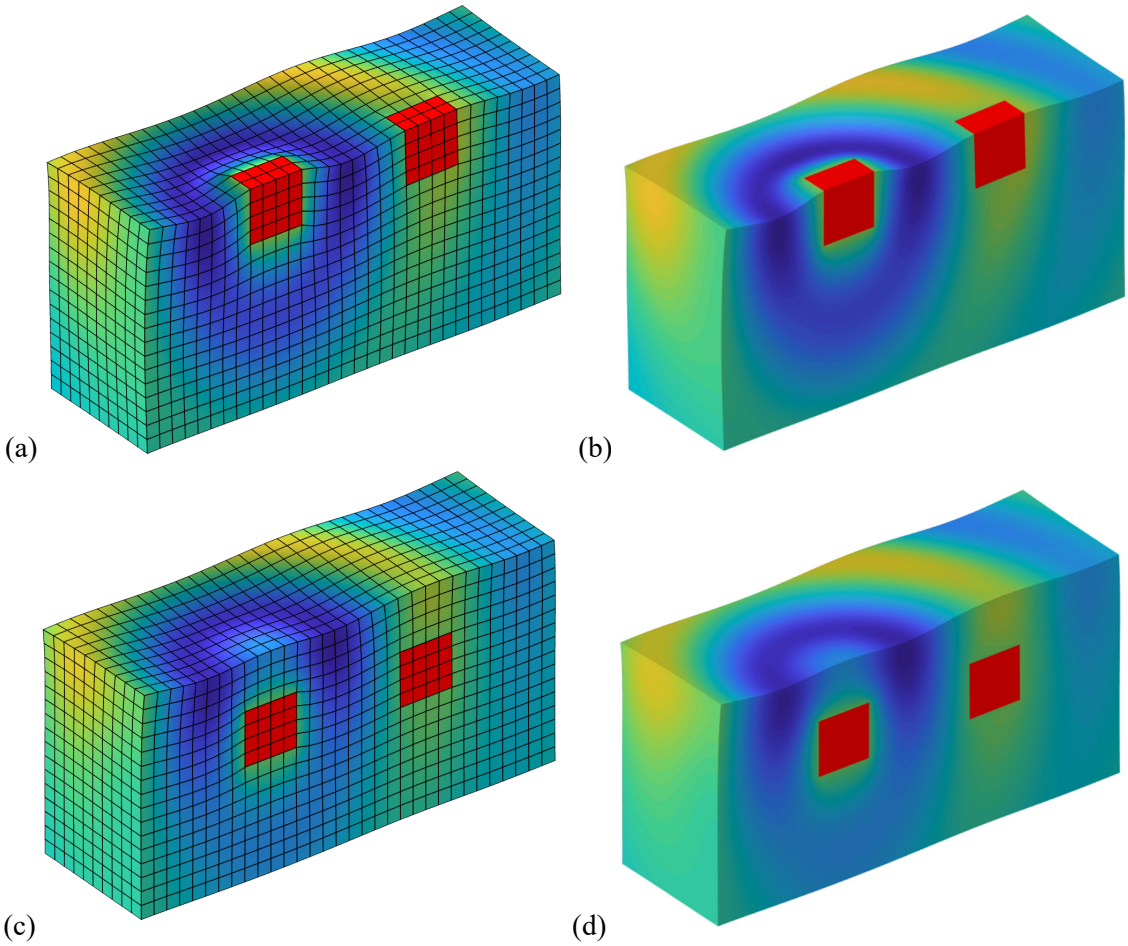

Figure 2. Field response at 30 Hz for two rigid blocks with vertical load: (a) Case A, FE-PML model; (b) Case A, semi-analytical model; (c) Case B, FE-PML model; (d) Case B, semi-analytical model. Bright yellow and dark blue shades indicate positive and negative vertical displacements in phase with the load. Note that subfigures (a) and (c) are produced with COMSOL Multiphysics, whereas subfigures (b) and (d) are produced with MATLAB, based on the in-house code for the proposed semi-analytical model.

and Kuhlemeyer [10], and perfectly matched layers (FE–PML) as first proposed by Bérenger [12] for electromagnetic waves and later developed for elastodynamics.

The BE–FE model created in BEASTS employs a BE model for the soil and an FE model for the rigid blocks, modelling these as a material with a stiffness 10^6 times higher than the stiffness of the soil and otherwise with the same properties. The BE model for the soil was based on quadrilateral nine-nodes elements with quadratic interpolation of the displacement and traction fields, following the theory outlined by Dominguez [33]. The FE model of the blocks used quadratic Lagrange interpolation of the displacements. Full integration was used for the FE part, and 6×6 Gauss points were used per boundary element for the non-singular terms. The procedure outlined by Andersen and Jones [34], and explained in detail by the same authors in [35], was applied for treatment of the strong singularities of the traction Green's function. The mesh size was 0.5 m, and the ground surface was discretized over a rectangular area that was 16 m long (in the x-direction) and 5 m wide (in the y-direction), exploiting the symmetry of the geometry and load around the (x, z)-plane. Hence, the model was truncated 4 m from the blocks in the x and y-directions, and only the elements at $y \geq 0$ were considered explicitly. The influence of the 'mirror image' of the modelled part was considered implicitly via the Green's functions, following the approach suggested by Andersen and Jones [35].

In order to be consistent with the dimensions and discretization of the BE–FE model analysed by the BEASTS software, the FE models constructed in COMSOL Multiphysics considered a block of soil that was 16 m long (in the *x*-direction), 5 m wide (in the *y*-direction) and 8 m deep (in the z-direction). Quadratic Lagrange interpolation was applied, and a structured mesh with an element size of 0.5 m was used everywhere. The mesh used for the two analysed cases can be seen in Figs. 2a and 2c. In total, the model had around 120 000 degrees of freedom for the considered soil domain and the rigid blocks which were again modelled with a stiffness 10^6 times higher than the stiffness of the soil and otherwise with the same properties. A further study, not reported in detail in this paper, indicated that no significant improvement of the accuracy in the considered frequency range would be achieved by mesh refinement or by using cubic interpolation instead of quadratic interpolation. Further, it was found that almost identical results were obtained with reduced and full integration.

On the boundary residing in the plane defined by $y = 0$, the FE model was pinned in the *y*-direction to enforce the symmetry around this plane. The boundary in the top, i.e. the ground surface, was assumed to be free of traction. However, the four remaining sides of the modelled domain can be considered artificial boundaries. As originally proposed by Lysmer and Kuhlemeyer [10], reflection of waves at the artificial boundaries of the FE model can be partially avoided by introduction of impedance conditions at the artificial boundaries:

$$\sigma_{ij}(x, y, z, \omega)\, \hat{n}_j(x, y, z) \;= -\mathrm{i}\omega\, z_{ij}(x, y, z)\, U_j(x, y, z, \omega), \tag{68}$$

where $\sigma_{ij}(x, y, z, \omega)$ is the Cauchy stress tensor in frequency–spatial domain, and $\hat{n}_j(x, y, z)$ is the unit outward normal to the boundary at the point (x, y, z). In the present model, the mechanical impedance was assumed to be isotropic: $z_{ij}(x, y, z) = \delta_{ij}\, \rho\, (c_\mathrm{P} + c_\mathrm{S})/2$, where ρ is the mass density of the soil and c_P and c_S are the corresponding P- and S-wave speeds, respectively. This provides a 'low-reflecting' boundary compared to a fixed or free boundary. As discussed by Krenk and Kirkegaard [11], the impedance condition may be improved by considering the direction of wave propagation at the boundary. However, in the present case, due to wave scattering by the rigid blocks, the direction of P- and S-wave propagation towards the boundary is not easily defined, and the simple isotropic impedance condition based on average wave speeds was therefore chosen. With this definition, the impedance conditions are expected to provide partial reflection of P- and S-waves, and the Rayleigh wave forming in the ground surface has not been treated properly.

As an alternative to the simple, local impedance conditions, an improved radiation of the waves from the modelled domain can be achieved by implementation of PMLs. In the present analyses, the standard formulation of PMLs available in COMSOL Multiphysics was applied, using the default stretching functions and adding PMLs with a thickness of 4 m to the model described above. The same mesh size was used for the PMLs as within the modelled domain, i.e. brick elements with a side length of 0.5 m, thus adding substantially to the number of degrees of freedom of the model. The external boundaries of the PMLs were considered free.

The results of the considered models are shown in Figs. 3 and 4 for Cases A and B, respectively. It can be observed that, when a load is applied in the vertical direction, the obtained vertical displacements match well between all the models, as seen in Figs. 3a and 4a. Similarly, a horizontal (*x*) load results in well-matching horizontal displacements (see Figs. 3d and 4d). This can be expected, as the observed displacements are governed mainly by the direct coupling between the degrees of freedom of the two blocks. However, the FE–IBC model shows some deviation at low frequencies due to partial reflection of waves at the artificial boundaries.

Analysing the couplings between two directions (horizontal load to vertical displacement and vice versa), the discrepancies between the different methodologies increase. Still, the semi-analytical model matches well with the FE–PML model, while the other models show some deviation. For the FE–IBC model, this was again expected due to partial reflection at the boundaries. For the BE–FE model, the truncation of the ground surface in the discretization is now seen to have an impact that could be reduced by modelling a larger part of the surface, farther away from the blocks, at the expense of longer computation times. Furthermore, it can be seen

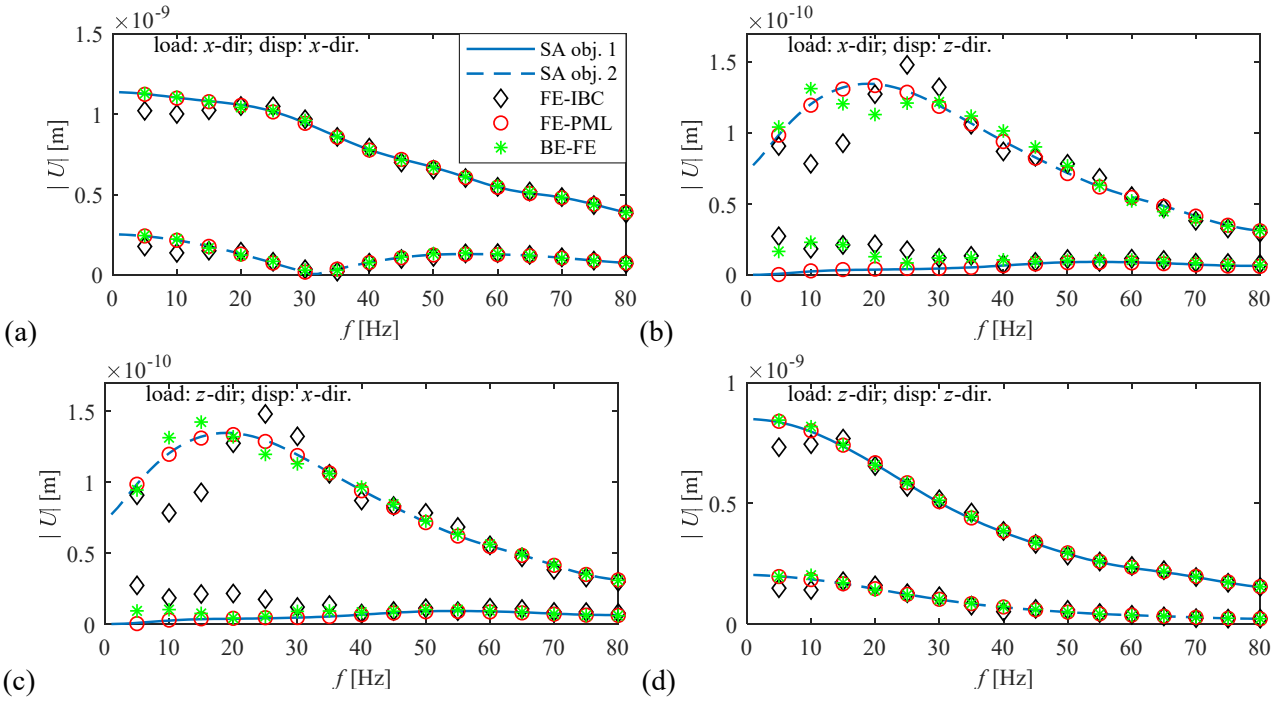

Figure 3. Case A—the top of the rigid blocks is placed at the ground surface: (a) Load applied in *x*-direction, displacements in *x*-direction; (b) load applied in *x*-direction, displacements in *z*-direction; (c) load applied in *z*-direction, displacements in *x*-direction; (d) load applied in *z*-direction, displacements in *z*-direction.

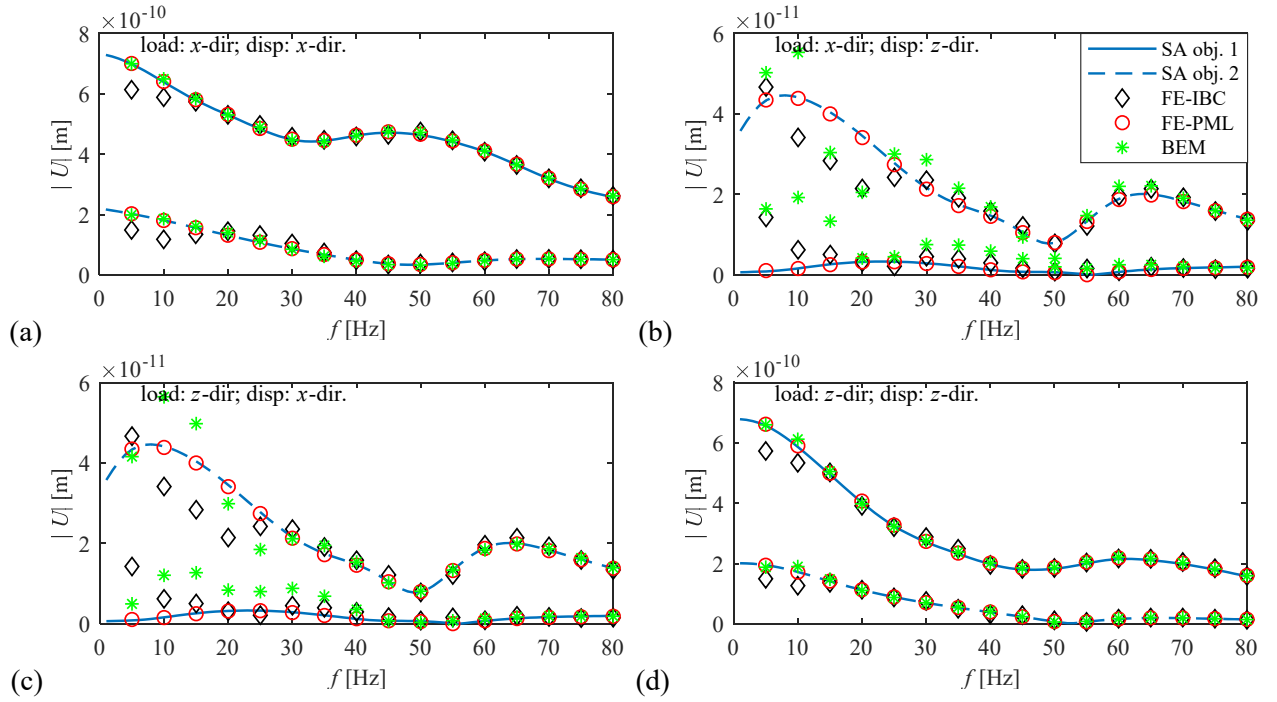

Figure 4. Case B—the top of the rigid blocks is buried 2 m below the ground surface: (a). load applied in *x*-direction, displacements in *x*-direction; (b) load in *x*-direction, displacements in *z*-direction; (c) load in *z*-direction, displacements in *x*-direction; (d) load in *z*-direction, displacements in *z*-direction.

that Figs. 3c and 3d (and Figs. 4c and 4d) are almost identical. This could be expected, as a well-represented linear system should exhibit symmetric behaviour. With increasing frequency, the differences between the

approaches are reduced, since the artificial boundaries lie farther away measured in terms of wavelengths.

For assessment of the model accuracy, the horizontal displacements of block number one due to a vertical load applied to the same block are of special interest (see Figs. 3c and 4c), since the horizontal displacements of this block are caused purely by the waves reflected from the other rigid block. Thus, these displacements are caused only by the weak coupling between the two footings. However, even in this case the match between the semi-analytical model and the FE–PML model is almost perfect, indicating a very high precision of the semi-analytical approach and the FE–PML. Even when comparing the resulting soil displacements, as shown in Fig. 2 for 30 Hz, the agreement between the semi-analytical model and FE–PML model is very good, throughout the whole domain. Especially, it can be concluded that the PML formulation indeed offers perfect transmission of the waves, and that the proposed semi-analytical approach provides highly accurate results with low computational cost.

4.2 Piles interacting with soil

For validation, two piles are modelled with 6 m distance centre-to-centre. Each pile has a circular cross-section with diameter of 1 m and is embedded 6 m into the soil. The material properties of the piles are: Young's modulus, 34 GPa, shear modulus, 13.1 GPa, mass density, 2 400 kg/m^3, and loss factor, 0.03. Two soil stratifications are studied. In the first case, the soil is modelled as a homogeneous half-space with the same material properties as given in Section 4.1. In the second case, a 6 m layer of the same material is placed over a half-space of stiffer soil with a Young's modulus of 600 MPa, a Poisson's ratio of 0.25, a mass density of 2 000 kg/m^3, and a loss factor of 0.05. The system is excited by placing a uniformly distributed load of magnitude 1 N/m^2 on the pile cap, in either the vertical direction or the horizontal direction.

The semi-analytical model uses the same wavenumber domain discretization settings as described in Section 4.1. The rigid discs representing the cross-sections of the piles are discretized into 19 SSI nodes, with five nodes along the diameter of the cross-section. This leads to the load distribution parameters $d_{s0} = 0.227\,3$ and $r_{c0} = 0.256\,4$. The vertical spacing for both the FE-model nodes and between the rigid discs is 0.5 m. The FE beam model of the piles is assigned the corresponding cross-sectional properties, while the Young's modulus, shear modulus and density are modified by subtracting the properties of the soil. The model can be seen in Fig. 5b, with the black line indicating the FE beams and the rigid disks shown in red. The figure shows only one half of the analysed model.

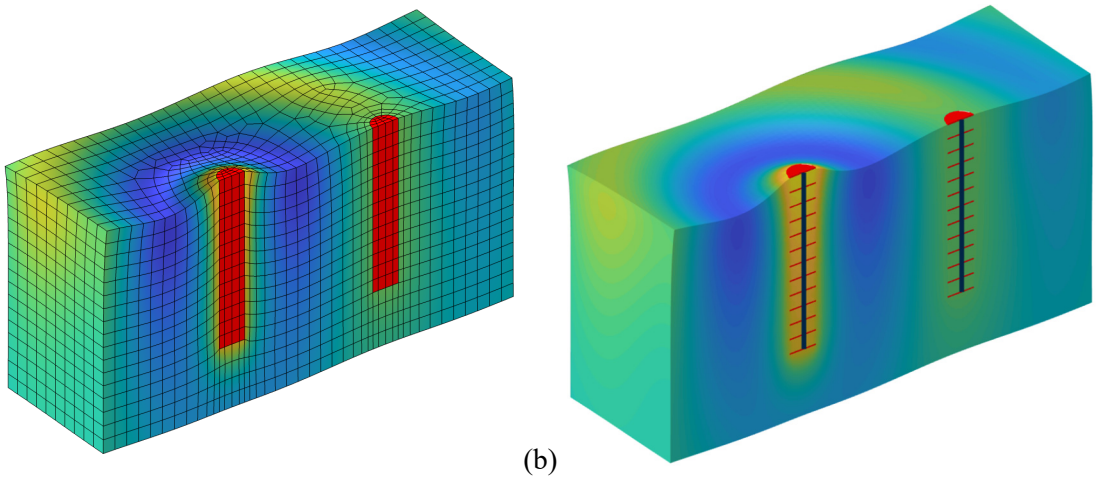

(a) (b)

Figure 5. Field response at 30 Hz, for two piles with vertical load: (a) Case A, FE-PML model; (b) Case A, semi-analytical model; (c) Case B, results from FE-PML model; (d) Case B, semi-analytical model. Bright yellow and dark blue shades indicate positive and negative vertical displacements in phase with the load.

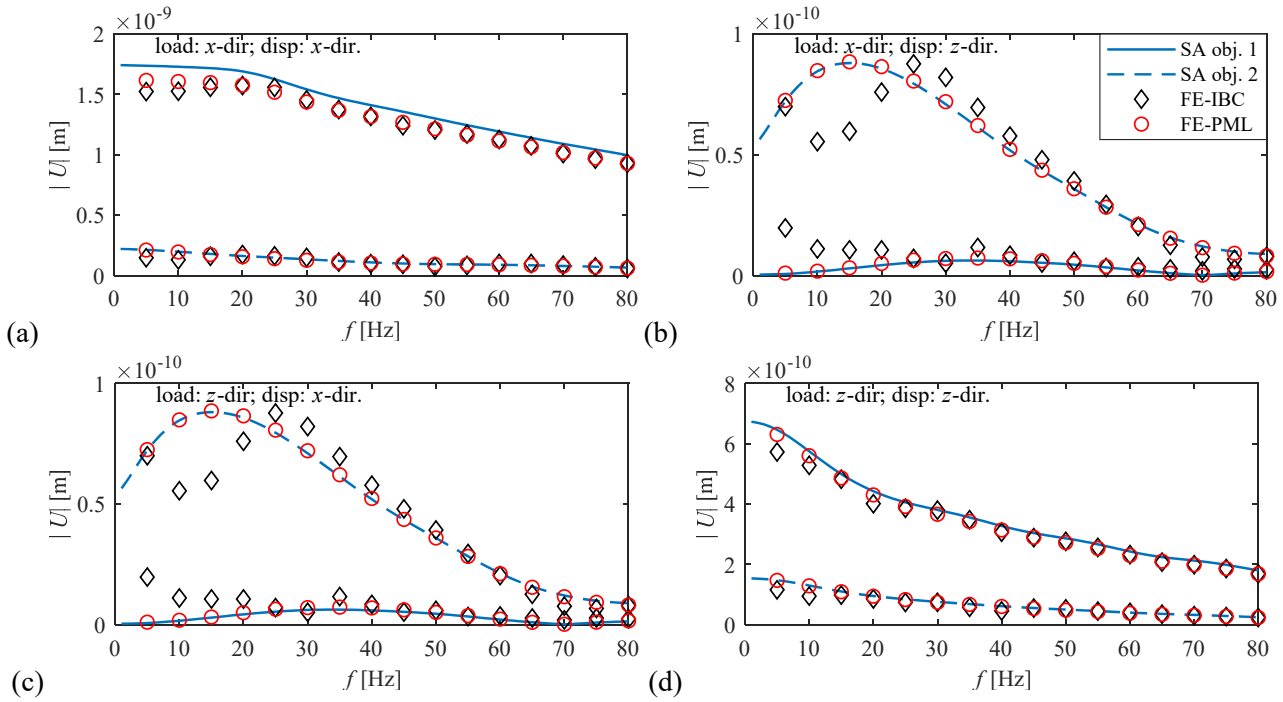

Figure 6. Two piles embedded into a half-space, with load applied on the first pile: (a) load applied in x-direction, displacements in x-direction; (b) load in x-direction, displacements in z-direction; (c) load in z-direction, displacements in x-direction; (d) load in z-direction, displacements in z-direction.

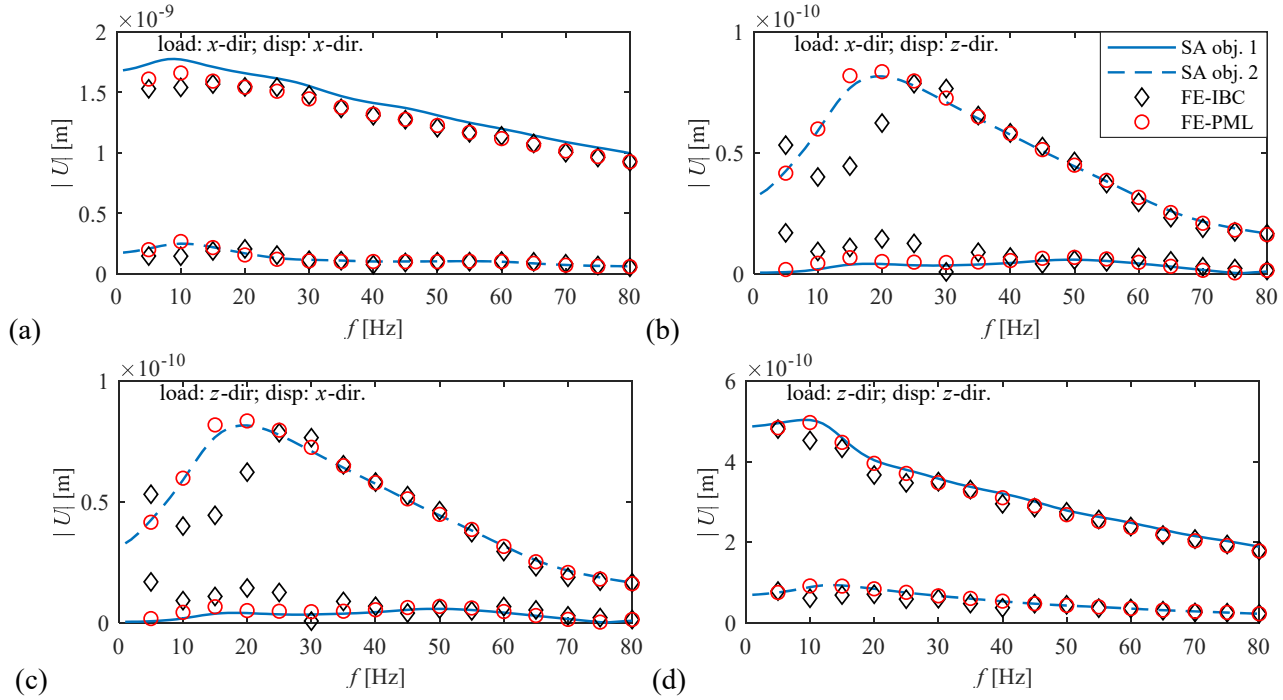

Figure 7. Two piles embedded into a layered soil, with load applied on the first pile: (a) load applied in x-direction, displacements in x-direction; (b) load in x-direction, displacements in z-direction; (c) load in z-direction, displacements in x-direction; (d) load in z-direction, displacements in z-direction.

The semi-analytical model was compared to FE models created in COMSOL Multiphysics. The overall modelled domain size was kept the same as in Section 4.1. Using a free, automatic meshing scheme, the

element size was allowed to vary between 0.05 m for the discretization of the piles and the adjacent soil, to 0.5 m at the boundaries of the modelled domain. Only one-half of the domain was analysed due to the symmetry across the plane defined by $y = 0$. The generated mesh can be seen in Fig. 5a. Both IBC and PML boundary conditions were tested. The FE model can be seen in Fig. 5a. For the FE–PML model, additional 4 m thick layers were added to the boundaries of the modelled domain.

The results are shown in Fig. 6 for the half-space case and in Fig. 7 for the layered-soil case. It can be seen that, for low frequencies, some differences between the modelling approaches exist. The FE–IBC model performs the worst, with the cross-directional terms (Figs. 6b, 6c, 7b, and 7c) showing a completely different behaviour compared to the other models. This is caused by the waves partially reflecting from the artificial boundaries of the modelled system. However, with increasing frequency the agreement improves, and above around 40 Hz all models agree quite well. Once again, the semi-analytical model shows good agreement with FE–PML model through the considered frequency range. However, the semi-analytical model tends to overestimate the vertical displacements of the loaded pile when loaded in the vertical direction, as seen in Figs. 6c and 7c. The largest difference between the two approaches is around 7 % at low frequencies. This is caused by the discretization of the piles that is used in the semi-analytical model, as the vertical discretization of the piles is only done through horizontal cross-sections. Further, the pure FE models allow the pile cross-section to deform locally, due to the use of solid elements, while the semi-analytical approach assumes rigid cross-sections and the FE beams are based on the Euler-Bernoulli beam theory.

Figure 5 shows the field response for the FE–PML and semi-analytical models excited at 30 Hz with a vertical load. Both subfigures are plotted with identical colourmaps and within the same colour range. Once again, the agreement between the two approaches is very good, even in the near field around the modelled piles.

4.3 Effects of cavities within the soil

As mentioned previously, the effects of cavities, trenches and other types of material removal from the soil cannot be directly accounted for using the semi analytical soil model. However, in the discretized system, the cavities can be simulated by subtracting the dynamic stiffness provided by solid FE blocks with the same material and geometry as the cavities. To validate the approach, the soil and two rigid blocks were modelled with the same discretization and material properties as in Section 4.2. The blocks were placed with the top lying in the ground surface (Case A in Section 4.2). The distance between the blocks was increased to 10 m, centre-to-centre. In between the blocks, a cavity inside the soil was created. The cavity was 3 m long (in the x-direction), 6 m wide (in the y-direction) and 2 m deep (in the z-direction). Horizontally, the cavity was placed exactly halfway between the two blocks, that is at 5 m distance from the cavity centre to either of the blocks' centre. Only one load case was analysed: a unit magnitude vertical load placed on the first rigid block. Once again, two cases were tested: Case A with the top of the cavity top at the ground surface, making it an open pit; Case B with a cavity embedded inside the soil, so that the distance between the crown of the cavity and the ground surface was 2 m. Case A is shown in Figs. 8a and 8b, while Case B can be seen in Figs. 8c and 8d.

Using the semi analytical model combined with FEM, special consideration needs to be taken when modelling cavities. The quality of the solution strongly depends on the discretization and convergence of the system. This is somewhat difficult to achieve as both approaches converge differently. On the one hand, the semi-analytical model tends to underestimate the stiffness of the system if the discretization is poor or if the loaded area of SSI nodes is too small. On the other hand, the FEM used to model the cavities tends to overestimate the stiffness when the discretization is poor. This can lead to numerical issues, when subtracting the dynamic stiffness matrix of the FE model from the dynamic stiffness of the semi-analytic soil model.

A system with numerical issues will show unphysical waves propagating in the boundaries between the created cavity and the soil. This behaviour is due to the dynamic stiffness of the two approaches 'overshooting' at certain nodes. The terms coupling different directions of loading and response, for example vertical load and horizontal displacement, are much more prone to these issues, while the direct coupling terms, for example

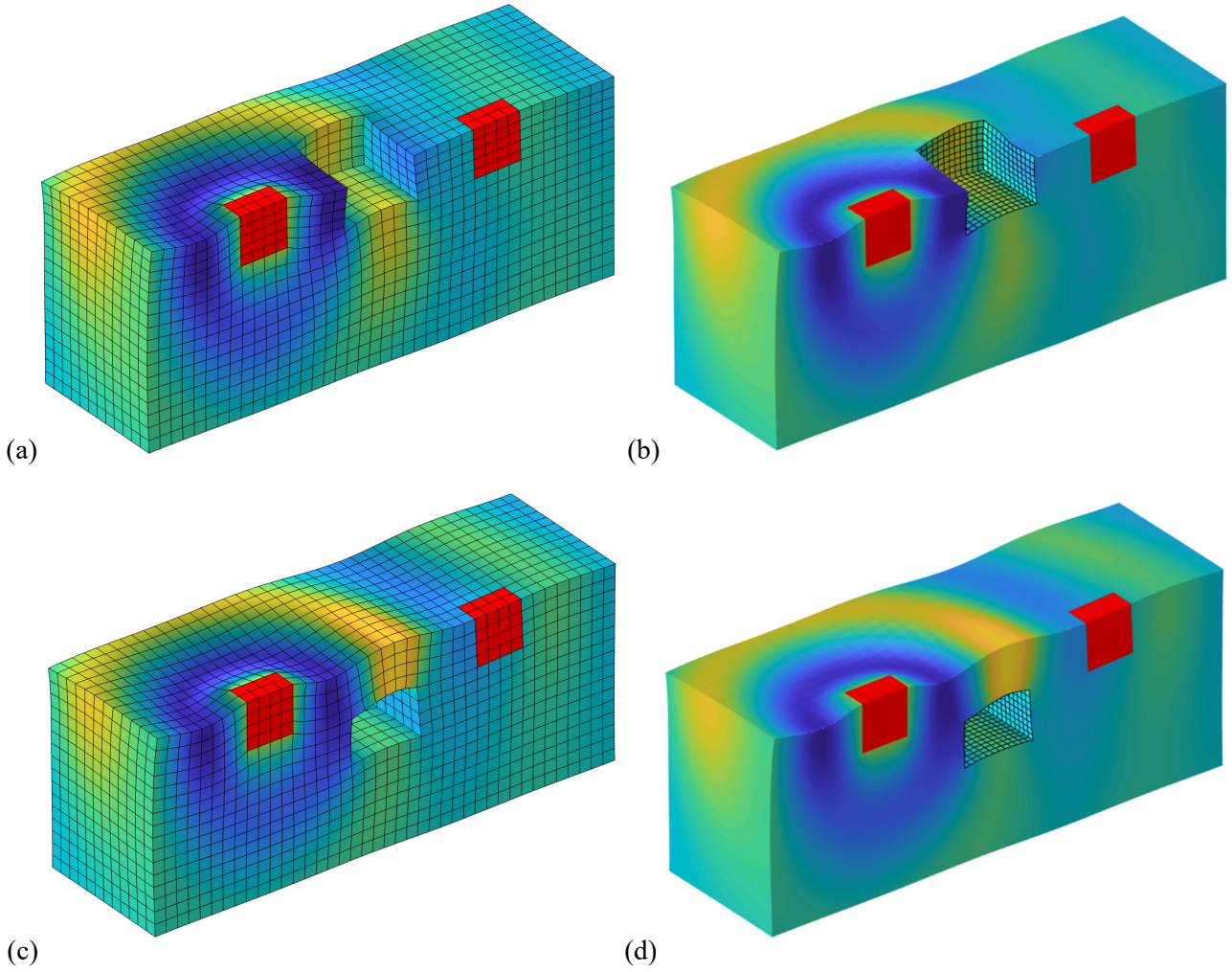

Figure 8. Field response at 30 Hz, for two rigid blocks with soil cavity: (a) Case A, FEM-PML model; (b) Case A, semi-analytical model; (c) Case B, FEM-PML model; (d) Case B, semi-analytical model.

vertical loading and vertical response, are less susceptible. Likewise, the results observed further away from the cavity are not affected significantly.

Using the coupled model, the cavity was discretised into solid linear brick finite elements with a mesh size of 0.25 m in all directions. Various values of the load distribution parameter r_{c0} were tested, with the value of $r_{c0} = 0.151\,3$ providing the most accurate results, without experiencing significant numerical issues. This is equivalent to around 60 % of the distance between two FE nodes. Therefore, there is some overlap between two nearby SSI nodes, spreading the load effects between them, which is similar to the linear interpolation functions used for the finite elements. It has been found that lower values of r_{c0} can lead to better matching results, while experiencing more stability issues at certain frequencies. By contrast, larger values of r_{c0} lead to more stable systems, but the agreement, when compared to pure FE solution, is not as good. The coupled model, including the FE mesh on the boundary of the cavity, can be seen in Figs. 8b and 8d.

COMSOL Multiphysics was again used for validation of the obtained results. The pure FE model is largely the same as described in Section 4.3. However, the modelled domain size was increased to be 20 m long (in the *x*-direction), 5 m wide (in the *y*-direction) and 8 m deep (in the *z*-direction). IBC as well as PML boundary conditions were tested. The models and their meshes can be seen in Figs. 8a and 8c.

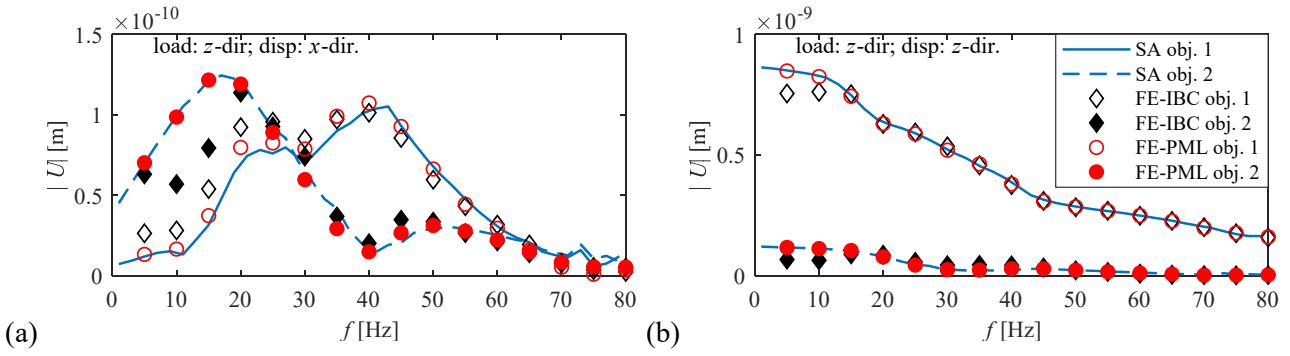

Figure 9. Case A—two rigid blocks with a cavity (pit) placed at the ground surface: (a) load applied in the *x*-direction, displacements in the *x*-direction; (b) load in the *x*-direction, displacements in the *z*-direction.

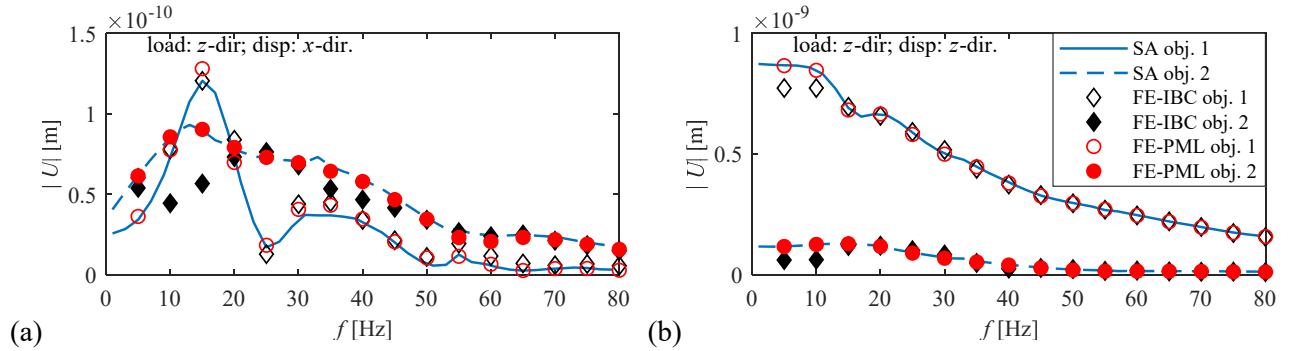

Figure 10. Case B—two rigid blocks with a cavity placed 2 m beneath the ground surface: (a) load applied in the *x*-direction, displacements in the *x*-direction; (b) load in the *x*-direction, displacements in the *z*-direction.

The results are shown in Figs. 9 and 10 for Cases A and B, respectively. Like the previously analysed cases, the FE–IBC model provides the worst matching results. Especially, at lower frequencies and for horizontal displacements, the observed differences are significant. The semi-analytical model and the FE–PML models show a good agreement through the whole analysed frequency range. Of particular interest for the validation of the proposed methodology, the horizontal displacements of the first rigid block, see Figs. 9a and 10a, match well between the semi-analytical approach with FE cavities and the FE–PML model, even though the displacements are caused solely by the waves reflecting from the cavity and the other rigid blocks. Additional peaks are present in the observed response, which would not be the case without the cavity, as it can be seen in Figs. 3c and 4c. A good agreement shows that both models are able to represent the complex dynamic coupling of the structures through the soil, including the effect of the cavity. However, the results of the semi-analytical model indicate some problems with the proposed approach. Additional peaks can be observed in Fig. 9a in the 70–75 Hz range. These are caused by the previously described convergence issues between the FE cavity model and the semi-analytical model, though the inaccuracy of the proposed methodology is small. Further, with increasing cavity size the number of SSI nodes needed also increases, reducing the computational efficiency of the proposed approach. Therefore, the semi-analytical soil model is better suited for cases where a limited amount of soil material is removed.

5. Conclusions

A computational approach for modelling various structures interacting with the soil was introduced. The approach uses a well-known semi-analytical model for layered soil that is coupled to structures that can be embedded in the soil. Modelling of three-dimensional rigid blocks was described in detail, considering proper discretization of the blocks without sacrificing the computational efficiency of the methodology. Further, a

short overview of modelling piles and cavities inside the soil was given. The proposed models were validated by comparison with well-established methods. The proposed model of rigid blocks was compared with coupled boundary-element–finite-element models as well as finite-element models employing local impedance boundary conditions (FE–IBC models) or perfectly matched layers (FE–PML models) to minimize the reflection of waves at artificial boundaries of the model. The pile and cavity modelling approaches were validated by comparison with the FE–IBC and FE–PML models.

The results show very good agreement between the proposed semi-analytical models and the FE–PML models for almost all the analysed cases. As an interesting finding, a 'universal' load distribution parameter to be used in the proposed semi-analytical methodology was identified heuristically.

The other tested approaches, i.e. the BE–FE model (only for rigid blocks) and FE–IBC model, generally tend to diverge at the low frequencies; but their accuracy improves with increasing frequency. All the tested modelling techniques show generally good agreement above 30 Hz.

Especially interesting are the results from the FE–IBC model that had the worst performance in all analysed cases. This demonstrates that the, commonly available in commercial software and thus widely used, boundary conditions do not provide accurate results within the low-frequency range, which is extremely important for structure–soil interaction problems.

The largest discrepancies between the semi-analytical models and the FE–PML models were observed when analysing horizontally loaded pile response. There, the semi-analytical model tends to overestimate the displacements of the loaded pile. This can be expected, since the differences between the two solution procedures are quite large when considering the local pile cross-section displacements and deformations. However, the differences never exceeded 7 % in the considered examples.

From the analysed cases, it can be concluded that the proposed semi-analytical modelling approaches provide very accurate results. Further, following previously described modelling techniques [23], the solution becomes extremely computationally efficient. It works well with modern multi-core computers, as the formulation can easily be adapted for parallel computations.

Another advantage of using the proposed techniques is a fair compatibility with FE formulations. In a frequency-domain formulation, the dynamic stiffness matrices obtained with any of the proposed approaches can simply be assembled into an FE model as a 'super-element', encompassing all of the soil-structure interaction nodes. This way, SSI effects can be included in the dynamic analysis of various structures without significant additional computational effort.

Future works could include a more in-depth analysis of modelling the cavities and resulting numerical issues, as well as a more in-depth analysis of the effects of the wavenumber domain discretization.

Acknowledgement

Part of the research was carried out in the framework of the project "Urban Tranquility" under the Interreg V programme. The authors of this work gratefully acknowledge the European Regional Development Fund for the financial support. Further, the first author would also like to acknowledge the generous support of the Graduate School of Science and Technology in Aarhus University.

References

[1] J.P. Wolf, Spring-dashpot-mass models for foundation vibrations, Earthquake Engineering and Structural Dynamics. 26 (1997) 931–949.

[2] H.L. Wong, J.E. Luco, Tables of impedance functions for square foundations on layered media, International Journal of Soil Dynamics and Earthquake Engineering. 4 (1985) 64–81.

[3] H.L. Wong, J.E. Luco, Dynamic interaction between rigid foundations in a layered half-space, Soil Dynamics and Earthquake Engineering. 5 (1986) 149–158.

[4] A. Mita, J.E. Luco, Dynamic response of a square foundation embedded in an elastic half-space, Soil Dynamics and Earthquake Engineering. 8 (1989) 54–67.

[5] S. Bu, C. Lin, Coupled horizontal-rocking impedance functions for embedded square foundations at high frequency factors, Journal of Earthquake Engineering. 3 (1999) 561–587.

[6] S.C. Dutta, R. Roy, A critical review on idealization and modeling for interaction among soil-foundation-structure system, Computers and Structures. 80 (2002) 1579–1594.

[7] A.M. Kaynia, E. Kausel, Dynamics of piles and pile groups in layered soil media, Soil Dynamics and Earthquake Engineering. 10 (1991) 386–401.

[8] G. Gazetas, N. Makris, Dynamic pile-soil-pile interaction. Part I: Analysis of axial vibration, Earthquake Engineering & Structural Dynamics. 20 (1991) 115–132.

[9] N. Makris, G. Gazetas, Dynamic pile-soil-pile interaction. Part II: Lateral and seismic response, Earthquake Engineering & Structural Dynamics. 21 (1992) 145–162.

[10] J. Lysmer, R.L. Kuhlemeyer, Finite dynamic model for infinite media, Journal of the Engineering Mechanics Division, ASCE. 95 (1969) 859–878.

[11] S. Krenk, P.H. Kirkegaard, Local tensor radiation conditions for elastic waves, Journal of Sound and Vibration. 247 (2001) 875–896.

[12] J.P. Berénger, J.P. Berenger, A Perfectly Matched Layer for the Absorption of Electromagnetic Waves, Journal of Computational Physics. 114 (1994) 185–200.

[13] E.A. Kausel, J.L. Tassoulas, Transmitting boundaries: A closed-form comparison, Bulletin of the Seismological Society of America. 71 (1981) 143–159.

[14] D. Clouteau, R. Cottereau, G. Lombaert, Dynamics of structures coupled with elastic media—a review of numerical models and methods, Journal of Sound and Vibration. 332 (2013) 2415–2436.

[15] R. Shahi, A. Noorzad, Dynamic Response of Rigid Foundations of Arbitrary Shape Using Half-Space Green's Function, International Journal of Geomechanics. 11 (2011) 391–398.

[16] J. Fu, J. Liang, B. Han, Impedance functions of three-dimensional rectangular foundations embedded in multi-layered half-space, Soil Dynamics and Earthquake Engineering. 103 (2017) 118–122.

[17] L.A. Padrón, J.J. Aznárez, O. Maeso, Dynamic structure-soil-structure interaction between nearby piled buildings under seismic excitation by BEM-FEM model, Soil Dynamics and Earthquake Engineering. 29 (2009) 1084–1096.

[18] R. Sanaz, D.K. Armen, A stochastic ground motion model with separable temporal and spectral nonstationarities, Earthquake Engineering & Structural Dynamics. 41 (2012) 1549–1568.

[19] W.T. Thomson, Transmission of elastic waves through a stratified solid medium, Journal of Applied Physics. 21 (1950) 89–93.

[20] N.A. Haskell, The dispersion of surface waves on multilayered media, Bulletin of the Seismological Society of America. 43 (1953) 17–43.

[21] X. Sheng, C.J.C. Jones, M. Petyt, Ground vibration generated by a harmonic load acting on a railway track, Journal of Sound and Vibration. 225 (1999) 3–28.

[22] X. Sheng, C.J.C. Jones, M. Petyt, Ground vibration generated by a load moving along a railway track, Journal of Sound and Vibration. 228 (1999) 129–156.

[23] L.V. Andersen, J. Clausen, Impedance of surface footings on layered ground, Computers and Structures. 86 (2008) 72–87.

[24] L.V. Andersen, J. Clausen, Efficient Modelling of Wind Turbine Foundations, Fundamental and Advanced Topics in Wind Power. (2011).

[25] E. Kausel, J.M. Roesset, Stiffness matrices for layered soils, Bulletin of the Seismological Society of America. 71 (1981) 1743–1761.

[26] J. Lysmer, G. Waas, Shear waves in plane infinite structures, Journal of Engineering Mechanics Division. ASCE 18 (1972) 85–105.

[27] R. Wang, A simple orthonormalization method for stable and efficient computation of Green's functions, Bulletin of the Seismological Society of America. 89 (1999) 733–741.

[28] P. Bucinskas, L.V. Andersen, Semi-analytical approach to modelling the dynamic behaviour of soil excited by embedded foundations, Procedia Engineering. 199 (2017) 2621–2626.

[29] P. Bucinskas, L.V. Andersen, Dynamic soil excitation from railway tunnels, Numerical Methods in Geotechnical Engineering IX. Volume 2 (2018) 1551–1556.

[30] L.V. Andersen, C.J.C. Jones, BEASTS - A Computer Program for Boundary Element, ISVR Technical Memorandum 868, Institute of Sound & Vibration Research, University of Southampton, 2001.

[31] L.V. Andersen, C.J.C. Jones, Finite Element Addendum for BEASTS, ISVR Technical Memorandum 881, Institute of Sound & Vibration Research, University of Southampton, 2003.

[32] COMSOL Multiphysics® v. 5.4. www.comsol.com. COMSOL AB, Stockholm, Sweden., (n.d.).

[33] J. Domínguez, Boundary Elements in Dynamics, Computational Mechanics Publications, 1993.

[34] L.V. Andersen, C.J.C. Jones, Coupled boundary and finite element analysis of vibration from railway tunnels-a comparison of two- and three-dimensional models, Journal of Sound and Vibration. 293 (2006) 611–625.

[35] L.V. Andersen, C.J.C. Jones, Three-Dimensional Elastodynamic Analysis Using Multiple Boundary Element Domains, ISVR Technical Memorandum 867, Institute of Sound & Vibration Research, University of Southampton, 2001.

Paper R1

Effects of railway track modelling to surrounding soil and structure excitation

Full reference:

P. Bucinskas, L.V. Andersen, Effects of railway track modelling to surrounding soil and structure excitation, 25th International Congress on Sound and Vibration, ICSV 25. (2018), 4148–4155.

Status:

The paper in this chapter has been presented at the international conference ICSV 25, 2018 July 8–12 in Hiroshima, Japan. It has been published in the proceedings of the conference. The contents and typesetting of this chapter are as submitted.

25th International Congress on Sound and Vibration
8-12 July 2018 HIROSHIMA CALLING
ICSV25

EFFECTS OF RAILWAY TRACK MODELLING TO SURROUNDING SOIL AND STRUCTURE EXCITATION

Paulius Bucinskas and Lars Vabbersgaard Andersen

Aarhus University, Department of Engineering, Aarhus, Denmark
email: pb@eng.au.dk, lva@eng.au.dk

Railway traffic can lead to significant ground borne vibrations in the surrounding areas. These effects are especially evident in urban environment, where even slow-moving trains generate significant vibrations, which can lead to annoyance and even health concerns of nearby inhabitants. A number of computational models have been created to model such systems, with varying degree of complexity. The most complex models are able to model the system in great detail, but are extremely computationally demanding, while the simple approaches often only consider very simple systems and provide limited insights, such as only the free-field response of the soil. In this work, the full vibration propagation path from a railway line through soil to a simple building structure is modelled. An approach based on a semi-analytical model of the soil is used, while the structures are modelled using finite elements. The method is computationally efficient and could be used in early project-design phases, where a large number of design choices and site conditions might need to be evaluated. However, the efficiency of the approach is greatly reduced with increasing number of nodes where structure and soil interact. Therefore, simplifying the model of a railway track as much as possible can be very advantageous. The aim of the paper is to investigate several different rail track models, with varying degree of simplifications, and to quantify the modelling effects to the system behaviour. Several different soil stratification cases are investigated. The results are obtained by comparing the system response at the soil surface as well as within the building structure.
Keywords: Railway track modelling, ground vibration, structure-soil interaction.

1. Introduction

Vibrations from railway lines is a serious concern in urban environment. Exposure to prolonged periods of environmental vibrations can lead to annoyance and health concerns to building inhabitants as well structural damage to the surrounding structures Further, close proximity to railway lines might reduce the value and desirability of nearby buildings or lead to unused plots of land inside a city. Therefore, estimation of vibrations is very important when building new rail lines or structures nearby. The increasing importance of estimation of railway ground vibration problems is illustrated in a review done by Connolly *et al.* [1], where it was found that for around half of investigated cases additional vibration mitigation measures had to be taken. Most often, the estimation of vibrations is performed using in-situ measurements, which is a time consuming and expensive endeavour. Ideally, the initial estimations could be performed with numerical simulations, reducing the need of in-situ measurements. Computational simulations are cheaper to perform and large number of configurations can be easily tested. Further, estimation of vibrations can be done for project that are only in the planning stages.

There is a wide range of computational approaches created to analyse the ground vibration problems. The models vary from the simplest analytical solutions to 3-dimensional numerical approaches as shown in a review done by Kouroussis *et al.* [2]. However, due computational limitations it is

preferable to use the more efficient—simplified models. The most simple approaches often model the track and underlying soil with Winkler foundations, e.g. by Fryba [3]. Further, a layered system connected through springs and dashpots can be introduced for better representation of a real track structure. Lei [4] uses two-layered track with the most important track elements such as rails, sleepers and the ballast, to analyse the vibrations caused by random track irregularities. However, these approaches do not represent the underlying soil well. This is especially true when the moving vehicle approaches the Rayleigh wave speed inside the soil, which can lead to very large deformations of the system. To account for more complex structure-soil interaction, more advanced models of the soil are introduced. Vostroukhov and Metrikine [5] model the soil as a single viscoelastic layer to which a track system, modelled as beams supported by springs and dashpots, is connected. The used approach does still allow for a closed form solution. However, in most cases finite element (FE) method is used. For example, the FE method has been used by Shih *et al*. [6] to investigate the effects of the modelling approach and by Vogiatzis and Kouroussis [7] to quantify the effects of floating slab track structure. The FE approach is often combined with boundary element (BE) method to represent the soil [8]. These approaches are very versatile and can be used for a wide array of cases. The main disadvantage when using FE or combined FE/BE approaches are the long computation times needed.

More computationally efficient way to represent the soil is to use semi-analytical approaches that can then be coupled to the track structure. A model where the railway track and other structures are modelled using FE while the soil is accounted for with a semi-analytical approach has been presented by Bucinskas [9]. This work uses the same approach to analyse the effects the track model has on the surrounding soil and structure excitation. Several track models are created with varying degree of simplifications in order to find the most efficient way to compute reliable results. The work is focused on the system response further away from the track and the track response itself is not analysed.

2. Computational approach

The applied semi-analytical soil model used was originally proposed by Thomson [10] and Haskell [11]. The soil is assumed viscoelastic, with horizontal interfaces between the soil layers. An analytical expression of the Green's function is found, based on a transfer matrix established between the top and the bottom of a single layer. Introducing the boundary conditions to the system of equations allows for an analytical solution. However, the solution is only possible in frequency domain and by Fourier transformation into the horizontal wavenumber domain. The original approach of assembling multiple layers might break down for large depths and high wavenumbers. Thus additional computational stabilisation techniques should be applied [12]. Further, an inverse Fourier transformation to spatial domain is needed, which can only be performed numerically. Using the obtained solution, a global flexibility matrix of the system can be established.

To couple the soil to FE, the area where the structure interacts with the soil is discretized into soil-structure interaction (SSI) nodes. Due to limitations of the semi-analytical model, the structure and soil can only interact to structures through layer interfaces. Therefore, special care needs to be taken when considering embedded structures—in that case additional interfaces need to be created inside the soil at depths where SSI nodes are present. However, in the considered cases, the rail track interacts only interacts with the soil at the ground surface, thus decreasing the needed computational effort. It has been found that FEs with linear interpolation provide better agreement with the soil model, compared to quadratic interpolation. This is due to the more even stiffness distribution through the nodes of each element as the weigh functions are similar for all nodes. Thus, eight-node solid and four-node shell elements are used. A more detailed description of the approach can be found in [9].

Modelling the soil with a semi-analytical model greatly reduces the computational times needed. While the FE method still allows a wide range of geometries and configurations of structures to be analysed. Of course, some drawbacks also exist. Analysis can only be performed in frequency domain, which does not allow non-linear system behaviour. Further, loads applied on a soil interface

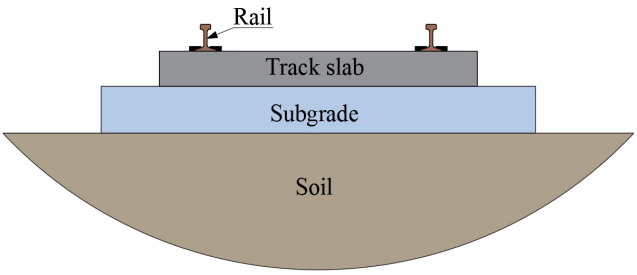

Figure 1. Simplified ballastless track structure.

can only be distributed horizontally. Therefore, the method performs better when analysing vertical system response.

3. Modelling data

In this paper, a ballastless railway track was considered. The more traditional system of sleepers and ballast is replaced by a continuous track slab to which the rails are attached. This type of track requires less maintenance and has a longer life span, when compared to traditional track structures. However, the installation costs are significantly higher, thus it is most often used for the most important track stretches, such as tunnels, viaducts, and areas with dense railway traffic. The modelled track structure is illustrated in Fig. 1. The main part of the structure is the track slab, which is constructed from concrete (properties for materials used in the paper are given in Table 1). The rails are discretely connected to the rail track with rail fastenings. Further, the track slab is placed on a layer of subgrade to ensure good connection to the underlying soil surface.

The described track structure was modelled with three different models, each of them with an increasing degree of simplifications. Three types of FE elements have been utilized: solid, shell and beam elements, each of the element types representing an increased level of simplifications. The overall system is modelled in three dimensions, while the track structure is simplified by essentially removing a dimension from the model. In all cases, the rails are modelled as Euler-Bernoulli beams discretely pinned to the underlying structure. Therefore, the loads acting on the rails can be applied in the same manner for all models. The rails are made of steel, with a cross-sectional area of 0.0076 m^2 and a moment of inertia of 3.038×10^{-5} m^4. The created numerical models are:

- *Solid model.* In this case, the track slab and the subgrade are modelled using eight-node FE solid elements. It provides the most accurate representation of the considered system, with both the track slab and the subgrade layers modelled with separate elements. The subgrade layer is then coupled to the soil surface through SSI nodes. The used solid elements contain three translational degrees of freedom per node, which corresponds to three degrees of freedom of the SSI node.
- *Plate model.* Here the track slab and subgrade layers are combined into a single plate constructed with four-node Mindlin shell elements. The constructed plate is coupled to the underlying soil. In this case, the thickness of the rail track structure is largely disregarded. This is especially evident when coupling the rails and the soil to the structure, where the offset from the embankment centre line is not modelled. Compared to the Solid model, the total number of

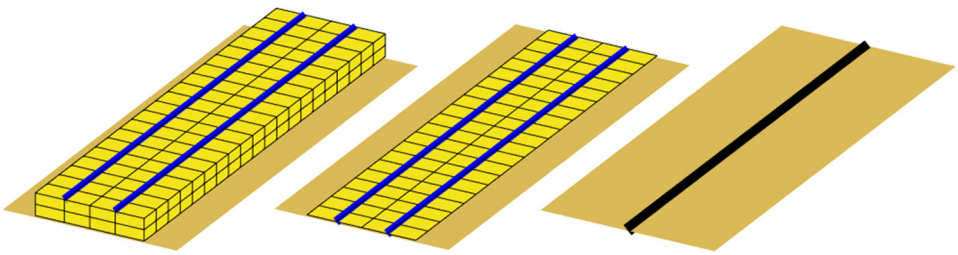

Figure 2. Considered track models. Left to right: Solid model, Plate model, Beam model.

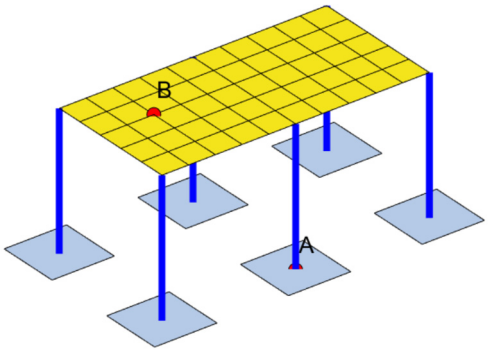

Figure 3. Modelled building structure.

degrees of freedom is reduced. However, the number of SSI nodes stays the same. Further, coupling to the soil is only possible for the first three translational degrees of freedom of the shell element, while the rotational degrees of freedom are not coupled. This could lead to a reduced stiffness of the structure compared to the previous case.

- *Beam model.* The track slab is modelled with two-node beam elements in three-dimensions, where bending is modelled using the Euler-Bernoulli beam theory. The subgrade layer is completely disregarded. Further, both rails are combined into a single beam pinned to the track slab at connecting nodes. Here, both the overall number of degrees of freedom and SSI nodes is greatly reduced. However, similarly to the Plate model, only the translational degrees of freedom of the beam are coupled to the structure.

All models are discretized in a similar fashion—nodes that are shared between models are kept in the same positions. The spacing between the nodes is around 0.6 m in both horizontal directions and 0.3 m in the vertical direction. The discretization of the models is illustrated Fig. 2. The ends of the track are not fixed, therefore it is ensured that the modelled track is long enough to minimise the effects of the free ends. Thus, the total length of the modelled track is equal to 60.0 m. Further, the rail gauge is 1.4 m and track slab width is 3.0 m. The track slab is made from concrete (material properties for concrete and other material used can be found in Table 1). For simplicity, the subgrade layer is modelled with the same width as the track slab. Both the track slab and the subgrade are 0.3 m thick.

Two soil stratification cases were considered: a homogeneous half-space of drained sand and a 5.0 m thick layer of soft clay over a half-space of drained sand. The first case represents a real world case with good soil conditions, while in the second case, the soil conditions are rather unfavourable. Travelling waves can reflect from the boundary between the two materials, trapping the wave in the upper soft layer. This can lead to slower attenuating waves and increased displacements.

The response of the system is analysed in several cases:

- A single massless rigid footing is placed at 15.0 m distance from the track. The footing is a square with a side length of 2.0 m. This case is used to determine the soil response without the added effects of the building structure.
- Further, a simplified one-storey building is analysed, as shown in Fig. 3. The structure is constructed from six columns that support a single floor slab. It is supported by the same type of rigid footings as in the previous case and one of the footings (Point A) is placed in the same position. The cross-section of the columns is square with a side length of 0.3 m, while the slab

Table 1: Material properties.

Material	Young's modulus (MPa)	Poisson's ratio (-)	Mass density (kg/m^3)	Damping ratio (-)
Concrete	30000	0.15	2400	0.040
Steel	210000	0.30	7900	0.020
Subgrade	120	0.35	2100	0.040
Sand	250	0.30	2200	0.045
Clay	80	0.48	2000	0.045

Table 2: Computation times for considered railway track models.

Computed model	Number of computed frequencies	
	1	100
Solid model	10.88 s	692.12 s
Plate model	7.35 s	496.61 s
Beam model	2.30 s	166.38 s

is 0.25 m thick. The columns are 3.0 m high and the spans between the columns are 3.0 m. The building centre is 16.5 m away from the railway track, with the longer side positioned along the track. Two points on the building structure are analysed: Point A is placed at the SSI node connecting the footing and the building column, while Point B is placed on the slab of the building. Mindlin shell and beam elements are used to model the structure. It is discretized with 0.6 m spacing between the nodes.

4. Results

4.1 Response from a harmonic stationary load

The previously described models were analysed in the frequency domain. A vertical unit load was split between the two rails and placed at the middle of the rails, except for the Beam model where the whole load was applied to the single combined rail. Analysis was performed in the 1–50 Hz range. Only the vertical response of the system was analysed, as it is assumed the most important characteristic of the system.

Table 2 shows the computational times needed for the considered models. The time to compute the results is given for 1 and 100 frequencies, as some overhead time can be saved when computing multiple frequencies at the same time. The computations were performed on a workstation with two Intel Xeon E5-2620v3 processors, with 2.40 GHz clock speed. It can be observed, that replacing the Solid model with the Shell model reduces the computation times by around 30%. Simplifying the system into the Beam model reduces the computation times even further by around 77%, when compared to the Solid model. Reducing the computation times can be especially important when considering wide frequency ranges or a wide array of cases. Thus, even a computation-time reduction of as little as 30% can be significant.

Fig. 4 shows the resulting vertical displacements of the single rigid footing for both soil stratification cases. The results are shown in the frequency domain. The observed behaviour is significantly different between the two soil stratification cases. The overall displacements are higher for the layered soil case, except for the very low 1–4 Hz frequency range where the homogeneous half-space provides higher displacements. Further, the layered soil case has a distinct peak at around 10 Hz, which is not present for the half-space soil stratification case.

It is clear that the Solid and Plate models provide almost identical behaviour through the analysed frequency range. The Beam model shows good agreement to about 10 Hz and is able to predict the peak of the layered soil case. However, for higher frequencies, the results diverge and the Beam model tends to overestimate the system response. This could be due to the lack of stiffness at higher frequencies in the system, caused by rotational degrees of freedom of the beam not coupling to the underlying soil. This could be solved by assigning a certain rigid area to each SSI node to obtain the rotational stiffness. However, that would lead to significantly longer computational times, making the model even less efficient than the Plate or Solid models.

Further, the building structure was added to the system. Firstly, Point A in the structure was analysed (position shown in Fig. 3). The rigid footing associated with this point is the same as in the previous case, thus the effects of added mass of the building and additional footings can be investigated. However, it has been found that adding the building does not change the system response at this point significantly. The obtained results are very similar to those shown in Fig. 4 and they are, therefore, not shown here. Further, Fig. 5 shows the behaviour of the floor slab of the building in Point B. Once again, the observed response in Solid and Plate models are almost identical. The Beam

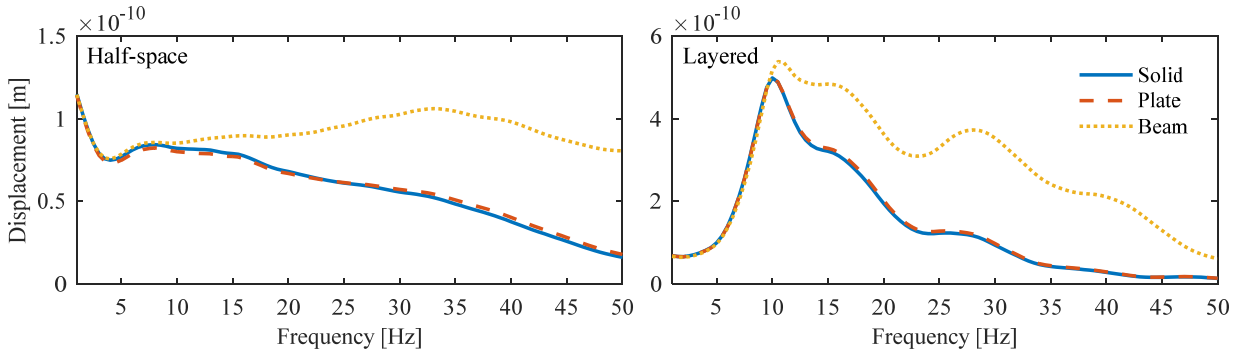

Figure 4: Vertical response of a single footing at 15 m distance from the rail track. Soil conditions: on the left—homogenous half-space of sand, on the right—5 m layer of soft clay over half-space of sand.

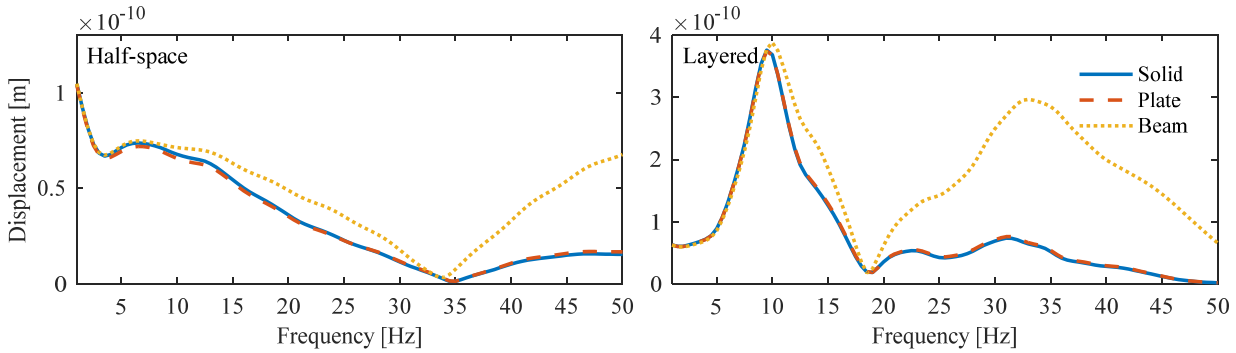

Figure 5: Steady state response on the first floor (Point B) of the building structure. Soil conditions: on the left—homogenous half-space of sand, on the right—5 m layer of soft clay over half-space of sand.

model still provides different results, especially at higher frequencies. However, the agreement between all models is better overall—the Beam model shows good agreement up to 35 Hz and 20 Hz for half-space and layered soil stratification cases, respectively. Further, it predicts the first peak of the layered case as well as the first large valley for both stratification cases. It can be concluded, that the effects of railway track modelling are reduced further away from the soil surface. It is possible that these effects can further increase when considering larger structures.

4.2 Response from a constant moving load

The system response from a stationary force might not reproduce the real-life system behaviour well. Thus, as an alternative, a moving unit load is introduced into the system. The modelled load is moving at 40 m/s along the track and is split between the two rails in the same way as in the previous subsection. The load is applied in the vertical direction downwards, for better representation of a passing train. The system is calculated at 1024 discrete frequencies up to 100 Hz, and inverse Fourier transformation is performed to obtain the time-domain solution. The previous subsection showed only minimal differences between the responses of a single footing in the free field and a building structure. Hence, only the building structure is considered in this section.

Fig. 6 shows the building footing response (Point A) from a moving force. Firstly, the resulting vertical response is given in time domain. Once again, different soil-stratification cases have a significant effect on the system behaviour. Interestingly, higher absolute displacements are observed for the homogeneous half-space, even though the soil stiffness is lower in the layered case. All considered numerical models provide very similar results. The Beam model does show some differences—higher positive peaks are observed, especially for layered soil stratification. Further, the results are converted into frequency domain (see bottom subfigures in Fig. 6). Here it is clear the Beam model significantly overestimates the response at higher frequencies—good agreement between all models is only observed up to 3.5 Hz. The Solid and Beam models still show very good agreement with only minor

deviations in both frequency domain and time domain. Similar system behaviour is also observed for different vehicle speeds.

The vertical response of the floor slab in Point B is shown in Fig. 7. Here, the agreement between all considered models is even better. For the homogeneous half-space, the Beam model fits the other models very well. In some instances, it fits the solid model better than the shell model. Overall, the Beam model still provides more excitation at higher frequencies. However, the differences are rather small and could be considered acceptable, especially when significantly reduced computation times are taken into account. As seen from the analysis with a stationary force, the building structure introduces additional damping to the system, thus reducing the importance of the railway track model.

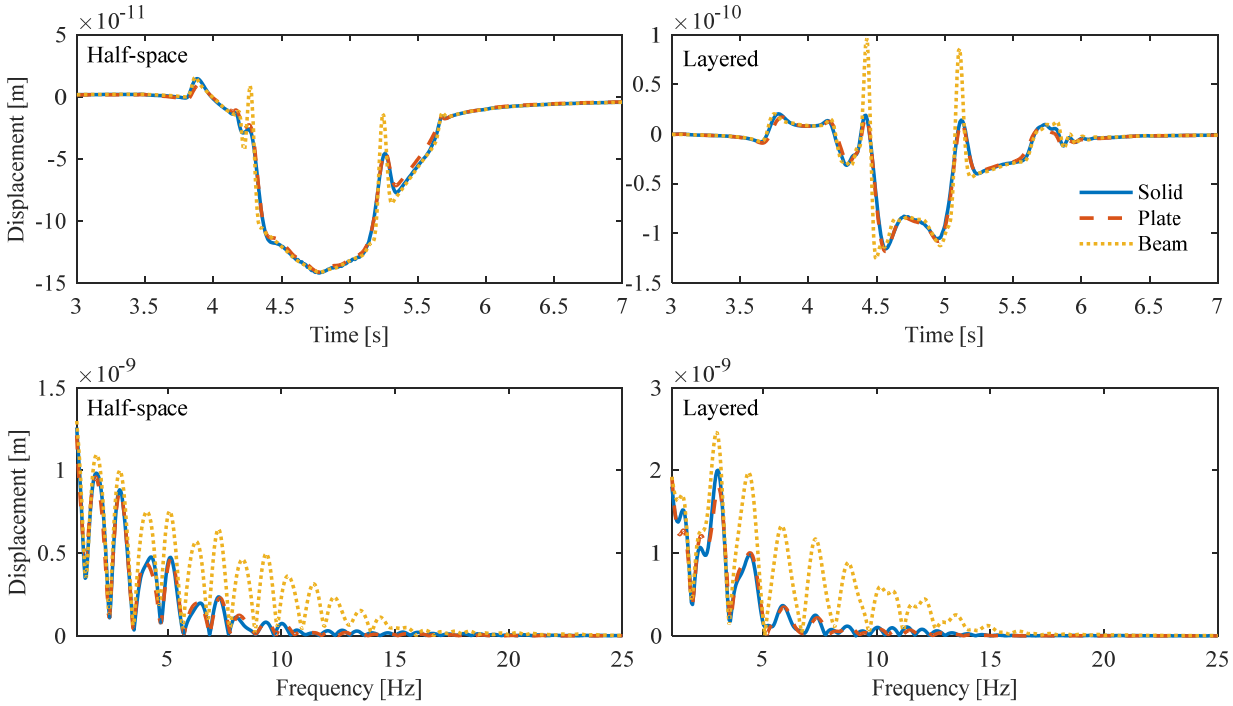

Figure 6: Vertical building footing (Point A) from unit load travelling at 40 m/s. Soil conditions: on the left—homogenous half-space of sand, on the right—5 m layer of soft clay over half-space of sand.

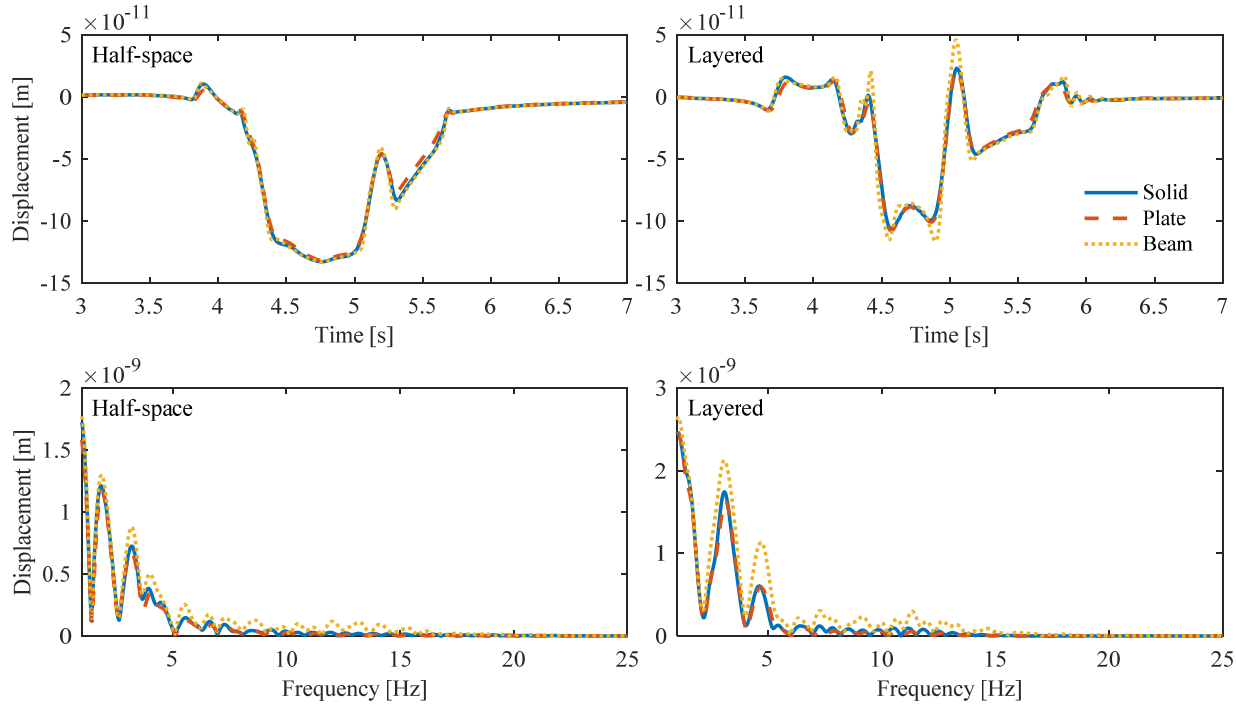

Figure 7: Vertical building floor (Point B) response from unit load travelling at 40 m/s. Soil conditions: on the left—homogenous half-space of sand, on the right—5 m layer of soft clay over half-space of sand.

5. Discussion and conclusion

The work shortly introduces a modelling approach where a semi-analytical soil model can be coupled via SSI nodes to a finite-element model of one or more structures. The approach was utilized to model a railway track and a neighbouring footing or building. Three different railway track models were created, with varying degrees of complexity. Created models were used to analyse the excitation of the soil and building structure near the railway track. Analysis was performed by calculating the steady state response from a stationary force and the response from a load traversing the railway track.

It has been found that in all considered cases, the Plate model provides almost identical results to the Solid model. This could be an attractive approach when modelling a railway track, as the Plate model offers 30% reduced computation times together with an easier modelling procedure. Further, the Beam model offers an additional 77% reduction of the computation time, and thus it would be very useful for studies requiring many computations. However, the model does not perform well in all cases. It has been found that the Beam model performs well in the low-frequency range at around 1-4 Hz. Further, introducing a building structure into the system reduces the differences between the approaches. The building structure damps some of the high frequency response, reducing the drawbacks of the Beam model. Therefore, when considering the building floor response from a moving load, the Beam model shows rather good agreement with the other models, especially for a homogeneous half-space of soil. It is possible that when larger and more complex structures are analysed, these effects would further amplify. The Beam model could also be considered when modelling slow-moving vehicles such as trams, where the excited frequency ranges are lower.

Acknowledgment

The research was carried out in the framework of the project “Urban Tranquility” under the Interreg V programme. The authors of this work gratefully acknowledge the European Regional Development Fund for the financial support.

References

1 Connolly D.P., Marecki G.P., Kouroussis G,. Thalassinakis I., Woodward P.K., The growth of railway ground vibration problems—a review. *Science of the Total Environment*, **568**, 1276-82, (2016).
2 Kouroussis G., Connolly D.P., Verlinden O., Railway-induced ground vibrations–a review of vehicle effects. *International Journal of Rail Transportation*, **2**(2), 69-110, (2014).
3 Frýba L., *Vibration of solids and structures under moving loads*. Springer Science & Business Media; (2013).
4 Lei X, Noda N.A. Analyses of dynamic response of vehicle and track coupling system with random irregularity of track vertical profile. *Journal of sound and vibration*, **258**(1), 147–65, (2002).
5 Vostroukhov A.V., Metrikine A.V., Periodically supported beam on a visco-elastic layer as a model for dynamic analysis of a high-speed railway track, *International Journal of Solids and Structures*, **40**(21), 5723-52, (2003).
6 Shih J.Y., Thompson D.J., Zervos A., The effect of boundary conditions, model size and damping models in the finite element modelling of a moving load on a track/ground system. *Soil Dynamics and Earthquake Engineering*, **89**, 12-27, (2016).
7 Vogiatzis K.E., Kouroussis G., Prediction and efficient control of vibration mitigation using floating slabs: practical application at Athens metro lines 2 and 3. *International Journal of Rail Transportation*, **3**(4), 215-32, (2015).
8 Galvín P., Romero A., Domínguez J., Fully three-dimensional analysis of high-speed train–track–soil-structure dynamic interaction. *Journal of Sound and Vibration*, **329**(24), 5147-63, 2010.
9 Bucinskas P., Andersen L.V., Excitation of structures near railway tracks—analysis of the wave propagation path, *COMPDYN 2017-6th International Conference on Computational Methods in Structural Dynamics and Earthquake Engineering*, (2017).
10 Haskell N.A., The dispersion of surface waves on multi-layered media, *Bulletin of the seismological Society of America*, **43**(1), 17–34, (1953).
11 Thomson W.T., Transmission of elastic waves through a stratified solid medium, *Journal of applied Physics*, **21**(2), 89–93, (1950).
12 Wang R, A simple orthonormalization method for stable and efficient computation of Green's functions, *Bulletin of the Seismological Society of America*, **89**(3), 733-41, (1999).

Paper R2

Modelling train-induced vibration of structures using a mixed-frame-of-reference approach

Full reference:

P. Bucinskas, E. Ntotsios, D.J. Thompson and L.V. Andersen, Modelling train-induced vibration of structures using a mixed-frame-of-reference approach. Under review in Journal of Sound and Vibration, initial submission 2019 September 17.

Status:

This chapter presents the manuscript submitted to Journal of Sound and Vibration on 2019 September 17. The contents and typesetting of this chapter are as submitted.

Modelling train-induced vibration of structures using a mixed-frame-of-reference approach

Paulius Bucinskas[1]*, Evangelos Ntotsios[2], David J. Thompson[2] and Lars V. Andersen[1],

[1] *Department of Engineering, Aarhus University, Aarhus, 8000, Denmark*
[2] *Institute of Sound and Vibration, University of Southampton, Southampton, SO17 1BJ, United Kingdom*
* *Corresponding author, e-mail address pb@eng.au.dk*

Abstract

A novel computational modelling approach for prediction of environmental vibration is introduced. The model is formulated in both moving and fixed frames of reference, with a mixed frame of reference formulation introduced to couple the two frames of reference. The resulting system is able to model a vehicle travelling on an infinite railway track, formulated in a moving frame of reference, interacting via the soil with a building structure, formulated in a fixed frame of reference. The method utilizes a semi-analytical soil model with the structures modelled using three-dimensional finite elements. Two solution procedures of the full system are proposed: partial coupling, where some secondary effects from reflected waves propagating through soil are disregarded, and full coupling, where the vehicle–track–soil–structure is modelled as a fully coupled system. Both proposed solution procedures offer a one-step approach for solving the whole system in the frequency–spatial domain. The usage of the model is demonstrated in two example cases: one analysing a simple building structure near a railway track, using the partial coupling solution procedure, and another one analysing the behaviour of a vehicle model traversing over a rigid block embedded inside the soil, using the full coupling solution procedure. The introduced modelling approach offers a computationally efficient solution procedure, at the same time being applicable to a wide array of application cases.

Keywords: soil–structure interaction, train induced vibration, mixed frame of reference

1. Introduction

Railway transportation has been seeing a resurgence in popularity in the recent years, as an efficient, fast and environmentally friendly form of transportation. This is especially evident in urban centres, where new metro and tramway lines are being continuously developed. However, constructing railway lines close to existing buildings or new buildings near existing lines leads to a set of challenges which need to be addressed. One of these challenges is the environmental vibration resulting from the passing trains. It propagates through the soil and enters the structures, causing annoyance to the inhabitants and, in worst case, leading to structural damage.

As shown in Connolly et al. [1], environmental vibration is a growing concern when planning new railway projects. The exact propagation mechanism of environmental vibration is an extremely complex phenomenon, and thus proper evaluation of its effects is difficult. A rough estimate of the vibration levels can be obtained by using the guidelines provided by, for example, the Federal Railroad Administration [2] that is commonly used in many countries. These estimates are generally based on empirical methods using on-site measurements before and during construction. However, for more precise estimations, costly and time-consuming in-situ investigations need to be performed. Alternatively, computational models can also be used to evaluate these effects. Their use is advantageous as analysis can be performed even before the construction begins, and different configurations and site conditions can be tested. However, detailed computational models often require sufficient engineering experience and long computation times, while simplified models assume significant reduction of site conditions, making their applications somewhat limited.

When modelling environmental vibration, the modelling of the soil strata is, in most cases, the highest time consuming and difficult task. A sizable soil domain must be modelled to account for the source–soil–structure interaction, and in numerical models based on, for example, the finite-element method (FEM), transmitting boundary conditions are required to ensure radiation of waves, thus mimicking the behaviour of an unbounded medium. This can be avoided to a degree by using analytical and semi-analytical approaches to model the underlying soil. Such models, utilizing purely analytical formulations of the Green's function, can be found in [3–5]. A widely used semi-analytical method, based on the soil layer transfer matrices formulated in frequency–wavenumber domain, was originally proposed by Thomson [6] and Haskell [7]. The semi-analytical method offers relatively short computation times and ensures radiation without the need of special boundary conditions. The approach has been expanded by introducing rigid objects as described by Andersen and Clausen [8]—or by coupling with a finite-element (FE) model of external structures as described by Bucinskas and Andersen [9]. An analytical railway track model coupled to a semi-analytical soil model was introduced by Sheng et al. for a stationary load [10] and a moving load [11]. The railway track was modelled analytically as an infinite structure consisting of beam and continuous springs and masses, this way accounting for the railway track behaviour at higher frequencies. The model was further expanded by introducing a multi-degree-of-freedom vehicle model and excitation from an uneven track [12]. The vehicle was modelled in two dimensions, accounting only for the vertical interactions between the wheels and the rails, with the whole system modelled in a moving frame of reference, and with the possibility to observe the resulting displacements at a non-moving receiver. The developed methodology offers relatively quick computations. However, the application range is limited by the assumptions made for the semi-analytical soil model (e.g. perfectly horizontal layers, homogeneity, isotropy etc.).

When more complex systems are investigated, the modelling effort increases accordingly. Three-dimensional (3D) problems can be analysed using the FEM. Examples of 3D FE models including surface railways can be found in [13–15]. The models can be formulated to account for a fully coupled vehicle–track–soil system, as shown by Connolly et al. [14]—or a two-step approach can be used, as shown by Kouroussis and Verlinden [15]. The biggest challenges of fully 3D models are the long computation times and the finite boundaries of the modelled domain. Another popular numerical approach is the boundary-element (BE) method. Like the semi-analytical approach, this method has an inherent ability to radiate waves. Hence, only the boundaries of the investigated domain need to be discretized. The boundary-element method (BEM) is commonly coupled to the FEM, to create FE–BE models where the structures are modelled using the FEM and the soil is modelled using the BEM. Examples of 3D BE analysis and its coupling with the FEM can be found in [16–18]. Similar to fully 3D FE models, the 3D BE models still suffer from long computation times. This can be remedied to some degree by using so-called 'two-and-a-half-dimensional' (2.5D) models, originally proposed by Yang and Hung [19]. The methodology assumes invariant geometry along the movement direction of the vehicle, enabling Fourier transformation into wavenumber domain in this direction, in essence discretizing only the two-dimensional (2D) cross section of the investigated domain. Then the 2D sections of the model are solved for different wavenumbers and, after inverse Fourier transformation, the 3D response can be obtained. The methodology is widely adopted and various approaches have been utilized to handle the non-reflecting boundary conditions: FE element models [19], FE–BE models [20,21], finite-element–perfectly matched layers models (FE–PML) [22] or finite-element–scaled-boundary-finite-element models [23]. Only a small part of computational approaches and models developed over the years is presented here. A much wider overview of the methods used can be found in review papers, i.e. [24,25] and in the comparative study of models by Connolly et al. [26].

When modelling the environmental vibration in a building induced by railway traffic, three main parts of the problem need to be considered: the vehicle–track system which is the vibration source, the underlying soil through which the vibration propagates, and the building structure which is the vibration receiver. Ideally, all the parts would be combined into a single model, including all coupling terms. However, due to complex analytical formulation needed and the limitations of computational models, this is rarely performed. Most

often, parts of the model are coupled together; for example, a coupled vehicle–track–soil model is calculated, and the obtained results propagate to the building structure [22,27–32]. This way, the secondary coupling terms are excluded from the system, such as the effect of the building structure to the response of the track and the vehicle. This is acceptable, as these coupling terms do not influence the system significantly. For example, Fiala et al. [27] used a two-step approach to obtain the response of a building structure by splitting the problem into a vehicle–track–soil source model and a structure–soil receiver model. With a similar approach, François et al. [28] studied road-traffic-induced vibration. The work also proposed a methodology to exclude the soil–structure interaction problem for cases of soft structures resting on stiff soils. A so-called sub-modelling technique was proposed by Hussein et al. [30], where the response of the soil surface from a tunnel structure was modelled using the pipe-in-pipe method [33] to find the response of a 2D frame. An almost identical system assembly method was also used by Lopes et al. [22]; however, the soil surface response from a tunnel structure was modelled using a 2.5D FEM–PML model and a 3D building structure was analysed.

Overall the prediction of environmental vibration using computational methods is a wide field, with a large variety of solutions developed over the years. However, an overall best method for the problem does not exist, and the decision on which approach to use depends largely on the available computational resources and acceptable level of simplification. The aim of this work is modelling the full vibration propagation path from the vehicle up to the building structure. The proposed novel method includes a moving vehicle model that is directly coupled to a stationary building structure, with interaction between them through the infinite underlying soil, without needing a multiple step solution. At the same time, the method offers a relatively quick and flexible solution procedure. A fully 3D system is modelled, with structures modelled using FE, allowing a wide variety of configurations. To limit the computational times needed, the semi-analytical soil formulation is utilized, with a surface railway track, also modelled analytically as proposed by Sheng et al. [10–12]. The system is excited by a multi-body vehicle model passing over an irregular track. The work introduces an approach of solving the coupled vehicle–track–soil–building system using a single step solution procedure. Two system assembly and solution methods are presented: *partial coupling* and *full coupling*. With the *partial coupling* procedure disregarding some effects caused by the reflected waves for a more computationally efficient solution, and the *full coupling* procedure including all the coupling terms. Additionally, the methodology for modelling rigid objects and FE structures interacting with the soil is described with its implementation into the proposed solution approaches.

The theoretical background of semi-analytical soil modelling is given in Section 2.1, together with the derivations of displacements observed in a fixed frame of reference (FOR) form a load in a moving FOR, in Section 2.2, and vice versa, in Section 2.3. The assembly of discretized soil and coupling it to FE is discussed in Section 3.1. Further, creating rigid objects interacting with the soil is introduced in Section 3.2. The vehicle–track system with the system excitation mechanism is introduced in Section 3.3. Section 4 presents the two assembly and solution procedures of a full system in a mixed FOR. The methodology is validated, by validating the analytically derived coupling terms, in Section 5.1, and comparing with another solution procedure, in Section 5.2. To show the capabilities of the proposed modelling approach two example cases are analysed in Section 6. Finally, the conclusions can be found in Section 7.

2. Semi-analytical soil model

2.1 Formulation in frequency–wavenumber domain

A semi-analytical soil model is used in the present work. The model utilizes a well-known approach based on an analytical solution to the Green's function in the frequency–wavenumber domain. For the linear hysteric half-space $z \leq 0$, the displacement field in time–space domain can be obtained using a convolution integral

$$u_i(x,y,z,t) = \int_{-\infty}^{t} \int_{-\infty}^{0} \int_{-\infty}^{\infty} \int_{-\infty}^{\infty} g_{ij}(x-x', y-y', z, z', t-t')\, p_j(x', y', z', t')\, \mathrm{d}x'\, \mathrm{d}y'\, \mathrm{d}z'\, \mathrm{d}t', \quad (1)$$

where the Green's function g_{ij} relates the displacement component u_i at the point (x, y, z) and time t to the loads p_j applied in direction j at all positions and times up to and including the time t. It should be noted that the Green's function is dependent explicitly on the vertical coordinates z and z' of the observation and loading points and not only on the distance between the points in the depth direction. Thus, while the soil is assumed invariant and infinite in both horizontal directions, the material properties vary over depth due to stratification.

The Green's function is challenging to find analytically in time–space domain for a layered half-space. Thus, a triple Fourier transformation is performed, transforming the two horizontal coordinates into the wavenumbers k_x and k_y, and time into the circular frequency ω. Further, introducing a discretization into a number of depths z_n, $n = 1, 2, 3, \ldots, N_z$, Equation (1) simplifies into

$$\bar{U}_i(k_x, k_y, z, \omega) = \sum_{n=1}^{N_z} \bar{G}_{ij}(k_x, k_y, z, z_n, \omega)\, \bar{P}_{n,j}(k_x, k_y, \omega). \quad (2)$$

Here $\bar{U}_i$ and $\bar{G}_{ij}$ are components of the displacement vector and the Green's function tensor, respectively, in the frequency–wavenumber domain. After the discretization over depth, $\bar{P}_{n,j}$ signifies the traction applied on a horizontal interface placed at the depth z_n. In the following, upper case symbols indicate Fourier transforms with respect to time, whereas overbar indicates Fourier transforms with respect to the horizontal spatial coordinates.

An analytical expression for the Green's function in frequency–wavenumber domain is available. Thomson [6] and Haskell [7] originally developed a transfer-matrix method, which relates the displacements and traction applied at the top of a single layer of material to the displacements and traction at the bottom of the same layer. For that purpose, it is assumed that every layer is composed of homogeneous and linear hysteric material and that the layers are infinite in both horizontal directions. Further, interaction with the soil is only possible through the interfaces between layers or the soil surface. Using the transfer matrices, multiple layers of material are assembled and, after applying the boundary conditions, the expression for the Green's function can be obtained analytically. However, the assembly of multiple layers is not a straightforward task and requires further consideration in order to avoid numerical instabilities. There are two major groups of approaches used to assemble multiple soil layers: the flexibility approaches and the stiffness approaches. One flexibility approach was proposed in the original works by Thomson [6] and Haskell [7]. There, the transfer matrices are multiplied together to propagate the displacements and traction through the layers. Since the considered transfer matrices are never bigger than six by six (three displacement components and three traction components for three-dimensional wave propagation), the approach is very quick to compute. However, the transfer matrices are relating both traction and displacements components to each other in the same matrix, and thus the matrices become badly scaled and eventually ill-conditioned when the frequency becomes higher or the layer thickness becomes greater [34,35]. Interaction between the waves propagating through the layers and reflecting from the interfaces can also cause instabilities due to the limits of the numerical precision in computers. The problems are caused by exponentially increasing and decreasing terms in the same system, which leads to the real behaviour of the system being lost as the rounding error. Therefore, the method is not well suited for problems where high frequencies or thick soil layers are considered.

Solving the numerical stability issues is possible by introducing additional stabilization techniques into the system. One approach, called the orthonormalization method, was proposed by Wang [35] for geophysical applications. In essence, the method 'rotates' the obtained traction and displacements components before propagating them to the next soil layer, this way removing the coupling terms between the primary (P) and the

vertically polarized secondary (SV) waves. The method was originally described for two dimensional cases that only contain P and SV waves, but it can easily be generalized to three-dimensional cases by introducing the horizontally polarized secondary wave (SH). The SH wave is naturally uncoupled from the other two waves; however, this should be enforced in computational codes as rotating the other waves might introduce weak coupling due to numerical precision errors. Further, the transfer matrices contain exponential terms that grow with increasing layer depth and frequency, thus very thick layers should be split into multiple smaller layers with the same material properties to not exceed the limits of floating-point numbers. Using these techniques, very efficient computer calculations can be achieved, as all the computations are still based on interaction between layer transfer matrices not bigger than six by six.

Another, and perhaps a more commonly used approach to solve the numerical instability issues, is the stiffness approach introduced by Kausel and Roesset [36]. Here, the original transfer matrix, as derived by Thomson [6] and Haskell [7], is reordered into a stiffness expression equivalent to those used in the FEM, assuming that the interface between two layers is interpreted as a connecting node. Then multiple layers can be assembled by overlapping the stiffness matrices at the connecting interfaces. Naturally, this approach leads to bigger matrices, especially when considering strata composed of many layers. However, the obtained system stiffness matrices are symmetric, and the approach does not suffer from the instability issues. The created system can then be used to obtain the Green's function of the system.

In terms of computation time, the two methods described above perform very similarly when implemented as a computer code. Further, they can both be used to obtain the Green's function in the frequency–wavenumber domain, and they provide identical results. In this work, both methods have been utilized: the flexibility approach with numerical stabilization for the fixed-frame-of-reference soil model and the stiffness approach for the moving-frame-of-reference model.

In the frequency–wavenumber domain, the displacements are calculated by multiplying the Green's function $\bar{G}_{ij}$ with the triple-Fourier-transformed load $\bar{P}_{n,j}$. Practise shows that using spatially distributed loads is advantageous, since such loads vanish at infinity in wavenumber domain. Contrarily, a concentrated force applied in a single spatial point produces a constant value of the Fourier transform for all wavenumbers—i.e. "white noise" in wavenumber domain—thus requiring, in principle, evaluation of the Green' function and inverse Fourier transformation up to infinite wavenumbers. A further discussion about the load distribution used in this work can be found in Section 5.2. After the displacements in the frequency–wavenumber domain are obtained, a double inverse Fourier transformation is performed into frequency–space domain:

$$U_{\mathrm{f}\,i}(x_{\mathrm{f}}, y, z, \omega_{\mathrm{f}}) = \frac{1}{4\pi^2} \int_{-\infty}^{\infty} \int_{-\infty}^{\infty} \bar{U}_i(k_x, k_y, z, \omega_{\mathrm{f}})\, \mathrm{e}^{\mathrm{i}(k_x x_{\mathrm{f}} + k_y y)}\, \mathrm{d}k_x\, \mathrm{d}k_y. \tag{3}$$

The above equation is used when both the load and the response in a fixed frame of reference (fixed FOR) is considered. The load is applied at a circular frequency ω_{f} and coordinate x_{f}, with subscript 'f' indicating a fixed FOR. As described by Andersen and Clausen [8], a load applied axisymmetrically around the point (x', y', z') can be treated effectively in the fixed FOR. Here, the inverse Fourier transformation can be carried out in semi-discrete form by adopting polar coordinates, since the integration with respect to the azimuthal angle can be done in closed form, leading to Bessel functions in the components $G_{\mathrm{f}\,ij}$ of the Green's function.

When the whole system is considered in a moving FOR, the Green's function and, at the same time, the response in the frequency–wavenumber domain lose the polar symmetry around the origin of the wavenumber domain, compared to a purely fixed FOR. Hence, a fully discrete inverse Fourier transformation from wavenumber domain into spatial domain is necessary. Assuming that a load is moving in the positive x-direction, the frequency used to compute the Green's function becomes wavenumber dependent. In that case, the inverse double Fourier transformation into frequency–space domain is defined as

$$U_{\mathrm{m}\,i}(x_{\mathrm{m}}, y, z, \omega_{\mathrm{m}}) = \frac{1}{4\pi^2}\int_{-\infty}^{\infty}\int_{-\infty}^{\infty}\bar{U}_i(k_x, k_y, z, \omega_{\mathrm{m}} - k_x v)\,\mathrm{e}^{\mathrm{i}(k_x x_{\mathrm{m}} + k_y y)}\,\mathrm{d}k_x\,\mathrm{d}k_y. \tag{4}$$

where v is the velocity at which the moving FOR travels through the fixed FOR. Subscript 'm' indicates values in the moving FOR.

2.2 Moving load observed in a fixed frame of reference

The methodology presented in this work uses both moving and fixed frames of reference. Thus, a mixed FOR is used, where the displacement response observed in a fixed FOR from a load applied at a stationary point in the moving FOR and vice versa are needed in order to obtain the coupling terms between the two frames of reference. An expression for fixed-frame-of-reference displacements from a moving load can be found in [11]. The same formulation is used in this work, and a short summary of the formulation is given below.

Consider a load moving along the x-axis at a constant velocity v. It is assumed that the (x_{m}, y, z)-coordinate system moves together with the load, with the origin placed at the centre of the loaded area. The system is excited at the circular frequency ω_{m}. If only a single excitation frequency is considered, the steady-state time-domain response in the same moving FOR can be expressed as

$$u_{\mathrm{m}\,i}(x_{\mathrm{m}}, y, z, t) = U_{\mathrm{m}\,i}(x_{\mathrm{m}}, y, z, \omega_{\mathrm{m}})\,\mathrm{e}^{\mathrm{i}\omega_{\mathrm{m}} t}, \tag{5}$$

where $u_{\mathrm{m}\,i}$ and x_{m} are the displacement and the coordinate along the x-axis in the moving FOR, respectively. The displacements at a stationary point in the fixed FOR can be observed by defining a relation between x-coordinates in the moving and fixed frames of references:

$$x_{\mathrm{m}} = x_{\mathrm{f}} - vt. \tag{6}$$

Note that here the moving coordinate x_{m} becomes a field quantity dependent on time and is offset from the origin of the fixed FOR. Thus, the response $\tilde{u}_{\mathrm{f}\,i}$ observed in the fixed FOR, caused by a load applied within the moving FOR, can be expressed as

$$\tilde{u}_{\mathrm{f}\,i}(x_{\mathrm{f}}, y, z, \omega_{\mathrm{m}}, t) = u_{\mathrm{m}\,i}(x_{\mathrm{f}} - vt, y, z, t) = U_{\mathrm{m}\,i}(x_{\mathrm{f}} - vt, y, z, \omega_{\mathrm{m}})\,\mathrm{e}^{\mathrm{i}\omega_{\mathrm{m}} t}, \tag{7}$$

where the tilde above the symbol indicates that the quantity depends on the frequency related to the other FOR than the frame in which is observed. In the present case, the displacement is observed in the fixed FOR but depends on the frequency in the moving FOR. Further, the response in the fixed FOR can be Fourier transformed using the fixed-frame-of-reference circular frequencies ω_{f}:

$$\tilde{U}_{\mathrm{f}\,i}(x_{\mathrm{f}}, y, z, \omega_{\mathrm{m}}, \omega_{\mathrm{f}}) = \int_{-\infty}^{\infty} U_{\mathrm{m}\,i}(x_{\mathrm{f}} - vt, y, z, \omega_{\mathrm{m}})\,\mathrm{e}^{-\mathrm{i}(\omega_{\mathrm{f}} - \omega_{\mathrm{m}})t}\,\mathrm{d}t. \tag{8}$$

The expression for x_{m} is introduced back into the equation and is used to replace the time variable t. Using integration by substitution, the time integral can be replaced with

$$\mathrm{d}x_{\mathrm{m}} = -v\mathrm{d}t. \tag{9}$$

Inserting this into Equation (8) and further reordering the expression, the following is obtained:

$$\tilde{U}_{\mathrm{f}\,i}(x_{\mathrm{f}}, y, z, \omega_{\mathrm{m}}, \omega_{\mathrm{f}}) = \frac{1}{v}\mathrm{e}^{-\mathrm{i}(\omega_{\mathrm{f}} - \omega_{\mathrm{m}})x_{\mathrm{f}}/v}\int_{-\infty}^{\infty} U_{\mathrm{m}\,i}(x_{\mathrm{m}}, y, z, \omega_{\mathrm{m}})\,\mathrm{e}^{\mathrm{i}(\omega_{\mathrm{f}} - \omega_{\mathrm{m}})x_{\mathrm{m}}/v}\,\mathrm{d}x_{\mathrm{m}}. \tag{10}$$

It is evident that a wavenumber in the direction of convection can be introduced as

$$\beta = \frac{\omega_{\mathrm{m}} - \omega_{\mathrm{f}}}{v}. \tag{11}$$

Thus, the expression in Equation (10) simplifies to

$$\widetilde{U}_{\mathrm{f}\,i}(x_\mathrm{f}, y, z, \omega_\mathrm{m}, \omega_\mathrm{f}) = \frac{1}{v}\mathrm{e}^{\mathrm{i}\beta x_\mathrm{f}} \int_{-\infty}^{\infty} U_{\mathrm{m}\,i}(x_\mathrm{m}, y, z, \omega_\mathrm{m})\, \mathrm{e}^{-\mathrm{i}\beta x_\mathrm{m}}\, \mathrm{d}x_\mathrm{m}\,, \qquad \beta = \frac{\omega_\mathrm{m} - \omega_\mathrm{f}}{v}. \tag{12}$$

An expression for the displacements in a moving FOR $U_{\mathrm{m}\,i}$ can be found in Equation (4). Replacing the wavenumber k_1 with β and inserting this into Equation (12) produces:

$$\widetilde{U}_{\mathrm{f}\,i}(x_\mathrm{f}, y, z, \omega_\mathrm{m}, \omega_\mathrm{f}) = \frac{1}{v}\mathrm{e}^{\mathrm{i}\beta x_\mathrm{f}} \int_{-\infty}^{\infty} \frac{1}{4\pi^2} \int_{-\infty}^{\infty}\int_{-\infty}^{\infty} \bar{U}_j(\beta, k_y, z, \omega_\mathrm{m} - \beta v)\, \mathrm{e}^{\mathrm{i}(\beta x_\mathrm{m} + k_y y)}\, \mathrm{d}\beta\, \mathrm{d}k_y\, \mathrm{e}^{-\mathrm{i}\beta x_\mathrm{m}}\, \mathrm{d}x_\mathrm{m}. \tag{13}$$

The obtained expression can be further simplified by removing the terms for forwards and backwards Fourier transformation related to x and k_x, obtaining the final expression:

$$\widetilde{U}_{\mathrm{f}\,i}(x_\mathrm{f}, y, z, \omega_\mathrm{m}, \omega_\mathrm{f}) = \frac{1}{v}\mathrm{e}^{\mathrm{i}\beta x_\mathrm{f}} \frac{1}{2\pi} \int_{-\infty}^{\infty} \bar{U}_i(\beta, k_y, z, \omega_\mathrm{m} - \beta v)\, \mathrm{e}^{\mathrm{i}k_y y} \mathrm{d}k_y\,, \qquad \beta = \frac{\omega_\mathrm{m} - \omega_\mathrm{f}}{v}. \tag{14}$$

From the above equation, it is evident that the displacements observed in a fixed FOR and caused by a load applied in a moving FOR are only dependent on a single wavenumber, β, when expressed in the frequency domain for both frames of reference. This allows for efficient calculations, as establishment of a full wavenumber-domain field is not necessary, and the integration is only performed for the wavenumbers in the y-direction.

2.3 Stationary load observed in a moving frame of reference

Similar to the case defined in the previous subsection, the steady-state time-domain response in a fixed FOR from a stationary load acting at a frequency ω_f can be expressed as

$$u_{\mathrm{f}\,i}(x_\mathrm{f}, y, z, t) = U_{\mathrm{f}\,i}(x_\mathrm{f}, y, z, \omega_\mathrm{f})\, \mathrm{e}^{\mathrm{i}\omega_\mathrm{f} t}. \tag{15}$$

The relation between the coordinates along the x-direction in fixed and moving frames of reference can be expressed from Equation (6) as

$$x_\mathrm{f} = x_\mathrm{m} + vt. \tag{16}$$

In this case, the fixed coordinate x_f becomes a time dependent field quantity. Repeating the same procedure as in the previous subsection, the fixed-frame-of-reference coordinate x_f is replaced by the expression for the moving-frame-of-reference coordinate x_m:

$$\tilde{u}_{\mathrm{m}\,i}(x_\mathrm{m}, y, z, \omega_\mathrm{f}, t) = u_{\mathrm{f}\,i}(x_\mathrm{m} + vt, y, z, t) = U_{\mathrm{f}\,i}(x_\mathrm{m} + vt, y, z, \omega_\mathrm{f})\, \mathrm{e}^{\mathrm{i}\omega_\mathrm{f} t}. \tag{17}$$

Further, Fourier transforming the obtained displacements using the moving-frame-of-reference circular frequencies ω_m, the following mixed-frequency-domain expression is obtained:

$$\widetilde{U}_{\mathrm{m}\,i}(x_\mathrm{m}, y, z, \omega_\mathrm{f}, \omega_\mathrm{m}) = \int_{-\infty}^{\infty} U_{\mathrm{f}\,i}(x_\mathrm{m} + vt, y, z, \omega_\mathrm{f})\, \mathrm{e}^{-\mathrm{i}(\omega_\mathrm{m} - \omega_\mathrm{f})t}\, \mathrm{d}t. \tag{18}$$

Back insertion of Equation (16) integration by parts provide the expression:

$$\widetilde{U}_{\mathrm{m}\,i}(x_\mathrm{m}, y, z, \omega_\mathrm{f}, \omega_\mathrm{m}) = \frac{1}{v}\mathrm{e}^{\mathrm{i}(\omega_\mathrm{m} - \omega_\mathrm{f})x_\mathrm{m}/v} \int_{-\infty}^{\infty} U_{\mathrm{f}\,i}(x_\mathrm{f}, y, z, \omega_\mathrm{f})\, \mathrm{e}^{-\mathrm{i}(\omega_\mathrm{m} - \omega_\mathrm{f})x_\mathrm{f}/v}\, \mathrm{d}x_\mathrm{f}. \tag{19}$$

Further, Equations (11) and (3) are inserted into the expression and after some simplification the following is obtained:

$$\widetilde{U}_{\mathrm{m}\,i}(x_\mathrm{m}, y, z, \omega_\mathrm{f}, \omega_\mathrm{m}) = \frac{1}{v}\mathrm{e}^{\mathrm{i}\beta x_\mathrm{m}} \frac{1}{2\pi} \int_{-\infty}^{\infty} \bar{U}_i(\beta, k_y, z, \omega_\mathrm{f})\, \mathrm{e}^{\mathrm{i}k_y y} \mathrm{d}k_y\,, \qquad \beta = \frac{\omega_\mathrm{m} - \omega_\mathrm{f}}{v}. \tag{20}$$

Comparing Equations (20) and (14) it is evident that the expressions are equivalent. That is, the displacements originating from a moving source and observed in a fixed FOR are equivalent to the displacements caused by a stationary source and observed in a moving frame:

$$\widetilde{U}_{\mathrm{m}\,i}(x_{\mathrm{m}}, y, z, \omega_{\mathrm{f}}, \omega_{\mathrm{m}}) = \widetilde{U}_{\mathrm{f}\,i}(x_{\mathrm{f}}, y, z, \omega_{\mathrm{m}}, \omega_{\mathrm{f}}), \tag{21}$$

given that the horizontal coordinates x_{m} and x_{f} have the same numerical value. In practise, this means that only Equation (14) or Equation (20) needs to be evaluated. Then the integral part of the equation is reused for the other FOR combination, with changed x-coordinate. It should be noted that this is only true in the mixed frequency domain. When inverse Fourier transformation is performed to obtain the time-domain response, this is no longer true—even if the circular frequencies ω_{m} and ω_{f} are equal:

$$\tilde{u}_{\mathrm{m}\,i}(x_{\mathrm{m}}, y, z, \omega_{\mathrm{f}}, t) \neq \tilde{u}_{\mathrm{f}\,i}(x_{\mathrm{f}}, y, z, \omega_{\mathrm{m}}, t). \tag{22}$$

3. Structures interacting with soil

3.1 Assembly in a single frame of reference

To couple the semi-analytical soil model to a finite-element (FE) model of one or more structures, a dynamic stiffness matrix of the soil is established. Firstly, the desired geometry of the soil–structure interface is discretized into a number of 'soil–structure interaction' (SSI) nodes. Further, pure output is requested at a range of 'observation' nodes. An example of the discretization is shown in Figure 1. The figure shows the two types of nodes used to model the system: the SSI nodes that are interacting with external structures, and the observation nodes which are only used to analyse soil displacements without direct interaction. The dynamic stiffness matrix is established using the SSI nodes, which is then coupled to structures and used to obtain the system displacements. The displacements of the observation nodes are obtained by post-processing the previously obtained results.

To establish the dynamic stiffness matrix of the soil, a global flexibility matrix relating all the degrees of freedom is needed. For a three-dimensional case, each SSI node has three degrees of freedom. Therefore, the receptance matrix $\mathbf{R}_{\mathrm{ss}}(\omega)$, also called the flexibility matrix, will be a square matrix with three times more rows and columns than the number of nodes in the system. To create the receptance matrix, a unit harmonic load $\bar{P}_{0,s_j}$ is applied to a single degree of freedom, s_j, and the resulting displacements are observed at all SSI degrees of freedom, including the loaded one. The procedure is repeated for every degree of freedom in the system. This way, the receptance relating all degrees of freedom to the loaded degree of freedom is established. The receptance between degrees of freedom s_i and s_j is found as

$$R_{s_i,s_j}(\omega) = \int_{-\infty}^{\infty}\int_{-\infty}^{\infty} \bar{G}_{d_i d_j}(k_x, k_y, z_{n_i}, z_{n_j}, \omega)\, \hat{\bar{P}}_{n_j,s_j}(k_x, k_y, \omega)\, \mathrm{e}^{\mathrm{i}\left(k_x(x_{n_i}-x_{n_j})+k_y(y_{n_i}-y_{n_j})\right)}\, \mathrm{d}k_x\, \mathrm{d}k_y. \tag{23}$$

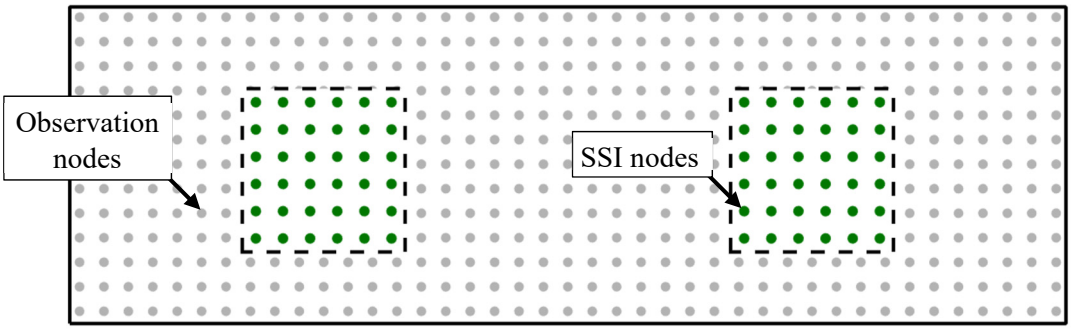

Figure 1. Discretization of a system using the semi-analytical soil model. The SSI nodes shown in green can be loaded directly or interact with external structures. The observation nodes shown in grey only show the displacement resulting from the displacements of the calculation nodes.

Here $\hat{\tilde{P}}_{n_j,s_j}(k_x,k_y,\omega)$ is the double spatial Fourier transform of a distributed harmonic load $\hat{P}_{n_j,s_j}(x,y,\omega)$ of unit magnitude acting within the frequency domain at the depth z_{n_j} in degree of freedom s_j. Further, corresponding to the SSI degrees of freedom s_i and s_j, d_i and d_j signify the local degrees of freedom, $d_i, d_j = 1,2,3$ for the three-dimensional solid, while n_i and n_j are the node numbers of the nodes to which SSI degrees of freedom s_i and s_j belong. Thus, it is assumed that the displacement is observed in direction d_i at a node with coordinates $(x_{n_i}, y_{n_i}, z_{n_i})$, while the load is applied in direction d_j at a node with coordinates $(x_{n_j}, y_{n_j}, z_{n_j})$. The same procedure can be performed in both fixed and moving frames of reference. The obtained results are placed in a single column of the receptance matrix and the process is repeated for every degree of freedom. Assuming there is a total of S SSI degrees of freedom in the system, the assembled receptance matrix becomes:

$$\mathbf{R}_{\mathrm{ss}}(\omega) = \begin{bmatrix} R_{s_1,s_1}(\omega) & R_{s_1,s_2}(\omega) & \cdots & R_{s_1,s_S}(\omega) \\ R_{s_2,s_1}(\omega) & R_{s_2,s_2}(\omega) & \cdots & R_{s_2,s_S}(\omega) \\ \vdots & \vdots & \ddots & \vdots \\ R_{s_S,s_1}(\omega) & R_{s_S,s_2}(\omega) & \cdots & R_{s_S,s_S}(\omega) \end{bmatrix}. \tag{24}$$

Notice that the set $s = \{s_1, s_2, \dots, s_S\}$ containing the numbering of all SSI degrees of freedom is not necessarily equal to the set $\{1, 2, \dots, S\}$, i.e. another ordering of the degrees of freedom may be used. When the soil model is coupled with FE models of structures and/or vehicles coming with their own sets of degrees of freedom, s will be a subset of the set containing all degrees of freedom. However, in any case, $\mathbf{R}_{\mathrm{ss}}(\omega)$ is a $S \times S$ matrix providing the flexibility of the S SSI degrees of freedom from loads applied to the same S degrees of freedom.

The receptance matrix can be established for the moving and fixed frames of reference. However, only in the fixed FOR, the matrix is symmetric, assuming that the applied load $\hat{P}_{n_j,s_j}(x,y,\omega)$ is the same for all degrees of freedom. If no external structures are connected to the semi-analytical soil model, it is possible to apply the loads and obtain the system displacements $\mathbf{U}_{\mathrm{s}}$ directly as:

$$\mathbf{U}_{\mathrm{s}}(\omega) = \mathbf{R}_{\mathrm{ss}}(\omega)\, \mathbf{P}_{\mathrm{s}}(\omega), \tag{25}$$

where $\mathbf{P}_{\mathrm{s}}$ is the vector of load magnitudes. It is implied here that the load acting in degree of freedom s_j has a spatial distribution defined by $\hat{P}_{n_j,s_j}$ and a magnitude defined by element j of $\mathbf{P}_{\mathrm{s}}$.

Next, to couple the soil model with an FE model of one or more structures, the dynamic stiffness matrix of the soil is needed. It can be obtained by inverting the receptance matrix:

$$\mathbf{K}_{\mathrm{ss}}(\omega) = [\mathbf{R}_{\mathrm{ss}}(\omega)]^{-1}. \tag{26}$$

Inversion of a matrix can be computationally expensive, especially for larger systems. Thus, using as few as possible SSI nodes is important for an efficient solution. After the dynamic stiffness matrix is obtained, it can be assembled in the single frame of reference (SFOR) with the dynamic stiffness matrix $\mathbf{K}_{\mathrm{FE}}$ of the FE model:

$$\mathbf{K}_{\mathrm{SFOR}}(\omega) = \begin{bmatrix} \mathbf{K}_{\mathrm{ss}}(\omega) + \mathbf{K}_{\mathrm{FE}}^{\mathrm{ss}}(\omega) & \mathbf{K}_{\mathrm{FE}}^{\mathrm{sn}}(\omega) \\ \mathbf{K}_{\mathrm{FE}}^{\mathrm{ns}}(\omega) & \mathbf{K}_{\mathrm{FE}}^{\mathrm{nn}}(\omega) \end{bmatrix}, \tag{27}$$

where superscript ‘s’ denotes the degrees of freedom through which the FE model interacts with the soil, while superscript ‘n’ denotes the degrees of freedom that are internal to the FE model. Combinations of superscripts ‘sn’ and ‘ns’ denote the coupling terms. Due to symmetry of the FE system matrices, $\mathbf{K}_{\mathrm{FE}}^{\mathrm{ns}}(\omega) = [\mathbf{K}_{\mathrm{FE}}^{\mathrm{sn}}(\omega)]^{\mathrm{T}}$. Further, the matrix $\mathbf{K}_{\mathrm{FE}}^{\mathrm{sn}}(\omega)$ is usually sparsely populated.

The displacements of the system can then be obtained by solving the system of equations:

$$\mathbf{K}_{\mathrm{SFOR}}(\omega)\, \mathbf{U}_{\mathrm{SFOR}}(\omega) = \mathbf{P}_{\mathrm{SFOR}}(\omega). \tag{28}$$

To obtain the displacements of the observation degrees of freedom, a flexibility matrix relating the SSI and observation degrees of freedom is needed. Assuming that the numbering of observation degrees of freedom is stored in a set $o = \{o_1, o_2, \dots, o_O\}$ with the number of degrees of freedom being O, the flexibility matrix will have O rows and S columns. The flexibility matrix for observation degrees of freedom is assembled as:

$$\mathbf{R}_{\mathrm{os}}(\omega) = \begin{bmatrix} R_{o_1,s_1}(\omega) & R_{o_1,s_2}(\omega) & \cdots & R_{o_1,s_S}(\omega) \\ R_{o_2,s_1}(\omega) & R_{o_2,s_2}(\omega) & \cdots & R_{o_2,s_S}(\omega) \\ \vdots & \vdots & \ddots & \vdots \\ R_{o_O,s_1}(\omega) & R_{o_O,s_2}(\omega) & \cdots & R_{o_O,s_S}(\omega) \end{bmatrix}. \tag{29}$$

To find the displacements of the observation nodes the observation flexibility matrix $\mathbf{R}_{\mathrm{os}}$ is multiplied by the soil displacements at the SSI degrees of freedom $\mathbf{U}_{\mathrm{s}}$, which are extracted from the whole system displacement vector $\mathbf{U}_{\mathrm{SFOR}}$:

$$\mathbf{U}_{\mathrm{o}}(\omega) = \mathbf{R}_{\mathrm{os}}(\omega)\,[\mathbf{R}_{\mathrm{ss}}(\omega)]^{-1}\,\mathbf{U}_{\mathrm{s}}(\omega) = \mathbf{R}_{\mathrm{os}}(\omega)\,\mathbf{K}_{\mathrm{ss}}(\omega)\,\mathbf{U}_{\mathrm{s}}(\omega). \tag{30}$$

The matrix inverse involved here was already performed in Equation (26). Thus, the result can be reused. Then, to obtain the displacements of the observation nodes, no further large matrix inversion is needed, making the calculations more computationally efficient. Observation nodes are especially useful when the displacements of large fields are of interest, for example, to observe the displacement of the ground surface in a large region.

3.2 Rigid structures interacting with the soil

The semi-analytical soil model allows modelling of completely rigid objects interacting with the soil. This is useful when modelling structures that are much stiffer than the surrounding material, for example building foundations. To create a three-dimensional rigid object, the object shape is discretized into a number of SSI nodes. The global flexibility matrix is created in the same way as in the previous subsection and inverted to obtain the dynamic stiffness matrix. However, condensation of the stiffness matrix must be performed in order to reduce the system such that the response can be determined in terms of the rigid body modes rather than the original degrees of freedom of the SSI nodes. This is achieved by assuming that SSI nodes belonging to the same rigid object are fixed relatively to each other and move together with the degrees of freedom of a reference master node that defines the motion of the rigid object. In principle, the master node can be placed at any position. However, it is most conveniently placed in the point at which coupling to an FE model should be done. That is, for example, in the centre of the topside of a footing. In the most common three-dimensional case, separate SSI nodes have three degrees of freedom each, i.e. three lateral displacements, while each rigid

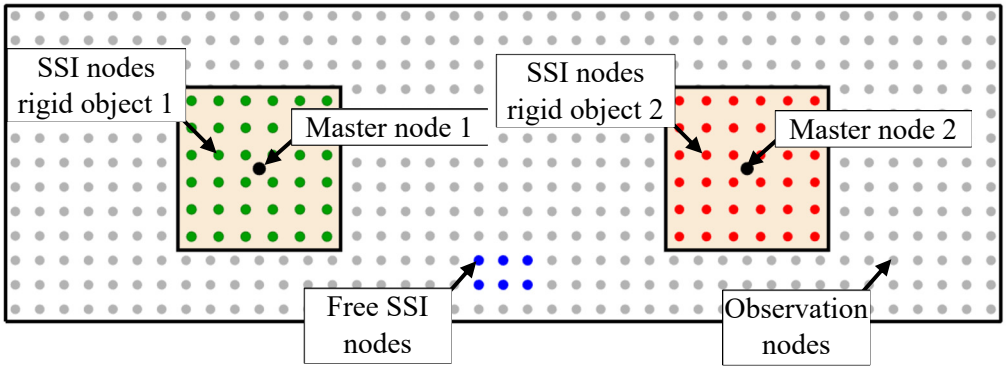

Figure 2. Discretization of a system with rigid objects. The SSI nodes shown in green belong to the rigid object number 1, with master node 1, while nodes in red belong to rigid object number 2, with master node 2. Further 'free' independent SSI nodes are also present in the system and shown in blue. The observation nodes are shown in grey.

object has six degrees of freedom: three for lateral displacements and three additional rotational degrees of freedom of the reference node. For a single rigid object composed of a number of SSI nodes, the transformation matrix $\mathbf{T}_{0,i}$ is created. Multiple rigid objects can also be a part of the same system. The global transformation matrix for a system with N rigid objects can be assembled as:

$$\mathbf{T}_\mathrm{s} = \begin{bmatrix} \mathbf{T}_{0,1} & \mathbf{0} & \cdots & \mathbf{0} \\ \mathbf{0} & \mathbf{T}_{0,2} & \cdots & \mathbf{0} \\ \vdots & \vdots & \ddots & \vdots \\ \mathbf{0} & \mathbf{0} & \cdots & \mathbf{T}_{0,N} \end{bmatrix}. \tag{31}$$

The system can also contain non-associated 'free' SSI nodes, which are not part of any rigid object. In that case, the local transformation matrix for such nodes will be the identity matrix with the same number of rows and columns as the number of degrees of freedom associated with the free node. An example of a two-dimensional system containing rigid objects, free nodes and observation nodes is shown in Figure 2.

To obtain the condensed stiffness matrix of the soil, Equation (26) is modified:

$$\mathbf{K}_\mathrm{s}(\omega) = [\mathbf{T}_\mathrm{s}]^\mathrm{T}\, \mathbf{K}_\mathrm{ss}(\omega)\, \mathbf{T}_\mathrm{s}. \tag{32}$$

The matrix can then be coupled to FE structures in the same way as described previously. Due to condensation of some SSI nodes, Equation (30) is also modified by introducing the transformation matrix:

$$\mathbf{U}_\mathrm{o}(\omega) = \mathbf{R}_\mathrm{os}(\omega)[\mathbf{R}_\mathrm{ss}(\omega)]^{-1}\, \mathbf{T}_\mathrm{s}\, \mathbf{U}_\mathrm{s}(\omega) = \mathbf{R}_\mathrm{os}(\omega)\, \mathbf{K}_\mathrm{ss}(\omega)\, \mathbf{T}_\mathrm{s}\, \mathbf{U}_\mathrm{s}(\omega). \tag{33}$$

The matrix inversion involved here was already performed in Equation (26). Thus, to improve the efficiency of the calculation, intermediate results should be saved and reused here. The formulation outlined here can be also used, if no rigid objects are present in the system. In that case each SSI node is treated as a 'free' node, creating a transformation matrix which is just a square identity matrix, with a number of rows and columns equal to the number of degrees of freedom in the system.

3.3 Vehicle, railway track and wheel–rail interaction

The system is excited by one or more vehicles travelling across a railway track. The vehicles can be modelled using various multibody systems, with varying complexity, depending in the application case. However, in the described model vehicles are only modelled in two dimensions and only the vertical wheel–rail interaction forces are considered. The dynamic stiffness matrix of the vehicle $\mathbf{K}_{\mathrm{vv},i}(\omega_\mathrm{m})$ is created in a moving FOR by combining the vehicle stiffness, damping and mass matrices. If multiple vehicles are needed, the dynamic stiffness matrix becomes:

$$\mathbf{K}_\mathrm{vv}(\omega_\mathrm{m}) = \begin{bmatrix} \mathbf{K}_{\mathrm{vv},1}(\omega_\mathrm{m}) & \mathbf{0} & \cdots & \mathbf{0} \\ \mathbf{0} & \mathbf{K}_{\mathrm{vv},2}(\omega_\mathrm{m}) & \cdots & \mathbf{0} \\ \vdots & \vdots & \ddots & \vdots \\ \mathbf{0} & \mathbf{0} & \cdots & \mathbf{K}_{\mathrm{vv},I}(\omega_\mathrm{m}) \end{bmatrix}, \tag{34}$$

Here it is assumed that there is a total number I of vehicles in the system. Further, there is no coupling between separate vehicles through the vehicle stiffness matrix, i.e. each car of a train acts like a separate vehicle.

The railway track model, as described by Sheng et al. [11], is utilized in this work. A layered track structure containing rail, rail-pads, sleepers and ballast is used. It is coupled to the underlying soil in the frequency–wavenumber domain. The railway track is placed along the x-axis on the soil surface and, similarly to the wheel–rail interaction forces, only the vertical interaction between the soil and the track is considered. An analytical formulation is used, in which the rail track is assumed to be infinite along the x-axis. A flexibility matrix $\mathbf{R}_\mathrm{rr}(\omega_\mathrm{m})$ relating the rail displacements between all vehicle wheel sets positions is constructed. This is achieved in a similar manner as described in the previous section, assuming a single degree of freedom of a rail in a moving FOR for every wheel. The matrix is later used to establish the stiffness matrix of a coupled-

domain stiffness matrix. However, considering a system only in the moving FOR with no additional structures coupled to the soil, the stiffness matrix for the rails can be found by inverting the flexibility matrix:

$$\mathbf{K}_{\mathrm{rr}}(\omega_{\mathrm{m}}) = [\mathbf{R}_{\mathrm{rr}}(\omega_{\mathrm{m}})]^{-1}. \tag{35}$$

To obtain the correct interaction between the rail and the wheels of the vehicle, Hertzian springs are used. However, the system is solved in the frequency domain assuming linear behaviour. Hence, the stiffness of the Hertzian springs is linearized according to the static load of the vehicle:

$$K_{\mathrm{H},l} = \frac{3\,(F_{\mathrm{dw}})^{1/3}}{G_{\mathrm{H}}}, \tag{36}$$

where G_{H} is a constant dependent on the wheel shape and size, and F_{dw} is the load acting on a single wheel from the weight of the vehicle. It should be noted that F_{dw} is the load acting on a single vehicle wheel, and is defined as half of the load acting on a single wheel set. The obtained values are placed into a diagonal matrix, whose size depends on the number of wheel sets L in the system:

$$\mathbf{K}_{\mathrm{H}} = \mathrm{diag}(K_{\mathrm{H},1} \quad K_{\mathrm{H},2} \quad \cdots \quad K_{\mathrm{H},L}). \tag{37}$$

The obtained matrix can then be used for coupling the vehicle model to the track model.

The whole system is excited by the deadweight of the vehicle and the uneven track, with the track unevenness being the largest contributor of higher frequency vibration. It is assumed, that the unevenness of the track can be Fourier transformed and split into separate independent components acting at certain wavenumbers. This way, it is possible to compute the response of the system at selected excitation frequencies ω_{m} from a unit track unevenness. Afterwards, the real response of the system can be found by multiplying the obtained unit response by the actual unevenness at the corresponding wavenumber. Since the vehicle–railway track system is considered in the frequency domain and in a moving FOR, the unit unevenness of the rails will become a complex number with a phase angle according to the wheel position. Vector containing the unit displacements for all wheel sets in the system is found as:

$$\mathbf{d}(\omega_{\mathrm{m}}) = \exp\left(\frac{\omega_{\mathrm{m}}}{v}\,\mathbf{x}_{\mathrm{w}}\right), \tag{38}$$

where $\mathbf{x}_{\mathrm{w}}$ is a vector storing the positions of the wheels in the moving FOR system. The coupled vehicle–track system response from a unit unevenness can then be found as:

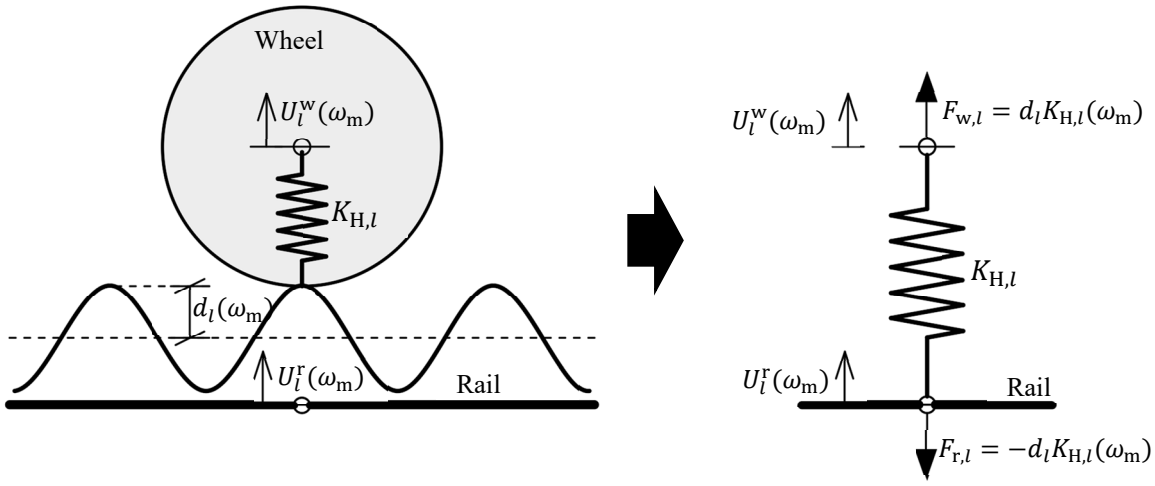

Figure 3. Wheel–rail excitation mechanism due to uneven track. Note that the track unevenness d_l is a complex number, as the system is solved in the frequency domain.

$$\begin{bmatrix} \mathbf{K}_{\mathrm{v}}^{\mathrm{uu}}(\omega_{\mathrm{m}}) & \mathbf{K}_{\mathrm{v}}^{\mathrm{uw}}(\omega_{\mathrm{m}}) & \mathbf{0} \\ \mathbf{K}_{\mathrm{v}}^{\mathrm{wu}}(\omega_{\mathrm{m}}) & \mathbf{K}_{\mathrm{v}}^{\mathrm{ww}}(\omega_{\mathrm{m}}) + \mathbf{K}_{\mathrm{H}} & -\mathbf{K}_{\mathrm{H}} \\ \mathbf{0} & -\mathbf{K}_{\mathrm{H}} & \mathbf{K}_{\mathrm{r}}(\omega_{\mathrm{m}}) + \mathbf{K}_{\mathrm{H}} \end{bmatrix} \begin{Bmatrix} \mathbf{U}_{\mathrm{v}}^{\mathrm{u}}(\omega_{\mathrm{m}}) \\ \mathbf{U}_{\mathrm{v}}^{\mathrm{w}}(\omega_{\mathrm{m}}) \\ \mathbf{U}_{\mathrm{r}}(\omega_{\mathrm{m}}) \end{Bmatrix} = \begin{Bmatrix} \mathbf{0} \\ K_{\mathrm{H}}\,\mathbf{d}(\omega_{\mathrm{m}}) \\ -K_{\mathrm{H}}\,\mathbf{d}(\omega_{\mathrm{m}}) \end{Bmatrix}. \tag{39}$$

Here the vehicle degrees of freedom are split into two parts: those relating to the wheels, denoted with the superscript 'w', and those that are not coupled to the track, denoted with superscript 'u'. It is assumed that each vehicle wheel has the same Hertzian spring stiffness K_{H} when calculating the acting forces. A system with a single vehicle wheel, showing the forces acting on the rail and the wheel due to the unevenness of the track, is shown in Figure 3. Solving the equation for the unknown displacement vector $\mathbf{U}$ produces the system behaviour. Note that in this case, the effects of external structures coupled to the railway track through the soil are not accounted for.

4. Assembly and solution of global system

4.1 Partly coupled global system

Parts of the model described in the previous sections are combined into a single global system. The resulting system combines parts formulated in a moving FOR, such as the vehicle and the track, and parts formulated in the fixed FOR, such as the structures interacting with the soil. To couple the two frames of reference together, the theory described in Sections 2.2 and 2.3 is used. For that purpose, the receptance matrix $\widetilde{\mathbf{R}}_{\mathrm{sr}}$, providing the interaction between the degrees of freedom of the rails and the degrees of freedom of the soil, is established. The matrix $\widetilde{\mathbf{R}}_{\mathrm{sr}}$ couples the moving and fixed frames of reference, and it is therefore dependent on two frequencies: ω_{m} and ω_{s}. Accordingly, the tilde indicates that the quantity is defined in the mixed FOR.

The receptance defining the response of degree of freedom i in the fixed FOR to a load applied to degree of freedom j in the moving FOR can be found as:

$$\tilde{R}_{\mathrm{f}\,i,j}(\omega_{\mathrm{m}}, \omega_{\mathrm{f}}) = \frac{1}{v} \mathrm{e}^{\mathrm{i}\beta(x_{\mathrm{f}\,n_i} - x_{\mathrm{m}\,n_j})} \frac{1}{2\pi} \int_{-\infty}^{\infty} \bar{G}_{d_i d_j}(\beta, k_y, z_{n_i}, z_{n_j}, \omega_{\mathrm{m}} - \beta v)\, \hat{\bar{P}}_{n_j,s_j} \mathrm{e}^{\mathrm{i}(y_{n_i} - y_{n_j})k_y}\, \mathrm{d}k_y, \tag{40}$$

where d_i and d_j are the directions associated with degrees of freedom i and j, while n_i and n_j are the node numbers of the nodes to which degrees of freedom i and j belong. In this case, all loaded degrees of freedom belong to the rails and are applied as unit loads on an Euler-Bernoulli beam. Therefore, the load $\hat{\bar{P}}_{n_j,s_j}$ is equal to one. The receptance matrix can now be assembled:

$$\widetilde{\mathbf{R}}_{\mathrm{sr}}(\omega_{\mathrm{m}}, \omega_{\mathrm{f}}) = \begin{bmatrix} \tilde{R}_{\mathrm{f}\,s_1,r_1}(\omega_{\mathrm{m}}, \omega_{\mathrm{f}}) & \tilde{R}_{\mathrm{f}\,s_1,r_2}(\omega_{\mathrm{m}}, \omega_{\mathrm{f}}) & \cdots & \tilde{R}_{\mathrm{f}\,s_1,r_R}(\omega_{\mathrm{m}}, \omega_{\mathrm{f}}) \\ \tilde{R}_{\mathrm{f}\,s_2,r_1}(\omega_{\mathrm{m}}, \omega_{\mathrm{f}}) & \tilde{R}_{\mathrm{f}\,s_2,r_2}(\omega_{\mathrm{m}}, \omega_{\mathrm{f}}) & \cdots & \tilde{R}_{\mathrm{f}\,s_2,r_R}(\omega_{\mathrm{m}}, \omega_{\mathrm{f}}) \\ \vdots & \vdots & \ddots & \vdots \\ \tilde{R}_{\mathrm{f}\,s_S,r_1}(\omega_{\mathrm{m}}, \omega_{\mathrm{f}}) & \tilde{R}_{\mathrm{f}\,s_S,r_2}(\omega_{\mathrm{m}}, \omega_{\mathrm{f}}) & \cdots & \tilde{R}_{\mathrm{f}\,s_S,r_R}(\omega_{\mathrm{m}}, \omega_{\mathrm{f}}) \end{bmatrix}, \tag{41}$$

where $s = \{s_1, s_2, \ldots, S\}$ is the previously defined set of SSI degrees of freedom, whereas $r = \{r_1, r_2, \ldots, R\}$ is the set of rail degrees of freedom.

Further, the receptance used for the backwards coupling from a load at degree of freedom i in fixed FOR to a displacement in degree of freedom j in a moving FOR is obtained. To avoid excessive additional computations, the similarity between the solutions for the two FOR combinations and the symmetry of the solution in the y-direction is used. Further, it is assumed that there is reciprocity of receptance between the rails and the soil. Thus, the coupling terms between loads applied in a stationary FOR and observed in a moving FOR can be found as:

$$\tilde{R}_{\mathrm{m}\,i,j}(\omega_{\mathrm{f}}, \omega_{\mathrm{m}}) = \frac{1}{v} \mathrm{e}^{\mathrm{i}\beta(x_{\mathrm{m}\,n_j} - x_{\mathrm{f}\,n_i})} \frac{1}{2\pi} \int_{-\infty}^{\infty} \bar{G}_{d_i d_j}(\beta, k_y, z_{n_i}, z_{n_j}, \omega_{\mathrm{m}} - \beta v)\, \hat{\bar{P}}_{n_j,s_j} \mathrm{e}^{\mathrm{i}(y_{n_i} - y_{n_j})k_y}\, \mathrm{d}k_y. \tag{42}$$

By keeping the same integrand as in Equation (40) and only modifying the x-coordinates, additional computations are avoided. The modification due to the x-coordinate is unavoidable as the solution is not symmetrical in the x-direction. The receptance matrix for backwards coupling can be assembled as

$$\widetilde{\mathbf{R}}_{\mathrm{rs}}(\omega_{\mathrm{f}},\omega_{\mathrm{m}})=\begin{bmatrix}\tilde{R}_{\mathrm{m}\,s_1,r_1}(\omega_{\mathrm{f}},\omega_{\mathrm{m}}) & \tilde{R}_{\mathrm{m}\,s_1,r_2}(\omega_{\mathrm{f}},\omega_{\mathrm{m}}) & \cdots & \tilde{R}_{\mathrm{m}\,s_1,r_R}(\omega_{\mathrm{f}},\omega_{\mathrm{m}})\\ \tilde{R}_{\mathrm{m}\,s_2,r_1}(\omega_{\mathrm{f}},\omega_{\mathrm{m}}) & \tilde{R}_{\mathrm{m}\,s_2,r_2}(\omega_{\mathrm{f}},\omega_{\mathrm{m}}) & \cdots & \tilde{R}_{\mathrm{m}\,s_2,r_R}(\omega_{\mathrm{f}},\omega_{\mathrm{m}})\\ \vdots & \vdots & \ddots & \vdots\\ \tilde{R}_{\mathrm{m}\,s_S,r_1}(\omega_{\mathrm{f}},\omega_{\mathrm{m}}) & \tilde{R}_{\mathrm{m}\,s_S,r_2}(\omega_{\mathrm{f}},\omega_{\mathrm{m}}) & \cdots & \tilde{R}_{\mathrm{m}\,s_S,r_R}(\omega_{\mathrm{f}},\omega_{\mathrm{m}})\end{bmatrix}^{\mathrm{T}}. \tag{43}$$

The matrix is assembled like Equation (41) and then transposed, accounting for the switched source and receiver positions. However, as the effects of the backwards coupling in most cases are negligible, the transpose of the forwards coupling matrix, $\widetilde{\mathbf{R}}_{\mathrm{sr}}(\omega_{\mathrm{m}},\omega_{\mathrm{f}})^{\mathrm{T}}$ can be also reused here with little loss of accuracy.

Further, the flexibility matrix, assembled in the fixed FOR and connecting all the degrees of freedom interacting with the soil, is added to the system. Using the created matrices, the full flexibility matrix for the so-called 'global' (indicated by subscript 'g') system can be constructed:

$$\widetilde{\mathbf{R}}_{\mathrm{g}}(\omega_{\mathrm{m}},\omega_{\mathrm{f}})=\begin{bmatrix}\mathbf{R}_{\mathrm{rr}}(\omega_{\mathrm{m}}) & \widetilde{\mathbf{R}}_{\mathrm{rs}}(\omega_{\mathrm{f}},\omega_{\mathrm{m}})\\ \widetilde{\mathbf{R}}_{\mathrm{sr}}(\omega_{\mathrm{m}},\omega_{\mathrm{f}}) & \mathbf{R}_{\mathrm{ss}}(\omega_{\mathrm{f}})\end{bmatrix}. \tag{44}$$

Further, if no rigid bodies are present in the soil model, the global flexibility matrix may be inverted to obtain the stiffness matrix of the global system:

$$\widetilde{\mathbf{K}}_{\mathrm{g}}(\omega_{\mathrm{m}},\omega_{\mathrm{f}})=\left[\widetilde{\mathbf{R}}_{\mathrm{g}}(\omega_{\mathrm{m}},\omega_{\mathrm{f}})\right]^{-1}. \tag{45}$$

If the system contains rigid objects, which are formulated as described in Section 3.2, the global stiffness matrix can be constructed using the global transformation matrix:

$$\mathbf{T}_{\mathrm{g}}=\begin{bmatrix}\mathbf{I} & \mathbf{0}\\ \mathbf{0} & \mathbf{T}_{\mathrm{s}}\end{bmatrix}, \tag{46}$$

where $\mathbf{I}$ is the identity matrix with dimensions equal to the number of rail degrees of freedom. It is assumed that there are no rigid bodies modelled in the moving FOR. In theory, it is possible to model rigid bodies in both the moving and the fixed frames of reference, given that the reference nodes for these bodies are not shared between the two frames of reference. In that case, the identity matrix would be replaced with local transformation matrices $\mathbf{T}_{0,i}$. However, for any practical applications, rigid bodies will only exist in the fixed FOR, where they may be used to model foundations or structures embedded in the ground. The global transformation matrix is introduced into Equation 45 as:

$$\widetilde{\mathbf{K}}_{\mathrm{g}}(\omega_{\mathrm{m}},\omega_{\mathrm{f}})=\left[\mathbf{T}_{\mathrm{g}}\right]^{\mathrm{T}}\left[\widetilde{\mathbf{R}}_{\mathrm{g}}(\omega_{\mathrm{m}},\omega_{\mathrm{s}})\right]^{-1}\mathbf{T}_{\mathrm{g}}. \tag{47}$$

After the stiffness matrix of the system has been obtained, the vehicle and the FE structures can be also added to the global system. The governing equation for partial coupling in the mixed FOR becomes:

$$\widetilde{\mathbf{K}}(\omega_{\mathrm{m}},\omega_{\mathrm{f}})\widetilde{\mathbf{U}}(\omega_{\mathrm{m}},\omega_{\mathrm{f}})=\widetilde{\mathbf{F}}(\omega_{\mathrm{m}},\omega_{\mathrm{f}}), \tag{48a}$$

where

$$\widetilde{\mathbf{K}}(\omega_{\mathrm{m}},\omega_{\mathrm{f}})=\begin{bmatrix}\mathbf{K}_{\mathrm{v}}^{\mathrm{uu}}(\omega_{\mathrm{m}}) & \mathbf{K}_{\mathrm{v}}^{\mathrm{uw}}(\omega_{\mathrm{m}}) & \mathbf{0} & \mathbf{0} & \mathbf{0}\\ \mathbf{K}_{\mathrm{v}}^{\mathrm{wu}}(\omega_{\mathrm{m}}) & \mathbf{K}_{\mathrm{v}}^{\mathrm{ww}}(\omega_{\mathrm{m}})+\mathbf{K}_{\mathrm{H}} & -\mathbf{K}_{\mathrm{H}} & \mathbf{0} & \mathbf{0}\\ \mathbf{0} & -\mathbf{K}_{\mathrm{H}} & \widetilde{\mathbf{K}}_{\mathrm{g}}^{\mathrm{rr}}(\omega_{\mathrm{m}},\omega_{\mathrm{f}})+\mathbf{K}_{\mathrm{H}} & \widetilde{\mathbf{K}}_{\mathrm{g}}^{\mathrm{rs}}(\omega_{\mathrm{f}},\omega_{\mathrm{m}}) & \mathbf{0}\\ \mathbf{0} & \mathbf{0} & \widetilde{\mathbf{K}}_{\mathrm{g}}^{\mathrm{sr}}(\omega_{\mathrm{m}},\omega_{\mathrm{f}}) & \widetilde{\mathbf{K}}_{\mathrm{g}}^{\mathrm{ss}}(\omega_{\mathrm{m}},\omega_{\mathrm{f}})+\widetilde{\mathbf{K}}_{\mathrm{FE}}^{\mathrm{ss}}(\omega_{\mathrm{f}}) & \mathbf{K}_{\mathrm{FE}}^{\mathrm{sn}}(\omega_{\mathrm{f}})\\ \mathbf{0} & \mathbf{0} & \mathbf{0} & \mathbf{K}_{\mathrm{FE}}^{\mathrm{ns}}(\omega_{\mathrm{f}}) & \mathbf{K}_{\mathrm{FE}}^{\mathrm{nn}}(\omega_{\mathrm{f}})\end{bmatrix}, \tag{48b}$$

$$\widetilde{\mathbf{U}}(\omega_\mathrm{m},\omega_\mathrm{f})=\begin{Bmatrix}\widetilde{\mathbf{U}}_\mathrm{v}^\mathrm{u}(\omega_\mathrm{m},\omega_\mathrm{f})\\ \widetilde{\mathbf{U}}_\mathrm{v}^\mathrm{w}(\omega_\mathrm{m},\omega_\mathrm{f})\\ \widetilde{\mathbf{U}}_\mathrm{g}^\mathrm{r}(\omega_\mathrm{m},\omega_\mathrm{f})\\ \widetilde{\mathbf{U}}_\mathrm{g}^\mathrm{s}(\omega_\mathrm{m},\omega_\mathrm{f})\\ \widetilde{\mathbf{U}}_\mathrm{FE}^\mathrm{n}(\omega_\mathrm{m},\omega_\mathrm{f})\end{Bmatrix},\qquad \widetilde{\mathbf{F}}(\omega_\mathrm{m},\omega_\mathrm{f})=\begin{Bmatrix}\mathbf{0}\\ K_\mathrm{H}\mathbf{d}(\omega_\mathrm{m})\\ -K_\mathrm{H}\mathbf{d}(\omega_\mathrm{m})\\ \mathbf{0}\\ \mathbf{0}\end{Bmatrix}. \tag{48c}$$

The superscripts relate to the degrees of freedom of: 'w'—wheels, 'r'—rails, 's'—soil in the fixed FOR, 'n'—parts of FE structures not coupled to the soil and 'u'—vehicles uncoupled from the track (e.g. the vehicle body). Vectors $\widetilde{\mathbf{U}}_\mathrm{v}$, $\widetilde{\mathbf{U}}_\mathrm{g}$ and $\widetilde{\mathbf{U}}_\mathrm{FE}$ store the displacements for the vehicle, global railway track–soil system and the FE structure, respectively. When the excitation frequency ω_m is equal to zero, the unevenness of the track does not excite the system. In that case, the loads corresponding to the deadweight of the vehicle are placed directly on the rails.

It can be seen that the whole system can be solved as a single-step solution without the need of computing the wheel–rail interaction forces before applying them to the system. This way, the weak coupling between the vehicle and the structures interacting with the soil are also included in the system. For most practical applications, these effects are very small. However, the increase in computational effort needed to compute the full system is also relatively low, as the added vehicle degrees of freedom do not increase the total size of the matrix by much.

It should be noted that the coupling between the two frames of reference introduced via Equations (40)–(48) only couples the two investigated frequencies and does not include further spreading through the frequencies. For the investigated case, this means that the effects from the waves propagating through the soil and being reradiated by rigid bodies or FE structures will only affect the vehicle at the frequency of excitation and will not spread to a wider range of frequencies. In order to account for the coupling due to the Doppler effect observed in the moving FOR, related to reradiated waves from footings, etc., in the fixed FOR, and vice versa, the problem must be solved simultaneously for a number of combinations of the frequencies ω_f and ω_m. This results in a system of equations that can be solved directly (see the next section) or by iteration.

After the system has been solved, the displacement for the observation degrees of freedom in the fixed FOR can be obtained. For that purpose, a receptance matrix $\widetilde{\mathbf{R}}_\mathrm{or}(\omega_\mathrm{m},\omega_\mathrm{f})$ between the rails and the observation nodes is established. The procedure is the same as shown in Equations (40) and (41). The receptance matrix between the observation nodes and global nodes is then constructed:

$$\widetilde{\mathbf{R}}_\mathrm{og}(\omega_\mathrm{m},\omega_\mathrm{f})=[\widetilde{\mathbf{R}}_\mathrm{or}(\omega_\mathrm{m},\omega_\mathrm{f})\quad \mathbf{R}_\mathrm{os}(\omega_\mathrm{f})]. \tag{49}$$

The displacements can then be obtained as

$$\widetilde{\mathbf{U}}_\mathrm{o}(\omega_\mathrm{m},\omega_\mathrm{f})=\widetilde{\mathbf{R}}_\mathrm{og}(\omega_\mathrm{m},\omega_\mathrm{f})\left[\widetilde{\mathbf{R}}_\mathrm{gg}(\omega_\mathrm{m},\omega_\mathrm{f})\right]^{-1}\mathbf{T}_\mathrm{g}\,\widetilde{\mathbf{U}}_\mathrm{g}(\omega_\mathrm{m},\omega_\mathrm{f}). \tag{5,}$$

When the displacements for both the global and the observation degrees of freedom have been obtained, the effects from J_m discrete excitation frequencies ω_m can be added together to obtain the total response in the fixed FOR:

$$\mathbf{U}_\mathrm{FE}(\omega_\mathrm{f})=\frac{1}{2\pi}\sum_{j=1}^{J_\mathrm{m}}\widetilde{\mathbf{U}}_\mathrm{FE}\big(\omega_{\mathrm{m},j},\omega_\mathrm{f}\big)\,D(k_{\mathrm{m},j})\,\Delta k_\mathrm{m}, \tag{51}$$

where $D(k_{\mathrm{m},j})$ is the rail unevenness obtained from a power spectral density (PSD) according to the wavenumber $k_{\mathrm{m},j}$, and Δk_m is the wavenumber step size. The wavenumber can be found as

$$k_{\mathrm{m},j}=\frac{\omega_{\mathrm{m},j}}{v}. \tag{52}$$

The displacement vectors $\widetilde{\mathbf{U}}_{\mathrm{g}}^{\mathrm{s}}$ for the global-system soil displacements and $\widetilde{\mathbf{U}}_{\mathrm{o}}$ for the observation node displacements, both relating to the fixed FOR, can be constructed using the same approach. Meanwhile, the displacement vectors $\widetilde{\mathbf{U}}_{\mathrm{g}}^{\mathrm{r}}$ for the global-system rail displacements and $\widetilde{\mathbf{U}}_{\mathrm{v}}$ for the vehicle displacements both relate to the moving FOR. Hence, they should be constructed by combining the effects of the entire considered range of frequencies ω_{f} in the fixed FOR.

Further, the time-domain response for the degrees of freedom associated with the fixed FOR can be obtained by performing an inverse discrete Fourier transformation of the displacements $\mathbf{U}_{\mathrm{FE}}(\omega_{\mathrm{s}})$:

$$\mathbf{u}_{\mathrm{FE}}(t) = \frac{1}{2\pi}\sum_{j=1}^{J_{\mathrm{f}}} \mathbf{U}_{\mathrm{FE}}(\omega_{\mathrm{f},j})\mathrm{e}^{\mathrm{i}\,\omega_{\mathrm{f},j}\,t}\,\Delta\omega_{\mathrm{f}}, \tag{53}$$

where J_{f} is the number of discrete frequencies in the fixed FOR. Note that J_{f} and J_{m} need not be equal. However, the step sizes $\Delta\omega_{\mathrm{f}}$ and Δk_{m} must be small enough, and the number of frequencies J_{f} and J_{m} large enough, to ensure proper discretization of peaks in the loads and resonances of the system while, at the same time, avoiding violation of the periodicity inherent in the frequency-domain solution. Thus, analysis of trains passing very slowly over a track with both short and long irregularities is computationally demanding.

The methodology presented here can be easily expanded for a wider variety of cases. Using the established coupling between two frames of reference, it is also possible to add FE structures in the moving FOR in order to model a more complex geometry of the track or vehicle. Further, the receptance matrices can be created with other methods, for example FE or BE methods, with the global system being assembled and solved in the same manner. Finally, it is noted that the methodology is well-suited for calculation on any computer system, ranging from laptops to large clusters, given that parallelization is possible at many levels.

4.2 Fully coupled global system

Using the matrices already created for the previously described solution procedure, it is also possible to assemble a fully coupled global system. Such a system accounts for the frequency spreading of the reflected waves due to the Doppler effect and might be useful for certain cases where the full coupling between the vehicle (the source) and the structures (the receivers) cannot be discarded.

Considering a discretized system with J_{f} frequencies in the fixed FOR and J_{m} frequencies in the moving FOR, the global receptance matrix for the fully coupled system is assembled as:

$$\overleftrightarrow{\mathbf{R}}_{\mathrm{g}} = \begin{bmatrix} \mathbf{R}_{\mathrm{rr}}(\omega_{\mathrm{m},1}) & \mathbf{0} & \cdots & \mathbf{0} & \widetilde{\mathbf{R}}_{\mathrm{rs}}(\omega_{\mathrm{f},1},\omega_{\mathrm{m},1}) & \widetilde{\mathbf{R}}_{\mathrm{rs}}(\omega_{\mathrm{f},2},\omega_{\mathrm{m},1}) & \cdots & \widetilde{\mathbf{R}}_{\mathrm{rs}}(\omega_{\mathrm{f},J_{\mathrm{f}}},\omega_{\mathrm{m},1}) \\ \mathbf{0} & \mathbf{R}_{\mathrm{rr}}(\omega_{\mathrm{m},2}) & \cdots & \mathbf{0} & \widetilde{\mathbf{R}}_{\mathrm{rs}}(\omega_{\mathrm{f},1},\omega_{\mathrm{m},2}) & \widetilde{\mathbf{R}}_{\mathrm{rs}}(\omega_{\mathrm{f},2},\omega_{\mathrm{m},2}) & \cdots & \widetilde{\mathbf{R}}_{\mathrm{rs}}(\omega_{\mathrm{f},J_{\mathrm{f}}},\omega_{\mathrm{m},2}) \\ \vdots & \vdots & \ddots & \vdots & \vdots & \vdots & \ddots & \vdots \\ \mathbf{0} & \mathbf{0} & \cdots & \mathbf{R}_{\mathrm{rr}}(\omega_{\mathrm{m},J_{\mathrm{m}}}) & \widetilde{\mathbf{R}}_{\mathrm{rs}}(\omega_{\mathrm{f},1},\omega_{\mathrm{m},J_{\mathrm{m}}}) & \widetilde{\mathbf{R}}_{\mathrm{rs}}(\omega_{\mathrm{f},2},\omega_{\mathrm{m},J_{\mathrm{m}}}) & \cdots & \widetilde{\mathbf{R}}_{\mathrm{rs}}(\omega_{\mathrm{f},J_{\mathrm{f}}},\omega_{\mathrm{m},J_{\mathrm{m}}}) \\ \widetilde{\mathbf{R}}_{\mathrm{sr}}(\omega_{\mathrm{m},1},\omega_{\mathrm{f},1}) & \widetilde{\mathbf{R}}_{\mathrm{sr}}(\omega_{\mathrm{m},2},\omega_{\mathrm{f},1}) & \cdots & \widetilde{\mathbf{R}}_{\mathrm{sr}}(\omega_{\mathrm{m},J_{\mathrm{m}}},\omega_{\mathrm{f},1}) & \mathbf{R}_{\mathrm{ss}}(\omega_{\mathrm{f},1}) & \mathbf{0} & \cdots & \mathbf{0} \\ \widetilde{\mathbf{R}}_{\mathrm{sr}}(\omega_{\mathrm{m},1},\omega_{\mathrm{f},2}) & \widetilde{\mathbf{R}}_{\mathrm{sr}}(\omega_{\mathrm{m},2},\omega_{\mathrm{f},2}) & \cdots & \widetilde{\mathbf{R}}_{\mathrm{sr}}(\omega_{\mathrm{m},J_{\mathrm{m}}},\omega_{\mathrm{f},2}) & \mathbf{0} & \mathbf{R}_{\mathrm{ss}}(\omega_{\mathrm{f},2}) & \cdots & \mathbf{0} \\ \vdots & \vdots & \ddots & \vdots & \vdots & \vdots & \ddots & \vdots \\ \widetilde{\mathbf{R}}_{\mathrm{sr}}(\omega_{\mathrm{m},1},\omega_{\mathrm{f},J_{\mathrm{f}}}) & \widetilde{\mathbf{R}}_{\mathrm{sr}}(\omega_{\mathrm{m},2},\omega_{\mathrm{f},J_{\mathrm{f}}}) & \cdots & \widetilde{\mathbf{R}}_{\mathrm{sr}}(\omega_{\mathrm{m},J_{\mathrm{m}}},\omega_{\mathrm{f},J_{\mathrm{f}}}) & \mathbf{0} & \mathbf{0} & \mathbf{0} & \mathbf{R}_{\mathrm{ss}}(\omega_{\mathrm{f},J_{\mathrm{f}}}) \end{bmatrix}. \tag{54}$$

The left–right arrow on $\overleftrightarrow{\mathbf{R}}_{\mathrm{g}}$ indicates the two-way coupling, and again subscript ‘g’ stands for ‘global’. The matrices that depend on single frequencies are assembled into a block diagonal matrices, while the coupling terms that depend on pairs of frequencies are fully populated submatrices. It can be seen that the previously uncoupled frequencies in a single FOR are now coupled through the other FOR. To consider rigid objects, the transformation matrix for the considered system is also needed. However, the transformation matrices are frequency independent and can be assembled simply by combining the previously obtained matrices into a block diagonal matrix, expanding Equation (46) into

$$\overleftrightarrow{\mathbf{T}}_{\mathrm{g}} = \mathrm{diag}\,\{\mathbf{I}_1 \;\; \mathbf{I}_2 \;\; \cdots \;\; \mathbf{I}_{J_\mathrm{m}} \;\; \mathbf{T}_{\mathrm{s},1} \;\; \mathbf{T}_{\mathrm{s},2} \;\; \cdots \;\; \mathbf{T}_{\mathrm{s},J_\mathrm{f}}\}, \tag{55}$$

where in total there are J_m identity matrices, $\mathbf{I}$, and J_f local transformation matrices, $\mathbf{T}_\mathrm{s}$. To obtain the stiffness matrix, the system is solved in the same manner as in the partly coupled system:

$$\overleftrightarrow{\mathbf{K}}_{\mathrm{g}} = \left[\overleftrightarrow{\mathbf{T}}_{\mathrm{g}}\right]^{\mathrm{T}}\left[\overleftrightarrow{\mathbf{R}}_{\mathrm{g}}\right]^{-1}\overleftrightarrow{\mathbf{T}}_{\mathrm{g}}. \tag{56}$$

In most cases, the matrix $\overleftrightarrow{\mathbf{K}}_{\mathrm{g}}$ will be fully populated. To add the vehicle and external FE structures to the system, the fully coupled stiffness matrix $\overleftrightarrow{\mathbf{K}}_{\mathrm{g}}$ is split into submatrices: $\overleftrightarrow{\mathbf{K}}_{\mathrm{g}}^{\mathrm{rr},j_\mathrm{m}j_\mathrm{m}}(\omega_{\mathrm{m},j_\mathrm{m}})$ corresponding to the rail degrees of freedom in a moving FOR at the discrete frequency $\omega_{\mathrm{m},j_\mathrm{m}}$, $\overleftrightarrow{\mathbf{K}}_{\mathrm{g}}^{\mathrm{ss},j_\mathrm{f}j_\mathrm{f}}(\omega_{\mathrm{f},j_\mathrm{f}})$ corresponding to the soil degrees of freedom at a discrete frequency $\omega_{\mathrm{f},j_\mathrm{f}}$ in the fixed FOR. Further, coupling terms between the moving FOR rails and fixed FOR soil are $\overleftrightarrow{\mathbf{K}}_{\mathrm{g}}^{\mathrm{rs},j_\mathrm{m}j_\mathrm{f}}(\omega_{\mathrm{m},j_\mathrm{m}},\omega_{\mathrm{f},j_\mathrm{f}})$ and $\overleftrightarrow{\mathbf{K}}_{\mathrm{g}}^{\mathrm{sr},j_\mathrm{f}j_\mathrm{m}}(\omega_{\mathrm{f},j_\mathrm{f}},\omega_{\mathrm{m},j_\mathrm{m}})$. Differently from the partly coupled system, the fully coupled system has terms coupling the soil degrees of freedom at one fixed-FOR frequency $\omega_{\mathrm{f},j_\mathrm{f}}$ to the soil degrees of freedom at another fixed-FOR frequency $\omega_{\mathrm{f},i_\mathrm{f}}$, such as $\overleftrightarrow{\mathbf{K}}_{\mathrm{g}}^{\mathrm{ss},j_\mathrm{f}i_\mathrm{f}}(\omega_{\mathrm{f},j_\mathrm{f}},\omega_{\mathrm{f},i_\mathrm{f}})$ and $\overleftrightarrow{\mathbf{K}}_{\mathrm{g}}^{\mathrm{ss},i_\mathrm{f}j_\mathrm{f}}(\omega_{\mathrm{f},i_\mathrm{f}},\omega_{\mathrm{f},j_\mathrm{f}})$. Similarly, the rail degrees of freedom are coupled between $\omega_{\mathrm{m},j_\mathrm{f}}$ and $\omega_{\mathrm{m},i_\mathrm{f}}$ in the moving FOR through $\overleftrightarrow{\mathbf{K}}_{\mathrm{g}}^{\mathrm{rr},j_\mathrm{m}i_\mathrm{m}}(\omega_{\mathrm{m},j_\mathrm{m}},\omega_{\mathrm{m},i_\mathrm{m}})$ and $\overleftrightarrow{\mathbf{K}}_{\mathrm{g}}^{\mathrm{rr},i_\mathrm{m}j_\mathrm{m}}(\omega_{\mathrm{m},i_\mathrm{m}},\omega_{\mathrm{m},j_\mathrm{m}})$.

Using the submatrices defined above, the vehicle is coupled to the rails at each moving-FOR frequency $\omega_{\mathrm{m},j_\mathrm{m}}$:

$$\overleftrightarrow{\mathbf{K}}_{\mathrm{mm}}^{j_\mathrm{m}j_\mathrm{m}}(\omega_{\mathrm{m},j_\mathrm{m}}) = \begin{bmatrix} \mathbf{K}_{\mathrm{v}}^{\mathrm{uu}}(\omega_{\mathrm{m},j_\mathrm{m}}) & \mathbf{K}_{\mathrm{v}}^{\mathrm{uw}}(\omega_{\mathrm{m},j_\mathrm{m}}) & \mathbf{0} \\ \mathbf{K}_{\mathrm{v}}^{\mathrm{wu}}(\omega_{\mathrm{m},j_\mathrm{m}}) & \mathbf{K}_{\mathrm{v}}^{\mathrm{ww}}(\omega_{\mathrm{m},j_\mathrm{m}}) + \mathbf{K}_{\mathrm{H}} & -\mathbf{K}_{\mathrm{H}} \\ \mathbf{0} & -\mathbf{K}_{\mathrm{H}} & \overleftrightarrow{\mathbf{K}}_{\mathrm{g}}^{\mathrm{rr},j_\mathrm{m}j_\mathrm{m}}(\omega_{\mathrm{m},j_\mathrm{m}}) + \mathbf{K}_{\mathrm{H}} \end{bmatrix}, \tag{57}$$

with subscript 'm' referring to all degrees of freedom in the moving FOR, i.e. the combination of the uncoupled vehicle 'u', wheel 'w' and rail 'r' degrees of freedom. The force matrix from the track unevenness is also created:

$$\overleftrightarrow{\mathbf{F}}_{\mathrm{m}}^{j_\mathrm{m}}(\omega_{\mathrm{m},j_\mathrm{m}}) = \left\{\mathbf{0} \quad D(k_{\mathrm{m},j})\Delta k_\mathrm{m} K_\mathrm{H}\left[\mathbf{d}(\omega_{\mathrm{m},j_\mathrm{m}})\right]^{\mathrm{T}} \quad -D(k_{\mathrm{m},j})\Delta k_\mathrm{m} K_\mathrm{H}\left[\mathbf{d}(\omega_{\mathrm{m},j_\mathrm{m}})\right]^{\mathrm{T}}\right\}^{\mathrm{T}}. \tag{58}$$

Note that the track unevenness D has to be inserted in the force matrix here, as the obtained displacements will only depend on a single frequency. If the moving-FOR frequency $\omega_{\mathrm{m},j_\mathrm{m}}$ is equal to zero, the deadweight of the vehicle is applied directly to the rails. However, the vehicle is still added to the system, since it reacts to the reradiated waves propagating back into the moving-FOR system from structures defined in the fixed FOR.

External FE structures can be coupled to the soil at fixed FOR frequency $\omega_{\mathrm{f},j_\mathrm{f}}$:

$$\overleftrightarrow{\mathbf{K}}_{\mathrm{ff}}^{j_\mathrm{f}j_\mathrm{f}}(\omega_{\mathrm{f},j_\mathrm{f}}) = \begin{bmatrix} \overleftrightarrow{\mathbf{K}}_{\mathrm{g}}^{\mathrm{ss},j_\mathrm{f}j_\mathrm{f}}(\omega_{\mathrm{f},j_\mathrm{f}}) + \mathbf{K}_{\mathrm{FE}}^{\mathrm{ss}}(\omega_{\mathrm{f},j_\mathrm{f}}) & \mathbf{K}_{\mathrm{FE}}^{\mathrm{sn}}(\omega_{\mathrm{f},j_\mathrm{f}}) \\ \mathbf{K}_{\mathrm{FE}}^{\mathrm{ns}}(\omega_{\mathrm{f},j_\mathrm{f}}) & \mathbf{K}_{\mathrm{FE}}^{\mathrm{nn}}(\omega_{\mathrm{f},j_\mathrm{f}}) \end{bmatrix}, \tag{59}$$

here the subscript 'f' refers to all degrees of freedom in a fixed FOR in the full system, it is a combination of soil 's' and uncoupled FE 'u' degrees of freedom. In this case they are all related to the building structure. Further, the coupling terms coupling the system through frequencies also need to be included. Nothing is directly coupled to them, thus only zero terms are added to the matrix to ensure the obtained matrices are sized correctly. For example, to include the coupling term $\overleftrightarrow{\mathbf{K}}_{\mathrm{g}}^{\mathrm{rs},j_\mathrm{f}j_\mathrm{m}}$ in the full system:

$$\overleftrightarrow{\mathbf{K}}_{\mathrm{mf}}^{j_\mathrm{m}j_\mathrm{f}}(\omega_{\mathrm{m},j_\mathrm{m}},\omega_{\mathrm{f},j_\mathrm{f}}) = \begin{bmatrix} \mathbf{0}^{(\mathrm{uw}\times\mathrm{s})} & \mathbf{0}^{(\mathrm{uw}\times\mathrm{n})} \\ \overleftrightarrow{\mathbf{K}}_{\mathrm{g}}^{\mathrm{rs},j_\mathrm{m}j_\mathrm{f}}(\omega_{\mathrm{m},j_\mathrm{m}},\omega_{\mathrm{f},j_\mathrm{f}}) & \mathbf{0}^{(\mathrm{r}\times\mathrm{n})} \end{bmatrix}, \tag{60}$$

where the superscripts of the zero matrices indicate the sizes of the submatrices, e.g. uw × n indicates that the submatrix has a number of rows equal to the number of degrees of freedom in the vehicle (combined uncoupled

and wheel degrees of freedom) and a number of columns equal to the number of degrees of freedom of not coupled FE structure. Similarly, the matrix coupling the soil degrees of freedom between two frequencies is defined as

$$\vec{\mathbf{K}}_{\mathrm{ff}}^{j_{\mathrm{f}}i_{\mathrm{f}}}\left(\omega_{\mathrm{f},j_{\mathrm{f}}},\omega_{\mathrm{f},i_{\mathrm{f}}}\right)=\begin{bmatrix}\vec{\mathbf{K}}_{\mathrm{g}}^{\mathrm{ss},j_{\mathrm{f}}i_{\mathrm{f}}}(\omega_{\mathrm{f},j_{\mathrm{f}}},\omega_{\mathrm{f},i_{\mathrm{f}}}) & \mathbf{0}^{(\mathrm{s}\times\mathrm{n})}\\ \mathbf{0}^{(\mathrm{n}\times\mathrm{s})} & \mathbf{0}^{(\mathrm{n}\times\mathrm{n})}\end{bmatrix}. \tag{61}$$

This is repeated to create the other coupling matrices in the full system, i.e. $\vec{\mathbf{K}}_{\mathrm{fm}}^{j_{\mathrm{f}}j_{\mathrm{m}}}(\omega_{\mathrm{f},j_{\mathrm{f}}},\omega_{\mathrm{m},j_{\mathrm{m}}})$, $\vec{\mathbf{K}}_{\mathrm{ff}}^{i_{\mathrm{f}}j_{\mathrm{f}}}(\omega_{\mathrm{f},i_{\mathrm{f}}},\omega_{\mathrm{f},j_{\mathrm{f}}})$, $\vec{\mathbf{K}}_{\mathrm{mm}}^{j_{\mathrm{m}}i_{\mathrm{m}}}(\omega_{\mathrm{m},j_{\mathrm{m}}},\omega_{\mathrm{m},i_{\mathrm{m}}})$ and $\vec{\mathbf{K}}_{\mathrm{mm}}^{i_{\mathrm{m}}j_{\mathrm{m}}}(\omega_{\mathrm{m},i_{\mathrm{m}}},\omega_{\mathrm{m},j_{\mathrm{m}}})$. These are created from the global system matrices $\vec{\mathbf{K}}_{\mathrm{g}}^{\mathrm{sr},j_{\mathrm{f}}j_{\mathrm{m}}}(\omega_{\mathrm{f},j_{\mathrm{f}}},\omega_{\mathrm{m},j_{\mathrm{m}}})$, $\vec{\mathbf{K}}_{\mathrm{g}}^{\mathrm{ss},i_{\mathrm{f}}j_{\mathrm{f}}}(\omega_{\mathrm{f},i_{\mathrm{f}}},\omega_{\mathrm{f},j_{\mathrm{f}}})$, $\vec{\mathbf{K}}_{\mathrm{g}}^{\mathrm{rr},j_{\mathrm{m}}i_{\mathrm{m}}}(\omega_{\mathrm{m},j_{\mathrm{m}}},\omega_{\mathrm{m},i_{\mathrm{m}}})$ and $\vec{\mathbf{K}}_{\mathrm{g}}^{\mathrm{rr},i_{\mathrm{m}}j_{\mathrm{m}}}(\omega_{\mathrm{m},i_{\mathrm{m}}},\omega_{\mathrm{m},j_{\mathrm{m}}})$, respectively.

The full system is assembled into submatrices related to the moving and fixed FORs and the coupling terms between them:

$$\vec{\mathbf{K}}_{\mathrm{mm}}=\begin{bmatrix}\vec{\mathbf{K}}_{\mathrm{mm}}^{11}(\omega_{\mathrm{m},1}) & \vec{\mathbf{K}}_{\mathrm{mm}}^{12}(\omega_{\mathrm{m},1},\omega_{\mathrm{m},2}) & \cdots & \vec{\mathbf{K}}_{\mathrm{mm}}^{1J_{\mathrm{m}}}(\omega_{\mathrm{m},1},\omega_{\mathrm{m},J_{\mathrm{m}}})\\ \vec{\mathbf{K}}_{\mathrm{mm}}^{21}(\omega_{\mathrm{m},2},\omega_{\mathrm{m},1}) & \vec{\mathbf{K}}_{\mathrm{mm}}^{22}(\omega_{\mathrm{m},2}) & \cdots & \vec{\mathbf{K}}_{\mathrm{mm}}^{2J_{\mathrm{m}}}(\omega_{\mathrm{m},2},\omega_{\mathrm{m},J_{\mathrm{m}}})\\ \vdots & \vdots & \ddots & \vdots\\ \vec{\mathbf{K}}_{\mathrm{mm}}^{J_{\mathrm{m}}1}(\omega_{\mathrm{m},1},\omega_{\mathrm{m},J_{\mathrm{m}}}) & \vec{\mathbf{K}}_{\mathrm{mm}}^{J_{\mathrm{m}}2}(\omega_{\mathrm{m},2},\omega_{\mathrm{m},J_{\mathrm{m}}}) & \cdots & \vec{\mathbf{K}}_{\mathrm{mm}}^{J_{\mathrm{m}}J_{\mathrm{m}}}(\omega_{\mathrm{m},J_{\mathrm{m}}})\end{bmatrix}, \tag{62a}$$

$$\vec{\mathbf{K}}_{\mathrm{ff}}=\begin{bmatrix}\vec{\mathbf{K}}_{\mathrm{ff}}^{11}(\omega_{\mathrm{f},1}) & \vec{\mathbf{K}}_{\mathrm{ff}}^{12}(\omega_{\mathrm{f},1},\omega_{\mathrm{f},2}) & \cdots & \vec{\mathbf{K}}_{\mathrm{ff}}^{1J_{\mathrm{f}}}(\omega_{\mathrm{f},1},\omega_{\mathrm{f},J_{\mathrm{f}}})\\ \vec{\mathbf{K}}_{\mathrm{ff}}^{21}(\omega_{\mathrm{f},2},\omega_{\mathrm{f},1}) & \vec{\mathbf{K}}_{\mathrm{ff}}^{22}(\omega_{\mathrm{f},2}) & \cdots & \vec{\mathbf{K}}_{\mathrm{ff}}^{2J_{\mathrm{f}}}(\omega_{\mathrm{f},2},\omega_{\mathrm{f},J_{\mathrm{f}}})\\ \vdots & \vdots & \ddots & \vdots\\ \vec{\mathbf{K}}_{\mathrm{ff}}^{J_{\mathrm{f}}1}(\omega_{\mathrm{f},J_{\mathrm{f}}},\omega_{\mathrm{f},1}) & \vec{\mathbf{K}}_{\mathrm{ff}}^{J_{\mathrm{f}}2}(\omega_{\mathrm{f},J_{\mathrm{f}}},\omega_{\mathrm{f},2}) & \cdots & \vec{\mathbf{K}}_{\mathrm{ff}}^{J_{\mathrm{f}}J_{\mathrm{f}}}(\omega_{\mathrm{f},J_{\mathrm{f}}})\end{bmatrix}, \tag{62b}$$

$$\vec{\mathbf{K}}_{\mathrm{mf}}=\begin{bmatrix}\vec{\mathbf{K}}_{\mathrm{mf}}^{11}(\omega_{\mathrm{m},1},\omega_{\mathrm{f},1}) & \vec{\mathbf{K}}_{\mathrm{mf}}^{12}(\omega_{\mathrm{m},1},\omega_{\mathrm{f},2}) & \cdots & \vec{\mathbf{K}}_{\mathrm{mf}}^{1J_{\mathrm{f}}}(\omega_{\mathrm{m},1},\omega_{\mathrm{f},J_{\mathrm{f}}})\\ \vec{\mathbf{K}}_{\mathrm{mf}}^{21}(\omega_{\mathrm{m},2},\omega_{\mathrm{f},1}) & \vec{\mathbf{K}}_{\mathrm{mf}}^{22}(\omega_{\mathrm{m},2},\omega_{\mathrm{f},2}) & \cdots & \vec{\mathbf{K}}_{\mathrm{mf}}^{J_{\mathrm{m}}J_{\mathrm{f}}}(\omega_{\mathrm{m},J_{\mathrm{m}}},\omega_{\mathrm{f},J_{\mathrm{f}}})\\ \vdots & \vdots & \ddots & \vdots\\ \vec{\mathbf{K}}_{\mathrm{mf}}^{J_{\mathrm{m}}1}(\omega_{\mathrm{m},J_{\mathrm{m}}},\omega_{\mathrm{f},1}) & \vec{\mathbf{K}}_{\mathrm{mf}}^{J_{\mathrm{m}}1}(\omega_{\mathrm{m},J_{\mathrm{m}}},\omega_{\mathrm{f},2}) & \cdots & \vec{\mathbf{K}}_{\mathrm{mf}}^{J_{\mathrm{m}}J_{\mathrm{f}}}(\omega_{\mathrm{m},J_{\mathrm{m}}},\omega_{\mathrm{f},J_{\mathrm{f}}})\end{bmatrix}, \tag{62c}$$

$$\vec{\mathbf{K}}_{\mathrm{fm}}=\begin{bmatrix}\vec{\mathbf{K}}_{\mathrm{fm}}^{11}(\omega_{\mathrm{f},1},\omega_{\mathrm{m},1}) & \vec{\mathbf{K}}_{\mathrm{fm}}^{12}(\omega_{\mathrm{f},1},\omega_{\mathrm{m},2}) & \cdots & \vec{\mathbf{K}}_{\mathrm{fm}}^{1J_{\mathrm{m}}}(\omega_{\mathrm{f},1},\omega_{\mathrm{m},J_{\mathrm{m}}})\\ \vec{\mathbf{K}}_{\mathrm{fm}}^{21}(\omega_{\mathrm{f},2},\omega_{\mathrm{m},1}) & \vec{\mathbf{K}}_{\mathrm{fm}}^{22}(\omega_{\mathrm{f},2},\omega_{\mathrm{m},2}) & \cdots & \vec{\mathbf{K}}_{\mathrm{fm}}^{2J_{\mathrm{m}}}(\omega_{\mathrm{f},2},\omega_{\mathrm{m},J_{\mathrm{m}}})\\ \vdots & \vdots & \ddots & \vdots\\ \vec{\mathbf{K}}_{\mathrm{fm}}^{J_{\mathrm{f}}1}(\omega_{\mathrm{f},J_{\mathrm{f}}},\omega_{\mathrm{m},1}) & \vec{\mathbf{K}}_{\mathrm{fm}}^{J_{\mathrm{f}}2}(\omega_{\mathrm{f},J_{\mathrm{f}}},\omega_{\mathrm{m},2}) & \cdots & \vec{\mathbf{K}}_{\mathrm{fm}}^{J_{\mathrm{f}}J_{\mathrm{m}}}(\omega_{\mathrm{f},J_{\mathrm{f}}},\omega_{\mathrm{m},J_{\mathrm{m}}})\end{bmatrix}. \tag{62d}$$

Further the full system displacement and load vectors are created:

$$\vec{\mathbf{U}}_{\mathrm{m}}=\left\{\left[\vec{\mathbf{U}}_{\mathrm{m}}^{1}(\omega_{\mathrm{m},1})\right]^{\mathrm{T}}\quad\left[\vec{\mathbf{U}}_{\mathrm{m}}^{2}(\omega_{\mathrm{m},2})\right]^{\mathrm{T}}\quad\cdots\quad\left[\vec{\mathbf{U}}_{\mathrm{m}}^{J_{\mathrm{m}}}(\omega_{\mathrm{m},J_{\mathrm{m}}})\right]^{\mathrm{T}}\right\}^{\mathrm{T}}, \tag{63a}$$

$$\vec{\mathbf{U}}_{\mathrm{f}}=\left\{\left[\vec{\mathbf{U}}_{\mathrm{f}}^{1}(\omega_{\mathrm{f},1})\right]^{\mathrm{T}}\quad\left[\vec{\mathbf{U}}_{\mathrm{f}}^{2}(\omega_{\mathrm{f},2})\right]^{\mathrm{T}}\quad\cdots\quad\left[\vec{\mathbf{U}}_{\mathrm{f}}^{J_{\mathrm{f}}}(\omega_{\mathrm{f},J_{\mathrm{f}}})\right]^{\mathrm{T}}\right\}^{\mathrm{T}}, \tag{63b}$$

$$\vec{\mathbf{F}}_{\mathrm{m}}=\left\{\left[\vec{\mathbf{F}}_{\mathrm{m}}^{1}(\omega_{\mathrm{m},1})\right]^{\mathrm{T}}\quad\left[\vec{\mathbf{F}}_{\mathrm{m}}^{2}(\omega_{\mathrm{m},2})\right]^{\mathrm{T}}\quad\cdots\quad\left[\vec{\mathbf{F}}_{\mathrm{m}}^{J_{\mathrm{m}}}(\omega_{\mathrm{m},J_{\mathrm{m}}})\right]^{\mathrm{T}}\right\}^{\mathrm{T}}, \tag{63c}$$

where it is assumed that only load in a moving FOR is considered. The full system can be solved to obtain the displacements as:

$$\vec{\vec{\mathbf{K}}}\,\vec{\vec{\mathbf{U}}} = \vec{\vec{\mathbf{F}}}, \qquad \vec{\vec{\mathbf{K}}} = \begin{bmatrix} \vec{\vec{\mathbf{K}}}_{\mathrm{mm}} & \vec{\vec{\mathbf{K}}}_{\mathrm{mf}} \\ \vec{\vec{\mathbf{K}}}_{\mathrm{fm}} & \vec{\vec{\mathbf{K}}}_{\mathrm{ff}} \end{bmatrix}, \qquad \vec{\vec{\mathbf{U}}} = \begin{Bmatrix} \vec{\vec{\mathbf{U}}}_{\mathrm{m}} \\ \vec{\vec{\mathbf{U}}}_{\mathrm{f}} \end{Bmatrix}, \qquad \vec{\vec{\mathbf{F}}} = \begin{Bmatrix} \vec{\vec{\mathbf{F}}}_{\mathrm{m}} \\ \vec{\vec{\mathbf{F}}}_{\mathrm{f}} \end{Bmatrix}. \tag{64}$$

In this case, the vector $\vec{\vec{\mathbf{F}}}_{\mathrm{f}}$ is all zeros as there are no loads acting in the fixed FOR. However, the system can be solved by applying loads in either FOR or both FORs at the same time. After the displacements have been obtained, the time-domain solution for both FORs can be obtained using Equation (53). To obtain the displacements of observation nodes, a receptance matrix equivalent to the two lower quarters of the matrix in Equation (54) should be constructed, relating the observation nodes to the rails and to the soil. However, for any considerable number of observation degrees of freedom, the matrix size becomes very large, which can be considered a computational drawback of the methodology.

It is evident that the computation of the fully coupled system is an extremely computationally demanding process, which involves double inversion of very large matrices. Thus, it should only be used when the secondary coupling effects arean important factor. The fully coupled system computation greatly depends on the random-access memory (RAM) available in the computer system used, as the matrices are generally fully populated. However, if the considered system is not too large and the matrices can be stored in computer RAM, the computation times for the system are almost equal to those the partly coupled system.

5. Validation

The methodology described in this paper is validated by comparison with other computational approaches. Firstly, considering a system with no structures or rigid objects interacting with the soil, the described system assembly and solution procedures provide identical results to the approach provided by Sheng et al. [10–12]. This is expected, as this work utilizes the same vehicle–track–soil interaction model, and, with no other structures interacting with the soil, the coupling terms cancel out. Further, modelling of rigid objects interacting with the soil was validated by comparison with BE and FEM–PML models. It was determined that the semi-analytical model provides a very good match, especially with the FEM–PML model, where even the secondary coupling terms show very good agreement. Sections 5.1 and 5.2 provide a more in-depth descriptions of validating the coupling terms used in the system assembly and the solution procedure including a structure interacting with the soil.

5.1 Coupling between moving and fixed frames of reference

In order to validate the coupling terms between the two frames of reference, especially the symmetry between a load applied in the moving FOR and the displacements observed in a fixed FOR and vice versa, some test cases were set up. The previously described mixed-FOR model was simplified by removing the railway track together with the vehicle and the FE/rigid structures interacting with the soil. This way, the effects of a single load with a single excitation frequency acting directly on the soil surface can be observed. The ground was modelled as a homogenous elastic half-space of dense sandy-type soil, with a Young's modulus of 250 MPa, a Poisson's ratio of 0.25, a mass density of 2000 kg/m^3 and a loss factor of 0.05. A stationary point in the fixed FOR was placed 3 m from the line along which the load was moving.

Firstly, a moving vertical load with constant speed v and frequency f_{m} was modelled. The vertical displacements were observed within a fixed FOR for a range of frequencies f_{f}. The system was modelled using the simplified mixed-FOR model. For the analysed case, only the coupling terms between the moving and the fixed frames of reference, as described in Section 2.2, have an effect for the obtained results. For comparison, a full model was established, modelled only in the moving FOR, using the semi-analytical approach.

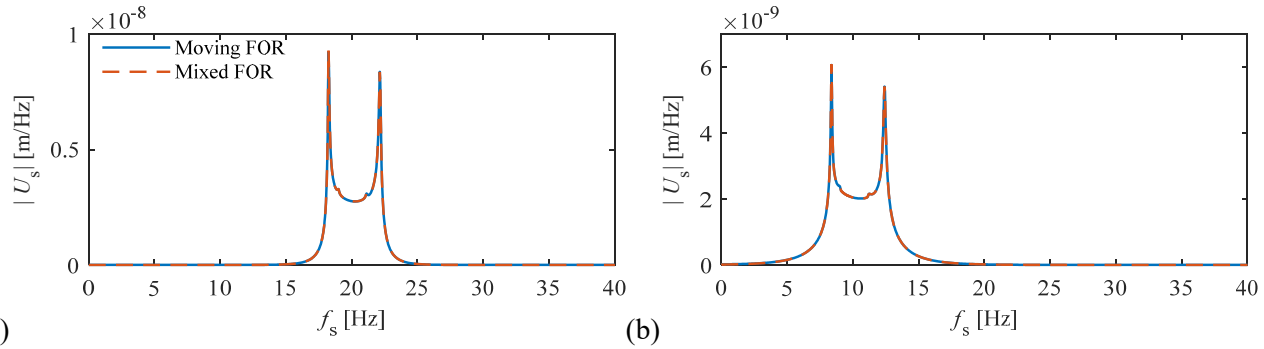

Figure 4. Displacements in a fixed FOR from a unit load applied in a moving FOR: (a) $v = 20$ m/s and $f_\mathrm{m} = 20$ Hz; (b) $v = 40$ m/s and $f_\mathrm{m} = 10$ Hz.

Using the created model, the displacement field of the soil surface in the moving FOR and within the time domain was obtained for a single excitation frequency. Then, a time signal for displacements of an observation point moving through the displacement field with speed $-v$ was found, considering that for every time step the position of the observation point changed. Fourier transforming the obtained time signal into frequencies f_s, the displacement spectra for a stationary observation point was obtained. Two combinations of speed and frequency in the moving FOR were investigated: Combination 1 with $v = 20$ m/s and $f_\mathrm{m} = 20$ Hz, and Combination 2 with $v = 40$ m/s and $f_\mathrm{m} = 10$ Hz. The comparison of both approaches are shown in Figure 4 where it can be seen that the two approaches agree, confirming the analytical derivation presented in Section 2.2.

Secondly, a similar test case was created to analyse the coupling between a load in a fixed FOR and the resulting displacements in a moving FOR. Here, the mixed FOR model was compared to a full solution formulated only in a fixed FOR. In the same way as for the previous case, using the full model, the displacement field of the soil surface was found in time domain. Then the vertical displacements for a moving observation point were obtained by changing the position of the point for every time step. Fourier transforming the time-domain response for frequencies f_m, the displacement spectra for a moving observation point were obtained. Two combinations of speed and stationary frequency were again investigated: Combination 1 with $v = 20$ m/s and $f_\mathrm{s} = 20$ Hz; Combination 2 with $v = 40$ m/s and $f_\mathrm{s} = 10$ Hz. Results of both approaches are given in Figure 5. Once again, the results agree well, this time confirming the derivation given in Section 2.3.

Comparing the two investigated cases, it is evident that the response spreads out through the observer frequencies due to the Doppler effect, independently of which FOR the load was applied in. The range of affected frequencies dependent on the speed of the moving FOR. However, a load applied in the fixed FOR produces two symmetric peaks around the excitation frequency, when observed in a moving FOR, while a load applied in a moving FOR produces two peaks in the fixed FOR. Further, comparing the results of

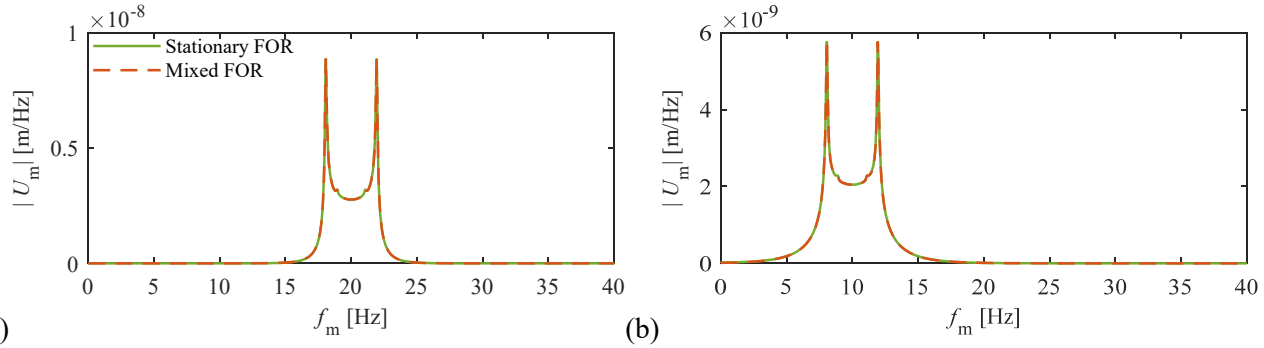

Figure 5. Displacements in a moving FOR from a unit load applied in a fixed FOR.: (a) $v = 20$ m/s and $f_\mathrm{s} = 20$ Hz; (b) $v = 40$ m/s and $f_\mathrm{s} = 10$ Hz.

Combination 1 for both cases, it can be observed that the result in Figure 4 at $f_s = 20$ Hz and the result in Figure 5 at $f_m = 20$ Hz show exactly the same response. This confirms the symmetry between the two frames of reference implied by Equation (21). The same result is obtained by comparing the responses of Combination 2 for both cases.

5.2 Validation of the modelling approach

To validate the modelling approach presented in this paper, it was compared to a sub-modelling technique, as described by [30]. A similar modelling approach was also used in [22]. In both cases the sub-modelling approach was used to model an underground railway tunnel with a vehicle travelling through it, in turn exciting a building structure above the soil. However, the solution procedure can also be applied to surface railways and the system analysed in this work. The method uses the free-field displacements of the soil caused by a passing vehicle, which are later modified by introducing the building structure. Ensuring equilibrium and compatibility between the degrees of freedom connecting the building and the soil, a solution for the building displacements can be found. Comparing the methodology proposed in this work with the sub-modelling technique, it becomes evident that the basic parts used for both solution procedures are identical. For example, the free-field displacements from a moving load used in the two-step approach are identical to the flexibility matrix $\mathbf{G}_{rs}$ used here. However, the assembly and solution of the full system is somewhat different, with the proposed methodology allowing a wider range of applications, such as modelling rigid inclusions or allowing a two-way coupling between the two frames of reference. Further, the sub-modelling technique, as applied in this work, is a two-step solution approach, as the wheel–rail interaction forces are obtained in the moving FOR before being used to obtain the displacements in the fixed FOR.

As, both approaches use the same basic parts, it is relatively easy to compare them. For comparison, a building structure, as described below in Section 6.1, was used. However, the sub-modelling technique cannot directly model rigid objects, thus the rigid surface footings underneath each column were replaced by a single flexible slab footing underneath the whole building. The foundation slab was modelled using shell finite elements with the same properties as the building floors. The soil is modelled as a half-space of sand, with the same properties as in Section 5.1. Both systems were excited by a single passing vehicle, travelling at 40 m/s, exposed to a unit rail unevenness, with a 4 m wavelength corresponding to an excitation frequency of 10 Hz. For analysis, only

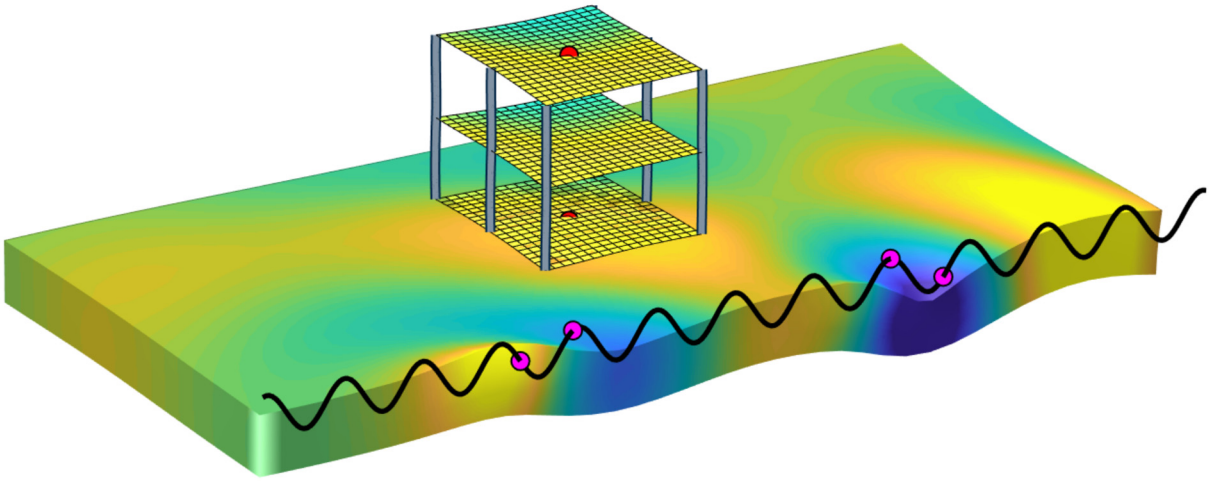

Figure 6. Investigated case for validating the modelling approach. The vehicle is travelling from left to right, with magenta nodes indicating the wheel positions. The red nodes indicate the observation points, while the shades of colour indicate the vertical displacements (bright yellow is up, dark blue is down). Track unevenness is not scaled.

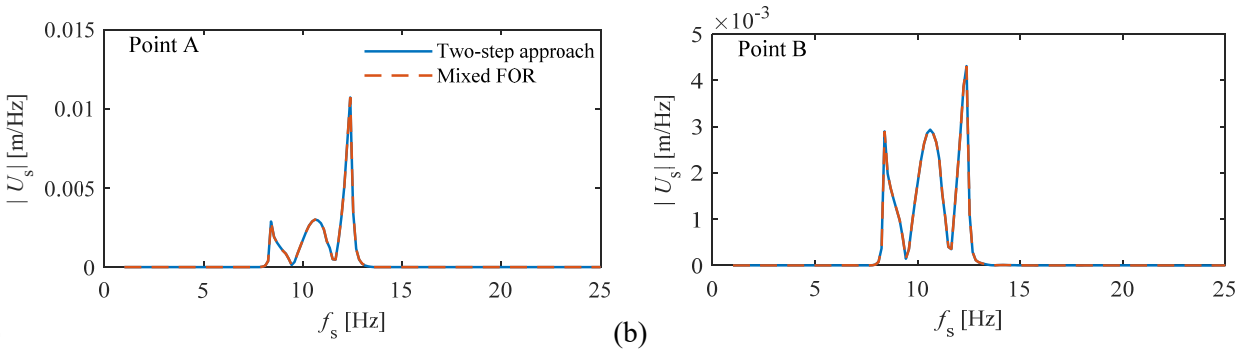

Figure 7. Comparison between two system solution procedures. Displacements are shown: (a) at the centre of the ground floor; (b) at the centre of the second floor of the building structure.

a single excitation frequency is used, as the effects from multiple excitations frequencies are just added together due to the principal of superposition. Thus, a single excitation frequency is enough to evaluate how well both models perform. The test case is illustrated in Figure 6.

Figure 7 shows the displacements of the building structure obtained at the centre of the ground floor and the second floor. It can be observed that both approaches provide almost identical results, showing that the proposed method is performing well. At the same time, almost identical results indicate that the back-coupling of the building structure to the railway track is insignificant. It can be concluded, that at least for the considered case, there is no significant difference whether on or the other approach is considered.

6. Example cases

6.1 Partly coupled system

To demonstrate the capabilities of the proposed partly-coupled-modelling approach, an example case was set up. A simple building structure that is excited by a vehicle travelling on a nearby railway track is modelled. The vehicle, railway track, soil and the building were all modelled in one coupled system. The soil was modelled as a 5 m layer of soft clay sitting over a stiffer half-space of sand. The clay had a Young's modulus of 80 MPa, a Poisson's ratio of 0.48, a mass density of 2100 kg/m^3, and a loss factor of 0.05. The underlying sand had the same properties as in Section 5. A soil stratification with two layers was chosen, as the waves reflecting from the interface between the two different materials can, in some cases, amplify the excitation of the building structure.

Only a single vehicle was modelled in the system. It was modelled as a 10-degree-of-freedom multibody system. The system consists of a rigid vehicle body, two rigid bogies and four wheels, with parts of the vehicle connected through a two-tier spring dashpot system. The vehicle was travelling at 40 m/s over the track

Table 1. Vehicle properties.

Mass of car body	40000	kg
Mass of bogie	5000	kg
Mass of wheel set	1800	kg
Car body pitch moment of inertia	$2.0 \cdot 10^6$	kg·m^2
Primary suspension stiffness	$2.4 \cdot 10^6$	N/m
Secondary suspension stiffness	$6.0 \cdot 10^5$	N/m
Primary suspension damping	30000	N·s/m
Secondary suspension damping	20000	N·s/m
Distance between bogies' centers	19.0	m
Distance between bogie's wheels sets	2.7	m
Herztian constant G_H	$5.14 \cdot 10^{-8}$	-

Table 2. Railway track properties.

Rail mass per unit length	60.0	kg/m
Rail bending stiffness	$6.4 \cdot 10^6$	N/m^2
Rail loss factor	0.01	-
Railpad stiffness	$5.0 \cdot 10^8$	N/m
Railpad loss factor	0.1	-
Sleeper mass per unit length	542.0	kg
Ballast vertical stiffness	$4.64 \cdot 10^9$	N·s/m
Ballast mass per unit length	1740	m
Ballast loss factor	0.04	-
Track width	3.2	m

structure, with the building 10 m away from the track centreline. The properties of the vehicle and the track are given in Tables 1 and 2, respectively. The system was excited by the deadweight of the vehicle and by the dynamic wheel–rail interaction forces caused by the uneven vertical track profile. To model the unevenness of the rails, a German track spectrum was used to obtain the PSD function, as described by Cantero et al. [37], with the track quality coefficient equal to $0.59233 \cdot 10^{-6}$, corresponding to a medium quality track. From it, the corresponding unevenness values for every wavenumber were obtained. The track unevenness was considered in the range 0.5–80 m, including both positive and negative wavenumbers to allow a double-sided Fourier transformation. The total amount of discrete wavenumbers considered was 800.

The modelled building structure can be seen in Figure 8. It is a simple structure with six columns supporting two floors. Underneath each column, a square rigid surface footing was modelled, with one side equal to 2 m. Each rigid footing was discretized into 100 SSI nodes. The building is facing the railway track with its narrow side, which is 8 m wide, and the building is supported by two columns at either side. The length of the building is 10 m in the direction orthogonal to the track. In addition to the four columns placed at the corners, a column is placed in the middle of each of the longer sides. Each storey is 4 m high. The whole building structure is constructed from concreate with a Young's modulus of 30 GPa, a Poisson's ratio of 0.15, a mass density of 2400 kg/m^3, and loss factor of 0.03. The columns have square cross-sections, with one side equal to 0.3 m, while the floors are 0.25 m thick slabs. 3D beam elements were used to model the columns, using Euler-Bernoulli beam theory to account for bending. The floors of the building were modelled using Mindlin-Reissner shell elements, accounting for bending as well as shear. All FE parts of the model were discretized

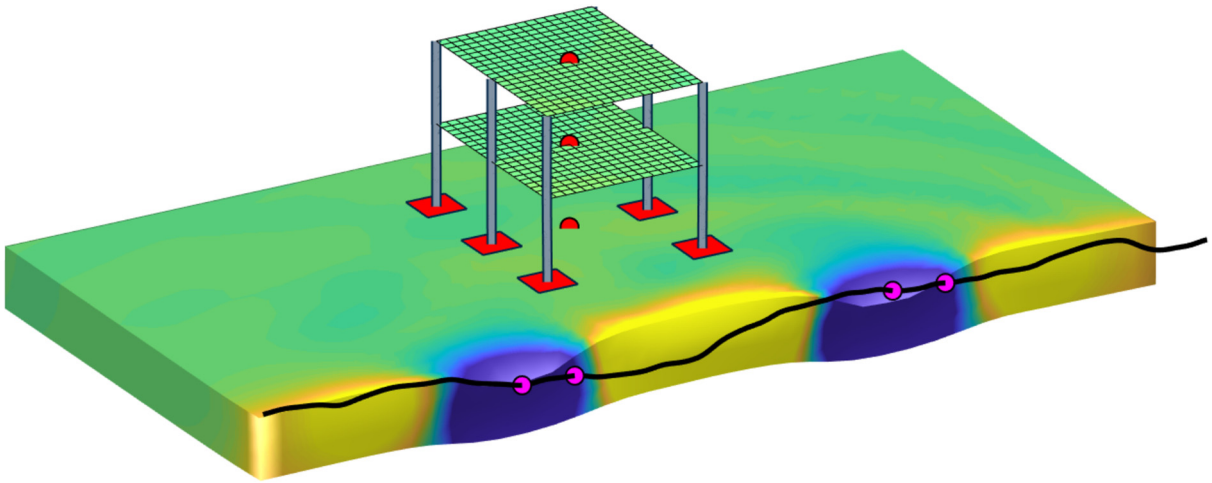

Figure 8. Investigated example case. The shades of colour indicate the vertical displacements (bright yellow is up, dark blue is down). The red nodes are the observation points, while the magenta nodes indicate the positions of the vehicle wheel sets placed on the exaggerated vertical rail profile.

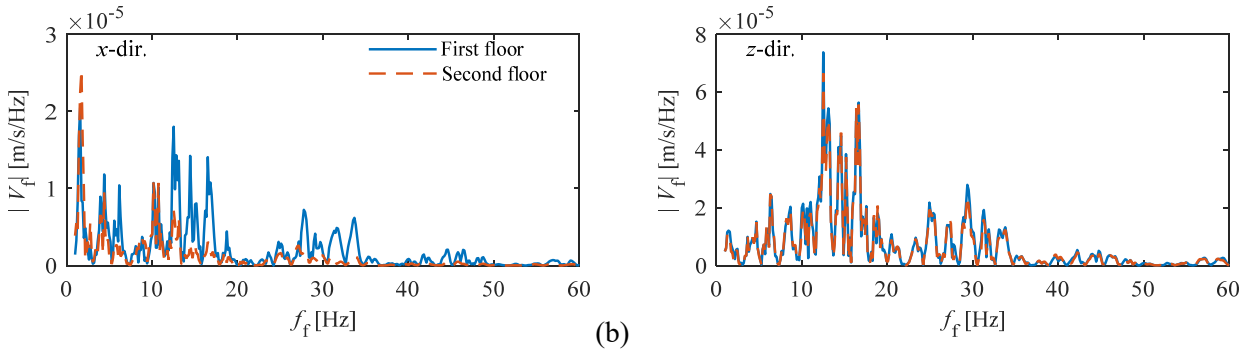

Figure 9. Velocities of the building structure in the frequency domain at the centre of the first and the second floors, (a) in *x*-direction; (b) in *z*-direction.

with mesh size of 0.5 m. Three points on the building structure were created, where the displacements and velocities are observed, as shown in Figure 8. The excitation of the building structure is observed within the frequency range 1–60 Hz, with 400 discrete fixed-FOR frequencies.

Figure 8 shows the system response in time domain at the instance where the centre of the vehicle is at the position right in front of the centre of the building. The positions of the vehicle wheels are indicated by magenta coloured nodes placed on the uneven track surface. The black line shows the exaggerated track surface profile, and it also indicates location of the railway track centre. It can be observed that the displacements from the deadweight of the vehicle have the largest effect on the system, especially near the track structure. However, the building is further away from the track and is affected more by the lower-amplitude, higher-frequency excitation. This is especially evident when the velocities in the frequency domain of the first and second floors are investigated, as shown in Figure 9. Here, it can be observed that, while the low-frequency response is still excited by the deadweight of the vehicle, higher-frequency excitation plays an important role—especially for the vertical velocities.

Comparing the response on the first and the second floors of the building, it can be observed that in the vertical direction both floors are excited almost identically to each other, while the differences for the horizontal *x*-direction (the vehicle travelling direction) are much larger. This is due to the relatively large axial stiffness of the columns, which propagates the excitation in the vertical direction well, exciting both floors almost equally. While, the bending stiffness of the columns is smaller and therefore the upper floor is isolated, especially at higher frequencies. This is seen on the left subfigure in Figure 9, where the high-frequency response is smaller for the second floor when compared to the first floor.

The time domain response of the system is obtained by assigning random phase angles to the unevenness of the rail corresponding to each considered wavenumber. This way, a random vertical rail profile is created and the response to it can be observed in the system. Figure 10 shows the time-domain response of the soil surface and the two floors from two different profiles of the uneven track. It can be observed that the track profiles have a significant effect on the observed system displacements in time domain, especially for the observed high-frequency components. However, the low frequencies are dominated by the deadweight of the vehicle and not affected much by different rail profiles. Further, the building structure acts as a filter of higher frequency vibration, significantly reducing the observed displacements when compared to the soil surface. This is especially evident for the horizontal displacements, where different rail profiles have a much smaller effect on the time domain displacements.

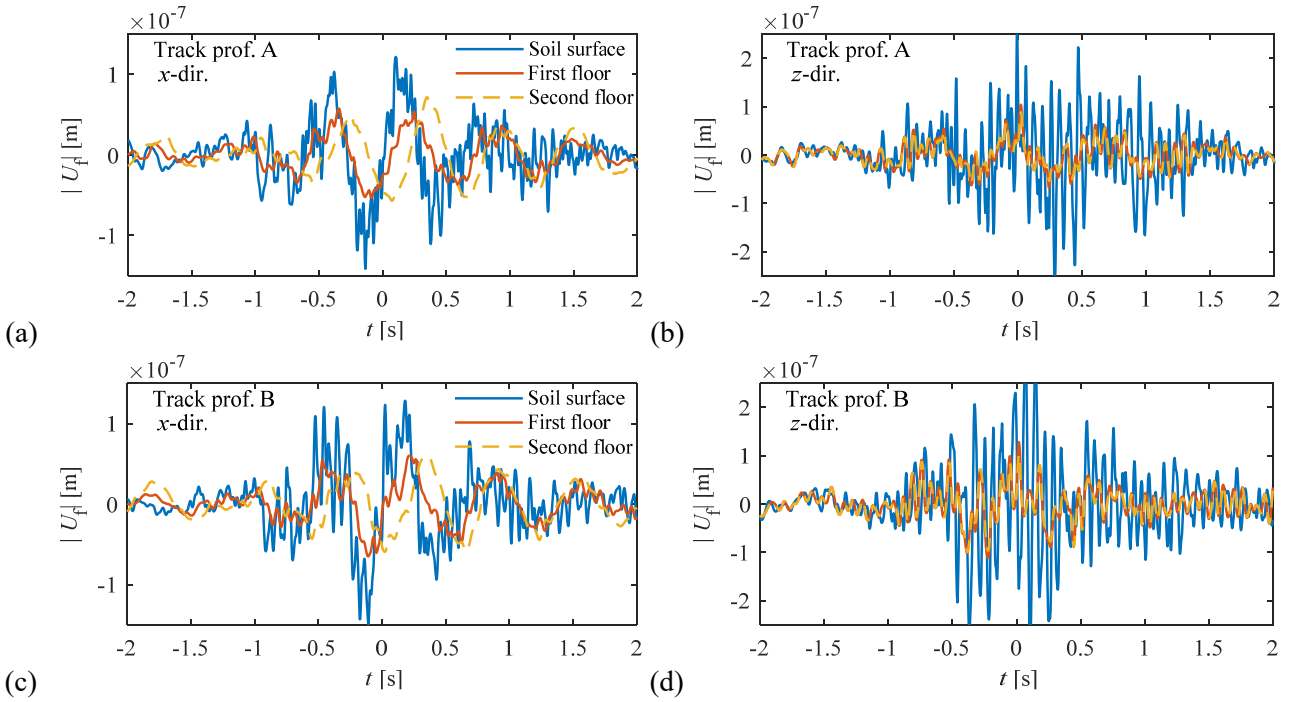

Figure 10. Displacements of the structure in the time domain generated from different rail unevenness profiles, (a) unevenness profile A and response in *x*-direction; (b) unevenness profile A, response in *z*-direction; (c) unevenness profile B, response in *x*-direction; (d) unevenness profile B, response in *z*-direction.

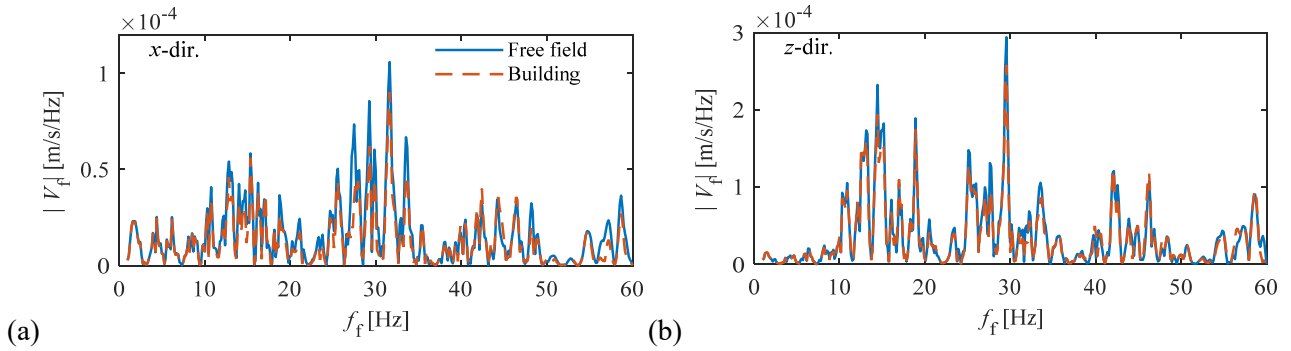

Figure 11. Velocities of the soil surface underneath the building compared to the free-field response, (a) response in *x*-direction; (b) response in *z*-direction.

The displacements of the soil surface are also affected by the building structure. Figure 11 shows the velocities of the soil from a model with a building structure compared to a free-field solution. The building structure reduces the observed velocities of the soil. However, the effects are not very large, with the largest change observed in the 10–35 Hz range. The frequency range corresponds well with the frequency range where the highest excitation of the building was obtained, as seen in Figure 9. Once again, these effects are more pronounced when analysing the horizontal displacements of the system.

6.2 Fully coupled system

A fully-coupled system solution approach might be necessary in cases where the modelled structures are close to the railway track, introducing a signifficant change of dynamic stiffness along the track. In that case, the rescattered waves can have an effect on the vehicle behaviour and the obtained wheel–rail interaction forces.

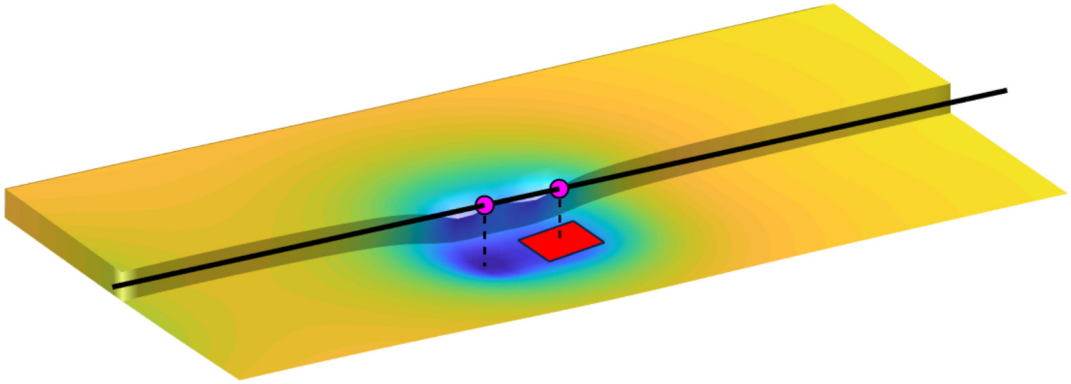

Figure 12. Vehicle passing over a buried rigid block, at an instance where the leading wheel of the vehicle is directly above the centre of the rigid block. The vehicle is travelling at 40 m/s from left to right. The black line indicates the vehicle traverse line, with the magenta nodes indicating the positions of the vehicle wheel sets. Only the two wheel sets of the front bogie are shown.

To examine such a case, a test case was set up modelling a single vehicle traveling across a railway track, as shown in Figure 12. The speed of the vehicle was 40 m/s. The vehicle and the track properties were the same as introduced in Tables 1 and 2. The soil was modelled as a half-space of clay, with material properties given in Section 6.1. Underneath the track, at a depth of 1 m, a rigid block was embedded within the soil. The block was centred at the position, where the travelling vehicle centre line was located at time 0. The block was modelled as a 2D plate, placed in the horizontal plane with one side equal to 2 m. It was discretized into 36 discretization nodes, with three degrees of freedom per node. The system was excited by the deadweight of the vehicle only applied at $f_{\mathrm{m}} = 0$ Hz, with no excitation from the rail unevenness. The system was assessed by the fully-coupled-modelling approach, described in Section 4.2. As only the quasi-static effects of the vehicle were modelled, the considered frequency ranges are reduced. The one-sided frequency range of the moving FOR was 0–30 Hz, and the one-sided frequency range of the fixed FOR is 0–25 Hz. In the computation, negative as well as positive frequencies were considered for either FOR, and each range was split into 200 discrete frequencies.

Figure 13 shows the velocities obtained for the vehicle in the moving FOR as well as the rigid block in the fixed FOR. It can be observed that the vehicle passing over a rigid block introduces a significant excitation into the system, with the rigid block as well as the vehicle reacting to the passage. In this system, the observed excitation of the vehicle is purely due to the weak coupling effects that are disregarded in the two-step procedure. The waves generated by the passing vehicle are scattered by the rigid block in the fixed FOR and in turn excite a range of frequencies in the moving FOR. These effects would not be accounted for when the weak coupling between the vehicle and structures is not modelled. Analysing the wheel velocities, as shown in Figure 12 top left, it can be seen that both leading wheels of separate bogies produce very similar results. However, the excitation due to the first wheel passage over the rigid block generates a wave that excites the third vehicle wheel, even before it reaches the rigid block. A similar effect is also observed after the third wheel passes over the rigid block, where the generated wave travels forward and excites the first vehicle wheel. A very similar behaviour is also observed on the bogies. Comparing these secondary excitations, it can be seen, that the reaction of the third wheel due to the first wheel passage is higher than the excitation of the first wheel due to third wheel passage. This is due to the Doppler effect of the wave travelling through the rail, as the third wheel is travelling towards the wave propagating form the first wheel, while the wave generated by the third wheel must ‘catch up’ to the first wheel. Analysing the rigid block displacements, it can be observed that the largest velocities are reached just before the leading wheel of a bogie reaches the centre of block. Interestingly, to obtain the same displacements of the rigid block, a fully-coupled-system-solution approach is unnecessary, as the partly coupled solution provides results that are almost identical. For the analysed case, it can be

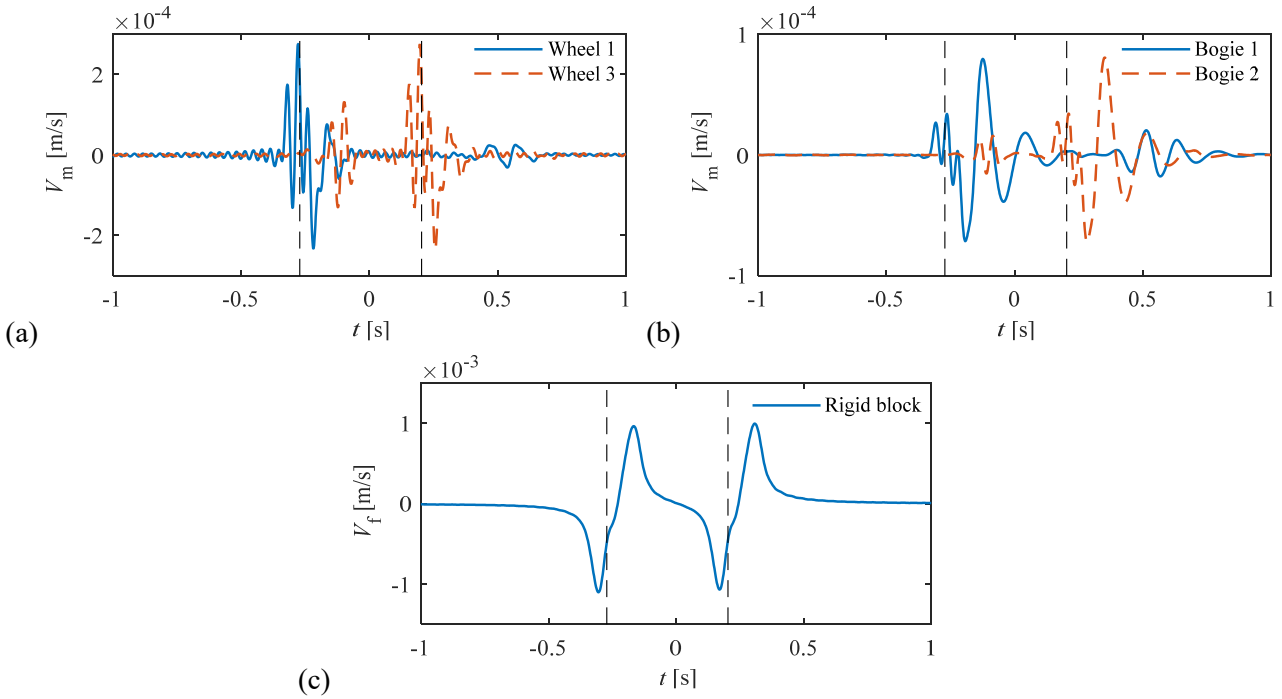

Figure 13. Vertical velocities for parts of the vehicle (in moving FOR) and the rigid block underneath the track (in fixed FOR). The vertical dashed black lines indicate time instance when the first and third vehicle wheels are directly above the centre of the rigid block. The response is shown for: (a) the first and the third vehicle wheels; (b) both vehicle bogies; (c) rigid block underneath the track.

concluded that the fully coupled solution approach is only necessary if the vehicle behaviour is of interest, for example for assessment of driver and passenger comfort, or if the track and wheel wear is to be assessed.

7. Conclusions

The paper introduced a new modelling approach for estimation of environmental vibration resulting from railway traffic. A model of a coupled vehicle–track–soil–building system was introduced with two approaches proposed for assembly and solution of the whole system: the partly-coupled approach and the fully-coupled approach. Both solution approaches use a single step procedure with one approach considering a fully-coupled system, while the other approach discards some secondary coupling effects for a more computationally efficient solution procedure.

A semi-analytical model was utilized to model the soil to which rigid objects and structures modelled by the FE were coupled. The proposed modelling approach uses the frequency-domain solution with some parts, such as the railway track, formulated in the moving FOR and other parts, such as building structures, formulated in a fixed FOR. The coupling terms between the two frames of reference are found by utilizing an analytical formulation of receptance between the two frames of reference. It has been established that due to the coupling between the fixed and moving frames of reference, the previously uncoupled discrete frequencies become coupled through the other FOR as a result of the Doppler effect and wave scattering. Thus, additional consideration is needed when modelling such systems.

The proposed methodology is a robust approach that does not suffer from numerical instabilities, due to the usage of frequency domain solutions. A wide range of cases can be assessed, including the modelling of rigid objects in or on the ground and flexible structures modelled by the FEM, interacting with the soil. Using the proposed partly-coupled-solution approach, the computations can be easily parallelized, thus providing a

relatively fast and efficient computational method. Further, the suggested fully-coupled-solution procedure is useful in cases where the weak coupling between the vehicle and structures cannot be discarded.

In this work, a railway track with a train was considered as an example case. However, the methodology can be easily expanded to other cases, e.g. modelling a road with road traffic exciting the system. Further, adding FE models to the formulation is possible in the moving FOR as well as the fixed FOR. Thus, a more detailed railway track model or vehicle could also be added to the system.

The analytically derived coupling terms between the two frames of reference were validated by comparing with models formulated in a single FOR. Further, the partly coupled solution procedure of the full system was compared to a solution procedure in which the weak coupling is completely discarded. The two solution procedures have been found to provide almost identical results, validating the proposed partly coupled solution procedure while, at the same time, indicating insignificant back-coupling in the considered case.

Finally, to demonstrate the capabilities of the numerical model, a building structure with rigid surface footings was analysed. The vibration levels at different floors were determined, as well as the effect of the structure on the surrounding soil, compared to a free-field solution. To demonstrate the potential of the fully-coupled-solution procedure, the response of a vehicle passing over a buried rigid block were investigated. It was been found that the fully coupled solution procedure can predict the weak coupling effects between the vehicle and the structure, producing a vehicle response distributed through frequencies, when the load is applied only at a single frequency. Thus, in the present example, the modes of the vehicle were excited parametrically by the waves scattered from the rigid inclusion as a result of the passing deadweight of the vehicle.

Acknowledgement

Part of the research was carried out in the framework of the project “Urban Tranquility” under the Interreg V programme. The first and the fourth authors of this work gratefully acknowledge the European Regional Development Fund for the financial support. Further, the first author would also like to acknowledge the generous support of the Graduate School of Science and Technology in Aarhus University. The second and third authors gratefully acknowledge the support of the EPSRC under the programme grant EP/M025276/1, 'The science and analytical tools to design long life, low noise railway track systems (Track to the Future)'.

References

[1] D.P. Connolly, G.P. Marecki, G. Kouroussis, I. Thalassinakis, P.K. Woodward, The growth of railway ground vibration problems — A review, Science of the Total Environment. 568 (2016) 1276–1282.

[2] High-Speed Ground Transportation Noise and Vibration Impact Assessment, Federal Railroad Administration, 2012.

[3] G. Degrande, G. Lombaert, An efficient formulation of Krylov's prediction model for train induced vibrations based on the dynamic reciprocity theorem, The Journal of the Acoustical Society of America. 110 (2002) 1379–1390.

[4] V. V. Krylov, F. Colin, Calculation of low-frequency ground vibrations from railway trains, Applied Acoustics. 42 (1994) 199–213.

[5] V. V. Krylov, Effects of track properties on ground vibrations generated by high-speed trains, Acta Acustica. 228 (1999) 129–156.

[6] W.T. Thomson, Transmission of elastic waves through a stratified solid medium, Journal of Applied Physics. 21 (1950) 89–93.

[7] N.A. Haskell, The dispersion of surface waves on multilayered media, Bulletin of the Seismological Society of America. 43 (1953) 17–43.

[8] L.V. Andersen, J. Clausen, Impedance of surface footings on layered ground, Computers and Structures. 86 (2008) 72–87.

[9] P. Bucinskas, L.V. Andersen, Semi-analytical approach to modelling the dynamic behaviour of soil excited by embedded foundations, Procedia Engineering. 199 (2017) 2621–2626.

[10] X. Sheng, C.J.C. Jones, M. Petyt, Ground vibration generated by a harmonic load acting on a railway track, Journal of Sound and Vibration. 225 (1999) 3–28.

[11] X. Sheng, C.J.C. Jones, M. Petyt, Ground vibration generated by a load moving along a railway track, Journal of Sound and Vibration. 228 (1999) 129–156.

[12] X. Sheng, C.J.C. Jones, D.J. Thompson, A theoretical model for ground vibration from trains generated by vertical track irregularities, Journal of Sound and Vibration. 272 (2004) 937–965.

[13] W. Zhai, Z. He, X. Song, Prediction of high-speed train induced ground vibration based on train-track-ground system model, Earthquake Engineering and Engineering Vibration. 9 (2010) 545–554.

[14] D.P. Connolly, A. Giannopoulos, M.C. Forde, Numerical modelling of ground borne vibrations from high speed rail lines on embankments, Soil Dynamics and Earthquake Engineering. 46 (2013) 13–19.

[15] G. Kouroussis, O. Verlinden, Prediction of railway induced ground vibration through multibody and finite element modelling, Mechanical Sciences. 4 (2013) 167–183.

[16] J. O'Brien, D.C. Rizos, A 3D BEM-FEM methodology for simulation of high speed train induced vibrations, Soil Dynamics and Earthquake Engineering. 25 (2005) 289–301.

[17] L.V. Andersen, C.J.C. Jones, Coupled boundary and finite element analysis of vibration from railway tunnels-a comparison of two- and three-dimensional models, Journal of Sound and Vibration. 293 (2006) 611–625.

[18] P. Galvín, A. Romero, J. Domínguez, Fully three-dimensional analysis of high-speed train-track-soil-structure dynamic interaction, Journal of Sound and Vibration. 329 (2010) 5147–5163.

[19] Y. Bin Yang, H.H. Hung, A 2.5D finite/infinite element approach for modelling visco-elastic bodies subjected to moving loads, International Journal for Numerical Methods in Engineering. 51 (2001)

1317–1336.

[20] X. Sheng, C.J.C. Jones, D.J. Thompson, Prediction of ground vibration from trains using the wavenumber finite and boundary element methods, Journal of Sound and Vibration. 293 (2006) 575–586.

[21] Q. Jin, D.J. Thompson, D.E.J. Lurcock, M.G.R. Toward, E. Ntotsios, A 2.5D finite element and boundary element model for the ground vibration from trains in tunnels and validation using measurement data, Journal of Sound and Vibration. 422 (2018) 373–389.

[22] P. Lopes, P.A. Costa, M. Ferraz, R. Calçada, A.S. Cardoso, Numerical modeling of vibrations induced by railway traffic in tunnels: From the source to the nearby buildings, Soil Dynamics and Earthquake Engineering. 61–62 (2014) 269–285.

[23] A. Yaseri, M.H. Bazyar, S. Javady, 2.5D coupled FEM-SBFEM analysis of ground vibrations induced by train movement, Soil Dynamics and Earthquake Engineering. 104 (2018) 307–318.

[24] G. Kouroussis, D.P. Connolly, O. Verlinden, Railway-induced ground vibrations – a review of vehicle effects, International Journal of Rail Transportation. 2 (2014) 69–110.

[25] D.J. Thompson, G. Kouroussis, E. Ntotsios, Modelling, simulation and evaluation of ground vibration caused by rail vehicles, Vehicle System Dynamics. 57 (2019) 936–983.

[26] D.P. Connolly, G. Kouroussis, O. Laghrouche, C.L. Ho, M.C. Forde, Benchmarking railway vibrations - Track, vehicle, ground and building effects, Construction and Building Materials. 92 (2015) 64–81.

[27] P. Fiala, G. Degrande, F. Augusztinovicz, Numerical modelling of ground-borne noise and vibration in buildings due to surface rail traffic, Journal of Sound and Vibration. 301 (2007) 718–738.

[28] S. François, L. Pyl, H.R. Masoumi, G. Degrande, The influence of dynamic soil-structure interaction on traffic induced vibrations in buildings, Soil Dynamics and Earthquake Engineering. 27 (2007) 655–674.

[29] G. Kouroussis, L. Van Parys, C. Conti, O. Verlinden, Prediction of ground vibrations induced by urban railway traffic: an analysis of the coupling assumptions between vehicle, track, soil, and buildings, International Journal of Acoustics and Vibration. 163 (2013) 163–172.

[30] M. Hussein, H. Hunt, K. Kuo, P.A. Costa, J. Barbosa, The use of sub-modelling technique to calculate vibration in buildings from underground railways, Proceedings of the Institution of Mechanical Engineers, Part F: Journal of Rail and Rapid Transit. 229 (2015) 303–314.

[31] D. López-Mendoza, A. Romero, D.P. Connolly, P. Galvín, Scoping assessment of building vibration induced by railway traffic, Soil Dynamics and Earthquake Engineering. 93 (2017) 147–161.

[32] D.P. Connolly, P. Galvín, B. Olivier, A. Romero, G. Kouroussis, A 2.5D time-frequency domain model for railway induced soil-building vibration due to railway defects, Soil Dynamics and Earthquake Engineering. 120 (2019) 332–344.

[33] M.F.M. Hussein, H.E.M. Hunt, A numerical model for calculating vibration from a railway tunnel embedded in a full-space, Journal of Sound and Vibration. 305 (2007) 401–431.

[34] P. Zheng, B. Ding, S.X. Zhao, D. Ding, 3D dynamic Green's functions in a multilayered poroelastic half-space, Applied Mathematical Modelling. 37 (2013) 10203–10219.

[35] R. Wang, A simple orthonormalization method for stable and efficient computation of Green's functions, Bulletin of the Seismological Society of America. 89 (1999) 733–741.

[36] E. Kausel, J.M. Roesset, Stiffness matrices for layered soils, Bulletin of the Seismological Society of America. 71 (1981) 1743–1761.

[37] D. Cantero, T. Arvidsson, E. OBrien, R. Karoumi, Train–track–bridge modelling and review of parameters, Structure and Infrastructure Engineering. 12 (2016) 1051–1064.